Robert Glaser

Symmetry, Spectroscopy, and Crystallography

Related Titles

Zhu, H.

Organic Stereochemistry
Experimental and Computational Methods

2015
Print ISBN: 978-3-527-33822-1; also available in electronic formats

Günther, H.

NMR Spectroscopy
Basic Principles, Concepts, and Applications in Chemistry

3rd Edition
2013
Print ISBN: 978-3-527-33004-1; also available in electronic formats

Zolotoyabko, E.

Basic Concepts of Crystallography

2011
Print ISBN: 978-3-527-33009-6; also available in electronic formats

Hermann, K.

Crystallography and Surface Structure
An Introduction for Surface Scientists and Nanoscientists

2011
Print ISBN: 978-3-527-41012-5; also available in electronic formats

Fleming, I.

Molecular Orbitals and Organic Chemical Reactions-Reference Edition

2010
Print ISBN: 978-0-470-74658-5; also available in electronic formats
ISBN: 978-0-470-68949-3

Berova, N., Woody, R.W., Polavarapu, P., Nakanishi, K. (eds.)

Comprehensive Chiroptical Spectroscopy
Applications in Stereochemical Analysis of Synthetic Compounds, Natural Products, and Biomolecules

2012
Print ISBN: 978-1-118-01292-5; also available in electronic formats

Robert Glaser

Symmetry, Spectroscopy, and Crystallography

The Structural Nexus

WILEY-VCH
Verlag GmbH & Co. KGaA

The Author

Prof. Dr. Robert Glaser
Ben-Gurion University of the Negev
Department of Chemistry
84105 Beer-Sheva
Israel

About the companion website

This book is accompanied by a companion website:
3D animations showing most of the molecules contained in this book can be found under
www.wiley.com/go/Glaser/Symmetry

Library of Congress Card No.: applied for

British Library Cataloguing-in-Publication Data
A catalogue record for this book is available from the British Library.

Bibliographic information published by the Deutsche Nationalbibliothek
The Deutsche Nationalbibliothek lists this publication in the Deutsche Nationalbibliografie; detailed bibliographic data are available on the Internet at <http://dnb.d-nb.de>.

Print ISBN: 978-3-527-33749-1
ePDF ISBN: 978-3-527-68420-5
ePub ISBN: 978-3-527-68421-2
Mobi ISBN: 978-3-527-68414-4
oBook ISBN: 978-3-527-68419-9

Cover Design Formgeber, Mannheim, Germany
Typesetting SPi Global, Chennai, India
Printing and Binding Markono Print Media Pte Ltd, Singapore

Printed on acid-free paper

To Darling Yael: a woman of valor (Eshet Hayil).

Contents

From the Author's Desk *XIII*

1 Symmetry/Pseudosymmetry: Chirality in Molecules, in Nature, and in the Cosmos *1*

1.1 Introduction *1*

1.2 Rudimentary Group Theory, Isometry, and Symmetry *4*

1.3 Asymmetric versus Chiral: The *I*-Symmetry of Viral Capsids *7*

1.4 The Birth of Chirality as a Chemical Concept *9*

1.5 Apparent Symmetry (High-Fidelity *Pseudo*symmetry) and the Quantification of Distortion from the Ideal *11*

1.6 Chirality in Form and Architecture: Symmetry versus Broken Symmetry *16*

1.7 Chirality in Nature: Tropical Storms, Gastropods (Shells), and Fish *17*

1.8 Extraterrestrial Macroscale Chirality: Spiral Galaxies, Martian Sand Devils, Jovian Great Red Spot, Neptune's Great Dark Spot, and Venusian South-Pole Cloud Vortex *20*

1.9 Analyses of Amino Acid Chirality in Extraterrestrial Samples with Gas–Liquid Chromatography Chiral Columns *23*

2 Enantiospecificity of Pheromones, Sweeteners, Fragrances, and Drugs *25*

2.1 Enantiospecificity of Pheromones, Sweeteners, and Fragrances *25*

2.2 The Importance of Chirality in Drug Therapy *27*

3 Bonding Parameters and the Effect of Local Environment on Molecular Structure *33*

3.1 Symmetry Arguments and the Effect of the Environment on Molecular Structure *33*

3.2 The Effect of Local Environment on Molecular Models and Molecular Structure *34*
3.3 Torsion Angles and Molecular Conformation *35*
3.4 Symmetry Considerations of Atomic Orbital Hybridization and Bonding Parameters *39*

4 Historical Development of Structural Chemistry: From Alchemy to Modern Structural Theory *41*
4.1 Hemihedralism in Quartz Crystals: Setting the Stage for the Birth of Stereochemistry *41*
4.2 Tartaric Acid and Alchemy *45*
4.3 Hemihedralism in Crystalline Tartaric Acid Salts: The Birth of Molecular Chirality *46*
4.4 Gift for Prelog's Retirement: A Matched Pair of u',x'-Hemihedral Faced Right- and Left-Handed Quartz Crystals *54*
4.5 Early Structural Representations of Organic Substances and the Development of Modern Structural Concepts *55*
4.6 Fischer Projections to Determine α- and β-Anomeric Configurations *64*

5 Chiroptical Properties *67*
5.1 The Language of Symmetry, Isomerism, and the Characterization of Symmetry Relationships within and between Molecules *67*
5.2 Chiroptical Properties: Circular Birefringence, Optical Rotatory Dispersion, and Circular Dichroism *68*
5.3 Miller Indices and Fractional Coordinates in Crystallography *74*
5.4 Scanning Tunneling Microscopy *78*
5.5 Direct Visualization of an Enantiomer's Absolute Configuration in the Gas Phase *82*

6 Symmetry Comparison of Molecular Subunits: Symmetry in Nuclear Magnetic Resonance Spectroscopy and in Dynamic NMR *85*
6.1 Symmetry in NMR Spectroscopy *85*
6.2 Symmetry Comparison of Molecular Subunits, Topicity Relationships *87*
6.3 Dynamic Stereochemistry, Dynamic Nuclear Magnetic Resonance Spectroscopy (DNMR) *90*
6.4 Use of Permutations in DNMR for Topomerization-, Enantiomerization-, and Diastereomerization-Exchange Processes *92*

7 Prochirality, Asymmetric Hydrogenation Reactions, and the Curtin–Hammett Principle *99*
7.1 Prochirality of Enantiotopic Subunits *99*
7.2 Homogeneous Hydrogenation by $Rhodium^{I}$/Achiral Diphosphine Catalysts Differentiates the Diastereotopic Prochiral Faces of Olefins *101*
7.3 Homogeneous Hydrogenation by $Rhodium^{I}$/(Chiral Diphosphine) Catalysts Differentiates the Enantiotopic Prochiral Faces of Olefins: The Curtin–Hammett Principle *104*

8 Stereogenic Elements, Chirotopicity, Permutational Isomers, and Gear-Like Correlated Motion of Molecular Subunits *113*
8.1 Stereogenicity, Stereogenic Elements, Chirotopicity, and the Ambiguity of Some Stereochemical Terms *113*
8.2 Triarylamine Propellers *115*
8.3 Dynamic Stereochemistry of Permutational Isomers: Correlated Motion in Triarylamines *116*
8.4 Relative Stereochemical Descriptors: *Retro-Inverso* Isomers *122*

9 Symmetry in Extended Periodic Arrays of Molecular Crystals and the Relevance of Penrose Tiling Rules for Nonperiodic Quasicrystal Packing *127*
9.1 Symmetry in Extended Arrays/Molecular Crystals *127*
9.2 Achiral Periodic Arrays of Chiral Objects and Racemic Compound Crystal Lattices *132*
9.3 Chiral Periodic Arrays *132*
9.4 Occupancy of Special Positions in Periodic Arrays *136*
9.5 The Bragg Law and X-Ray Diffraction *139*
9.6 The Interferogram Phenomenon in Single-Crystal X-Ray Crystallography *140*
9.7 X-Ray Fiber Diffraction *143*
9.8 Penrose Tiling Matching Rules, Quasicrystal Packing, and Dodecahedrane *145*

10 Multiple Molecules in the Asymmetric Unit, "Faking It"; Pseudosymmetry Emulation of Achiral Higher Order Space Filling in Kryptoracemate Chiral Crystals *149*
10.1 Multiple Molecules within an Asymmetric Unit *149*
10.2 "Faking It": *Pseudo*symmetry Emulation of Achiral Higher-Order Space Filling in Kryptoracemate Chiral Crystals *151*
10.3 Desymmetrization of Platonic-Solid Geometries Resulting from Crystallographic Symmetry Constraints *161*

10.4 Mobility of Cubane and Dodecahedrane $(CH)_n$ Spherical Molecules within a Crystal Lattice *164*

11 Platonic-Solid Geometry Molecules and Crystallographic Constraints upon Molecular Geometry, Symmetry Distortions from Ideality *169*
11.1 Geometrical Considerations in High-Symmetry Molecules *169*
11.2 Syntheses Strategies of High-Symmetry Chiral Molecules *171*
11.3 Ethano-Bridge Enantiomerization of *T*-Symmetry Molecules *173*
11.4 Self-Assembly of *T*-Symmetry Chiral Molecules *176*
11.5 Enantiomerization of T-Symmetry Clusters *180*
11.6 Tetradentate Edge-Linker Units Separated by a Spacer *183*
11.7 Self-Assembly of *O*-Symmetry Chiral Molecules *184*
11.8 *O*-Symmetry Ferritin Protein Octahedral Shell *185*
11.9 Desymmetrization Resulting from Symmetry and Chemical Constraints *186*

12 Solid-State NMR Spectroscopic/X-Ray Crystallographic Investigation of Conformational Polymorphism/Pseudopolymorphism in Crystalline Stable and Labile Hydrated Drugs *189*
12.1 Divalent Anions Linking Conformationally Different Ammonium Cations *189*
12.2 Cross Polarization/Magic Angle Spinning Solid-State NMR and X-Ray Crystallographic Studies on the Elusive "Trihydrate" Form of Scopolamine·Hydrobromide, an Anticholinergic Drug *191*

13 NMR Spectroscopic Differentiation of Diastereomeric Isomers Having Special Positions of Molecular Symmetry *205*
13.1 NMR Anisochronism of Nuclei at Special Positions of Molecular Symmetry *205*
13.2 Pattern Recognition: A Graphical Approach to Deciphering Multiplet Patterns *207*

14 Stereochemistry of Medium Ring Conformations *213*
14.1 A Short Primer on Medium Ring Stereochemistry *213*
14.2 Assignment of *Equatorial-/Axial*-Substituent Descriptors to Rings of Any Size *214*
14.3 NMR Structure Determination of Medium-Ring Solution-State Conformations *216*
14.4 Dynamic Disorder in Crystals *221*

15 The Pharmacophore Method for Computer Assisted Drug Design *229*
15.1 The Pharmacophore, Neurotransmitters and Synapse *229*
15.2 The Pharmacophore Method for Computer Assisted Drug Design *231*
15.3 Determination of the Dopamine Reuptake Site Pharmacophore *233*
15.4 Methylphenidate (Ritalin·HCl) and (−)-Cocaine·HCl *235*
15.5 Ritalin Versus Cocaine: Binding Affinity and Inhibitory Concentration *238*
15.6 Second Generation Pharmacophore: The Orientation of the NH Proton *242*
15.7 Avoidance of Adjacent Gauche^{+}Gauche^{-} Interactions *244*
15.8 Static Disorder in *N*-Methyl Ritalin Crystals *246*
15.9 Development of Specific Dopamine Reuptake Inhibitors (SDRI) *250*

16 The X-Ray Structure–Based Method of Rational Design *255*
16.1 X-Ray Crystallographic Structure–Based Molecular Design *255*
16.2 The Different Primary Ammonium and Quaternary Aminium Binding Modes *258*
16.3 Search for Unused Binding Sites *263*
16.4 Primary Ammonium and Quaternary Aminium Binding Modes in CB[7 and 8] Complexes of Diamantane-4,9-Substituted Guests *265*

17 Helical Stereochemistry *269*
17.1 Helical Stereochemistry *269*
17.2 $2n_n$-Symmetry Achiral Helical Pathways *273*
17.3 "*La Coupe du Roi*": Chiral Apple Halves Produced by a 4_2-Bisection *278*
17.4 Intermeshing Molecular Threefold Helices: Symmetry, Chemical, and Phase Considerations *281*
17.5 *X*-Ray Fiber versus Single-Crystal Diffraction Models *289*

References *293*

Index ***301***

From the Author's Desk

This book is the outgrowth of a graduate-level "Special Topics in Structural chemistry and Symmetry Course" taught concurrently in Hebrew at Ben-Gurion University of the Negev, Beer-Sheva, and in English at the Feinberg Graduate School, Weizmann Institute of Science, Rehovot, Israel. One educational goal of the course was to expose the participants to a path toward stereochemical knowledge different than the one ordinarily presented in standard organic stereochemistry lectures. In recent years, this course has become part of the advanced undergraduate curriculum of the Cross-Border Program in Biological Chemistry administered by the Johannes Kepler Universität Linz and the Jihočeská Univerzita v Českých Budějovicích, (University of South Bohemia, Budweis, Czech Republic) – two neighboring universities on either side of a common, and now peaceful, international frontier. It is hoped that similar binational programs integrating students in a common goal toward mutual cultural exchange and tolerance through advanced science education will one day be the norm between my own country and its Arab neighbors. Over the past three decades, this course has been given, in whole or in part, around the world (Australasia: Uni. Wollongong AU; Uni. Auckland NZ; Massey Uni., NZ; Uni. Kyoto JP; Uni. Mandalay, Myanmar MM; Europe: Uni. Twente NL; Uni. Zagreb HR; Serbian Acad. Sci., Belgrade RS; Boğaziçi Uni., Istanbul TR; and the Americas: UCLA; Uni. Syracuse; Nacional Autonom. Univ. Mexico MX; CINVESTAV – Nacional Polytech. Inst. Mexico MX; Uni. Nacional Costa Rica CR; Uni. Fed. Rio de Janeiro BR; Fluminense Fed. Uni. BR; Uni. National Córdoba AR; and Uni. Nacional Tucumán AR).

One important secondary goal of this book is to demonstrate a common interface between the aesthetic world of form and that of structural chemistry. Structural chemistry is unfortunately often not understood at the time of important career-making decisions in secondary school. Many labor under the misconception that chemistry is a daily regimen of titrations and/or balancing redox equations. Another objective was to stress the intimate impact of environment upon a molecule's conformation and structure: change the first and the other is not invariant. In a limited-size book, such as this, the various subjects

that can be discussed can obviously not be comprehensive. They were chosen to be a limited sampling of those that exhibited basic principles and provided vehicles for the exposition of stereochemistry.

Without the patience, encouragement, and understanding of Yael Burko-Glaser, my dear wife and life partner of 53 wonderful years, this dream of writing a book could not have come to pass. To my immediate family: daughter Yardenna, son Gil, daughter-in-law Adva Almog-Glaser, grandsons Ron Zeev, Tal David, and granddaughters Or and Hadar, now an IDF commander, it is my hope that intellectual and scientific endeavor will make their world a better and more peaceful place than it was at their birth. To them all, this book is dedicated.

Finally, it is both fit and proper to remember the teachers who shaped our minds and events that changed our lives. George Noyes was my inspiring 1958 11th grade chemistry teacher at Great Neck North Senior High School (Long Island, NY) who enthralled his class with the wonders of chemistry and also told us of the introduction of electric light in his boyhood home. Madeleine M. Joullié (University of Pennsylvania, Philadelphia), my undergraduate professor, showed us the world of functional group organic chemistry. Upon graduation in 1964, I was employed as a Development Chemist at PPG Industries, Structural Adhesives Division, Bloomfield, NJ. The PPG Employee Education Program rejected my enrollment in the New York University Graduate School of Business Administration, despite my already approved admission. Instead, they encouraged me to upgrade my Penn Chemistry B.A. into a full B.Sc. degree and then undertake part-time evening M.Sc. studies at the Polytechnic Institute of Brooklyn (a center of excellence in polymer chemistry). Dr Lincoln Hawkins next affected my life by informing me that acceptance of the Bell Laboratories (Murray Hill, NJ) job offer, having only the M.Sc. Chemistry degree, meant that I could not reach the highest echelons of their Scientific Staff. This provided the impetus to return to full-time studies. The Soviet Union Space Exploration program's Sputnik success prompted the United States Congress to pass the National Defense Education Act (NDEA). This provided me, and others, with predoctoral fellowships in the physical sciences. While at Rutgers University School of Graduate Studies, the scientific acumen of Donald J. Cram and George S. Hammond, in their revolutionary text "*Organic Chemistry*," Second Edition, McGraw-Hill: New York, 1959, did more than anything else to reveal that there was a wonderful logical chemical-intermediate-based foundation to organic chemistry rather than reliance on rote memory. The provisions of a 2-year US National Institutes of Health Postdoctoral Fellowship did not permit its use abroad, despite my prior arrangements with the Israeli biophysicist Ephraim Katchalski-Katzir to be a postdoctoral research associate at the Weizmann Institute of Science, Rehovot. In 1971, Prof. Katzir, who later became the fourth President of Israel, encouraged me not to take his job offer at WIS, but rather to start out at the new University of the Negev and to have the pleasure ("nachas" in Yiddish) of building, designing, and molding the nascent Beer-Sheva Department of Chemistry. This is not the time, nor the place, to go into the reasons

for immigration to the Jewish State in 1971. Suffice it to say, the feared destruction of the Jewish people in Israel prior to the Six Day War did not come to pass. However, those tension-filled prewar days brought about a radical change of mind and heart, and I then desired to do something for my people, and for myself, rather than continue a comfortable existence in the United States of America, the land of my birth.

Special mention must be given to my very talented and inspiring scientific mentors/advisors. First and foremost, the late Edmond J. Gabbay (Rutgers University, Chemistry Department), my PhD mentor and friend, who opened the door to the intriguing world of nucleic acid/diammonium ion interactions. I remember coming home after my first meeting with him, bubbling over with excitement about the "scientific" research project that was proposed to me (after having performed routine polymer chemistry development work at PPG Industries for 3 years). At Princeton, I owe my thanks to Paul von Rague Schleyer, who introduced me to the exciting and aesthetic world of adamantane chemistry. The second year of my NIH-funded postdoctoral studies was in X-ray crystallography with Robert Langridge at the Biochemical Sciences Department.

I have left the most significant for last: a 1978 sabbatical with Kurt Mislow back in Princeton probably had more impact upon my scientific development than any other single year in my career. I remember a conversation with K.M. in his office to this very day. He said "Robert, you are working in asymmetric hydrogenation where the rate determining transition-state is ephemeral. There is so much to be learned from ground-state stereochemistry, where at least you know what the structures are." It was sage advice from a learned scholar. It is thus both an honor and a pleasure to also dedicate this book to all my teachers. Finally, throughout the years, I have had the honor to tutor many research students. Without their sense of inquiry, determination, hard effort, and thirst for knowledge, this book could not have been written.

"הרבה למדתי מרבותי... ומתלמידי – יותר מכולם"

תלמוד בבלי, תענית ז', ע"א

Much have I learned from my teachers … but even more from my students
Talmud Bavli, Ta'anit 7a'

Robert Glaser
Omer (Negev), Israel, February 2015

1
Symmetry/Pseudosymmetry: Chirality in Molecules, in Nature, and in the Cosmos

1.1
Introduction

Symmetry and emulation of symmetry (*pseudo*symmetry) play a major role in the world of esthetics and science. In our macro-surroundings, symmetry and *pseudo*symmetry are an ever-present source of "visual pleasure" whose origins may arise from our genes. At times, prior to the achievements of modern medical science, symmetrical appearance of a prospective mate may have symbolized physical well-being (health) – an essential attribute for both the child bearer/parent and the successful hunter/defender. Often, our perception of beauty and form is related to the observation of physical proportions whose ratio approximates the "golden ratio" ϕ (an irrational number $(1 + \sqrt{5})/2$) where $\phi = 1.6180339887\ \ldots$ The golden ratio is derived from a Fibonacci sequence of numbers 0,1,1,2,3,5,8,13,21, … ,a,b whereby $\phi = b/a$.

Leonardo da Vinci's "Vitruvian Man" drawing (**1**) illustrates the beauty of *ideal human proportions* as described by Vitruvius, an architect in ancient Rome. The proportions of the circle's radius (centered at the navel) and the square's side (the human figure's height) are 1.659, which approximates the 1.618 value of the golden ratio. It is doubtful whether da Vinci and other great artists thought to themselves that they should paint figures and objects according to the dimensions specified by the golden ratio. Instead, they knew in their creative minds "what looks good" in their mind's eye in terms of proportions. They were probably gifted from birth (i.e., their genes) and did not have to learn about the importance of painting with the golden ratio as a novice students in art school.

Symmetry, Spectroscopy, and Crystallography: The Structural Nexus, First Edition. Robert Glaser.

Companion Website: www.wiley.com/go/Glaser/Symmetry

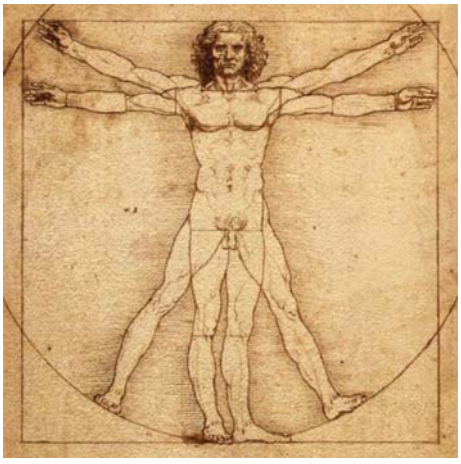

1

Prehistoric man's predilection to symmetry can be seen in anthropological findings of stone axe-heads. Increasingly symmetric stone axe-heads were unearthed at sites populated by progressively more developed societies. As the society of early prehistoric man matured, these finds seem to suggest that the hunter-gatherer crafted increasingly more functional hand tools that were also more visually pleasing [1]. David Avnir and coworkers have developed algorithms to measure distortion from an ideal symmetry and applied them to a morphological study of stone axe-heads unearthed at Pleistocene Age sites in the Jordan Valley. This enabled a quantitative correlation between increasing stone axe-head mirror *pseudo*symmetry and the decreasing age of the site. Illustrations **2**–**4** depict axe-heads dated 1.84 million years ago (the oldest site, (**2**)) 0.6(2)

2 **3** **4**

million years ago (intermediate aged site, (**3**)), and 0.3(2) million years ago (the youngest site, (**4**)) [1].

The visual pleasure we receive from the "classic proportions" of the Municipal Arch (**5**, photo: Yael Glaser) in the Roman ruins of Glanum (Provence) is undoubtedly related to the golden ratio of its dimensions (8.8 m width and 5.5 m height). It is clear that its intimately related symmetry and esthetics were concepts well understood by talented architects in ancient times.

5

Our ancestors seem to have been greatly fascinated by objects of "*high symmetry*" (i.e., objects with more than one C_n rotation axis of order $n \geq 3$, where n denotes the number of times the rotation is performed on a subunit in order to return it to its original orientation). Gray illustration **6** illustrates a late Neolithic/Bronze Age (about 4500 – 5200 years ago) elaborately carved *regular tetrahedron* stone specimen with three of its knobs decorated with spirals or dots and rings. It was unearthed at Towie in Aberdeenshire, North-East Scotland. Simple carved regular tetrahedron (**7**) and octahedron (**8**) geometry objects were also unearthed in Aberdeenshire (*hedron* means "face" in Greek). The esthetically pleasing five convex regular polyhedra (tetrahedron, hexahedron, octahedron, dodecahedron, and icosahedron) were a source of learning, contemplation, and discussion for Plato and his students. In modern times, these geometrical structures were the impetus for creative organic syntheses of high-symmetry hydrocarbon molecules [2, 3].

6

7

8

1.2 Rudimentary Group Theory, Isometry, and Symmetry

Symmetry is based upon *mathematical transforms,* and to understand it, a short introduction to simple *Group Theory* will be presented. The *elements* (members) of a mathematical *set* all share some common trait. For example, the elements of a *symmetry set* are all the *symmetry operations* that can be performed for a particular object. This set may be acted upon by a *mathematical operation* (*multiplication* or *successive application*, that is, performing one operation followed by another). The combination of a set and an operation defines a *mathematical group.* The identity (E) element must be present in the set of every group. Multiplication of two elements always affords a third element that must also be an element of the set. For example, in the symmetry group C_2, the elements E and C_2 ($360°/2 = 180°$ rotation about an axis) are the symmetry operations of the set, and $C_2 \times C_2 = C_2^2 = E$. Every element has its own *inverse element* whereby multiplication of the element by its inverse affords identity. The inverse element must also be an element of the set. In the case of C_2, it is its own inverse. Symmetry groups that result in at least one point within the object remaining spatially invariant are called *point groups*. Mathematical group elements should not be confused with *symmetry elements.* Symmetry elements in an object are those single points, linear arrays of points (*axes*), or flat surfaces composed of points (*planes*) that remain *spatially invariant* after a symmetry operation is performed. Symmetry elements in an object (or between objects) are generated by calculating the array of midpoints between all pairs of symmetry-equivalent points.

Symmetry is a subset of *isometry* (*isos* in Greek means "equal," *metron* in Greek means "measure"), where the *distance matrix* between a set of points in one object is preserved when the operation generates a second object. Two objects are said to be *isometric* when their distance matrices are identical. The spatial orientation of two isometric objects may differ relative to external axes of reference. *Symmetry* should have actually been written as *sy**n**metry* (*syn* in Greek means "together"),

but the letter "*n*" cannot precede the letter "*m*." Symmetry is an isometry in which full objects (or molecules), or subunits of an object, are exchanged while keeping their spatial orientations invariant. All symmetry operations are mathematical transforms performed using *symmetry operators*. These act upon a set of [*x*, *y*, *z*] coordinates of points defining an object to generate a new *exact copy* of the original object. One method (but not the only one) to make an exact copy is to generate the mirror image. When the mirror-image copied object or subunit is superimposable upon the original, then the object or subunit lacks the property called "*handedness.*" In other words, the object is *achiral*. When the mirror-image object is nonsuperimposable on the original, then it is *chiral* (from the Greek χειρ, pronounced "cheir", meaning "hand"). Objects that are chiral possess the property of (right- or left-) handedness or *chirality*.

Four of the eight known symmetry operations preserve an object's handedness. By this, we mean that after the operation is performed, a "right-handed" object/molecule remains "right," and a "left-handed" one remains "left," that is, they are *congruent*. These operations are denoted as being of the *First Kind*. Operations of the First Kind include *identity* (*E*), *rotation* around a "proper axis" (C_n, where "*C*" means *cyclic* and "*n*" is the *order* of the rotation operation, that is, the number of times the operation is performed on a subunit until it returns to its original orientation and position), *translation* (linear movement by a fixed distance), and n_m *screw-rotation* or *helical displacement* (combination of translation by *m/n*-th of the distance required for a full-turn of a helix plus rotation by 360/*n* degrees). Note: the *m/n* translation distance is the inverse of the descriptor's symbol n_m.

As noted earlier, when the mirror-image object or subunit is nonsuperimposable upon the original, then the object possesses the property of *chirality* or handedness. By this, we mean that the object's or subunit's "handedness" has been inverted by a symmetry operator, that is, a "right-handed" object/subunit becomes "left," and a "left-handed" one becomes "right."

The remaining four of the eight symmetry operations are those that invert the handedness of an object via symmetry transforms of the *Second Kind*. These are *reflection* (σ, where *sigma* comes from "Spiegel," which is German for "mirror"), *inversion* (*i*), *rotatory-reflection* (S_n, a combination of reflection and rotation by 360/*n* around an "improper axis"), and *glide-reflection* (*g*, a combination of reflection plus translation by one-half of the repeating distance in a linear periodic array of objects or molecules). Three of the eight known symmetry operations involve translation and, thus, can leave no point invariant in space. These are pure *translation, screw-rotation* (translation + rotation), and *glide-reflection* (translation + reflection). These three operations are found only in the 230 different *space groups* (groups of operations that describe the symmetry of a *periodic array* of objects or molecules). The remaining five (E, C_n, σ, i, and S_n) of the eight operations are found in both *point groups* and space groups.

There are 32 point groups and just five have sets containing only operations of the First Kind (those that preserve handedness). These five are known as *chiral point groups*: C_n (cyclic), D_n (dihedral), and the "high symmetry" T (tetrahedral, *tetra* in Greek means "four" and *hedron* in Greek means "face"), O (octahedral, *octa* in Greek means "eight"), and I (icosahedral, *icosa* in Greek means "twenty"). The other 27 point groups are *achiral* as their sets contain operations of both the First and Second Kinds.

In periodic ordered arrays of molecules (i.e., those within a crystal lattice), there is a sideways (or laterally or diagonally*) translational repeat unit* called a *unit cell* that builds the entire extended mosaic. Its volume is determined from the *cell parameters: a,b,c-axes lengths* (Å) and the *α,β,γ-angles* (°), where α is the angle between the *b,c*-axes, and so on. For ease of usage, crystallography uses *decimal fractions* of a unit cell axis length rather than Cartesian coordinates.

A *symmetry transform* is the mathematical basis for performing a symmetry operation. In this procedure, the set of $[x, y, z]$ coordinates defining all the atoms of a molecule or subunit is changed by a particular *symmetry operator* to generate the exact copy's new set of atoms. For example, the $[-y, x, z]$ symmetry operator engenders a C_4 rotational symmetry operation (C_n, where $n = 4$). When applied to the set of a molecule's *fractional* atomic coordinates, it produces a new same-handedness superimposable copy that has been rotated by $360°/n = 360°/4 = 90°$ about the Z-axis. The operator for a +180° (*clockwise*) symmetry-equivalent position is $[-y, -x, z]$, and for a +270° position, it is $[y, -x, z]$. What does this mean? It means that a +90° *clockwise rotation* about the $+Z$-axis of an atom with coordinates $[x, y, z]$ will reposition that atom to $x_{\text{new}} = -y$, $y_{\text{new}} = x$, and $z_{\text{new}} = z$. For example, if $[x, y, z] = [0.0047(1), 0.2321(1), 0.0479(5)]$ for an initial atomic position, then a +90° rotated atom will be at [−0.2321(1),0.0047(1),0.0479(5)] based upon the $[-y, x, z]$ *symmetry operator.* The number in parenthesis is the *estimated standard deviation* (esd) of the *experimentally measured* position, that is, its *precision.* Note: the rotational *tropicity* (*tropos* means "directionality" in Greek) of all symmetry operations is *arbitrarily but consistently* chosen to be *always clockwise.* Why? Answer: by historical convention.

The symmetry operation for a −90° rotation is C_4^3 (i.e., performing C_4 three times, i.e., $C_4 \times C_4 \times C_4 = C_4^3$). In a symmetry comparison, one compares only the *initial* and *final* objects. Thus, any intermediate steps leading up to C_4^3 (i.e., C_4 and $C_4 \times C_4 = C_4^2 = C_2$) are neglected. It is clear that the final position of the rotated atom is identical whether it was rotated either by −90° or by $3 \times 90° = 270°$. An $[x, y, -z]$ symmetry operator acting upon all the original atoms of a molecule would afford a new exact copy that has been reflected through the xy-plane. Similarly, a $[-x, -y, -z]$ operator would produce a new exact copy that was *inverted* through the unit cell origin, while a $[-x, 1/2 + y, -z]$ operator would generate a new copy that has been 2_1 screw-rotated about the b-axis (combination of 180° rotation about the *b*-axis plus translation of 1/2 the unit cell repeating distance on that

axis). The meaning of the 2_1 screw rotation operation will be explained later. The main purpose of this discourse is to emphasize that *genuine symmetry is a mathematical ideality.*

1.3 Asymmetric versus Chiral: The *I*-Symmetry of Viral Capsids

Asymmetry is a special case, since only objects exhibiting solely the *identity* operation are both *asymmetric* and *chiral*, that is, they have C_1 point group symmetry. Thus, while all asymmetric objects are chiral, certainly not all chiral objects are asymmetric. "Asymmetric" is definitely not a synonym for "chiral." The human adenovirus has an *I*-symmetry viral *capsid* (a protein shell without DNA or RNA; see **9** [4–6]. The cryo-electron microscopy and X-ray crystallography structure is presented in Protein Data Bank (PDB) entries 3IYN [7] and 1VSZ [8], respectively. *I*-symmetry is the highest chiral symmetry point group. The 120 I_h achiral group elements are: E, i, $6(C_5, C_5^2, C_5^3, C_5^4, S_{10}; S_{10}^3; S_{10}^7; S_{10}^9)$; $10(C_3, C_3^2, S_6; S_6^5)$ $15C_2$, and $15\sigma_h$, that is, $1 + 1 + (6 \times 8) + (10 \times 4) + 15 + 15 = 120$. The presence of only L-amino acids in the capsid removes the 60 group elements of the Second Kind, whereby the *I*-symmetry chiral group elements that remain are just E, $6(C_5, C_5^2, C_5^3, C_5^4)$; $10(C_3, C_3^2)$; $15C_2$, that is, $1 + (6 \times 4) + (10 \times 2) + 15 = 60$. The 60 C_n-rotation operations, where $n = 1, 2, 3,$ and 5, preserve the L-(*levo*)-handedness of all the capsid's amino acids.

The geometric considerations of the capsid's structure will be discussed next. The *asymmetric unit* of a unit cell is that minimal structural entity that will build the entire contents of the unit cell repeat unit using all of the symmetry operations of the point or space group (with the exception of translation for space groups). Molecules (or objects) that contain a symmetry element within themselves will have an asymmetric unit that is a fraction of the entity itself. The *Hexon* is the main structural protein of capsid **9**, and it is organized as a trimer. Four hexon trimer units reside within the capsid's *asymmetric unit* – a triangular shaped wedge extending from the interior center to the surface where it fills one-third of an equilateral triangular face (see dashed line triangular segment in **9**). Asymmetric units will be discussed in detail later on. Suffice it to say that the 12 hexons (3 hexons/*trimer* × 4 trimers/*asymmetric unit*) in this building-block unit will be duplicated by all the *I*-symmetry operations to generate the entire capsid. A threefold rotation axis through the face center copies the asymmetric unit's 12 hexon proteins 2 more times for a total of 36 hexon proteins/*face* (3 hexons/*trimer* × 4 trimers/*asymmetric unit* × 3 asymmetric units/*face*). Since there are 20 faces, this means a total of 720 hexon proteins reside within the capsid assembly. Obviously, this chiral supramolecular *I*-symmetry assembly, exhibiting 60 operations of the First Kind, can in no way be referred to as "asymmetric" [5].

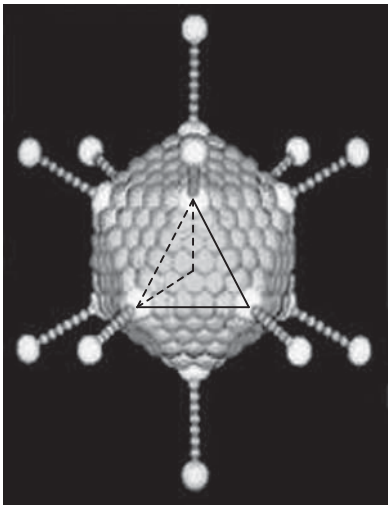

9

Rod units (protein helical fibers with *knobs* at the very end) are located at each of the 20 locations of fivefold symmetry. The human adenovirus structure provides a useful example of how Nature sometimes modifies a symmetry motif in order to attain a particular functional advantage. Why do this? Symmetry causes structural constraints that sometimes need to be partially removed to facilitate a particular functional effect (in this case, it is a biological effect). For this *particular virus*, there is a *symmetry mismatch* between the capsid's fivefold axes of symmetry and the threefold symmetry within the knob domain. The reasons for this are yet to be discovered. Usually, the rods show fivefold symmetry.

Due to the mismatch, the adenovirus only shows *I-pseudo*symmetry both in the solid and solution states. The Flock House virus is an RNA virus isolated from insects and exhibits near-perfect *I*-symmetry. One wonders why Nature has chosen such high symmetry for many viral particles? One obvious reason is that icosahedral symmetry enables efficient packing of the viral constituents within the capsid. The genetic material (DNA or RNA), packed within, often also has *I*-symmetry geometry. However, perhaps the high symmetry of the capsid also imparts a statistical advantage so that its knobs can attain auspicious orientations required for effective binding to the cell surface no matter how it lands upon it.

David Goodsell [6] has discussed the function of the *adenovirus* in his Protein Database "Structure of the Month" webpage. The viral capsid's function is to locate a cell and deliver the viral genome inside. Most of the action occurs at the knobs located at each vertex. The purpose of the long knobs is to selectively bind to transmembrane receptors called *integrins* located on the

cell's surface. Once the virus attacks this surface, it is drawn into *vesicles* (a small bubble within the cell's hydrophobic phospholipid bilayer membrane) by a process called *endocytosis*. Endocytosis is an energy-consuming process by which the cell *absorbs* molecules (i.e., large polar molecules) by engulfing them so that they can pass through the hydrophobic outer membrane. The next step involves breaking through the vesicle membrane and releasing the viral DNA into the cell. In the final stage, the *adenovirus* enters the cell's nucleus and builds thousands of replicas of new viruses. The ultimate result will cause the unfortunate recipient to suffer from respiratory illnesses, such as the common cold, conjunctivitis (eye infections), croup, bronchitis, and also pneumonia.

Note, for a lethal virus (e.g., ebola) to cause an epidemic, it has to kill the infected person slowly enough so that many people can come in contact with the dying victim (as with ebola). If the virus kills the sufferer too quickly, then a critical number of new victims will not arise to cause a chain reaction.

In the time of Louis Pasteur, rotationally symmetrical objects were called *dissymmetric*, while only achiral objects were referred to as symmetric. However, the prefix "*dis*" implies "a lack" of something, and thus, dissymmetric appears to be a synonym of asymmetric, which it is not. Since symmetry operations are both of the First and Second Kinds, there is no logical basis to restrict the general concept of "symmetry" to encompass only the second of the two types. On the other hand, the term chirality makes no distinction between asymmetric objects and those (like viral capsids) that exhibit high symmetry of the First Kind. Bottom line: all nonasymmetric objects are symmetrical by definition. Obviously, viral capsid **9** cannot be described as being *asymmetric*.

1.4
The Birth of Chirality as a Chemical Concept

The use of the term "chirality" in a scientific sense owes its conception to Lord Kelvin (Sir William Thomson), who stated, in his lecture to the Oxford University Junior Scientific Club (1893), "I call any geometrical figure, or group of points, chiral, and say that it has chirality if its image in a plane, ideally realized, cannot be brought to coincide with itself." Its present use in a chemical context to mean the structural property giving rise to two nonsuperimposable mirror-image molecular structures, or right- and left-handedness, can be traced to one of the eminent scholars of stereochemistry, Kurt Mislow. For nonphysicists, such as the author, Mislow says that the phrase "ideally realized" refers to "geometrical chirality" coming from a "mathematical idealization" which is common in physics and science in general (K. Mislow, personal communication, January 13, 2014).

Kurt Mislow was the first to use the terms *chiral* and *chirality* in chemistry. To see how this came about, we should first set the stage and discuss some important aspects of stereochemistry in the 1950s. Carl Djerassi, Luis Miramontes, and George Rosenkranz were at the Mexico City laboratories of the Syntex Corporation and were performing research in the developing field of steroid chemistry. In 1951, they invented the first oral contraceptive drug, progestin norethindrone, which, unlike progesterone, remained effective when taken orally. The drug triggers a hormonal response that stops further egg production in the female body during the period of pregnancy. This discovery radically changed the manner in which men and women interact as they heed the call of primordial hormonal urges originally designed to ensure the continuation of our species. In 1978, at the Knesset (Parliament) in Jerusalem, Carl Djerassi was awarded the first Wolf Prize in Chemistry for his work in bioorganic chemistry and for the invention of the first oral contraceptive drug.

At the time of his work, a very useful empirical link was discovered between steroidal absolute configuration and the (+ or −) sign of the "Cotton Effect" (a *chiroptical* property based on ***O***ptical ***R***otatory ***D***ispersion (ORD) of *plane polarized light* in the $n \rightarrow \pi$ transition of steroidal saturated ketones). This was the empirically based *Octant Rule*. While the "rule" seemed to work nicely for steroidal ketones (**10**), later on, it was found that different (+ or −) signs of the Cotton Effect, versus those predicted by the Octant Rule, were experimentally observed for optically active, known absolute configuration 8-alkyladamantan-2-ones (**11**). Since this phenomenon was then dubbed the *Anti-Octant Rule*, it is logically apparent that, alas, *there is no rule.* The ORD chirotopical technique and octant rule will be discussed later when details of its related subtopics *circular birefringence* and *circular dichroism* are presented as a separate section.

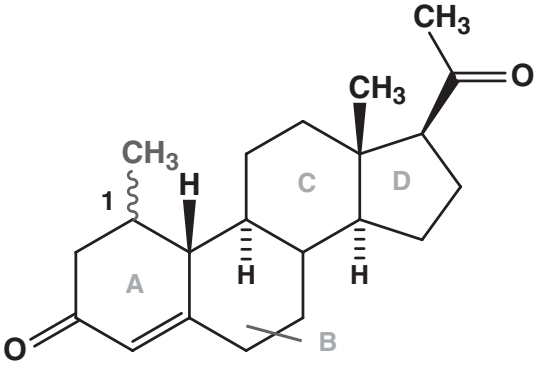

10

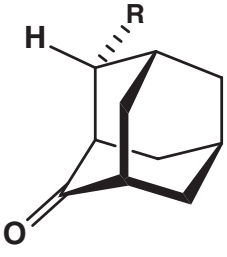

11

The principal investigators of a project involving steroidal α,β-unsaturated ketones (**10**) and the sign of their Cotton Effects were a group of distinguished chemists Carl Djerassi, Kurt Mislow (a stereochemist), and Albert Moscowitz (a chemical physicist). In a letter to Djerassi dated 7 October 1961, Mislow was discussing the Cotton Effect's sign for 1-methyl epimers of 1-methyl-19-norprogesterones (see wavy gray line in **10**). Mislow wrote "In the α-isomer the 1-methyl group is *equatorial,* but in the β-isomer the 1-methyl is *axial,* and interaction with C_{11}-methylene forces A (the 1-methylcyclohex-4-ene-3-one ring, A) into a boat and changes the sense of chirality." The ketones in the letter, and other steroids, were then discussed at length in their paper where the following is written: " … Dreiding models point definitely to a given chirality … " [9] A copy of the original letter was published in an article on language and molecular chirality written by chemical historian Joseph Gal [10].

1.5
Apparent Symmetry (High-Fidelity *Pseudo*symmetry) and the Quantification of Distortion from the Ideal

It is common to use "symmetry" in a logically "*fuzzy*" manner, that is, a concept whose borders or limitations are not absolutely well defined, such as the usual about 95% probability of finding electron densities in atomic orbitals. The pleasurable symmetry that one observes in our macro-world obviously does not exist via mathematical transforms, and yet viewers often perceive nonmathematically symmetrical objects as being "symmetrical." This is the realm of *pseudo*symmetry. High-fidelity *pseudo*symmetry (rather than genuine symmetry) is the norm in our macro-world. Genuine symmetry in our world manifests itself as reflections in a plane mirror of high quality or in a pristine lake's windless surface (see **12**, photo courtesy of Shaul Barkai, Switzerland).

Aside from the aforementioned special cases of reflection symmetry, our senses do not, or cannot, note the small deviations from an ideal geometry when confronted with "almost symmetrical/nonmathematically symmetrical" objects. A second look at da Vinci's "Vitruvian Man" (**1**) shows that it does not have true mirror reflection symmetry. Illustration **13** shows a pseudo left-half (inverted right-hand) drawing next to a genuine right-half drawing, while **14** depicts a real left-half next to a pseudo right-half (inverted left-half) drawing. Since these differences between the right and left halves are clearly noticeable, one wonders if they were intentionally made by the artist for esthetic purposes.

Many objects "look symmetrical" since their *pseudo*symmetry *fidelities* are very high. At first glance, starfish **15** appears to have multiple symmetry elements (five-fold rotational symmetry and five mirror planes, each one passed through a leg), that is, C_{5v} point group symmetry. But, careful inspection of **16** and **17** shows that the left leg of starfish **15** is very slightly higher than its right leg. Note the very

12

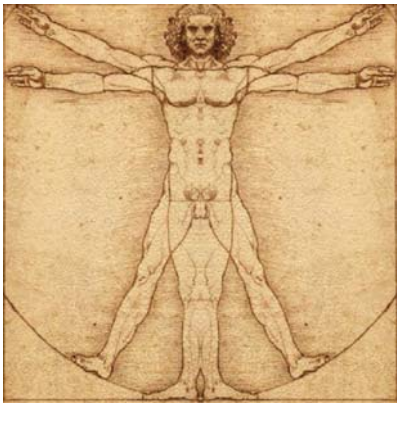

13

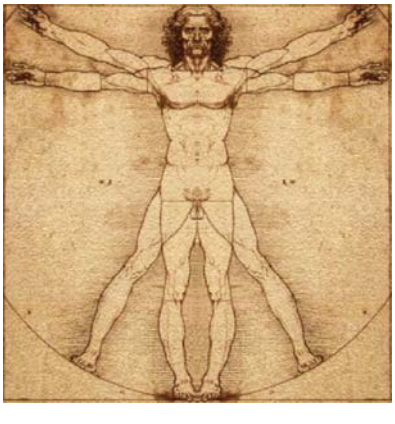

14

small differences between **16** (inverted right next to a real right starfish) and **17** (genuine left next to inverted left) make **15–17** all appear to be *almost* identical.

15 **16** **17**

Our genes have programmed us to overlook minor distortions from ideal symmetry. Avnir and his students have provided us with very useful mathematical algorithms to quantify the *continuum of distortion from a genuine symmetry* element within an object [11]. Genuine symmetrical geometry is only the origin-point terminus of an ever-decreasing sliding scale of *pseudo*symmetrical fidelity, that is, the *less* an object is distorted from the ideal symmetry, the more it shows a *higher-fidelity pseudo*symmetry. Therefore, *pseudo*symmetry is a sliding-scale variable, while true symmetry is an ideal state (a mathematical singleton, a set with only one element). Molecules either possess a particular symmetry, described by mathematical transforms, or do not. On the other hand, what is undisputable is that objects or molecules can readily exhibit a "continuum of distortion" from a particular ideal geometry. In other words, they can appear to exhibit various degrees of being "almost symmetrical."

Avnir and his coworkers at the Hebrew University of Jerusalem have shown that distortions from ideal point group symmetry or from an ideal shape should be considered to be continuous properties. The Avnir algorithms are commonly referred to as "*Continuous Symmetry Measures*" (CSMs) [11–17]. The broad utility of the CSM tools has been extensively demonstrated for quantification of symmetry distortion within objects or molecules and has led to correlations of these values with a wide range of physiochemical phenomena [18–23]. *Continuous Chirality* [24] and *Continuous Shape Measures* (CShMs) have also been reported [25, 26]. The application of Symmetry Operation Measures to inorganic chemistry [27] and the use of CShM [28–31] measurements for analysis of complex polyhedral structures have also been reported by Alvarez and coworkers.

It is useful to take the time to understand (in a very simplified and general manner) some of the methodology of the important Avnir [18–23] symmetry distortion algorithms. The "S(X)" CSM numerical index calculated for an object or a molecule distorted from any *generic* ideal X-symmetry (**18**, where X is any point group) is a *normalized root-mean-square distance function* from the closest theoretical geometry object (**19**) that exhibits the ideal X-symmetry [11, 12, 14,

16]. The theoretical object is simply the *closest geometrical construct* exhibiting ideal point group X-symmetry that is calculated from the distorted input structure. Despite the fact that the construct was derived from a molecule's structure, its geometry is not real in terms of its *bonding parameters* (i.e., bond lengths, bond angles, and torsion angles).

For simplicity, the distance geometry algorithm is based on Eq. (1.1), where P_k = Cartesian coordinates of the actual shape (e.g., distorted trigonal bipyramid colored black in **18**); N_k = coordinates of the nearest ideal C_3-symmetry "geometrical construct" (colored gray in **19**); n = number of points (1 to n); and D = a normalization factor so that two objects differing solely in size will afford the same $S(C_3)$ value [11, 16].

$$S(C_3) = \frac{1}{nD^2}\sum_{k=1}^{n}\left|P_k - N_k\right|^2 \times 100 \tag{1.1}$$

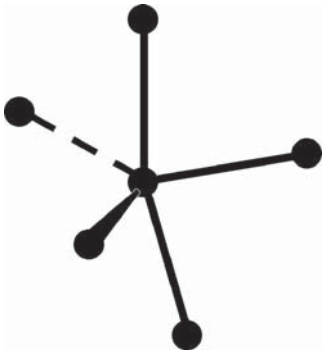

18

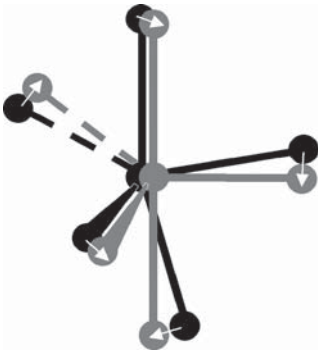

19

Any object with ideal generic X-symmetry will afford an S(X)-value equal to *integer number zero*, that is, it is a *special case* as it results from *symmetry constraints* upon the object's geometry. S(X)-values that are not integer zero are *general cases* (e.g., $S(X) = 0.0000001$ does NOT result from symmetry considerations). As the object is distorted more and more from $S(X) = 0$ *ideal* X-symmetry, the $S(X)$ value will increase. The $S(X)$ scale has been designed to range from 0 to 100, and users may refer to this scale as a continuous measure of the ability to perceive the existence of a particular generic *X-pseudo*symmetry element within an object. Ranges of $S(X)$-parameter numerical values have been interpreted in terms of either a *negligible loss, small loss, moderate loss,* or the *perceivable absence* of a generic symmetry element-X [11, 23]. Thus, one may paraphrase this interpretation by proposing a rule of thumb, which states that S-values of 0.01 or less indicate *negligible distortion* from an ideal symmetry

(i.e., *high-fidelity pseudo*symmetry that is not perceivable by the naked eye) [11], whereas values up to 0.1 correspond to *small deviations* from the ideal, which may or may not be visibly perceivable (i.e., moderate-fidelity *pseudo*symmetry). Larger S-values up to 1.0 signify *structurally significant divergences* from the ideal (i.e., low-fidelity *pseudo*symmetry) [11, 23]. Values larger than 1.0 testify to important distortions that are large enough so that the absence of a particular *pseudo*symmetry element within an object is visually recognized. For example, an Avnir CSM quantification of mirror-plane distortion in the stone axe-heads (**2**–**4**) as a function of the archeological site's age was reported to be 1.84 $S(\sigma)$ for the *oldest* specimen (**2**), 0.77 $S(\sigma)$ for the *intermediate*-aged one (**3**), and 0.29 $S(\sigma)$ for the *youngest* axe-head (**4**) [1]. Inspection of axe-heads shows **4** to exhibit the highest fidelity mirror *pseudo*symmetry and the lowest $S(\sigma)$ value.

The closer the Avnir $S(X)$-value approaches integer zero (the object's distortion from an ideal generic symmetry), the harder it is for our eyes to differentiate between high-quality *pseudo*symmetric objects and those exhibiting genuine symmetry. In the world around us, it is only our knowledge that *perceived symmetry* is almost always nonmathematical that enables us to be cognizant that an object's shape or form is actually only a *high-quality emulation of symmetry* rather than being the real thing. When does our perception of *pseudo*symmetry end and our realization of *gross distortion* or a complete loss of *pseudo*symmetry begin? It is not simple, since the *pseudo*symmetry continuum's frontier with perceivable asymmetry is mathematically *fuzzy,* rather than being an easily recognized step-function.

Should experts in symmetry proclaim, to one and all, that only *pseudo*symmetry (and not mathematical symmetry) primarily exists in our macro-world? Definitely not! There is nothing wrong with using fuzziness in communication unless the distinction between *pseudo*symmetry and genuine symmetry is absolutely required to explain a particular phenomenon. Communication and language should be free and not hampered by awkward phraseology and unnecessary accuracy. As a corollary, does this mean that one should use the adjective "*pseudo*symmetrical" to describe objects in our world? Probably not a good idea, since many will not understand the term. There is nothing wrong in using the concept of symmetry in its *fuzzy* sense. However, as scientists studying molecular structure, we should be aware of the conceptual differences between *pseudo*symmetry and genuine symmetry.

The concept of chirality seems to be a continuum without an end, since the generation of *achiral* geometries is a very special case due to specific *symmetry constraints.* Avnir has elegantly shown that when one of the two reflection symmetry-related vertices of the isosceles triangle **20** (*isos* and *skelos*, respectively, mean "equal" and "leg" in Greek) is ever so slightly depressed, then the formerly achiral figure is transformed into scalene triangle **21** (a two-dimensional chiral object). It exhibits a "*small amount of chirality*" as the ideal σ-plane has ceased to exist. The amount of this chirality can increase as the vertex is moved further

downward. It is thus clear that it is almost impossible to observe ideal achirality in our macro-world. The general case is that an object's geometry will have some finite degree of chirality. In other words, chirality is the "general rule" in our universe, while achirality is a "special case" since it requires structural and mathematical constraints.

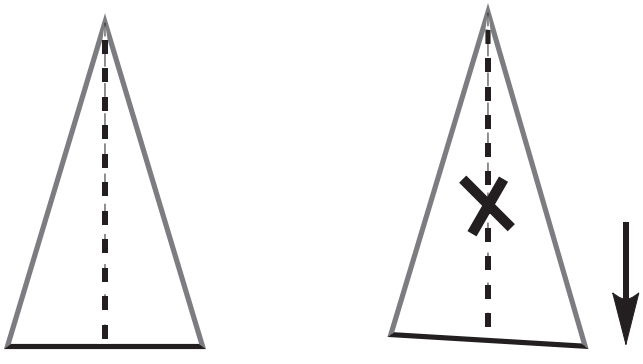

1.6
Chirality in Form and Architecture: Symmetry versus Broken Symmetry

Lest one thinks that esthetics in design, beauty of structure, and form are only expressed by dimensions of the golden ratio, Avnir and Huylebrouck have recently reported on the nexus between chirality and awe-inspiring cutting-edge architectural design [32]. To paraphrase the Nobel laureate Roald Hoffman (during a past visit to our university), he noted that breaking symmetry often imparts a warmer feeling of visual pleasure than that realized from "colder" symmetrical objects. While esthetic taste is certainly subjective, to the author (at least), broken symmetry can be as esthetically pleasing to the eye as genuine symmetry. The following two examples show different aspects of this subject. The first case deals with the graceful and prize-winning Mode Gakuen Spiral Towers building (**22**) in Nagoya, Japan (architects: Nikken Sekkei Ltd). Gakuen in Japanese means "academy." They were built to house three vocational schools: fashion, information technology, and medicine/welfare. The truncated gently spiraled edifice is composed of three unequal width, right-handed helical "tower" wings mutually connected to a common central core (i.e., similar to a spiraled triple helix). The tallest and widest wing gradually increases to a height of 36 stories, the "grooves" on either of its sides are equally larger than the third groove separating the two thinner wings. Photo **22** shows the widest helical tower facing the viewer and spiraling upward toward the

right (the wider grooves are clearly seen on either side). The second highest helical tower is partially seen on the left-hand side, while the third and lowest helical tower is hidden.

The second example is Mercedes House (**23**) at 555 West 53rd street, Manhattan, New York. It is an apartment building built in the shape of an inclined letter "Z" gradually zigzagging upward from the 6th to the 32nd floor. It was ingeniously designed by Mexican architect Enrique Norten to provide the maximum number (60) of Hudson River view roof-top luxury apartments resulting from the 30 indentations of its gradually slopping roof. The building sits atop a large Mercedes-Benz dealership (hence the name) and is one of the latest structures built as part of urban renewal of the "Hell's Kitchen" section of Manhattan.

22

23

1.7
Chirality in Nature: Tropical Storms, Gastropods (Shells), and Fish

One observes numerous examples of chirality in our macro-world around us: arms and legs, flowers, right- or left-flounder flatfish, wind patterns in low-pressure regions, tornados, whirlpools, spiral sea shells, galaxies, and so on. For example, stationary orbit weather satellites view Northern hemisphere hurricanes as *anticlockwise* vortexes of clouds (see **24**, a hurricane off the Mexican Pacific coast), while Southern hemisphere cyclones/typhoons (**25**, a typhoon off the Queensland coast of Australia) are seen from space as a *clockwise* vortex of clouds. It should be noted that the terms *clockwise/anticlockwise* are relative to

the orientation in which one views a *transparent* clock, that is, the tropical storms' *tropicity* (directionality) would be inverted when viewed from the ground to the sky.

24

25

The spiral sense of 90% of gastropods (shells, class: *Gastropoda*) show *dextral* (right-handed) coiling. It is very rare to walk along the seashore and find a left-handed specimen. However, there are large predatory sea snails called *Whelk*, which can be found not only in the common right-handed form, but also in the more unusual left-handed variety. The *Busycon carica* (**26**) species, representative of the overwhelming widespread *dextral* coiled sea shells, is found off North Atlantic coasts especially between New Jersey and Georgia. *Busycon contrarium* is a species found in the Gulf of Mexico with *sinistral* spirals (**27**: 20 cm length and 11 cm maximum width). It belongs to the *Busycon* genus within the *Buccinidae* family.

26

27

Amphidromus perversus butoti subspecies is an Indonesian air-breathing tree mollusk that exhibits either dextral or sinister coiling. These terrestrial gastropods (of 4–5 cm length and 2 cm maximum width) are *amphidromine* snails since both the dextral (**28**) and sinistral (**29**) forms can be found within the same population. This means that the *Amphidromus* genus is quite remarkable since a *single species* usually shows only one direction of coiling. For example, in the *Busycon* genus just discussed, the directionality of coiling is *species-specific.* Taking an overview of the situation, both the aforementioned examples of gastropods are quite remarkable since the vast majority of shells exhibit only dextral spiral sense.

28

29

Flatfish (e.g., flounder, skate) are another fascinating example of chirality in Nature. Flounder are *demersal* fish (bottom feeders) and are classified as *benthic* since they rest upon the sea floor. They belong to the *Pleuronectiformes* order in which one of the two eyes migrates to the other side of the fish so that it can then lie flat upon its side on the seabed. Right-eye flounders (**30**, e.g., the *Pleuronectidae* family) lie upon the sea floor on their *left sides.* Similarly, left-eye founders (**31**, e.g., the *Paralichthys lethostigma* species) rest upon the sea bottom on their *right sides.* Note: right- and left-eye descriptors are derived from the particular eye that has migrated to the other side (not the side of fish that faces upward). At birth, the tiny hatchlings appear achiral and swim upright like normal fish. But, after 6 months, one eye migrates to the other side of the fish (called *metamorphosis*), and the fish flips over on its side to lie in the sand of the seabed. A color change occurs as the stationary side darkens to blend in with the seafloor, while the other side remains white.

30

31

1.8
Extraterrestrial Macroscale Chirality: Spiral Galaxies, Martian Sand Devils, Jovian Great Red Spot, Neptune's Great Dark Spot, and Venusian South-Pole Cloud Vortex

In a similar manner to Terran (adjective of Latin name for "earth") tropical storms, the clockwise/anticlockwise tropicity of *spiral galaxies* is reversed when viewed from one side and then from the other. However, these spiral galaxies cannot be achiral, since the stars within do not symmetrically reside around the galactic mean plane. While not all galaxies are spiral, these galaxies are a common sight in the astronomer's telescope. Like the revolving cloud patterns of hurricanes and typhoons (photo **24**), the *tropicity* of a spiral galaxy will be reversed if viewers were able to observe it from the other side. NASA Photo **32** shows an edge-on view of galaxy NGC 5746 with a halo of hot blue gas around it. But can spiral galaxies, such as this, have a plane of reflection making them *achiral*? The answer is negative since the component stars are positioned about the equatorial belt according to gravitational forces and not by symmetry. Our telescopic images are simply not high enough in resolution to observe that the star distribution is actually asymmetric about the horizontal axis of rotation.

NASA photo **33** shows two colliding clockwise spiral galaxies NGC 5426 and NGC 5427 (collectively known as Arp 271). While they appear to be dangerously close to each other, the vastness of the galactic scale is such that researchers tell us that they will not collide. Instead, they will pass through each other, although it is expected that new stars will form out of the "bunching" of gas due to *gravitational tides.* Scientists predict that our own galaxy (the Milky Way – called the "Pharaoh's River" by the ancient Egyptians) will undergo a similar encounter with the neighboring Andromeda galaxy in a few billion years.

Counterclockwise columns of swirling Martian dust move across the surface in a similar manner as the same phenomenon on Earth and have been often photographed from rover exploration vehicles or by orbiting surveillance satellites. The Mars *Spirit Rover* photographed the anticlockwise dust devil in 2005

32

33

(**34**). On 14 March 2012, the NASA *Mars Reconnaissance Orbiter,* as part of a high-resolution imaging experiment, photographed an anticlockwise dust devil (**35**) as it flew over the Amazonis Planitia region of Northern Mars. This particular dust devil is quite large (30 m in diameter and 800 m in height).

34

35

Another extraterrestrial analogue of tropical storms is the Jovian (adjective of the gas giant planet Jupiter named after the Roman god) anticlockwise "***G***reat ***R***ed ***S***pot", GRS, (**36**, NASA). Jupiter's GRS is the vortex of an atmospheric storm raging in the Jovian atmosphere of the South Equatorial Belt for at least 400 years (when early telescopes first observed it). Three Earths can fit into its diameter.

As opposed to the extremely long-lived Jovian GRS, the anticlockwise ***G***reat ***D***ark ***S***pots (GDS-89) in the Southern Hemisphere of Neptune are storms that form and dissipate once every few years or so. About half the time, Neptune has one of these spots. They are smaller than the GRS, since their volume is only about the same size as Earth. Its winds have been measured at about 2400 km h^{-1}

36

37

and are the fastest in the solar system. These dark spots have different shapes and are thought to be vortices in the methane clouds of Neptune (similar to the hole in the ozone layer of Earth). The *Voyager 2* spacecraft photographed the Southern Hemisphere GDS (with white cirrus-like clouds that change over a small period of time) and below it a smaller spot called "Scooter" with a bright center; see **37,** Jet Propulsion Laboratory, California Institute of Technology. Both spots rotate at different speeds.

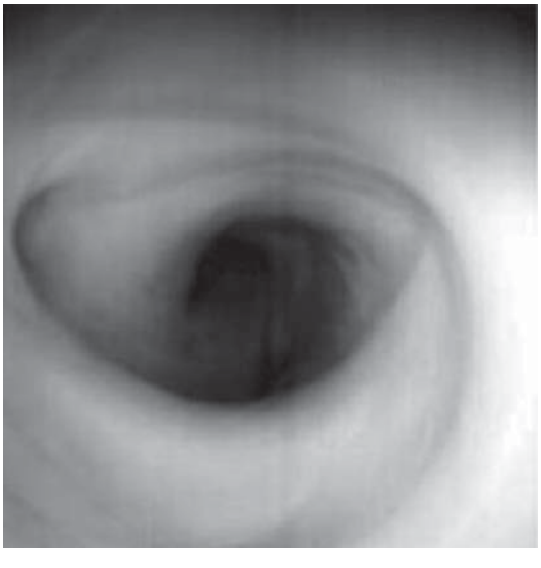

38

The Venusian South Polar Giant Vortex (**38**) is another example of an anticlockwise cloud pattern. It was thermally imaged with infrared light by the Infrared Thermal Imaging Spectrometer of the European Space Agency's *Venus Express* spacecraft. The vortex is 65 km in height. Finally, while there is a 30 September 2013 report of a giant planet (1.5 times larger than Jupiter) outside our solar system (an *exoplanet*) called Kepler-7b, the image of its high clouds to the West and clear skies in the East unfortunately does not show chiral cloud patterns.

1.9
Analyses of Amino Acid Chirality in Extraterrestrial Samples with Gas–Liquid Chromatography Chiral Columns

In 1966, Emanuel Gil-Av and coworkers at the Weizmann Institute of Science reported the first instance of a reproducible α-amino acid enantiomer separation using gas–liquid chromatography with an optically active stationary phase [33]. The column used a dipeptidic phase *N*-TFA-L-valyl-L-valine cyclohexyl ester, but required that samples be derivatized to their *N*-TFA(trifluoroacetamido)-*O*-*tert*.-butyl esters prior to analysis. The drawback was that such esters of amino acids are not readily prepared. The dipeptidic column was later used in 1970 to analyze for α-amino acids in moon samples retrieved from the surface of the Sea of Tranquility by the crew members of Apollo 11 [34]. However, no measurable amounts of amino acids were found under conditions that would have detected less than 0.1 ppm of any amino acid. In 1971, Benjamin Feibush [35] reported a very highly efficient diamide phase, *N*-lauroyl-L-valine *tert*-butylamide, which could be used with more readily prepared *N*-TFA-α-amino acid methyl esters. However, the column suffered from relatively high column bleeding, which limited its working temperature to 130–140 °C [35]. This disadvantage was later overcome by the preparation of higher homologue chiral phases: *N*-docosanoyl-L-valine *tert*-butylamide and *N*-lauroyl-L-valine 2-methyl-2-heptadecylamide, which showed no loss of weight by thermogravimetric analysis (TGA) until 190° and 180°, respectively [36]. As this chapter was being written, an enantioselective column by Volker Schurig (a former postdoctoral research associate of Gil-Av) was onboard the ESA Rosetta mission spacecraft. The orbiter successfully landed the Philae rover on 12 November 2014 after an incredible 10 year 317 million mile journey to the 2.5 mile wide comet 67P/Churyumov–Gerasimenko. His chiral column has been selected for future space missions to Mars: Mars Science Laboratory (MSL) and ExoMars 2016.

2
Enantiospecificity of Pheromones, Sweeteners, Fragrances, and Drugs

2.1
Enantiospecificity of Pheromones, Sweeteners, and Fragrances

Pheromones are chemicals released by animals and insects to elicit a behavioral response or activity in others of the same species. Gas chromatographs can be outfitted with an *electroantennographic detector* (EAD) [37] (i.e., an insect antenna), some of which can register the presence of pheromones at concentrations as low as two molecules per cubic meter. Many pheromones elicit increased activity by one enantiomer relative to the other. For example, the (*S*)-enantiomer of 4-methylhepta-3-one (**39**), the alarm pheromone of leaf-cutting ants, is 100 times more active than the (*R*)-enantiomer. Other pheromones produce different responses according to their chiral sense. The bis-cyclohexyl spiro compound known as "olean" (**40**), the sex pheromone produced by fruit flies, is excreted as a racemate. The (*R*)-enantiomer activates males, while the (*S*)-enantiomer attracts females. Other pheromones, for example, the aggregation pheromone of the ambrosia beetle (6-methylheptan-5-ene-2-ol, "sulcatol," **41**), require the presence of both enantiomers to be active.

It still has not been unequivocally proved that humans produce pheromones, although the primates, our biological ancestors, certainly do so, without a doubt. The validity of studies of menstrual synchrony in women living together is still under debate. Nature does everything for a purpose. We would like to think that Nature deems it important that species continue in their existence on our planet. When we consider human olfactory hormones, one wonders about the existence and function of pubic hair (may the author be forgiven for mentioning this very intimate part of our anatomy). We can ponder if the large surface area of hair provides the means for our perspiration to broadcast a physiological message to others?

A recent 2012 study by Noam Sobel of the Weizmann Institute of Science was conducted on a group of women who were shown a sad film that made them

Symmetry, Spectroscopy, and Crystallography: The Structural Nexus, First Edition. Robert Glaser.

Companion Website: www.wiley.com/go/Glaser/Symmetry

cry. Their tears were collected and the fluid was held under men's noses. Standard laboratory statistical tests showed reduced sexual arousal and testosterone levels in the men. Perhaps this signaled to them that "romance was now out of the question?"

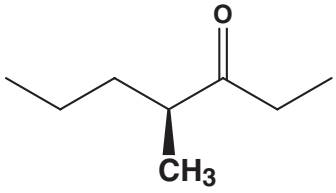

39

40

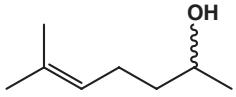

41

Our *gustatory* (taste buds) and *olfactory* receptors are also sensitive to molecular chirality. The L,L-dipeptide Aspartame® (Refcode FUPFAX [38] structure listed in the *Cambridge Structural Database* [39], CSD), the well-known artificial sweetener, is composed of phenylalanine and aspartic acid, while its enantiomer, prepared from the corresponding D-amino acids, is tasteless. When on sabbatical leave at UCSD La Jolla, the author was told by Murray Goodman, the laboratory director, that only he did the tasting of peptidomimetic sweeteners, since changes like chirality radically altered the sweet taste to such a degree of bitterness that he did not want to have his students suffer.

Not surprisingly, our *olfactory* receptors are also sensitive to the chirality of the molecules that stimulate them. A pleasant fresh citrus, orange-like aroma is perceived from (*R*)-limonene (**42**), which is a major component of the oil extracted from citrus rinds, while the (*S*)-enantiomer produces a turpentine-like odor. The carvone enantiomers, another group of cyclic diterpene natural products, are also used in many essential oils. The (*R*)-(−)-enantiomer has spearmint fragrance, while (*S*)-(+)-carvone (**43**) smells like caraway. The odors are indicative of the plant sources from which these fragrances are isolated and then purified.

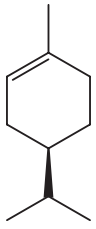

42

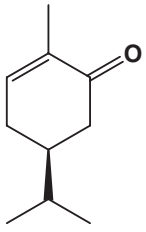

43

2.2
The Importance of Chirality in Drug Therapy

The last quarter of the twentieth century saw regulatory agencies require chiral drugs to be marketed as only one enantiomer (the bioactive enantiomer or *eutomer* – from the Greek *eutrophos* meaning "well-nourished," "healthy") unless they racemize within the body *and* both enantiomers are separately proven safe. The requirement of enantiomerically pure drugs only became possible when the manufacturing technology could produce only the eutomer, and analytical methods became sensitive enough to assay very small amounts of the unwanted enantiomer (the *distomer*) as a possible impurity in the enantiomerically pure drug. Chiral HPLC and chiral electrophoresis are the current sensitive methods of choice for the analysis of enantiomeric purity. While solid-state NMR spectroscopy can detect as little as 0.5% of a polymorphic impurity, it lacks the sensitivity of the two aforementioned techniques. It should be mentioned that the use of polarimetric *optical purity* as a measure of enantiomeric purity is definitely not a reliable analytical technique since chiral (*R*–*R*)/(*S*–*S*) and achiral (*R*–*S*) diastereomeric aggregates can form as a function of increasing analyte concentration. Therefore, the correct analytical procedure first separates and then quantifies the enantiomers.

Unfortunately, the distomer is not just inert, and economically wasteful "excess molecular baggage." Its presence may be responsible for severe deleterious side effects, which could be very different from those arising from the eutomer. A good example of different pharmacological activities of the enantiomers of chiral drugs is provided by penicillamine. The D-enantiomer of penicillamine (**44**, Refcode PENILA10) [40] is used for the treatment of rheumatoid arthritis and in chelation therapy, while the L-enantiomer is toxic since it inhibits the action of pyridoxine (vitamin B6) important for our health. Pyridoxine deficit may cause anemia, nerve damage, seizures, skin problems, and sores in the mouth.

The drug thalidomide is probably the most infamous drug in history. Its history will be explained in detail (even if it is a tad biological) since it dramatically demonstrates the important role of chirality in drug therapy. The (*R*)-(−)-eutomer of thalidomide (Refcode THALID11 [41], **45**) is an effective sedative/soporific (sleep inducer) and also an antiemetic (antivomiting drug) for morning sickness, while the (*S*)-(+)-distomer was unfortunately found to be *teratogenic* (*teratos* + *gen*, Greek for "monster producing") when the racemic drug was taken in the first trimester of pregnancy.

So, why not just prescribe enantiomerically pure (*R*)-(−)-thalidomide as a sedative? The problem is not so easily solved, since the drug undergoes racemization in the blood. The mechanism of *embryopathy* (diseases resulting from abnormal embryonic development) of thalidomide will be briefly explained.

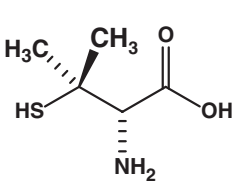

44

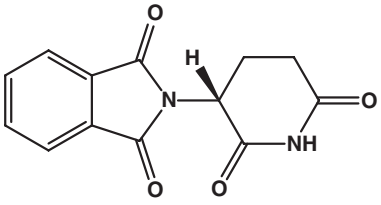

45

But, first, there is some terminology to be presented. The production of RNA from DNA is called *transcription* and is the first process in gene expression. A *promoter* is a region of DNA that initiates *transcription* of a particular gene (a DNA segment) and is located near that gene. Accessibility to the promoter region is controlled by a DNA sequence-specific DNA-binding factor protein known as a *transcription factor*. A gene cannot be expressed if the transcription factor control protein is bound to the DNA promoter region. The intimate geometrical matching of a control protein's structure with double-helical DNA is illustrated by the X-ray crystallographically determined structure of a complex between the Cro gene regulating protein and a 20 bp DNA fragment; see **46**. The DNA imprinted geometry of the protein has been bioengineered by Nature to accommodate the sequence-dependent right-handed helical geometry of the DNA duplex via intimate contacts between the two interacting surfaces. Polynucleotide helix-to-coil transitions are influenced by two helix stabilizing interactions (base-pairing and base-stacking) but are destabilized by *electrostatic interactions* between charged phosphate groups in the two polyanions that are separated by the 11 Å minor groove. Edmond Gabbay and Glaser [42] have demonstrated that small alkane-α,ω-diammonium cations bind to adjacent phosphate anions on the same strand and thereby stabilize the electrostatic interactions between the two close-spaced polyanionic DNA chains. Similar electrostatic interactions occur within the DNA-bound Cro dimer transcription factor complex **46** (see Protein Data Bank entry 3CRO [43]). The interactions arise from the protein's high content of basic amino-acid ammonium ions that intimately interact with phosphate anions on the polynucleotide duplex and thereby inhibit accessibility to the promoter region.

The promoter region also contains binding sites for RNA polymerase used during the initiation of transcription. During the first trimester of pregnancy, the (*S*)-(+)-thalidomide distomer was found to specifically bind to the GC-rich promoter region of the DNA responsible for the production of genes needed for normal *angiogenesis* in developing limb buds. Angiogenesis is the physiological process through which new blood vessels form from preexisting vessels. Unfortunately, the gene's decreased transcription efficiency resulted in truncation of the limb, thus causing the neonate to be born without limbs.

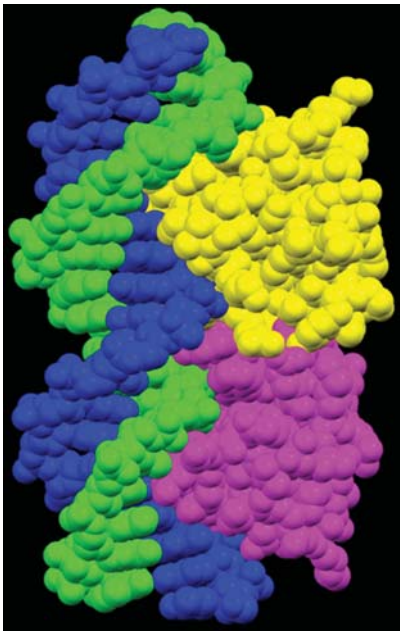

46

The historical aspects of the development of thalidomide will be presented next to show how this tragedy unfolded. In the Cold War era after World War II, sleeplessness was a common medical problem. At that time, there was an increasing use of tranquilizers and sleeping pills. There was a great demand for thalidomide in Europe since it was presumed to be safe, and the fact that it was a nonbarbiturate sedative gave the drug massive appeal. It entered the German market in 1957, and to make matters worse, it was sold as an *over-the-counter remedy* due to its maker's safety claims. After only 3 years (1960), it was already marketed in 46 countries, and its sales almost matched those of aspirin. Advertisements touted that thalidomide was "completely safe" even for mothers and children and "even during pregnancy." The pharmaceutical developers claimed that they " … could not find a dose high enough to kill a rat." However, its clinical trials never included pregnant test animals, and later human females, in all the important stages of pregnancy.

Even more unfortunate was the fact that physicians started to recommend it to patients for treatments unrelated to its original use as a sedative. Dr William McBride, an Australian obstetrician, found that the drug also alleviated morning sickness and recommended it to his patients. By then, the stage had been set for a

horrible human tragedy. In 1961, Dr McBride began to suspect that the drug was associated with severe birth effects in the babies that he delivered. These unfortunate babies suffered from a condition called *phocomelia* that results in shortened, absent, or flipper-like limbs. By March 1961, it was banned in most countries where it was previously sold. But, this was not before approximately 10 000 children in Europe, Australia, and Japan were born with birth defects.

By a quirk of fate, the United States Food and Drug Administration never approved the sale of thalidomide in America *for general use.* This stroke of serendipity resulted from insufficiencies in some of the results of the clinical trials' testing protocols. They obviously had no premonition of the impending disaster that was about to take place in Europe with thalidomide. FDA inspector Frances Kelsey felt that the drug application did not contain complete and sufficient data on its safety and *effectiveness*. Among her concerns was the dearth (insufficiency) of data relating to how the drug crosses the placenta into a developing fetus. As a result of the thalidomide disaster, FDA and other regulatory agencies have since markedly tightened up their regulatory powers and review procedures. They now demand that all new applications of chiral drugs include separation of the enantiomers, followed by statistically meaningful clinical trials of each one separately, and, finally, the marketing of only the eutomer.

Despite thalidomide's adverse effects, in 1962, it was found to be effective at the Hadassah Hospital in Jerusalem for the treatment of inflammation associated with Hansen's disease (leprosy). Today, it is also used as a chemotherapeutic agent for patients suffering from multiple myeloma. Thalidomide has now been approved to treat these conditions only.

A word about clinical trials. Clinical trials (I, II, and III) are performed under the supervision of qualified physicians upon an increasing number of patients. Try as they do, the number of patients in the study (even if it is in the thousands for a Phase III trial) is never truly is *statistically representative* of the total patient population (with all their varied other maladies and conditions) who will begin to take the drug during its first year of release on the market. Many approved drugs have to be recalled when very serious side effects are discovered during this critical first year of usage. While this text is not the venue to discuss the price of *ethical drugs* (drugs prescribed by physicians or veterinarians), a word should be said that pharmaceutical successes have to cover the investment of millions and millions of dollars (at least $500–600 million) already spent to bring a drug to market and then have it recalled.

Another point to be mentioned is that clinical trials are performed under *double-blind* conditions, that is, neither the dispensing physician nor the patient knows whether or not a placebo or the trial drug has been given to the patient. This is to prevent bias on the part of the physician in the evaluation and reporting of the testing results and also to prevent the nonunderstandable psychological therapeutic effect of patients "successfully willing themselves" to get better. The

final word has yet to be written on the fascinating power of the human psyche to overcome diseases based solely upon faith and hope (the so-called *placebo effect*). One last point to note is that if an experimental drug has been developed to fight a fatal disease and a terminally ill patient is used as a subject of a clinical trial, then placebos are certainly not used, and both physician and patient understand exactly what has been prescribed.

3
Bonding Parameters and the Effect of Local Environment on Molecular Structure

3.1
Symmetry Arguments and the Effect of the Environment on Molecular Structure

Symmetry arguments in chemistry are powerful tools of logic and exposition that are used to predict identities/differences in chemical and physical phenomena based solely upon the symmetry equivalence or nonequivalence of molecules within their environmental surroundings. An important attribute of a symmetry argument is that it is based only upon a symmetry comparison and never needs to be proven. It is even said that trying to disprove a symmetry argument is a fruitless task and is illogical to begin with. It is shown throughout this text that the surroundings of a molecule influence the molecular structure. For example, symmetry equivalence of two molecules also implies that their surroundings are invariant. But, when two assumedly "identical" molecules reside in different surroundings, then a symmetry comparison must show nonequivalence. Why? The surroundings will influence molecular geometry to one extent or the other. Therefore, different surroundings mean different molecular geometries and the molecules then cannot be considered to be "identical." However, one has to always remember that the symmetry argument never tells us just how different they will be (i.e., the *magnitude* of difference). If we know that there is structural nonequivalence, but it cannot be measured, does this mean that the symmetry argument is invalid? No, it just means that we must use a more sophisticated, or more precise, or more expensive instrument to observe the very small differences. One has to remember that all numerical measurements have an estimated standard deviation (esd) of error. One cannot discount the possibility that the real but very small differences between two measurements might fall within their error limits.

In addition, if we are measuring the (+ or −)-signed numbers of a *pseudoscalar* phenomenon (e.g., optical rotation), then one could accidentally choose the conditions where the measurement "just happens to be zero" (this is known as a *chiral zero*). The symmetry argument predicts nonequivalence of molecular structure whenever its immediate environment is varied. Therefore, by

Symmetry, Spectroscopy, and Crystallography: The Structural Nexus, First Edition. Robert Glaser.

Companion Website: www.wiley.com/go/Glaser/Symmetry

changing the measurement conditions either gently or drastically, an inherently zero-number will remain that way, but not for the case of a chiral zero.

3.2 The Effect of Local Environment on Molecular Models and Molecular Structure

It is time to consider molecular structure. One should always remember that molecular structure is based on an ensemble of atoms that continually vibrate around their well-defined *equilibrium* positions in space. When we consider molecular symmetry, we are always assuming a weighted time average of all the vibrational substructures. Moreover, the chemical and physical properties of real molecules are based on their *time-averaged structures*. To say it differently, at any particular instant, vibrations will cause even the highest symmetry molecule to appear to be momentarily asymmetric – but one usually ignores this. Molecular models (whether in our mind, or held in our hand, or drawn on a computer monitor as a result of a computational study, or arising from single-crystal X-ray diffraction) are just abstractions based on real assemblies of fuzzy spherical atoms in which carbon, oxygen, nitrogen, protons, and so on, are definitely not color-coded red, blue, or white. A molecule's structure (even that arising from single-crystal X-ray crystallography) is only a model based on an interpretation of experimental data. What makes X-ray crystallography typically produce high-quality models to explain the electron density within the unit cell is the fact that there usually are many data measurements (about 10×) than there are unknown positional parameters to be solved. However, it should be always remembered that not all X-ray crystallographically generated models have the same quality. This is particularly true of macromolecular X-ray crystallography where it is not uncommon that 15–25% of the electron density in the unit cell still remains to be explained by the particular model. However, it is reasonable to say that if about 10% of the electron density in the cell is still unaccounted for, then the basic experimentally determined molecular conformation will be known. This is true even if the precision of the three *bonding parameters* (bond lengths, bond angles, and torsion angles) is still far from optimum under these conditions.

As noted earlier, a molecule's structure depends on the local environment surrounding it, that is, the local environment in which it resides. One can readily understand that, when the environments surrounding two or more molecules are different, then a *symmetry argument* states that various structural determination techniques will afford nonidentical molecular geometries. The *dihedral angles* of molecular models interpreted from nuclear magnetic resonance (NMR) data are dependent on solution-state or solid-state data acquisition conditions and the type of solvent and temperature and may be conformationally time-averaged or not. The NMR and X-ray crystallography determined models can be slightly, or

completely, different since the latter are dependent on crystal growing conditions. Different crystals may sometimes (but rarely) be found even within the *same flask*, and their crystal structures can have similar or different conformations. Clearly, crystal structures represent weighted time-averaged thermal vibrations of the atoms. Computational models are dependent on the type of computational algorithm used, usually represent the structure at bottom of a potential energy well, and are also dependent upon the theoretical sophistication of the algorithms used.

The *bioactive conformation* in an enzyme's active site or in a receptor's binding site is not necessarily the same as the NMR-based solvated models or the crystallographically derived solid-state structures, but are usually within 1 – 3 kcal of the computed ground-state *global minimum energy structure.* Why? Nature makes use of low-energy structures since she is uninterested in being challenged to use high-energy structures. Since the molecular structures of granular active pharmaceutical ingredients (APIs) are also environmentally dependent, they may differ in solution state or as an amorphous solid or in their "*crystal form*" (packing arrangement) and the presence or absence of molecules of solvation. The crystal form can also change after the pressures of tabletation, or during storage conditions (humidity, temperature), or a manufacturing change of *excipients* (everything else in the tablet except the API).

3.3
Torsion Angles and Molecular Conformation

The *torsion angle* between four atoms A–B–C–D is a three-dimensional *bonding parameter.* It is the highest member of the set of three bonding parameters that includes one-dimensional A–B bond lengths and two dimensional *bond angles* (A–B–C). The atoms do not necessarily have to be ligated to each other when analyzing molecular structure. In this case, they are just *interatomic* distances, angles, or torsion angles between nonbonded atoms. Torsion angles are 3D *pseudoscalar* parameters since either a (+) or a (−) sign must be affixed to the magnitude of these angles. Scalar properties (such as *dihedral angles*) only have magnitude, while pseudoscalar properties are based upon vectors that change their sign under space inversion using the parity operator P $[-x, -y, -z]$, which inverts the coordinates of all the particles in a system through the coordinate origin. The only torsion angle descriptors that are unsigned are the special cases of *ideally synperiplanar* (integer-0°) and *ideally antiperiplanar* (integer-180°) achiral spatial arrangements. All other torsion angle descriptors represent chiral arrangements of the four atoms and hence must be signed. The sign of the torsion angle A–B–C–D (or nonbonded A· · ·B· · ·C· · ·D) is determined by orienting the central B–C bond to be perpendicular to the viewer and then looking down it away from the viewer to ascertain if the *tropicity* (directionality) of the front substituent to the

rear substituent is either *clockwise* (+)-sign or *anticlockwise* (−), as illustrated by Newman projections **47** and **48**, respectively. Like right- and left-handed screw-sense, the sign of torsion angle A–B–C–D is *invariant* irrespective of viewing the B–C bond from either bond terminus (either atoms B or C facing front), as demonstrated by **47** and **49**. In comparison, *dihedral angles* are *scalar* parameters since they have the same magnitudes as the corresponding torsion angles, but are unsigned. For example, the dihedral angles for projections **47 – 49** are the angles between two nonparallel planes A–B–C and B–C–D that intersect at line B–C.

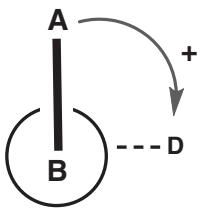

47

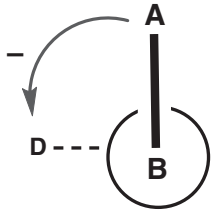

48

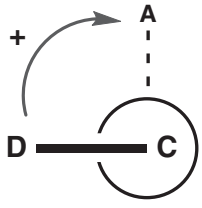

49

Conformational descriptors are often based upon the names or descriptors of torsion angles. They are often used in a *fuzzy* manner since they can also describe nonideal geometries. Saying that two or more molecules have the *same conformation* is simply a statement testifying to their *similar* spatial dispositions. It should be noted that "similar" is never a synonym for "identical." Identical spatial dispositions afford an ideal superimposition (congruency) of atoms where the root mean square (RMS) superimposition difference is *integer-zero.* Comparison of anhydrate and monohydrate crystal structures of the same molecule may show differences of as much as about 10° in some of the torsion angles, and yet their molecular conformations can still be called "*the same.*" For example, the O–C–C–N torsion angle in crystalline (±)-nefopam·HCl·anhydrate (Refcode entry DEHSEO11 [44], **50**, a nonnarcotic analgesic drug) is 57.7° and 48.8° in the (+)-nefopam·HCl·monohydrate chiral crystal (Refcode entries DUJVUZ, DUJVUZ10 [45]). Yet, the symmetry-nonequivalent eight-membered rings of the two crystal structures appear to visually exhibit the "*same*" eight-membered ring *boat–boat* conformation despite the 8.9° difference in solid-state torsion angles. The small differences in octagonal ring conformations are seen in the very low 0.081 Å RMS difference for the superimposition of corresponding atoms in the two crystal structures. Throughout this chapter, we discuss differences between two ideal structures versus those involving two similar nonsymmetry-equivalent surroundings (e.g., the aforementioned low 0.081 Å. RMS value). Furthermore, we will see that a molecule's environment also plays an important role on

its molecular geometry. For instance, dissolving either of the two different nefopam·HCl crystals in CD_2Cl_2 gives a solution-state ^1H NMR determined *boat–boat* O–C–C–N *dihedral* angle of 58.3(9)° that is statistically significantly different from the monohydrate's 48.8° value (but statistically the same as the anhydrate crystal's 57.7° value). Since solution-state NMR spectroscopy *cannot* differentiate between enantiomers, it is a dihedral angle (and not a torsion angle). However, solid-state CP/MAS (cross polarization/magic angle spinning) ^{13}C NMR spectra can differentiate between achiral and chiral crystals as well as anhydrates versus hydrates. Furthermore, the major species in a solution-state equilibrium need not necessarily be the solid-state structure. For example, *vicinal* $^3J_{HH}$ spin–spin coupling constants and ***N***uclear ***O***verhauser ***E***ffect (NOE) intensity enhancements were consistent with *slow exchange* kinetics for the interchange of *boat–boat* conformation *axial/equatorial N*-methyl-nefopam diastereomers (3 : 2 ratio at ambient temperature) [45]. The point to be stressed is that the solid-state X-ray crystal structure's *equatorial N*-methyl disposition and *boat–boat* conformation were consistent with the *minor* isomer's solution-state NMR spectral parameters but not with those of the *axial N*-methyl *major* solvated species [45]. More will be said later on about the phenomenon of slow exchange kinetics for conformational interchange.

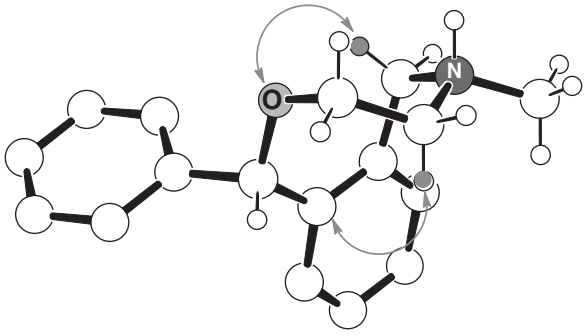

50

The concept of *same conformation* may be used in comparisons of nonsymmetry-equivalent molecules, since it may be applied to molecules of different atomic compositions. For example, since cyclohexane, cyclohexanol, and cyclohexylamine are clearly different molecules (*heteromers*, where *hetero* and *mer*, respectively, mean "different" and "unit" in Greek), their cyclohexane *chair* conformational geometries will never be observed to have exactly identical bonding parameters. Therefore, the term "*same conformation*" is a statement of *similar* but not necessarily *identical* spatial dispositions.

The semiquantitative descriptors of torsion angles for four atom segments exhibiting thermodynamically stable *staggered* conformations are (±)-*synclinal* (in Greek: *syn* means "together," and *clinare* means "to lean" in Latin, that is, a four-atom segment's termini both "lean" in the same direction) about (±)-60° and *antiperiplanar* (in Greek: *anti* means "opposite," *peri* means "periphery," and *planar* means "residing in the same plane," that is, the peripheral atoms of the segment are on opposite sides and are disposed in a planar arrangement) about 180°. The torsion angle descriptors of four atom segments having less thermodynamically stable *eclipsed* conformations are *synperiplanar* (*syn* "together," *peri* "periphery," and *planar,* that is, the peripheral atoms of the segment are on the same side and reside in a planar arrangement) about 0° and (±)-*anticlinal* (in Greek: *anti* means "opposed," and *clinare* means "to lean" in Latin, that is, the segment's termini lean in opposite directions) about (±)-120°. Torsion angle descriptors should be qualified so as to enable their use in a *fuzzy* or imprecise manner since they refer to a spatial disposition exhibiting a step-function range of angular values, for example, *synperiplanar* (0± ∼ 15°), (±)-*synclinal* (60± ∼ 15°), (±)-*orthogonal* (90± ∼ 10°), (±)-*anticlinal* (120± ∼ 15°), and *antiperiplanar* (180± ∼ 15°). For example, a *general* extended staggered spatial disposition of a molecular segment is really not perceivably different to our eyes if an *antiperiplanar-type* torsion angle is actually 179° or −176° or 169°. Further qualification can be used for angles whose magnitudes fall on either side of the ±∼15° ranges noted earlier. For instance, a 24° torsion angle may be described as "*synperiplanar-like.*" However, there are torsion angle values that are "*very close*" (another *fuzzy* term) to the borderline between two distinct angular regions. A case in point is an approximately 30° angle where the term "*midway between synperiplanar and synclinal*" can adequately describe the geometry of the segment. When molecular symmetry dictates *integer values* of 0°, 60°, 120°, 180°, these torsion angle descriptors are *special cases* and should be described as "*ideally antiperiplanar*," due to a segment's residence in a symmetry plane, and so on. The basic concept behind these angular descriptors is to convey a spatial disposition to the reader/listener without recourse to a graphical representation.

Torsion angles are also symmetry dependent. Since a threefold axis of rotational symmetry coincides with the C–C bond of ethane, there is no additional reason to explain why all the staggered H–C–C–H torsion angles are alternatively signed ±360°/*n*, where $n = 6$ (i.e., integer ±60°). However, once the C_3-axis is not present (e.g., as in *n*-butane), then one should expect that none of the *synclinal* torsion angles will show the ideal integer-60° value. For example, the solid-state cyclohexane solvate molecule within the Refcode entry FAYREE [46] crystal has alternating signed ±46(1)° C–C–C–C torsion angles. In summary, bond and torsion angles of 360°/*n* (where *n* = an integer) are special numerical cases whose existence depends upon a molecular symmetry. When symmetry does not permit these special values to exist, then "*general*" values either "closer to" or "farther from" the ideal will be found.

There are stereochemical terms such as *rectus, sinister, gauche,* and so on, which are commonly used today due to historical precedent, but have a second emotional often prejudicial social connotation often applied to trusted or feared acquaintances or revolutionaries versus the conservative political elite. Perhaps these terms refer to a time in our past history where "*simple*" common people could not understand why left-handed people were different from the majority. An intolerant simpleton might have thought that they were "possessed by spirits." The well-known term "*gauche*" when applied to a person's social behavior is not a compliment in France. Some of these terms such as "*rectus,*" and "*sinister*" can be readily changed to *dextro* (*dexter* in Latin means "right"), and *levo* (*laevus* in Latin means "left"), while *gauche* can be replaced by *synclinal.*

3.4 Symmetry Considerations of Atomic Orbital Hybridization and Bonding Parameters

Hybridization of atomic orbitals is also based on symmetry. It is common practice in introductory chemistry courses to affix sp^3, sp^2, and sp hybridization descriptors to all "tetrahedral," "trigonal," or "linear" bonding arrangements irrespective of their particular symmetry or lack thereof. The integer-3, 2, or 1 *hybridization indices* ("*x*") in "sp^x" are actually "special cases" due to molecular symmetry and are derived from the *Valence Shell Electron Pair Repulsion* (VSEPR) paradigm. These ideal superscript values are the result of special geometries exemplified by a T_d-symmetry regular tetrahedral carbon bound to four identical ligands (CL_4, e.g., CH_4), or a D_{3h}-symmetry trigonal flat carbon with three identical ligands (CL_3, e.g., $[CO_3]^{-2}$), or a $D_{\infty h}$-symmetry *palindromic* linear carbon with two identical ligands (CL_2, e.g., CO_2) [47]. Lowered symmetry in "tetrahedral-like," "trigonal-like," and "linear-like" bonding arrangements requires the use of non-integer *x*-values for the sp^x atomic orbitals (AOs) of a particular bond, and this is the general case. Similarly, *bond angles* of integer-360°/*n*, where $n = 2$ or 1, can only arise from the respective trigonal and linear *special geometries* noted earlier, while regular tetrahedral atoms (where $n = 3$) have six identical bond angles of $\arccos(-1/3)$ [47].

Mislow has discussed the use of $^1J_{CH}$ heteronuclear coupling constants measured in a nonproton decoupled ^{13}C NMR spectrum to calculate the percent of *s*- and *p*-character of the carbon atom's sp^x hybrid AO contribution to the C–H bond, where *x* is the *hybridization index* [47]. It is the noninteger *x*-values that give rise to nonideal bond angle values. A good example is the bond angles in the crystal structure of C_i-symmetry *antiperiplanar* conformer *n*-butane in Refcode entries DUCKOB04 [48] and ESILOI [49], measured, respectively, at 90 and 185 K. The crystal structures exhibit two different sets of *internally* inversion-symmetry-equivalent C(methyl)–C(methylene)–C(methylene) bond angles at each temperatures. An internal comparison is one between segments

within the same molecule, while an external comparison is one between segments residing in different molecules. The 113(1)° average value for the two structures is certainly not the ideal tetrahedral angle, nor should it be, since no butane carbon has ideal sp^3 hybridization. The corresponding symmetry-equivalent H–C(methylene)–H bond angles are 107.9(2)°. These C–C–C and H–C–η bond angles are typical for unstrained straight-chain alkanes and are readily explained by the symmetry argument that none of the carbons exhibits true T_d-symmetry. A chemical argument based upon the relative steric demands of the C and H atoms must then be promulgated to explain the opening of the C–C–C bond angle (vis-à-vis the ideal regular tetrahedral angle) and the subsequent closure of the H–C–H angle.

C–L bond lengths will obviously be symmetry equivalent only in an ideal tetrahedral, trigonal, or linear bonding arrangement. The difference between ideality and structural reality is seen in some molecular modeling programs. Ideal tetrahedral, trigonal, and linear geometry building blocks are often used to readily construct an initial (nongeometry optimized) model. To convince oneself that these idealized bonding geometry models are inappropriate for the molecule's actual symmetry, a so-called "*zero-point energy*" calculation is performed. This method simply calculates the input structure's energy while keeping the ideal-geometry building-block atoms invariant in space. Once this is performed, a full geometry optimization (energy minimization) calculation is then made. In the molecular graphics window, one observes the molecular structure change to a more realistic geometry as the energy decreases to its minimum value.

4
Historical Development of Structural Chemistry: From Alchemy to Modern Structural Theory

4.1
Hemihedralism in Quartz Crystals: Setting the Stage for the Birth of Stereochemistry

> Let us examine a crystal. We are at once interested by an equality between the sides and between the angles of one of its faces: the equality of the sides pleases us; that of the angles doubles the pleasure. On bringing to view a second face in all respects similar to the first, this pleasure seems to be squared; on bringing to view a third it appears to be cubed, and so on. I have no doubt indeed, that the delight experienced, if measurable, would be found to have exact mathematical relations such as I suggest; that is to say, as far as a certain point, beyond which there would be a decrease in similar relations.
>
> *Edgar Allen Poe (1809–1849), Rationale of Verse, 1843.*

The esthetic pleasures that most people experience upon beholding the beauty of crystalline minerals have undoubtedly played an important role in stimulating the development of stereochemistry as a scientific discipline. It is thus fitting to dwell upon some of the historical aspects of early structural chemistry in a chapter such as this. The tenets of stereochemistry, recognized today as part and parcel of our daily scientific endeavors, did not just drop out of the sky. Throughout the years of the nineteenth and twentieth centuries, discoveries of new concepts and explanations, followed by their public dissemination, stimulated additional discoveries. As a result of this, the foundation of knowledge and logical thought grew and broadened.

The sensation of awe and wonder derived from the symmetry of quartz crystals (the most common mineral on earth) prompted many early scientists to investigate their properties. Having said this, we will begin a discussion on the contribution of quartz crystals toward the inspiration of the scientific community at the turn of the eighteenth century. Astronomers in those times ground their own telescope lenses from quartz crystals (rock crystal or "bergkristall") due to the

Symmetry, Spectroscopy, and Crystallography: The Structural Nexus, First Edition. Robert Glaser.

Companion Website: www.wiley.com/go/Glaser/Symmetry

generally poor quality of factory-made glass at that time. The *crystal habit* (external form) of almost all of these crystals gave the mistaken appearance that they were *centrosymmetric,* that is, achiral by virtue of an "*apparent*" center of inversion. Most of these hexagonal shaped double-headed crystals *"seemed to have"* D_{3d} achiral symmetry (**51**), while a few "appeared to have" higher D_{6h} achiral symmetry (**52**). This impression arose from the *holohedral* faces of the crystal (from the Greek *holos,* whole or entire) bearing descriptors *m, r,* and *z.* Holohedral means that there are as many plane faces as required for complete symmetry described by one of the seven crystal *systems* (i.e., the triclinic, monoclinic, orthorhombic, tetragonal, trigonal, hexagonal, and cubic *lattice systems*). Finding a double-headed quartz crystal is quite unusual compared to the ordinary "garden-variety" single-headed crystals broken off from their nucleation site within a geode cavity's interior. The exception to this are the beautiful, but somewhat irregular, double-headed so-called "Herkimer diamonds" found in cavities within a gray porous fossilized sand matrix in the vicinity of Herkimer, in the Mohawk Valley of central New York State between Buffalo and Albany.

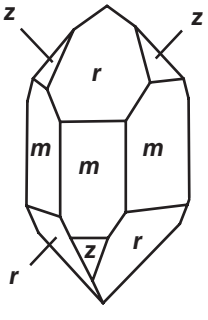

51

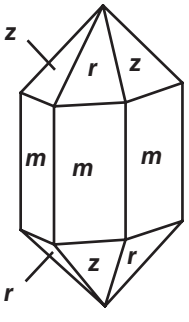

52

Before we continue, it is time to introduce some terminology that we will use in the following paragraphs. The adjective enantiomorphous (*enantio* and *morphous*, respectively, mean "opposite" and "form/shape" in Greek, where opposite is used in the sense of nonsuperimposable mirror image) was proposed by the German crystallographer Carl Friedrich Naumann in 1856 [50]. It should be noted that in those days a crystallographer was someone who studied crystals. Today, when we say "crystallographer," most of us mean a "single-crystal or powder X-ray diffraction crystallographer." In other words, nowadays, a crystallographer is usually someone who uses an X-ray beam to investigate their diffraction from single crystals or from ground powder. The term *enantiomorphs* is usually used to describe nonsuperimposable mirror image objects in our macro-world, while *enantiomers* are applied to the realm of molecules. The use of the adjective *enantiomeric* first appeared in 1915, while the noun *enantiomers* appeared in the literature only in 1926 [50].

In 1801, the French mineralogist René Just Haüy noted the presence of certain small facets (crystal faces) that reduced the symmetry of quartz crystals. Today, these are known as *hemihedral* faces since the crystal exhibits half the number of planes required for the symmetry of the holohedral form. Compare the more commonly observed D_{3d} *pseudo*symmetry achiral habit of hexagonal shaped double-headed quartz **51** with the much less frequently found D_3-symmetry chiral habit of left-(**53**) and right-handed quartz (**54**) idealized models. Haüy did not remark about the faces appearing to be related as nonsuperimposable mirror images (i.e., enantiomorphic). This might have been due to irregular crystal geometry arising from the presence of one of the three hemihedral face (facet) subtypes for quartz (*vide infra*) or from the different ordinary D_{3d} versus less common D_{6h} *pseudo*symmetric crystal habits for quartz crystals. The author can testify that after years of going through endless "rock shops," it is a very rare day when a hemihedral quartz head is found that enantiomorphically matches one of the examples in his own collection. Haüy did notice that in some of the quartz crystals, the hemihedral facets leaned to the right, and in others, to the left, when he viewed the crystals in a consistent manner. He used the adjective "*plagihedral*" (from *plagio,* meaning "oblique" in Latin, that is, neither perpendicular or parallel to a given line or surface) to describe these oblique facets but did not recognize the enantiomorphism produced by the facets in such crystals.

The fact is that the phenomenon of "enantiomorphism in quartz" was unknown when Haüy first noticed these hemihedral faces on some of the quartz crystals he was studying. As opposed to holohedral faces, hemihedral faces do not have a centrosymmetric partner on the other side of the crystal. There are three types of x'-, u'-, and s'-hemihedral faces. But, most quartz crystals do not express these faces at all. Those that do usually have only face per crystal rather than the multiple faces in the idealized models **53** and **54.** It is extremely doubtful if real specimens exist whose habits match those of the models.

In accord with the C_3-axis for D_3 chiral *pseudo*symmetry ($D_3 = C_3 + 3C_2$) of *ideal* double-headed single crystals, a C_2-axis on the crystal's equator should appear at each midpoint of the six vertical edges. A C_2-axis on one side of the

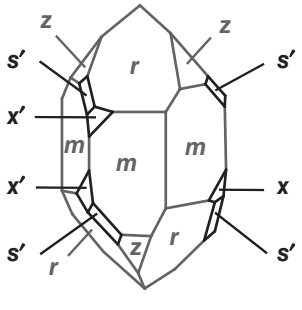

53

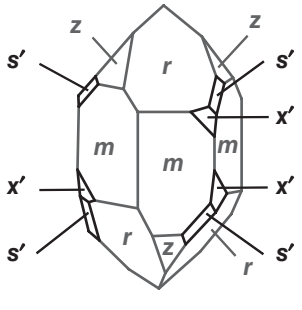

54

crystal goes through the midpoint of the common edge between two holohedral *m*-faces with *r*-face termini, see **53**, **54.** This axis exits the crystal at the midpoint of an edge linking two hemihedral *x′*-faces. This leaves the remaining three equally spaced vertical edges without contact with any of the hemihedral faces.

Haüy may be rightly referred to as the "Father of Crystallography." The noted crystallographer Howard D. Flack [51] published an excellent review of Pasteur's crystallographic and chemical work in 2009. It is apparent to many readers of this paper that Haüy developed many of the basic ideas of crystallography that have withstood the test of time. He explained crystal matter in terms of *atomism,* which was in vogue in France at that time, and is associated with such luminaries as Lavoisier and Laplace. His thoughts of repetitive subdivision of a crystal led to the idea of a geometrically well-defined basic structural unit for a crystal, which he referred to as "*molécules intégrantes*." This is what we now consider to be the *unit cell* translational repeat unit of a crystal. According to Haüy, units were to be put together into parallelepipedal building blocks to form layers producing a geometrically regular shape (now referred to as a *periodic lattice*). In 1809, he proposed that the external shape of a crystal was intimately connected to the internal shape of the repeating unit (Haüy's theorem).

The brilliant French astronomer, mathematician, physicist, and chemist Jean-Baptiste Biot was elected to the French Academy of Sciences at the tender age of 29. Using plane polarized light, recently discovered by Étienne Louis Malus in 1808, Biot developed the *polarimeter* instrument, which used the intense yellow doublet band emission of sodium light centered at $\lambda = 589$ nm (referred to as the sodium-D line, λ_D, "D" for doublet) as a monochromatic light source. In 1813, the already renowned Biot, working with the French astronomer François Arago, made a very significant discovery using his polarimeter to investigate specimens of quartz plates. He found that quartz plates cut at right angles to the crystal axis rotated the plane of polarized light through an angle proportional to the thickness of the plate. Unaware of Haüy's observations 2 years earlier, it was not understandable why quartz crystals could be divided into two subgroups: plates that rotated the plane of polarized light to the right (*dextrorotatory*) and those that rotated the light to the left (*levorotatory*).

In 1815, Biot reported his polarimetric measurements on what we now refer to as *natural product* organic molecules (e.g., ethanolic spirits of turpentine, laurel, camphor, and aqueous sugar solutions) and showed that such substances also rotated the plane of polarized light, crucially, *in the noncrystalline state,* that is, in solution or in the neat liquid or, in one instance, even in the gas phase. Among Biot's findings was that aqueous solutions of *Weinsaure* (German for "wine acid" – now known as D-(+)-tartaric acid) were dextrorotatory (+) when irradiated with plane polarized light at $\lambda = 589$ nm. He referred to these materials as being "*molecularly active.*" Much later on, he found that a mysterious substance, thought at that time to be an "*isomer*" of (+)-tartaric acid, was optically

inactive (*vide infra*). This material was called "*acide racémique*" (racemic acid) and was also referred to as "paratartaric acid," a name coined by Berzelius.

One of Biot's most important discoveries was the quantification of optical rotation measurements on the aforementioned solutions. He found that the degree of rotation of plane polarized light was directly proportional to the concentration and path length of the samples. Today, this is known as *Biot's law*, which is given as $\alpha = [\boldsymbol{\alpha}]_{\lambda}^{T} cl$, where "$\alpha$" is the degree of rotation of plane polarized light, $[\alpha]_{\lambda}^{T}$ is the measurement wavelength and temperature-T-dependent *specific rotation* constant, "c" is the concentration in g/100 ml, and "l" is the path length in *decimeters.* Note the close similarity to the *Beer–Lambert law* of energy absorbance: $A = [\boldsymbol{\varepsilon}]_{\lambda}^{T} cl$, where "$A$" is the optical density or absorption of light and $[\varepsilon]_{\lambda}^{T}$ is the measurement wavelength and temperature-T-dependent *absorption coefficient* constant. Rotation of plane polarized light, better known as *circular birefringence*, will be explained in detail later on.

In 1821, the English astronomer Sir John Herschel performed a careful morphological study of quartz crystals. He recognized a relationship that Biot had missed, namely, that there was a correlation between Haüy's right- or left-leaning plagihedral facets, on the one hand, and the direction of optical rotation by quartz plates observed by Biot. That is, Herschel found that slices from left plagihedral-face crystals rotated polarized light consistently in one direction, while plates cut from right plagihedral-face crystals consistently rotated the light in the opposite direction. For the first time, the direction of rotation could be linked with an observable property (the handedness of the *plagihedral* faces of the quartz crystals). Today, one uses the term *hemihedral* rather the more erudite *plagihedral* of that time.

However, even Herschel did not note that the plagihedral facets produced enantiomorphism in the crystals, perhaps because they were likely to have been of different dimensions and were probably far from being consistently the same in the shape and size of their expressed faces. In addition, it is highly likely that the quartz crystals also might have shown different *s*-, *u*-, or *x*-hemihedral subtype faces. Due to the foundation of knowledge provided by these pioneers of chemistry, and others, all of us are much more sophisticated today in defining and in recognizing spatial relationships. However, one has to remember that in those days, such basic concepts as "enantiomorphism" and "enantiomerism" and even "molecular structure" were yet to be discovered.

4.2
Tartaric Acid and Alchemy

(+)-Tartaric acid is isolated from a substance called *tartar*, which is crude potassium hydrogen (+)-tartrate that precipitates during the fermentation of grape juice. It was first reported in about 800 AD by the prominent Persian alchemist

Abu Musa Jabir Ibn Hayyan (from Arabic *ibn,* "son of" Hayyan and *abu,* "father of" Musa, from the Hebrew name "*Moshe*," later Anglicized to "Moses"). The Latin version of the Persian name *Jabir,* from the Arabic *jaaber* meaning "(the) conciliator, consoler, or comforter," was written as "Geber" in early European texts and most likely pronounced as "jeh-bear." Jabir also discovered antimony and bismuth, and among his many notable written works is his *Katab Al-Kimya* (literally "*Writings on Alchemy*"). He was a true *polymath* (a person whose expertise spans many fields) since he was a chemist and alchemist, astronomer and astrologer, engineer, philosopher, physicist, pharmacist, and a physician. He lived during the Golden Age of Arab culture, when Hebrew translators provided the human interface for transfer of knowledge written in Arabic into Latin for the scholars in medieval European monasteries. Many of them lived in Moorish *Al-Andalus,* later Christian Andalusia, until their expulsion from Spain by Ferdinand and Isabella in 1492. Many families to this day still bear the last name of *Turjeman,* now associated with a "translator" (but in Hebrew, this was also the name for a Talmudic spokesman who repeated a rabbi's lesson for all the students to hear).

4.3
Hemihedralism in Crystalline Tartaric Acid Salts: The Birth of Molecular Chirality

The first modern report on the isolation of crystalline tartaric acid was in 1769 by a Swedish pharmaceutical chemist named Carl Wilhelm Scheele. His raw material was also the thick crusty tartar fermentation residue from wine production. As an interesting anecdote, the writer Isaac Asimov had dubbed him "hard luck Scheele," since a number of his very important chemical discoveries were credited to others who had the good fortune to publish their results before he did. For example, in today's parlance, he was "scooped" by Joseph Priestley for one of his most notable discoveries, oxygen, before he could get his findings in print. There is a lesson here to learn from this for all of us, as often "time is of the essence."

(+)-Tartaric acid (Refcode TARTAL04) [52] was used in large quantities in the textile industry as a *mordant* (from *mordre*, which in French means "to bite"). Mordants form coordination complexes with dyes, which then bind to the fabric. Hence, it was produced industrially on a large scale in France, and elsewhere, to be sold as large milky crystals. In 1819, a strange incident occurred during the production of tartaric acid at a chemical factory (Fabrique de Produits Chimiques, SA) owned by Philippe-Charles Kestner in Thann, France. He did not own vineyards, but purchased the raw tartar that was deposited inside fermentation vats of European vineyards. Upon purification of one particular batch of raw material, several hundred kilograms of crystalline by-product was isolated. It was quickly noted that its solubility differed from that of the normal tartaric acid product, and it was originally thought that it might be oxalic acid. Much later, it was shown

that a reasonable explanation for the formation of the new acid by-product might have been that the temperature in one of the purification stages was too high. Indeed, it was later found that overheating (160–170°) engenders both *racemization* and *epimerization* under these conditions. The former process interconverts (+) and (−)-enantiomers, while the latter generates a diastereomer (an *epimer*) resulting from inversion of only one of tartaric acid's two *stereogenic* atoms. A common example of a "stereogenic" atom, but not the only one, is a maximally substituted tetrahedral atom (i.e., one with *four different substituents*) where a spatial exchange of any two substituents generates a new stereoisomer (see the following separate section on Stereogenicity and Local Site symmetry). Why *meso*-tartaric acid was not reported at that time remains a mystery to this day. Perhaps it was formed in very small quantities and was lost in the purification process due to solubility differences?

Seven years later, in 1826, the French chemist and physicist Joseph Louis Gay-Lussac (known for his two laws related to gases) visited Kestner's factory since he was intrigued upon hearing reports of the new acid and received a sample to study. The conventional wisdom at that time was that elemental composition uniquely characterized every chemical substance. However, the elemental composition (empirical formula, "the" analytical method available at that time) of the new acid was found to be exactly the same as that of (+)-tartaric acid. In 1828, in *Principes de Chimie*, he reported his findings that the elemental composition of the material was the same as that of (+)-tartaric acid and suggested that it be called acide racémique (Refcode ZZZDUI [53], *racemic acid*, from *racemus*, the Latin term for "a cluster of grapes"– -since its source was also from wine). Another analytical tool available at that time was the polarimeter, and Biot used it to observe that solutions of racemic acid did not rotate plane polarized light.

In 1830, the Swedish chemist Jöns Jacob Berzelius developed the important concept of *isomerism*. It was based upon finding identical empirical formulae for a number of pairs of molecules exhibiting different physical properties. For example, Justus von Liebig in 1822 determined the elemental composition of an explosive, silver fulminate [AgC≡NO], while Friedrich Wöhler found the same composition for a stable silver salt of cyanic acid (silver cyanate [AgOC≡N]). In 1828, Wöhler synthesized urea [$H_2NC(=O)NH_2$], which had the same empirical formula as ammonium cyanate [$NH_4OC{\equiv}N$] salt. The difference in optical rotation of tartaric and racemic acids was yet another known example. As an aside, Berzelius apparently was not very fond of using the term "acide racémique," and renamed it "paratartaric acid." It was Berzelius who found that there were solubility differences between the two acids. He noted that to dissolve paratartaric acid required a quantity of water equal to five times the weight of the crystals, while dissolution of (+)-tartaric acid occurred with a weight of water equal to only one-half of that of the crystals. These findings, and others, were the impetus for Berzelius to promulgate his concept of *isomerism.* In 1831, he asked Eilhardt Mitscherlich, a German chemist (later to be called the "Prince of Prussian

chemistry"), to prepare and investigate the salts of the two isomeric acids isolated from grape fermentation. Mitscherlich wrote to Biot in 1844 and informed him that not only were the empirical formulae of the sodium ammonium salts of the two diacids identical, but also a morphological study of their crystals showed *no discernable difference*, that is, the habits of sodium ammonium double salt crystals prepared from the two acids appeared to be *isomorphous* and differed only in their optical activity and solubility.

After Herschel's discovery, the conventional wisdom at the time was that optical rotation and crystal habit were somehow linked, although the optical rotation of liquid natural products, such as oil of lemon, still remained a mystery. Biot recognized that the rotation of plane polarized light was a function of the nature of dissolved molecules in liquids, while it was a function of the physical properties of the crystallized form of minerals. Furthermore, while the optical rotation of cooled molten quartz disappeared (it became *amorphous*), that from dissolved (+)-tartaric acid still remained.

Mitscherlich's report of isomorphic crystals for both the optically active sodium ammonium tartrate (tetrahydrate Refcode SATART03 [54], $P2_12_12$ chiral space group, D-(+)-**55**-symmetry-equivalent light gray oxygen added) and the inactive racemate was an enigma to Biot and to others steeped in the French scientific tradition of crystal-optical studies. Mitscherlich asked Biot to communicate his findings to the Académie des Sciences Française. Biot was intrigued by Mitscherlich's work and experimentally confirmed Mitscherlich's claim concerning the optical activity differences between the tartrate and paratartrate salts. However, Biot did not repeat Mitscherlich's crystallographic measurements, which showed the complete crystallographic identity of the two salts. Biot was also unable to explain Mitscherlich's findings. In retrospect, Biot (whose main interest was optics) was not a crystallographer with experience in observing and measuring the facets of crystals.

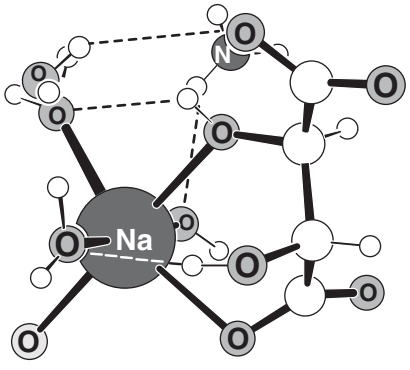

55

In 1848, a promising young French scientist named Louis Pasteur undertook detailed studies of the crystallography of (+)-tartaric acid, racemic acid, and a series of their salts. These studies of Pasteur were primarily prompted by Auguste Laurent (1807–1853), described by Mauskopf [55] as one of the greatest French chemists of the nineteenth century. Pasteur had already proved his scientific abilities with his work on *dimorphism* in crystals of saltpeter (potassium nitrate). He crystallized it in a round-bottom flask and obtained *rhomboid crystals* in the center and *hexagonal prisms* at the edges. This phenomenon in modern-day crystallography is known as *polymorphism* since different crystal forms can be found under diverse crystallization conditions and sometimes even in the same vessel. Polymorphism is the existence of more than one crystal packing arrangement. Since polymorphic crystals are different (i.e., diastereomorphous, nonsymmetry equivalent), it is no surprise that this gives rise to dissimilar solid-state properties (e.g., melting point, solubility, density, unit cell parameters, solid-state NMR, X-ray powder diffraction patterns). The well-known crystallographer Walter C. McCrone stated, "*every compound has different polymorphic forms, and that, in general, the number of forms known for a given compound is proportional to the time and money spent in research on that compound*" [56].

Biot managed to obtain a small quantity of the then 'world's supply' of racemic (paratartaric) acid for his young colleague Pasteur and let him use his polarimeter. Pasteur worked in the École Normale Supérieure de Paris laboratory of Prof. Antoine Jérôme Balard. As was common practice at that time, he also performed his own independent research as well as that for the senior professor.

Pasteur set out to undertake a systematic crystallographic and optical-rotational study of (+)-tartaric and paratartaric acids, as well as a series of their salts. His findings can be generalized as follows: crystals derived from (+)-tartaric acid and its salts were found to have hemihedral facets and their solutions were optically active and dextrorotatory, while those from paratartaric acid, with one exception, had holohedral morphology and their solutions were optically inactive. The important point is that the habit of the one exception (sodium ammonium paratartrate) differed from those of the other salts of paratartaric acid. That is, sodium ammonium paratartrate also had hemihedral facets. Now, Pasteur was aware of the findings of Mitscherlich, but, reports state that he was very disappointed in observing hemihedral facets in the paratartrate salt. Since solutions of this sodium ammonium salt were also optically inactive, he expected that these crystals would also be holohedral, as were all the other paratartrate salts that he had studied up to that point (and also the parent paratartaric acid itself). He decided to take a second look at the sodium ammonium paratartrate crystals. It is known that Pasteur's eyesight was poor, which necessitated him wearing thick-lens glasses. From this we can imagine that he probably held the crystals close to his glasses as he carefully examined them. As he was a crystallographer, he lined all the crystals up in a

particular systematic orientation according to crystallographic protocol. Pasteur found that he could organize the crystals into two groups. His crystallographic background enabled him to recognize nonsuperimposable mirror-image facets when he saw them. In other words, he realized that the two kinds of crystals of sodium ammonium paratartrate had nonsuperposable mirror-image morphology, that is, they were *enantiomorphous,* as we say today. It should be pointed out in this context that, in a broader sense, Pasteur's discovery of molecular chirality was clearly rooted in the French scientific traditions of the first half of the nineteenth century, specifically crystallography, optics, and chemical structuralism [50].

Why did crystallization of so many paratartrate salts and the parent acid yield achiral crystals? We now know that 90% of the crystallizations of racemic mixtures yield achiral crystals called *racemic compounds*. These crystals contain both enantiomers in equal quantities and in well-defined lattice locations. Only about 10% of the time does the crystallization produce a *spontaneous resolution* that yields a mechanical mixture (*conglomerate*) of (+)- and (−)-enantiomorphous chiral crystals. In most cases, there is only one molecule in the *asymmetric unit* (the smallest molecular entity that will generate the entire 3D packing within the *unit cell* translational repeat unit using *all the symmetry operations of the space group,* with the exception of *translation*). A detailed discussion of asymmetric units, unit cells, and crystallographic symmetry will be presented later on. Suffice it to say that since the crystals are chiral, then their space groups must also be chiral. As a result, all the symmetry operations of the chiral space group must also be chiral. Having said this, it stands to reason that the chiral single molecule within the asymmetric unit cannot coexist with its enantiomer in the unit cell's other asymmetric units as the space groups of these crystals lack symmetry operations of the Second Kind that invert the molecule's handedness. Therefore, only one handedness of a chiral molecule may reside within a chiral crystal. Where then is the enantiomer? The enantiomeric molecule must reside within the enantiomorphous crystals of the conglomerate mixture. The packing of (+)- and (−)-molecules together as a racemic compound can never ever be identical to the packing arrangement within chiral crystals containing only one enantiomer. This is the reason why all the physical properties that are 3D solid-state packing-dependent must be different for the racemic compound achiral crystal versus a chiral crystal of the conglomerate.

1848 was a year of political and social turmoil in France and in Europe in general. Nonetheless, Pasteur worked on in April 1848 and performed detailed morphological examinations of the sodium ammonium (+)-tartrate and paratartrate double salt crystals that were not only based upon subjective visual examination, but also included quantitative studies on the crystal's geometry. To do this, crystals were mounted on a *goniometer* (from the Greek *gonia,* angle; an optical instrument for measuring angles between crystal faces). Pasteur observed that

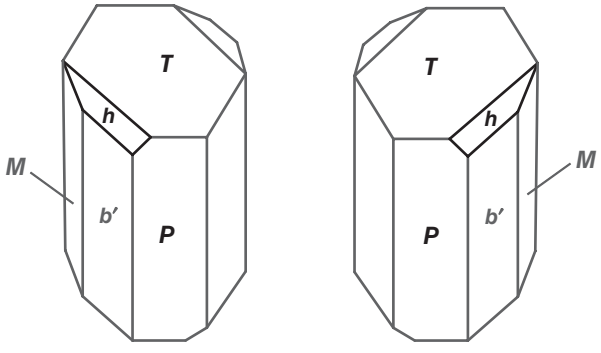

56 **57**

one of the crystal facets was longer (hemihedral face *h*) than the others. This gave the sodium ammonium (+)-tartrate and paratartrate crystals an asymmetric appearance (like those of quartz) since the *h*-hemihedral face was to either to the left or to the right of the adjacent *T*- and *P*-holohedral faces (see left-handed **56** and right-handed **57**). Moreover, he noted a correlation between the right-hand disposition of the elongated face and the maintenance of this asymmetry when the (+)-tartrate double salt crystals were dissolved to afford a dextrorotatory solution. This was the first time that anyone had observed that sodium ammonium tartrate double salt crystals were "*dissymétrique*," that is, the archaic and sometimes confusing term for "chiral" (introduced with that meaning by Pasteur himself).

Since the crystals were fairly large, with patience he was able to perform a manual separation. This was followed by measuring the optical rotation of solutions of equal concentration on the Biot polarimeter. To his delight, the left-handed crystals rotated plane polarized light to the left, while the others rotated the light to the same extent but in the opposite direction. To make it even better, when equal volumes of the two solutions were mixed, optical rotation was not observed. While this fantastic discovery is known as the birth of *molecular chirality*, the concept of a molecule's structure was still an enigma in 1848.

It should be noted that there was some degree of serendipity in Pasteur's landmark discovery, since sodium ammonium paratartrate double salt was later found to exist in a second crystalline form. The first discovered chiral crystals would today be called *Form 1*, as at a later date, crystallization at temperatures greater than 28° of the same racemic sample afforded an achiral crystal monohydrate containing both enantiomers (Refcode NAMTRB [57], $P2_1/a$ monoclinic achiral space group, D-(+)-dianion is depicted on the right side of (±)-**58**, *Form 2* in today's parlance). Nowadays, the mechanical mixture of enantiomorphic Form 1 (+)- and (−)-crystals is known as a *conglomerate of chiral crystals*, while the achiral Form 2 crystals are the more prevalent solid-state *racemic compounds.*

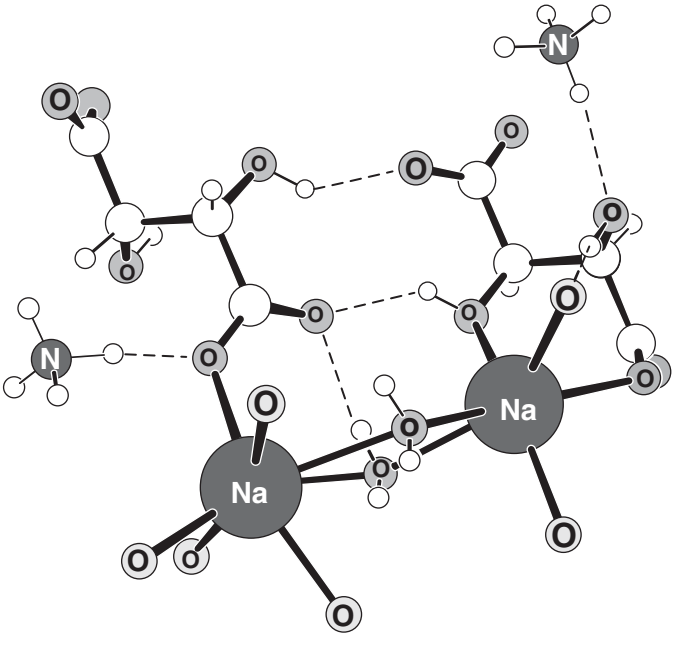

58

Real-estate agents are known to say that three things are important in buying or selling a home: "location, location, location." When one considers that diethyl ether boils in an Erlenmeyer flask placed on the bench top in a laboratory with a broken air conditioner here in the Negev Desert, then it is clear that Pasteur would not have made his discovery while working under these conditions.

Publishing scientific results in those days was not as it is today (there were no peer-reviewed journals). Instead, French scientific custom demanded that new important findings be announced by one of the members of the French Academy of Sciences. Pasteur contacted his friend, the now aged Biot, who then told him "I will be glad to verify your experiments with you when you have written them up, if you are willing to send them to me confidentially." Pasteur rationalized that if he could convince the illustrious Biot, then he could gain the support of a very important and influential patron who could help his scientific career progress.

Biot asked Pasteur to repeat the entire crystallization process from scratch (as well as the optical rotation measurements). Biot even prepared the sodium ammonium paratartrate double salt solution himself and verified that it was optically inactive. Biot witnessed each and every step. As luck would have it,

hemihedral-faced enantiomorphic chiral crystals were indeed obtained, and the wondrous polarimetric measurements were also duplicated. Legend has it that there were tears in Biot's eyes after witnessing the rotation experiments. He took Pasteur by the arm and said "My dear boy, I have loved science so much all my life that this stirs my heart." It was now very clear to both that Pasteur had made an extremely important discovery, despite the fact that knowledge in structural chemistry was quite primitive in those days. On 22 May 1848, Pasteur read his first memoir on his discovery to the Académie des Sciences [57a]. In October 1848, a commission appointed by the Académie (consisting of Biot and other distinguished scientists including the celebrated chemist Jean-Baptiste Dumas) presented a highly favorable report on Pasteur's chirality work affording Pasteur the recognition he so much deserved [57a].

In lectures made after his discoveries were announced, Pasteur compared his work with what was known about quartz crystals. He noted that the hemihedral right- and left-handed quartz crystals lost their optical activity upon melting and subsequent solidification into what we now know is an amorphous "*frozen-liquid*". This is exactly what happens to quartz sand crystals in the manufacture of glass. On the other hand, he added, while the chiral morphology of the hemihedral (+)-tartrate *crystals* was lost when they were dissolved, the resulting solution of the same substance retained its chirality. He reasoned that it was the *arrangement of the atoms* within the quartz crystals that was *dissymmetric* and that melting the crystals destroyed this arrangement. Moreover, he went on to state that it is the *molecules of tartaric acid* that are themselves dissymmetric, and hence they keep their chiral geometry when the crystals are dissolved. This was quite a quantum leap in molecular structure theory for that time, since in a later section we will see how primitive the molecular representations were when they first started to be proposed 20 years *after* Pasteur's discovery of *molecular chirality.* Once again, one must admire Pasteur because his 1848 findings were made at a time when molecular model sets were unknown, 3D molecular structure could not even be contemplated, and very basic concepts and nomenclature (that we take for granted today) were unheard of (such as the tetravalency of carbon, tetrahedral carbon atom geometry, nonsuperimposable mirror images, enantiomers and diastereomers). In closing this historical section dealing with the birth of molecular chirality and stereochemistry, one should note that in his lectures, Pasteur seems to have recognized a difference between asymmetry and chirality (or dissymmetry, as he called it). This conclusion is based on the fact that he did not use the terms *asymmetry* or *asymmetric* in his writings, and lectures, to refer to the phenomenon of dissymmetry. The author strongly recommends the writings of Joseph Gal, a renowned chemical historian, to all those readers interested in more details of the Pasteur story and of the times in which he performed his experiments [50, 58].

4.4
Gift for Prelog's Retirement: A Matched Pair of *u′*,*x′*-Hemihedral Faced Right- and Left-Handed Quartz Crystals

Photograph **59** shows a pair of left- and right-handed quartz crystals with hemihedral *x′* and *u′* faces. This photograph was a gift to the author from the Nobel laureate during a visit on 17 August 1982. The morphologically matched crystals had been presented to Prelog by his present and past students and colleagues upon his retirement from the Swiss Federal Institute of Technology (ETH) in 1976. Vladimir Prelog received the 1975 Nobel Prize in Chemistry for his research into the stereochemistry of organic molecules and reactions. Among his many achievements is his work with Cahn and Ingold on the use of *R*,*S*-descriptors for describing the *absolute configuration* of organic molecules. Prelog shared the Nobel Prize with John Cornforth, who was honored for his work on the stereochemistry of enzyme-catalyzed reactions.

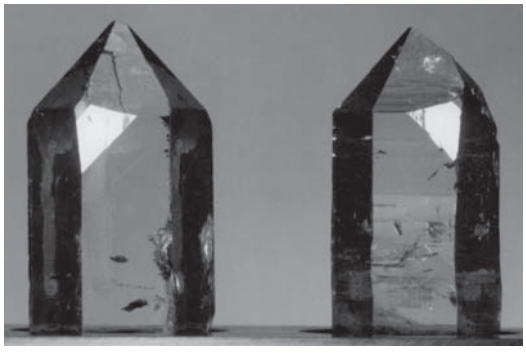

59

Photographs **60** and **61** (by Yael Glaser) show large elongated skewed diamond-shaped *s′*-hemihedral faces in an almost matched pair of left- and right-handed quartz crystals from the author's private collection. It obviously is much more of a challenge to observe the particular handedness of the *s′*-hemihedral-faced chiral crystal heads **60** and **61,** although it certainly is possible with prior knowledge. Look carefully at the diamond-shaped faces in the figure and you will find that the right-side vertex of *s′*-facet diamond in **60** is higher than the left side, while the higher and lower side vertices are reversed in **61.** This observation will usually not help our eyes *unequivocally* ascertain the handedness of these chiral habit quartz crystals. However, there is another trait of the *s′*-facet that is more definitive. It is very common to observe parallel *striation lines* in these faces by holding the crystal up to a light and slowly rotating it so that the *s′*-facet shines. The lines go

from (lower-*right*) → (upper-*left*) in *left-handed* **60**, while they are reversed in the enantiomorphous *right-handed* **61.**

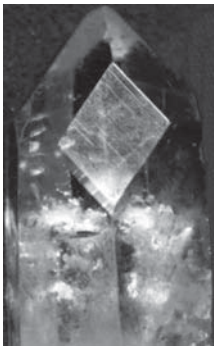

60

61

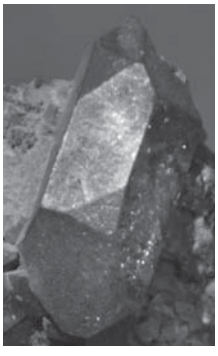

62

Finally, before leaving the subject of quartz morphology, the subject of *twinned* crystals should be mentioned. Carefully compare double-headed quartz crystal **62** (called a *Brazilian twin*) with the doubled-headed models **53** and **54**. There is a subtle difference between the real crystal and the models. Can you find it? Models **53** and **54** represent *single* crystals of the type required by X-ray crystallography, but **62** does not. Crystal **62** is twinned since every vertical edge contacts an x'-hemihedral face (rather than every other edge in **53** and **54**). In terms of morphological symmetry, note something else, the C_2-axes in models **53** and **54** transverse vertical edges having hemihedral faces *on both termini.* But, the C_2-axis in twinned **62** is located in the *middle* of the holohedral *m*-face. Twinned crystals were once the bane of crystallographers due to pairs of double reflections that are very close together as opposed to only one spot. Nowadays, with the advent of charge-coupled device (CCD) area detectors in modern X-ray diffractometers, the twinning mode can often be determined and the intensity of the appropriate partner in the each pair can be measured – thus enabling the molecular structure to be solved. The essentials of X-ray crystallography will be presented later on.

4.5 Early Structural Representations of Organic Substances and the Development of Modern Structural Concepts

Five years after his seminal work on sodium ammonium paratartrate, Pasteur prepared the *meso*-diastereomer of (+)-tartaric acid in 1853, and a year later, he

conducted what was then the first *asymmetric destruction* experiment (a kinetic method of partial resolution). A plant mold was used with racemic tartaric acid to exclusively metabolize (+)-tartaric acid while leaving the "unnatural" (−)-enantiomer untouched. As noted earlier, these findings were all done before chemical structural representations were promulgated. Pasteur did understand that helical staircases were *dissymmetric* (a now archaic term for *chiral* or handed), and thus he likened the arrangement of atoms in (±)-tartaric acids to be similar to right- or left-handed *helical staircases,* while those in the *meso*-diastereomer were thought of as being akin to an achiral *ladder.* He also clearly understood the conceptual difference between the terms "asymmetric" and "dissymmetric."

In 1858, Archibald Scott Couper presented a crude structural formula for ethanol (**63**) with the wrong valency for oxygen. August Kekulé, in a footnote within an article published in 1865 [59], discussed and illustrated his 1859 structural formulae for *n*-propanol (**64**) and benzene (**65**). The straight lines in **65** are intended to show that benzene's six carbon atoms are arranged in a cycle. These models are now referred to as *sausage formulae* that depicted " … the atomic composition of molecules." He further noted that "this form is nearly identical to those used by (Charles Adolphe) Wurtz in his beautiful lectures on chemical philosophy." In the same publication, he went on to present a newer and more familiar ball-and-stick representation of a "not-so-symmetrical" benzene, see **66.**

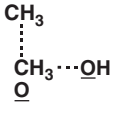

63

64

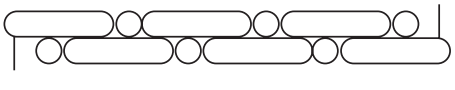

65

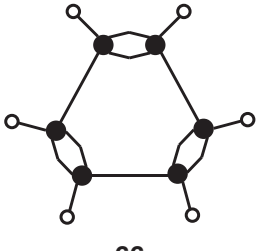

66

In 1861, the Russian chemist Alexander Butlerov used the concept of *chemical structure* for the first time in order to discuss atomic connectivity (a concept that we now refer to as the *constitution* of a molecule, see a detailed explanation later on). August Wilhelm Hofmann presented croquet-ball-and-stick planar models for water (**67**), "marsh gas" (methane, **68**), and 1,1-dichloroethane (**69**), which he called "Dutch liquid," in 1865. Dutch liquid got its name because it was discovered in 1795 by four Dutch chemists. In 1867, Alexander Crum Brown described a different kind of model for phenol (**70**).

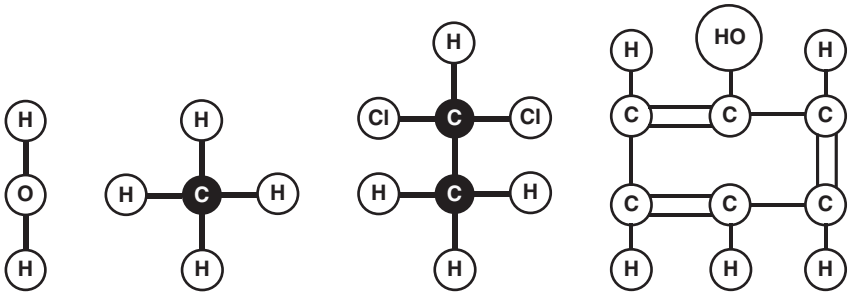

The earliest molecular graphics models that are the closest to those used nowadays was proposed by the Italian chemist Emmanuel Paterno in 1869. He made a breakthrough in the use of two eclipsed *tetrahedral carbon atoms* linked together to illustrate the 3D structures of dibromoethane. His models tried to address the question of how many isomeric structures can dibromoethane (**71**) have? He noted "It is superfluous to say that this is only a way of representing the facts, and that the whole concept needs experimental proof." Despite the fact that his use of a tetrahedral carbon atom was 5 years ahead of van't Hoff and LeBel (1874), he had the misfortune to publish his results in a relatively obscure journal (*Giornale di Scienze Naturale ed Economiche di Palermo*) [60]. Even today, this should be a take-home lesson to all of us.

In 1874, the Dutch physical chemist Jacobus Henricus van't Hoff at the age of 22 (and independently LeBel at the same time) proposed his salient theories on bonding geometries for organic compounds in a publication entitled "*The Arrangement of Atoms in Space*." Note that he also illustrated eclipsed conformations of single-bonded tetrahedral carbon atoms (**72–74**). The arrows show rotation about the single-bond as he wrote "It is then evident that [**72–74**] do not represent isomers, but the same structure in two phases of movement (arrows) around the axis uniting the carbon atoms," (i.e., rotamers).

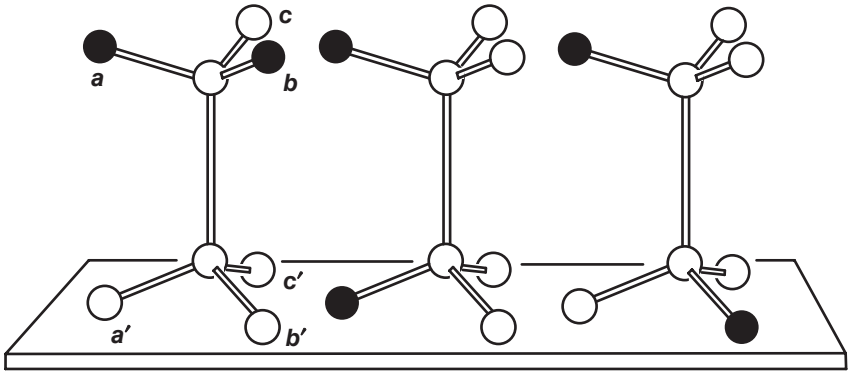

71

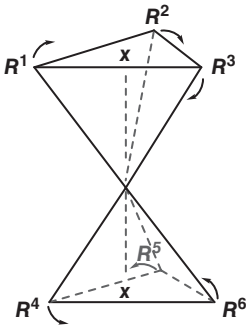

72

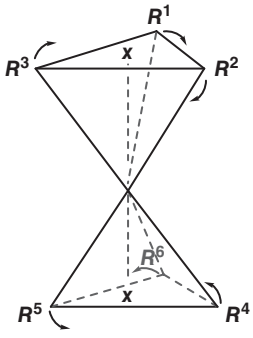

73

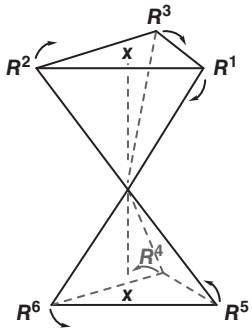

74

The models of double-bond compounds also addressed the question of *cis*/*trans*-isomerism in double bonds (maleic acid *cis*-**75**, versus fumaric acid *trans*-**76**). The ligation of two tetrahedral carbon atoms via two vertices explained the structural differences between the two *planar* diacids. A model for the triple bond in acetylene (**77**) was also proposed wherein two tetrahedral carbons were joined by a common face to engender a *linear* structure. In this publication, he went on to describe the case of the *asymmetric carbon* atom in which four different substituents were ligated to a tetrahedral carbon atom. Unfortunately, the meaning of "*asymmetric carbon atom*" is ambiguous. It is usually taken to mean that exchange of any two of the atom's four nonidentical substituents affords a new stereoisomer (what is now referred to as *stereogenicity*). However,

it can just as well refer to an atom's asymmetric local site-symmetry (what is now referred to as *chirotopicity*). This dichotomy of meanings will be discussed later on in more detail. In 1901, van't Hoff won the first Nobel Prize in Chemistry for this work on solution chemical dynamics and osmotic pressure.

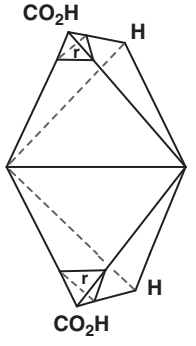

75

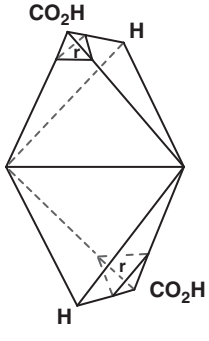

76

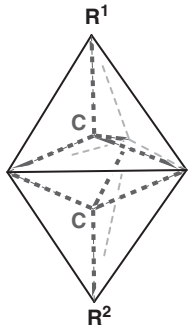

77

It was only in 1886 that the German chemist Aemilius Wunderlich introduced the term *configuration*. A few years later (1889), another German chemist, Viktor Meyer brought us the concept of *stereochemistry*. Finally, as lecture blackboards and paper are both planar, it is often both time-consuming and awkward to draw three-dimensional structures of molecules during a lecture. Emil Fischer in 1891 proposed a useful projection formula that could be quickly drawn by the lecturer/writer. He also made a "wild guess" about the absolute configurations of L-amino acids and D-sugars. It was only in 1952 that the Dutch crystallographer Johannes Martin Bijvoet (pronounced "By-foot") using the *anomalous dispersion* technique of X-ray crystallography confirmed that Fischer's lucky guess was indeed correct. We will now explain the drawing protocol for a Fischer projection for a generic L-amino acid. The carboxyl and R-groups of amino acids are vertically graphed on the vertices of a tetrahedron as top and bottom groups on the rear of the structure (**78**). The (L)-α-amino group and H(α) are, respectively, disposed horizontally left and right of the tetrahedron's front. The tetrahedron construction lines are then removed and are replaced by the addition of appropriate wedge- and dashed-shaped lines ligated to the C(α)-atom as in **79.** Usually, the configurational carbon is not labeled as C(α). Finally, the wedges- and dashed-lines are then replaced by simple straight lines to yield the well-known planar projection **80,** since the viewer is supposed to know the 3D equivalent (**79**). A word of caution for L-serine where R = CH_2OH and L-*cysteine* where R = CH_2SH. Beware that while both are drawn as in **79**,

since they are L-amino acids, their *R,S* Cram, Ingold, Prelog (CIP) descriptors are reversed. Why? The *R,S*-priority rules are based on *atomic number* and not on group size. Therefore, while most L-amino acids have an (*S*)-descriptor affixed for their absolute configuration, L-*cysteine* is the "odd man out" since α-sulfur has a higher priority than an α-oxygen. Therefore, L-*cysteine* bears an (*R*)-descriptor.

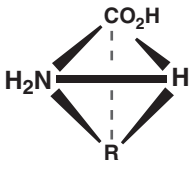

78

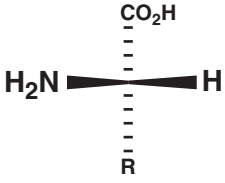

79

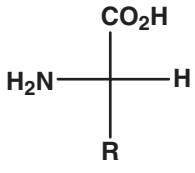

80

Fischer projections work fine for amino acids and sugars that possess a single stereocenter. The Fischer drawing protocol for sugars (**81–83**) is based upon D-glyceraldehyde. Larger aldo-sugars have additional H–C–OH units vertically inserted between C=O and the gray colored H*C*OH(CH_2OH) underlined italic *configurational carbon* of the linear open-chain form **82.** In other words, all additional H–C–OH units in the residue are vertically stacked, and their 3D translation involves wedges drawn in the same manner as the horizontal configurational H*C*(α)OH unit in **82.**

However, if one does not remember the three-dimensional wedge–dash translation protocol of a Fischer projection, then Fischer projections break down when they are used to ascertain the correct symmetry element responsible for *meso*-tartaric acid's optical inactivity. University lecturers typically use compounds like *meso*-tartaric acid as an example of an optically inactive diastereomer. Many readers have seen Fischer projection **84** (in Figure 4.1) in a First Year Organic

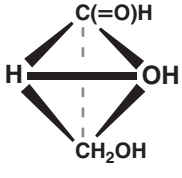

81

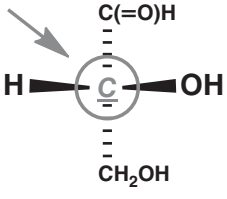

82

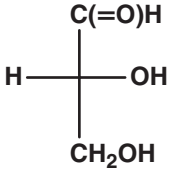

83

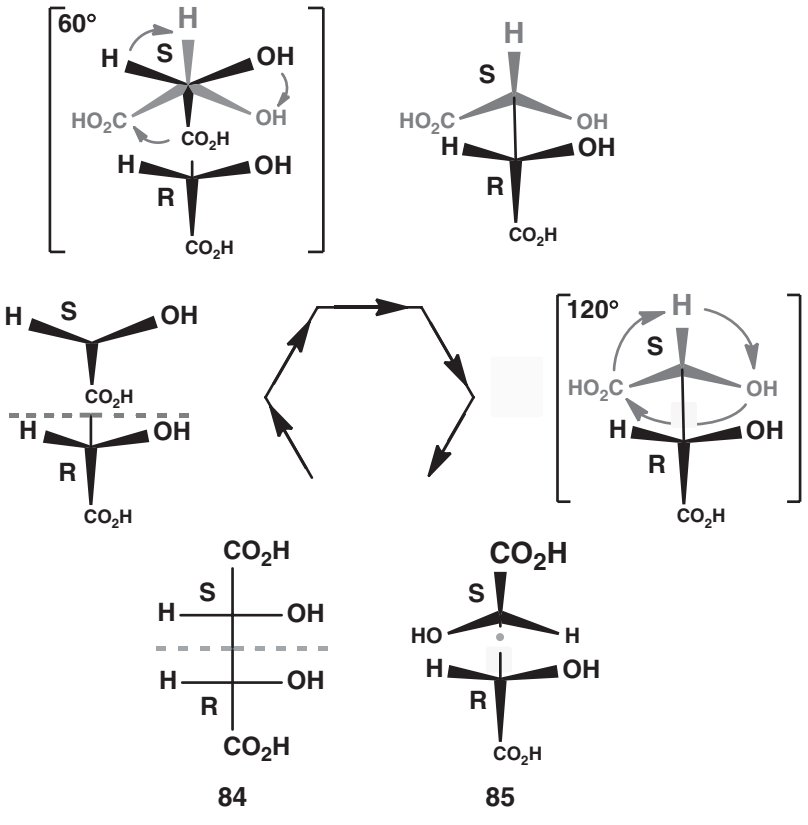

Figure 4.1 The achiral symmetry element in *meso*-tartaric acid is an inversion center (*i*) within stable staggered conformer **85** and definitely not a σ-plane in the Fischer projection eclipsed transition state **84**.

Chemistry lecture. Most likely the lecturer said words to the effect that "the σ-plane is responsible for the loss of optical activity." What is the problem here? The problem is that the Fischer projection breaks down when a molecule has two *adjacent* stereogenic atoms. Thus, the truth is that the molecule is indeed inactive, but due to a different symmetry element. To understand this, one should first "translate" Fischer projection **84** in Figure 4.1 into a 3D representation. It then becomes very clear that the σ-plane exists in an *unstable and nonpopulated eclipsed* transition-state rather than within a stable staggered conformation. Now, go upward and clockwise round the partial circuit of Figure 4.1. The (*S*)-top half of the 3D eclipsed structure is rotated 60° clockwise to generate a stable staggered structure. This conformer is asymmetric and, hence, optically active. Next, rotate

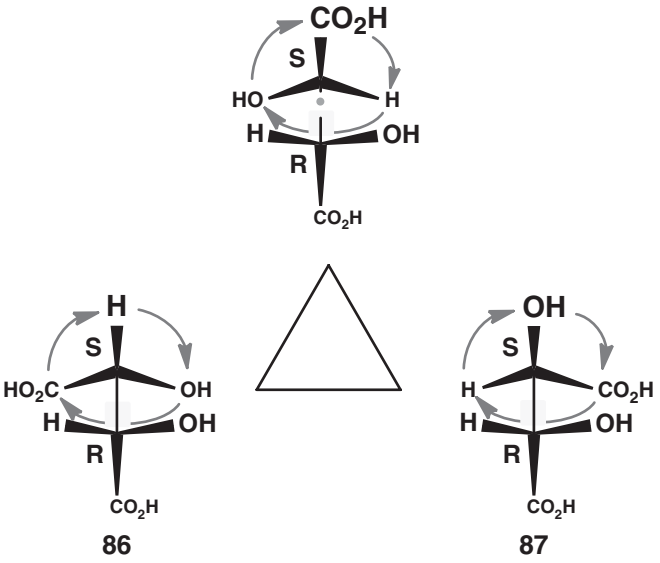

Figure 4.2 The *dynamic stereochemistry* of *meso*-tartaric acid is exemplified by three stable nonidentical staggered conformations interconverted by rapid 120° flips the (*S*)-half of the molecule about the central C–C bond.

the (*S*)-top half 120° clockwise to form an achiral C_i-symmetry *antiperiplanar* (180° C–C–C–C dihedral angle) *meso*-conformer (Refcode TARTAM [61], **85**), which is obviously nonoptically active.

But, the C_i-symmetry *meso*-rotamer is only one of three interconverting staggered structures. Figure 4.2 shows that consecutive 120° clockwise rotations (actually rapid flips) of the (*S*)-top half-molecule generate a circuit interconverting the three *stable staggered conformers* ((+)-asymmetric **86** → achiral **85** → (−)-asymmetric **87** →). Since chiral **86** and achiral **85** are the previously illustrated conformers in Figure 4.1, it logically follows that the new asymmetric third conformer **87** must be the enantiomer of **86** in order to have a nonoptically solution. However, the orientation of **87** does not give the appearance of being enantiomorphous to **86.**

A clockwise partial circuit through Figure 4.3 will convince the viewer that the proper orientation of **87** is indeed enantiomorphous to **86** via by a σ-plane. Starting with left-bottom **86,** a 120° anticlockwise rotation of the molecule's *(S)-half* about the C–C bond generates gray colored rotamer **87** just as depicted in the middle left of Figure 4.3. From now on, no C–C bond will be permitted since we do not want to change the rotamer. Instead, only rotations of the *entire molecule* **87** will be made for reorientation. Going clockwise, a horizontal 180° *out-of-plane*

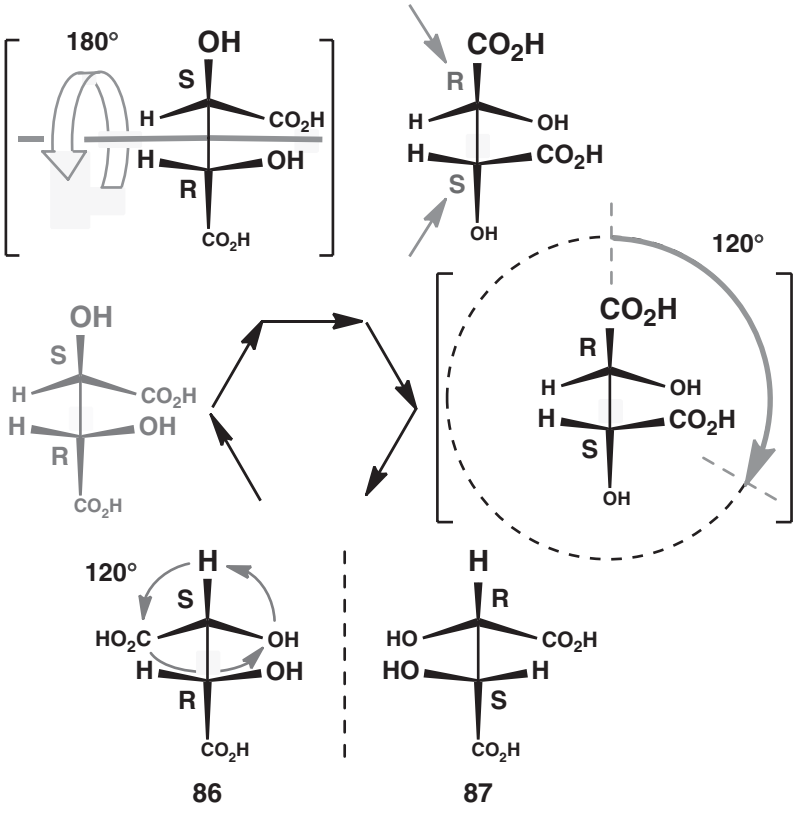

Figure 4.3 Reorientation of rotamer **87** (middle left) of Figure 4.2 by a 180° out-of-plane rotation of the entire molecule is then followed by a 120° in-plane rotation to afford **87** in the enantiomorphous disposition of **86**.

of the entire molecule rotation changes (*R*)-bottom half into an (*S*)-half (see upper right structure). This is followed by 120° *in-plane* rotation of the entire molecule to generate right-bottom **87** in the enantiomorphous orientation of **86.**

Unless we are dealing with compounds like *cis*-1,2-dimethyloxirane (**88**) with its geometrically constrained *eclipsed* mirror-symmetry structure, most *meso*-compounds have *staggered bond* inversion-symmetry. Although they are relatively more rare, there are also some *meso*-compounds having rotation-reflection S_4-symmetry, such as the spiro quaternary ammonium cation **89.** One understands from these examples that the presence of any point group operation of the Second Kind relating two opposite handed stereogenic atoms will make the compound optically inactive (i.e., a *meso* compound).

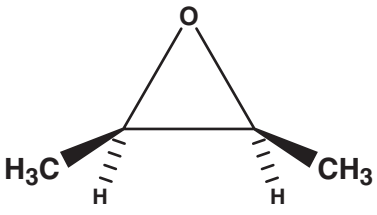

88

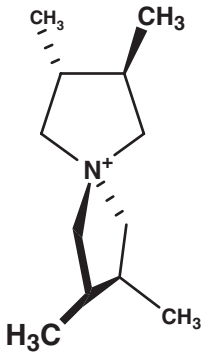

89

4.6
Fischer Projections to Determine α- and β-Anomeric Configurations

The assignment of α- or β-anomeric configuration in carbohydrates is based upon the pyranose- or furanose-ring *anomeric hydroxyl group's* relative orientation vis-à-vis the linear form's D or L-*configurational hydroxyl group,* that is, HC***OH***(CH_2OH). α-Anomers have their hydroxyl on the *same side* of the ring as that of the configurational hydroxyl, while β-anomer and configurational hydroxyls are located on the sugar cycle's *opposite faces.*

L-Galactopyranose is an appropriate carbohydrate to use for illustrative purposes, since most readers feel that they understand the nomenclature of D-glucopyranose α- and β-anomers. A number of marine organisms produce L-galactose. For example, 3-*O*-(α-D-glucopyranosyluronic acid)-L-galactopyranose is an aldobiouronic acid isolated from extracellular polysaccharides produced by the brackish water, unicellular, red alga *Rhodella reticulata*. Its structure determination was performed by Geresh, Arad, Glaser, and coworkers [62]. The configurational hydroxyl group of the vertically oriented linear form of L-galactose (**90**) (marked with an arrow and dashed circle in Figure 4.4) is on the left side of the vertically oriented molecule (lower left Fischer projection). One can imagine the configurational hydroxyl oxygen attacking the *prochiral* carbonyl aldehydic carbon to afford an anomeric OH-group on either the left or the right side. For the purpose of assignment of an α-anomer to an L-carbohydrate, the anomeric OH will be on the left-hand side. What is important here is the relative location of the *new anomeric OH* (labeled with a full circle) relative to the Fischer projection's *old configurational OH* (labeled with a dashed circle in **90**). Therefore, the α-anomer *axial* anomeric OH and *equatorial* methylol (CH_2OH) L-α-galactopyranose **91** has been drawn in the more stable ^{1}***C$_4$-chair*** conformation rather than as its ^{4}***C$_1$-chair*** *invertomer* (shown above **91** slightly to

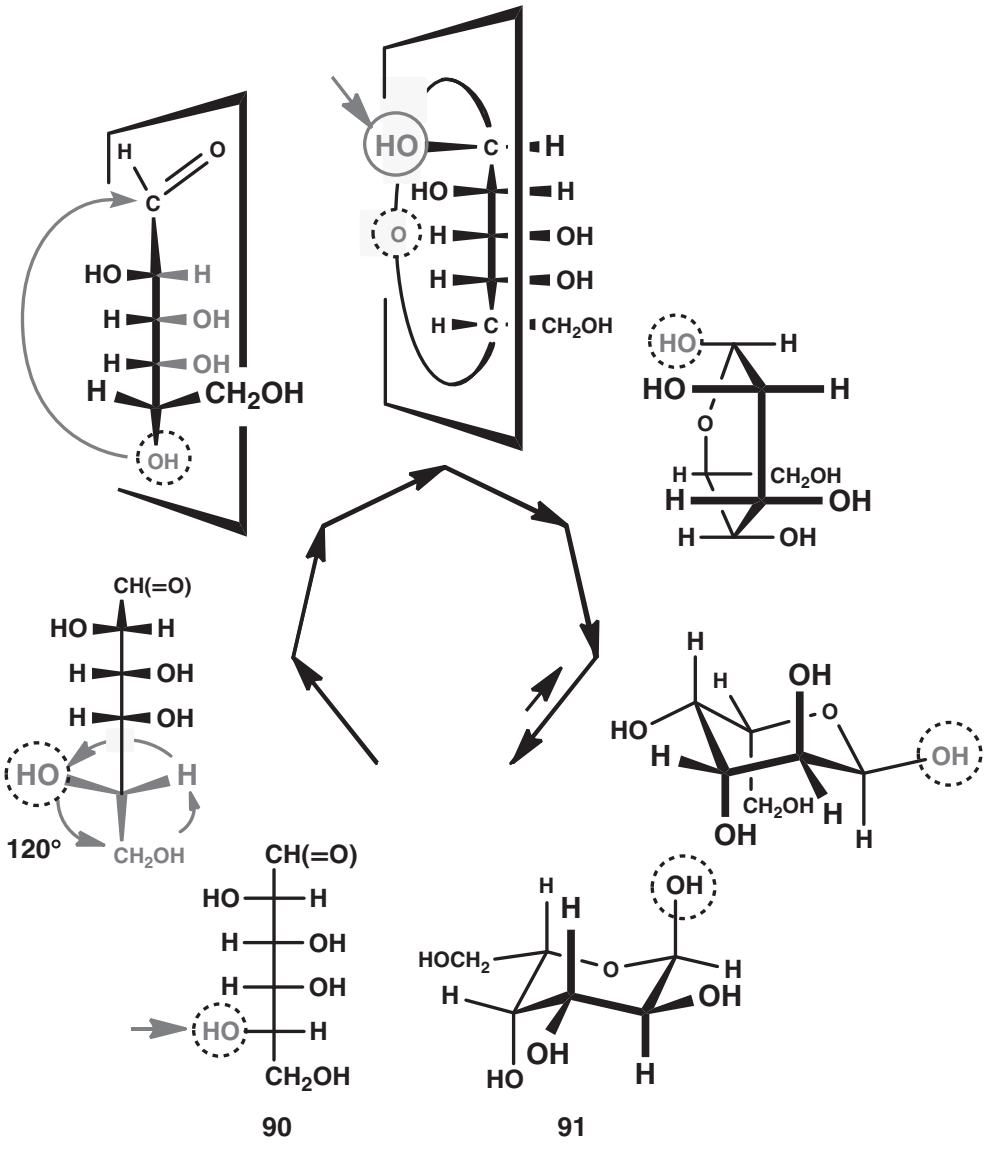

Figure 4.4 Both the configurational hydroxyl group of the vertically oriented linear form of l-galactose (**90**) (marked with an arrow) and the anomeric hydroxyl (upper most structure) are disposed toward the same left side of the drawings. Therefore, pyranose ring formation affords **91** (the more stable $^{1}C_{4}$-*chair* conformation of the two possible α-anomers).

the right). The $^{4}C_{1}$-*chair* pyranose conformation *ring-invertomer* is less stable by virtue of *cis*-1,3-diaxial-type interactions involving the C(3)-hydroxyl and methylol moieties. Ring inversion should not be confused with *mutarotation,* since the latter process involves bond-breaking and bond-making. Bottom line: ring inversion determines the stabilities of *equatorial/axial* orientations of the two possible α-anomeric hydroxyls, and only then should mutarotation be considered for the subsequent generation of the most stable α/β-anomers. Didactically, the commonly recognized $^{4}C_{1}$-*chair* D-β-glucopyranose (**92**) structure was not utilized, since the all *equatorial* disposition of its substituents makes it a less challenging model compound.

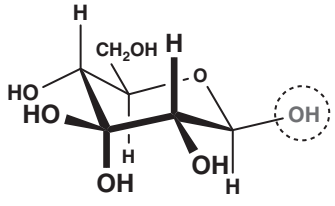

92

5
Chiroptical Properties

5.1
The Language of Symmetry, Isomerism, and the Characterization of Symmetry Relationships within and between Molecules

At the beginning of this section, it is useful to review some basic terminology in light of the fact that Mislow [63] (the author's stereochemistry mentor) has reorganized the concept of *isomerism* based on the principles of *isometric/anisometric* molecular geometry, superimposition, and *constitution* (atomic connectivity). The advantage of this reorganization is its ability to predict the conditions where one may experimentally differentiate between pairs of isomers. Molecules with the *same chemical formulae* (i.e., molecular formula: number and types of atoms) are *isomers* (equal units) and those that are not are *heteromers* (different units). All the physical and chemical properties of heteromeric pairs must be different since they are obviously not symmetry equivalent. Isomers are either *isometric* or *anisometric. Isometric isomers* have the same distance matrix and are either superimposable upon themselves (i.e., *homomers*, a congruent pair) or not (*enantiomers*). All the physical and chemical properties of an isometric pair of molecules are identical providing that the properties depend only upon the first and second dimensions. Anisometric isomers have different distance matrices but may have either the same *constitution* (*diastereomers*) or not (*constitutional isomers*). It is noted that *diastereomer* is a structure that differs from another "across"-"space"-"unit" molecule. It is derived from the Latin prefix *dia* meaning "across" (as in *diagonios* – "diagonal," i.e., "across the angle" since *gonia* means "angle," as in pentagon – a figure with five angles), *stereo* "space," and *mer* "unit."

Isometric isomers are symmetry equivalent (homomeric pairs by operations of the First Kind and enantiomeric pairs by operations of the Second Kind). The logic of placing homomers and enantiomers within the same isometric subfamily is that the corresponding properties of a pair of homomers are identical under all measurement conditions, while only the corresponding properties of a pair of enantiomers that do not depend on the third dimension are also identical (e.g., melting and boiling points, IR, and nuclear magnetic resonance (NMR) spectrum are

Symmetry, Spectroscopy, and Crystallography: The Structural Nexus, First Edition. Robert Glaser.

Companion Website: www.wiley.com/go/Glaser/Symmetry

the same). Enantiomers may be differentiated only by measurements that probe chirality. Examples of chiral probes are metabolism by enzymes, chiral chromatography, and chiroptical measurements.

In structural chemistry, the *bonding parameters* (*bond lengths* – a one dimensional parameter, *bond angles* – a two dimensional parameter, and *torsion angles* – a three dimensional parameter) are all identical for a pair of homomers, while just bond lengths and bond angles are identical for a pair of enantiomers. The respective torsion angles in enantiomers exhibit identical magnitudes but *inverted signs.* Similarly, grouping anisotropic diastereomers and constitutional isomers together makes sense since, by definition, both of these pairs of isomer types are symmetry nonequivalent, that is, they are *inherently different* in ALL their physical and chemical properties. In short, diastereomers and constitutional isomers are different molecules, and hence, one should not expect identities in any comparison of their chemical and physical properties. This is a symmetry argument, and it can "never, ever, be disproved." The only unknown is just "how different are they?" and "is our available instrumentation sensitive enough to measure the difference?" Many organic chemistry courses discuss chirality, enantiomers, and then optical activity followed by diastereomers, since the topics are considered to be pedagogically related by many textbook authors. However, the concept of diastereoisomerism, *per se*, has nothing to do with chirality, nor with optical activity, since the term can be readily applied to describe *cis-/trans*-but-2-ene diastereomers (*anisometric* and having the same *constitution*).

5.2 Chiroptical Properties: Circular Birefringence, Optical Rotatory Dispersion, and Circular Dichroism

In spite of loss in rigor, often for *heuristic* (teaching) purposes, quantum mechanical phenomena are sometimes more easily explained in terms of argumentation drawn from our macro-world as a "first approximation to the real truth." This is especially beneficial when quantum mechanics are being explained to nonphysicists. We will take such liberties when discussing chiro-optical (*chiroptical*) properties. Consider an electromagnetic beam to consist of an electric field's oscillating sine-wave plane perpendicular to that of the magnetic field. Sine waves are achiral and may be thought of as horizontal plane projections of either right- or left-handed enantiomorphous *in-phase* helical chiral-twisted oscillating fields. Note that the projection shadow upon a flat surface of a pair of right- or left-handed *in-phase* helices is the *same identical sine wave.* Furthermore, let us consider a photon's path to *propagate* outward from the source at a particular velocity (v) on one of the aforementioned *helical* pathways. What significance does this have? The helix diameter represents the vertical distance between the sine wave's *maxima*

and minima, that is, the sine wave's *intensity.* Furthermore, the horizontal axial distance between two consecutive coil maxima symbolizes the *wavelength.* For the sake of argument and heuristic purposes, let us further stipulate that a red-colored dot appears at the same single end of a mixture of parallel enantiomorphous helical pathways. Next, imagine placing the laterally disposed helices in such a manner that their red-colored termini all touch a transparent barrier. When our eyes look through the clear barrier down the *non-phase-restricted* parallel helices, the red dots will appear to have an infinite number of orientations. One can think of a *polarizer* as removing all the helices (our gross oversimplification for vector components of light) whose red dot is nonaligned with the polarizer's arbitrarily chosen vertical plane orientation.

In this case, only right- and left-handed *in-phase* helical pathways with red-dotted ideally vertical termini will remain in our collection. We can then metaphorically say that these right- and left-handed helices represent a plane polarized light racemic mixture of right and left enantiomorphous *circular polarized light* vector components. Since it is not easy for nonphysicists to conceptualize a photon's "*vector components*," let us bend the truth and state that our light beam is simply composed of a racemic mixture of achiral photons traveling at a particular velocity (v) down one of two *in-phase* enantiomorphous helical pathways. Bearing in mind that these "enantiomeric" *in-phase* non-quantum-mechanical helical paths of photons symbolize plane polarized light, we can now start to explain a large number of chiroptical phenomena in a nonrigorous manner.

So, as a macro-world very crude first approximation of a quantum mechanical phenomenon, if the helices' left-termini in Figure 5.1 denote a monochromatic light source, then we can imagine photons departing the source and propagating

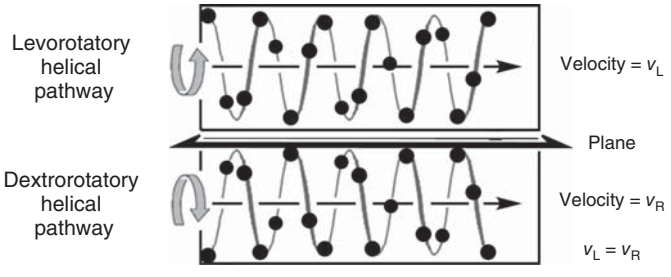

Figure 5.1 Photon locations (black dot distances from the left-handed edge) on parallel left and right *in-phase* helical pathways traversing an achiral medium are depicted at constant time intervals. Since the photons travel on enantiomorphous helical propagation pathways through an achiral medium at exactly identical velocities, the polarization plane never rotates since the vector-sum remains constant.

down one of the two in-phase helical parallel pathways through a vacuum or air. If we stipulate that the black dots in Figure 5.1 are photon locations at set time intervals (t) on the right and left circularly polarized pathways, then the vector sum of all their positions generates the same linear polarization mean plane as the polarizer. Continuing this analogy, since the circularly polarized pathways are enantiomorphous, and the achiral photons all travel through air at the identical velocity (v_{air}), then at any particular time interval (t), photons on either the right and left in-phase helical pathways will have always traveled the same propagation distance (x), since $v_L = v_R$. The velocities of both photons on circularly polarized pathways are then reduced *by the same extent* upon entering an achiral medium. These analogies to concrete, readily understandable helical pathways, show that the photon's reduced velocities through a medium relative to their higher velocities in a vacuum are akin to the concept of *index of refraction*, n (the ratio of the velocity of light in a vacuum to that in a medium). Thus, $n_R = n_L$ through an achiral medium, where n_R and n_L are the indices of refraction of right and left *circularly polarized light*, respectively.

Next, consider an enantiomerically pure chiral medium, (e.g., an arbitrarily chosen right-handed chiral medium). Now, the photon's velocity traversing one helical pathway within the spectrometer's quartz cuvette will not be identical to that of the photon traveling the enantiomorphous route, that is, $n_L \neq n_R$ since they are no longer constrained by symmetry. If we *schematically depict* the interaction of right circularly polarized light within a right-handed chiral medium as "($right_{circularly\ polarized\ light} \cdots (+)\text{-}_{medium}$)," then there is a *symmetry mismatch* when one compares it to the diastereomeric "($left_{circularly\ polarized\ light} \cdots (+)\text{-}_{medium}$)" interaction. This mismatch causes a *phase shift* of $+\alpha$ degree between the two helices, which then rotates the mean polarization plane by the same amount. Obviously, the plane of the polarized light would rotate in the opposite direction ($-\alpha$ degrees) if the light traversed through an enantiomeric sample. Figure 5.2 illustrates $v_L > v_R$ relative photon velocities through a chiral medium. Only 15 location measurements for the levorotatory path *faster* photon (top horizontal axis) were made during the drawing's total elapsed time period, compared to 18 for the dextrorotatory path *slower* photon. The difference in photon velocities rotates the vector-sum plane anticlockwise by $-\alpha°$. This $n_L \neq n_R$ phenomenon is known as *circular birefringence*.

The rotation of plane polarized light through chiral media is measured on a *polarimeter* at a particular wavelength, usually the sodium D unresolved-doublet lines (588.9950 and 589.5924 nm). See Biot's law discussed earlier. Like the Beer–Lambert law, there is a danger of aggregation if the concentration becomes too high. Under these high concentration conditions, $[\alpha]_\lambda^T$, the wavelength and temperature-T-dependent *specific rotation constant* is no longer concentration invariant. The polarimetric measurement of chiral molecules is also solvent-specific, since they are *solvated*. Similarly, the solvent–solute mean distance is obviously temperature dependent. Change the solvation-sphere or

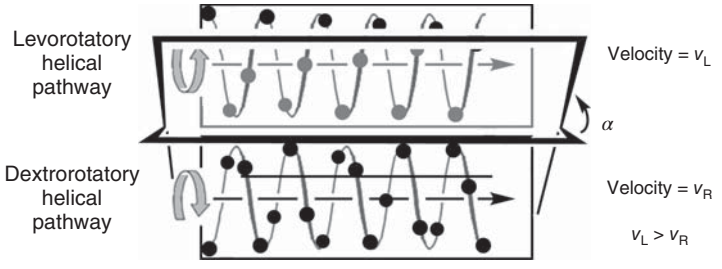

Figure 5.2 Photon locations (black dots) on parallel left- and right-handed helical pathways traversing an achiral medium are depicted at the same constant time interval. In this example, the photon's *faster* velocity on the left circularly polarized path enables it to travel farther along the top axis relative to the distance of its *slower* counterpart on the right circularly polarized bottom axis path and results in a $-\alpha°$ rotation of the vector-sum plane.

the temperature T, and the new solvated species exhibits different properties, for example, the magnitude, and even sometimes the sign, of $[\alpha]_\lambda^T$ changes.

The difference in refractive indices for the right and left circularly polarized components that make up plane polarized light was discovered in 1822 by Augustin-Jean Fresnel. A plot of α versus wavelength is called ***O**ptical **R**otatory **D**ispersion* (ORD). A positive ORD plot is depicted as **93**. It consists of two positive *plain curves* (sometimes called "wings") separated by a *discontinuity* at the UV/vis absorption λ_{max}. The discontinuity region is called a *Cotton Effect*. Where have you observed dispersion curves before? We see them all the time when phasing an NMR frequency-domain spectrum. If you are the primary NMR operator, then you have seen them when optimizing an NMR acquisition parameter, for example, P1 (the microseconds 90° pulse duration time). A series of increasing P1 pulse duration times generates a sine-wave intensity plot with a maximum 90° value, minimum at 270°, and zero intensities for a 180° or 360° pulse. However, instead of a zero-intensity signal, one usually observes a very low intensity dispersed signal (which integrates for zero).

Observe the plain curve wings of plot **93** carefully. Irrespective of the sign of α at any particular wavelength, increasing λ values afford *more positive* α-values (i.e., either *increasing positive* left-wing values or *decreasing negative* right-wing values). Early in the twentieth century, Paul Drude proposed an empirical curve fitting equation to describe the wings of the dispersion curve and their abrupt discontinuity at $\lambda = \lambda_{max}$, (see Eq. (5.1)) [64].

$$\mathrm{ORD}(\lambda) = \frac{C}{\lambda^2 - \lambda_{max}^2} \tag{5.1}$$

A solution of the enantiomer would give an enantiomorphous negative ORD plot **94**. ORD may be measured on a recording *polarimeter* equipped with

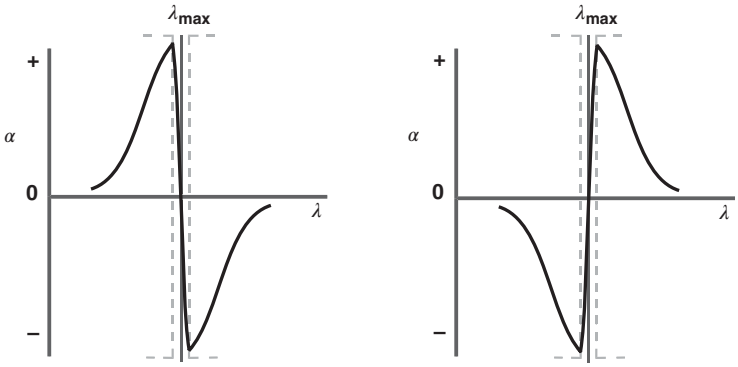

continuous light sources (e.g., deuterium lamp for UV or quartz-iodine lamp for Vis). Optical rotation (α) has an advantage of providing chiroptical data at wavelengths (e.g., $\lambda = \lambda_D$) far removed from a sample's λ_{max}.

Figure 5.3 schematically depicts parallel helical pathways for circularly polarized photons traversing first air and then an achiral medium with a solvated *achiral chromophore*. The same amount of light is absorbed by both circularly polarized light components since the chromophore's molecular orbitals have Second Kind symmetry, that is, they are achiral. Therefore, absorption of photons on the right

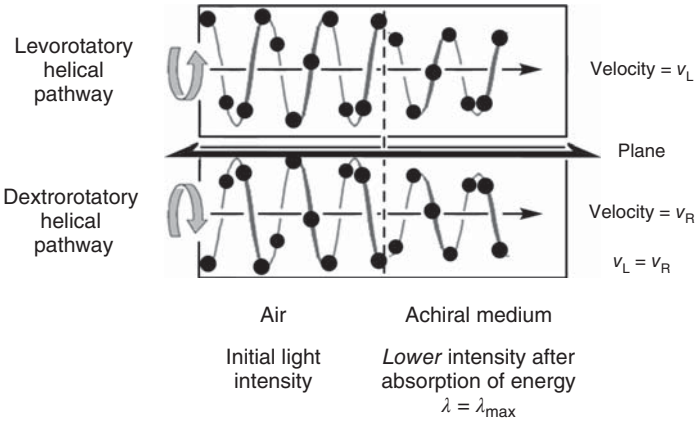

Figure 5.3 Constant time interval photon locations (black dots) on parallel left- and right-handed helical pathways traversing an achiral medium depict equal absorption and equal indices of refraction of right and left circularly polarized light energy by an achiral chromophore at $\lambda = \lambda_{max}$.

and left circularly polarized paths must be *identical.* In other words, their $\varepsilon_L = \varepsilon_R$ *molar extinction coefficient* constants are identical as in the Beer–Lambert law where absorption (optical density OD) $= [\varepsilon]_\lambda^T cl$. The two *equal-length* rotating right and left circularly polarized light vectors have swept out an identical-radius helical path through air, and then both are *equally reduced* when transiting an achiral medium. In other words, *absorption* of light energy has equally reduced the cross-sectional diameters of both the right- and left-helical pathways, while the indices of refraction remain the same ($n_L = n_R$) within air and in the achiral medium. As a result, the detector records a lower intensity signal with no change in the polarization plane.

Next, consider a chiral medium. As before, the two photons upon circularly polarized light helical pathways transverse air with equal velocities and no energy absorbance (see left side of Figure 5.4). However, when light enters a chiral medium with λ equal to the chiral chromophore's λ_{max}, then the oppositely handed circularly polarized light components will exhibit *unequal energy absorbance* ($\varepsilon_L \neq \varepsilon_R$) concomitant with *unequal photon velocities* $v_L > v_R$ and arising from unequal indices of refraction ($n_L \neq n_R$). The two *unequal-length* rotating right and left circularly polarized light vectors will now sweep out an *elliptical* figure at unequal velocities. None of ellipsoid's major/minor axes coincide with the original plane of polarization ($n_L \neq n_R$). The unequal intensity components of circularly polarized incident light on the detector are called *elliptical* polarized light. Observe that in Figure 5.4 the faster photon on the levorotatory (upper)

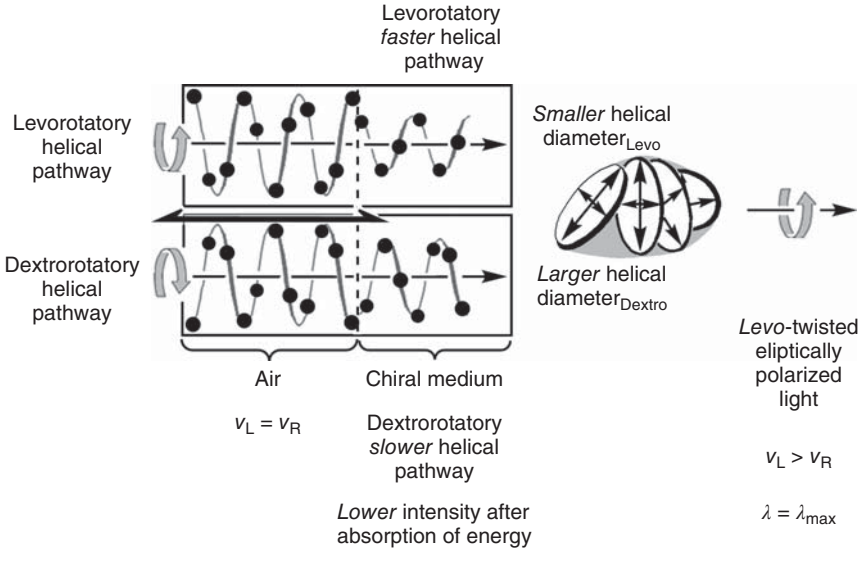

Figure 5.4 *Circular dichroism* is the unequal absorption of right and left circularly polarized light energy ($\varepsilon_R \neq \varepsilon_L$) combined with $n_L \neq n_R$.

path is measured only six times, while seven positions are observed for the *slower* photon on the dextrorotatory (lower) path during the same time period. The combined $\varepsilon_L \neq \varepsilon_R$ and $n_L \neq n_R$ phenomenon is referred to as *circular dichroism* (CD). The parameter that is measured by a CD instrument as a function of wavelength is called *molecular ellipticity*, θ, and the concentration-independent proportionality constant is denoted as $[\theta]$, the *molar ellipticity coefficient*. A CD spectrum shows a very considerably narrower $W_{1/2}$ line-width at half-height $(+)_{net}$- or $(-)_{net}$ signal(s) compared with broad UV/Vis electronic transitions.

5.3 Miller Indices and Fractional Coordinates in Crystallography

A *right-hand axes convention* is utilized by the crystallographic community. In this system, the *thumb* points upward (the X-axis), the index finger points the Y-axis, and the *middle finger* (the Z-axis) is bent toward the viewer (see **95**). Once these axes have been defined, they may be oriented according to esthetics and the contingencies of the illustration. When looking at a *unit cell* (the omnidirectional translational repeat entity of an extended array) the X-, Y-, and Z-axes become the cell's respective *a*, *b*, and *c sides.* The three faces of a parallelepiped unit cell will be described next. The γ angle lies between the *a* and *b* sides and the sides define the *ab*-plane (X,Y-plane), the β angle is between the *a* and *c* sides and the sides are the *ac*-plane (Y,Z-plane), and finally, angle α subtends the *b* and *c* sides. The fractional coordinates along each of the *a*, *b*, and *c* sides range from 0.0 to 1.0. Values greater than "1," or less than 0, take us into adjacent unit cells. By the way, since we are dealing with periodic crystalline arrays, one should not be concerned if the crystallographer provides us with coordinates whereby part of a molecule extends into an adjacent cell (this is quite common). If we desire to generate the enantiomer from the fractional coordinates of an oppositely handed chiral molecule, then this is readily done by multiplication of the original molecule's positive fractional coordinates by the $[1-x, 1-y, 1-z]$ inversion operator. Multiplication with the $[-x, -y, -z]$ inversion operator places the enantiomer in the three negative axes adjacent unit cell on the origin's other side.

The following section deals with the ***S***canning ***T***unneling ***M***icroscope (STM). STM specimens are coated upon surfaces of *atomically flat* electrodes, for example, *specific* planes usually cleaved from cubic crystals of copper. The chosen plane has a *specific symmetry relationship* between the surface's exposed metal atoms. To describe a specific crystal plane to be coated, one makes use of a triple integer descriptor called a *Miller index* (first used by the British mineralogist William Hallowes Miller in 1839).

It is good to begin with crystallographic notations. As we said before, $[x, y, z]$ are fractional atomic coordinates since "*x*, *y*, *z*" are all separated by commas within

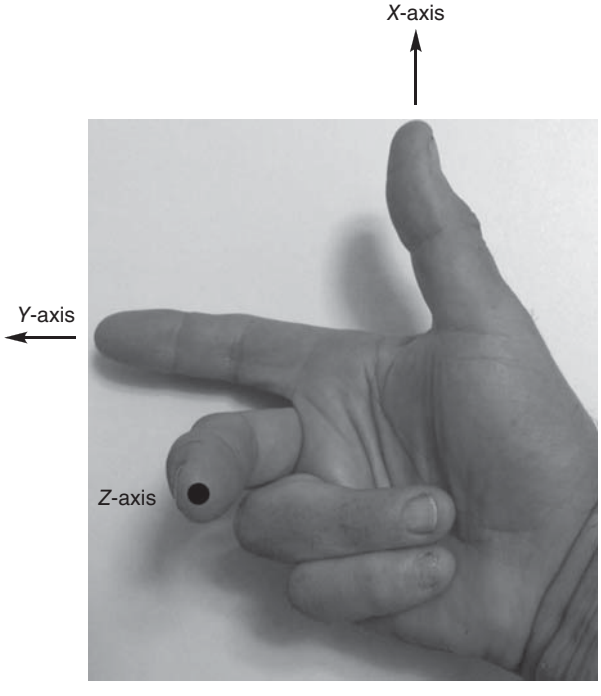

95

the square brackets. These coordinates can be either *decimals* (e.g., 0.2510, 0.3339, 0.4900, and 0.75070) or *rational numbers* (any number that can be expressed as the quotient or the fraction-(p/q) of two integers, with $q \neq 0$, e.g., 1/4, 1/3, 1/2, 3/4, etc.). On the other hand, (**hkl**) **boldfaced** Miller indexes are commonly denoted by three bold-faced "***h***," "***k***," and "***l***" integers, which are *not separated by commas* and are placed within parentheses. They describe a specific plane within a crystal. Three arbitrarily chosen planes in a cubic copper crystal will now be discussed. Let us begin to analyze Miller index plane (**100**). The $1/1 = 1$ *inverse* of the 100s digit (***h***) shows that the plane goes through fractional coordinate point **1** on the *a*-axis. The $1/0 = \infty$ inverses of the 10s (k) and unit's (l) digits signify that *no points* for the plane are on either the *b*- or the *c-axis*, that is, plane (**100**) is orthogonal to the *a*-axis at $x = 1$ and thus cannot intersect with the *b*- and *c-axes*, see (**96**). Inspection of the drawing clearly shows that cubic lattice plane (**100**) exhibits a *fourfold rotational-axis* perpendicular to the face. This is denoted by the crystallographic *black square symbol* in the middle of the gray (**100**)-face, that is, a C_4-axis passes through fractional coordinates [0, 1/2, 1/2] and [1, 1/2, 1/2] and the cube's center.

The $1/1 = 1$ *inverse* of the 100s (***h***) and 10s (***k***) digits indicates that the (**110**) plane goes through fractional coordinate points **1** on both the *a*- and *b*-axes. The

$1/0 = \infty$ inverse of the unit's (*l*) digit shows that there is *no point* for the plane on the *c-axis,* that is, plane (**110**) is rectangular (*twofold symmetry*) and passes through fractional coordinates [0, 0, 1/2] and [1, 1, 1/2] and the cube's center, see **97**. The crystallographic symbol for twofold rotational symmetry is a black ellipse.

Plane (**111**) in a Cu cubic lattice will be the last to be discussed. The $1/1 = 1$ *inverse* of the 100s (***h***), 10s (***k***), and unit's (***l***) digits shows that the (**111**) plane passes through fractional coordinate points **1** on all *a*-, *b*-, and *c*-axes. This plane appears to have *trigonal* threefold symmetry, see **98**. The crystallographic

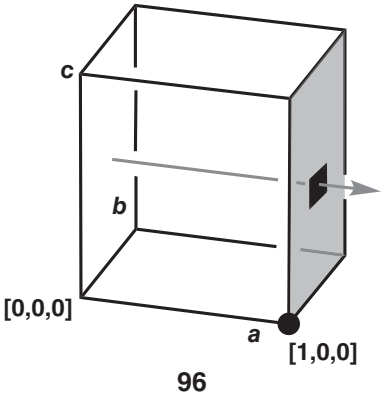

96

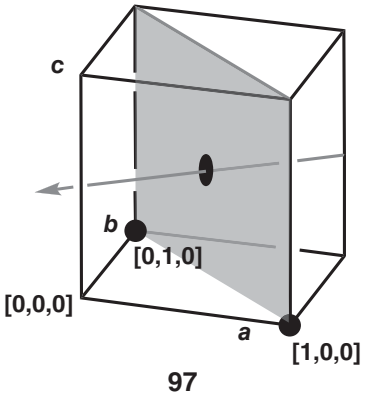

97

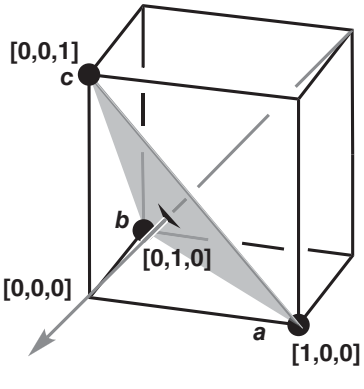

98

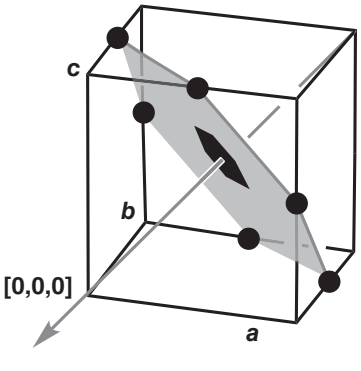

99

symbol for threefold rotational symmetry is a black equilateral triangle. However, one can generate a *family* of symmetry-equivalent {**111**} planes, (the bold-faced

braces denote that the descriptor refers to a family of symmetry related planes, for example, the two parallel (**111**)-planes of **98** and **99**). Note: the (**111**)-plane **99** bisects the mid-points of each of the cube's six edges, and its *actual symmetry is hexagonal,* not trigonal. Is there a discrepancy here? Certainly not! One has to remember that *six adjacent equilateral* triangles form a regular hexagon (*vide infra* **103**), and the unit cell is part of a periodic array.

In the case of a cubic crystalline Cu metal STM electrode, one can perform different cleavages of a crystal to expose a variety of surfaces exhibiting specific symmetry relationships between the metal atoms. The surface metal atoms on the fourfold symmetry (**100**)-plane are depicted in **100**. The second layer is

100

101

102

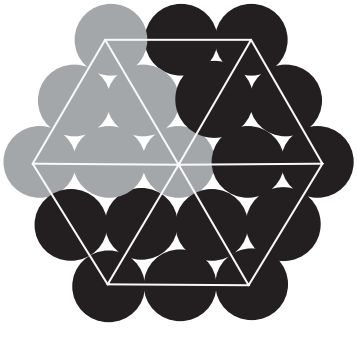

103

visible as gray colored atoms. Illustration **101** depicts the first atomic layer of the rectangular twofold symmetry (**110**)-surface. Inspection of the drawing shows that the (**110**)-surface of metal atoms is much less closely packed than the (**100**)-surface. Finally, the sixfold (hexagonal) symmetry (**111**)-surface (**102**) is the *most densely packed* arrangement of metal atoms or balls. As

mentioned earlier, the impression that arrangement **102** appears to be trigonal is incomplete since we are dealing with a *hexagonal*-symmetry *periodic array* of equilateral triangular unit cells **103**. A more detailed explanation of crystallography in general and *molecular* unit cells will be provided later on in the text.

5.4 Scanning Tunneling Microscopy

The remarkable STM is able to view molecules and even *tert*-butyl groups. It uses an atomically flat electrode. In order to obtain the desired flat surface of a cubic Cu *fcc*-symmetry crystalline metal, the crystal is carefully split along a *cleavage plane*. *Fcc* means ***f**ace-**c**entered **c**ubic* as in plane (**100**) **99**. Cleavage is known to produce *atomically flat* surfaces. These cleaved planes represent different layers of the crystal lattice. The author will do his best to explain the quantum-mechanical phenomena for the STM, despite an amusing quote attributed to Richard P. Feynman and which jokingly stated "… *I think that I can safely say that nobody understands Quantum Mechanics.*" Feynman, Sin-Itiro Tomonaga, and Julian Schwinger were awarded the 1965 Nobel Physics Prize for their fundamental work on quantum mechanics. The STM is an instrument for imaging surfaces with atomic resolution. It is based upon a principle known as *quantum tunneling* through the space between two electrodes with a proper voltage bias. This quantum-mechanical effect can be explained by the *wave-particle dualism* of electrons. In the STM, the electron is a quantum-mechanical particle that behaves as its wave function. The electron's wave functions can extend with an exponentially decaying tail out of an electrode into a *barrier.* The "barrier" is the space between a sharpened wire tip electrode and a conducting monolayer (i.e., the sample to be observed) deposited on an atomically flat second electrode composed of highly oriented pyrolytic graphite or a crystalline Cu metal surface. Why use the term "barrier"? The reason is that according to the laws of *classical physics*, a flow of electrons requires a conducting wire to move between two metal surfaces. So, physicists say that the electrons *tunnel* through the barrier in the STM.

The sharpened metal tip-electrode is composed of tungsten or platinum–iridium alloys. It is sharpened to an ultrafine atomic-scale tip by techniques such as mechanical cleavage or electrochemical etching. The tip is carefully adjusted to bring it close (4–7 Å) to the surface of the *conducting monolayer* (also called the "substrate" or specimen). A voltage *bias* (difference) is then applied so that the tip electrode is at higher potential than that for the conducting substrate monolayer adsorbed upon the flat surface electrode. The voltage is adjusted to cause the Fermi level heights of the electrons in the two electrodes to shift so

that the tails of the electron's wave functions begin to overlap within the barrier. The electrons then *tunnel* from the tip surface through the monolayer sample to the second electrode that is at a lower potential. This "tunneling" is a *forbidden process* according classical physics for reasons already noted earlier. However, quantum mechanics assures us that there is a finite probability that electrons on the higher potential tip will "*jump through the barrier*" to the lower potential flat surface. The resulting *tunneling current* exponentially decays with an increase of the separation distance (i.e., the barrier). This exponential dependence leads to exceptional resolutions of the order of 0.01 Å in the perpendicular direction and ~1 Å in the parallel directions. The tunneling current is also dependent on the applied voltage and the *local electronic-state density-functionals* of the atoms within the conducting monolayer. These molecular density functionals are directly related to their theoretically generated counterparts used to perform geometry optimization calculations by the density functional theory (DFT) B3LYP technique using a particular basis set (e.g., the relatively high 6−311 + *g*(*2d*,*p*) basis set used for NMR *spin*−*spin* coupling constant calculations).

Piezoelectrically based control circuits precisely maintain the tip at a constant vertical height from the surface atoms and also enable it to scan within the *X*,*Y*-plane across the sample. The vertical position (derived from the tunneling current) is measured as the tip moves across the surface, so that atomic information of the surface can be mapped out resulting in a *local density of states* (i.e., density functional) modulated image. The influence of this modulation is often neglected, since it is common practice to represent the image without further processing.

Besenbacher and coworkers [65] studied the organization of achiral 2,5,8,11,14,17-hexa-*tert*-butylbenzo[*bc*,*ef*,*hi*,*kl*]coronene (Refcode IVACOY [66], **104**) molecules that chirally self-assembled within a *close-packed monolayer* adsorbed on a crystalline copper (**110**)-surface electrode. The intense spots in the pair of STM images **105** arise from the more bulky *t*-butyl groups, while the relatively thinner (less dense) aromatic center appears in the image as a lighter tone. The use of *square brackets* in the $\mathbf{1\bar{1}0}$ notation in **105** denotes a *direction vector* within a Miller Index plane, and $\mathbf{\bar{1}}$ (read as "1-bar") is the −1 direction. For *chiral organization* of the molecules to come to pass, the adsorbed achiral molecules must interact with each other along specific directions, which are *not symmetric* with respect to any of the crystalline electrode's *mirror planes.* The power of the STM image is such that it alone enables the researchers to make this statement of fact based solely upon experimental observation. In the case of the achiral hexa-*t*-butyl-coronene-type star-shaped molecules, the self-assembled monolayer is chiral due to asymmetric intermolecular interactions arising from *organizational chirality* within the absorbed array of molecules. In this case,

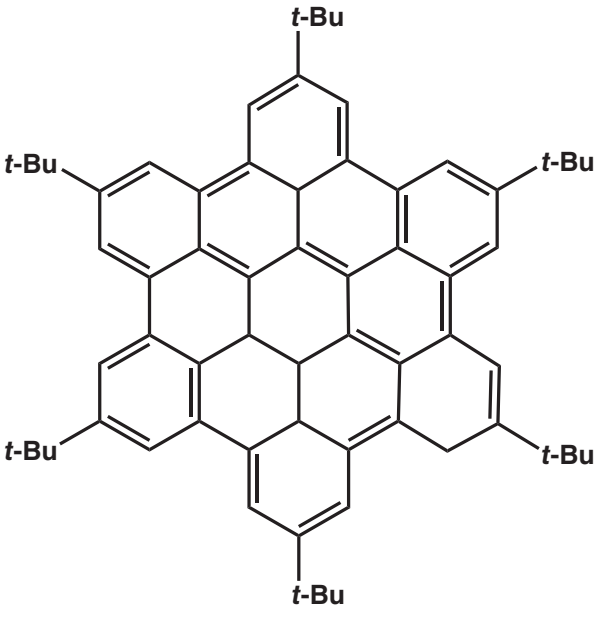

104

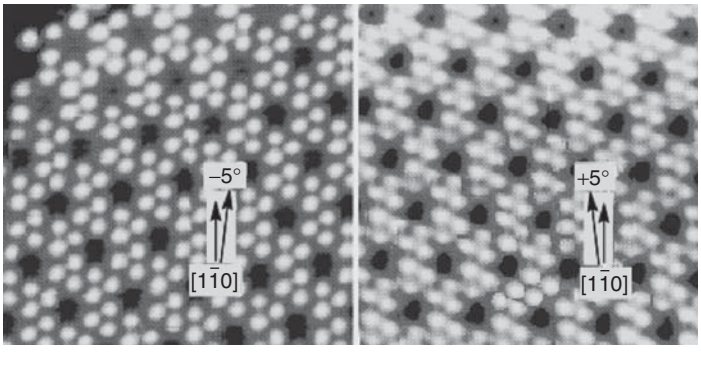

105

chirality is *induced* as the molecules enter the growing monolayer. It results from a reproducible statistical +5° or −5° *mismatch* (during the initial stages of the adsorption process) between the solution-state molecule's symmetry planes and those of the exposed metal ions upon the electrode's (**110**)-surface (see **105**).

Intermolecular lateral close-contact interactions propagate the induced chirality outward as the close-packed monolayer grows. If monolayer absorption on new (**110**)-surface electrodes is performed enough times, then there will be a 50 : 50 statistical probability of generating either right or left supramolecular assemblies. Since molecular structure is environmentally dependent, once the D_{6h}-symmetry solution-state achiral coronene enters the chiral monolayer, coronene may *no longer* express symmetry operations of the Second Kind. In other words, it must undergo a finite *skewing* deformation resulting in a desymmetrization to a chiral point group. The *maximum* chiral *pseudo*symmetry that the adsorbed molecules may express is now D_6.

Will the absorbed specimen's *pseudo*symmetry really be D_6? How about complete desymmetrization all the way to asymmetric C_1 (although to the naked eye it will appear to be D_6)? The resolution of the STM image will never provide an answer to this question, although we can say that the molecules appear to possess C_6-*pseudo*symmetry. One may ask the following: "OK, I can visually observe the disappearance of the σ_v vertical reflection planes, but what about the σ_h horizontal reflection plane?" It also has to disappear since the purpose of a reflection symmetry plane is to *exchange the space above and below* the plane. Well, the space below the plane is the Cu (**110**)-surface electrode, while the space above the plane is a small gap under the tip electrode. Obviously, these two spatial regions cannot be exchanged. We should remember that for all intents and purposes, the adsorbed molecules are very close to being ideally planar, although this is due to chemical and mechanical constraints and not by symmetry.

Before leaving this example, we should ask ourselves why was there a $\pm 5°$ *mismatch* in the first place? The only real answer to this is to state that since we have observed it in an STM-image, Nature must consider this skewing to be a low-energy arrangement between the molecular neighbors as they undergo adsorption upon the electrode's surface. How does one know this? Well, repeating the coating upon a new electrode gives either an STM observed $-5°$ mismatch or a $+5°$ enantiomorphous skewed monolayer.

The work of Held and coworkers [67] will be used as an example of chiral molecules that form supramolecular dimeric arrays whose directionality is skewed either to the right or to the left relative to that of the Cu (**110**)-surface electrode. Enantiomerically pure L- or D-serine, in its deprotonated (anionic) form, was adsorbed in separate experiments upon the electrode's surface at 300 K. The scale given in **106** (1 nm = 10 Å) testifies to the fact that the peanut-shell-type elongated features are too large to represent individual serine molecules. These structures were attributed to be *islands* of serene dimers, since circular termini can be discerned within the flat peanut shell structures. Comparison of the two images in **106** shows that the dimer's orientation with respect to the Cu (**110**)-surface depends on the molecular chirality. The dimers then aggregate into

superstructures with chiral lattices. The unit cells for the enantiomorphous L- or D-domains are shown by the b_1 and b_2 vectors drawn in the figure. Dimer and superlattice formation was explained in terms of intra- and interdimer bonds involving carboxylate, amino, and β-OH groups.

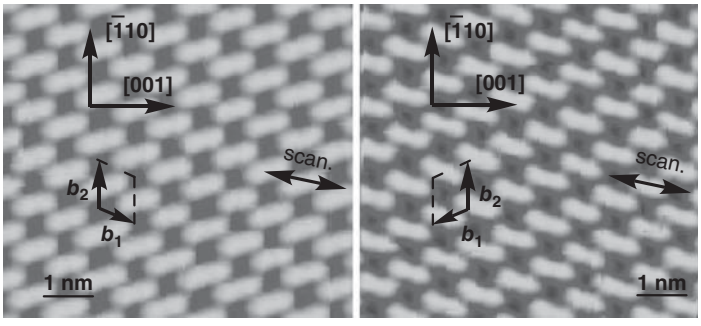

106

It is interesting to note that *spontaneous resolution* occurred when racemic mixtures were applied to the electrode surface. Domains of small ordered enantiopure L–L and D–D dimer islands with same enantiospecific elongated shapes as in the enantiopure monolayers were observed in the STM image. The formation of homochiral dimers (versus unobserved *meso*-dimers) appears to be driven by lower energy formation of homochiral dimer subunits and the directionality of interdimer hydrogen bonds.

5.5
Direct Visualization of an Enantiomer's Absolute Configuration in the Gas Phase

Dextrorotatory glucose was arbitrarily defined by Fischer [68] in 1894. Fifty years later, this lucky guess was experimentally confirmed by Bijvoet *et al.* [69] using *anomalous single-crystal X-ray diffraction* of sodium rubidium tartrate. This method has withstood the test of time to become a standard procedure for determination of absolute configuration in molecules within chiral crystals. *Vibrational CD* [70] and *vibrational Raman optical activity* [71] were then found to meet this task for liquid-phase samples. These methods require high-level computational simulation and subsequent comparison of spectral differences between two enantiomers. A new, very recent technique was reported in 2013 by Trapp, Kreckel, and coworkers [72] that is based upon foil-induced ***C****oulomb* ***e****xplosion* ***i****maging* (CEI) of individual molecules in the gas phase. In

this exciting method, isotopically labeled (*R*,*R*)-2,3-dideuteriooxirane could be visually differentiated from samples containing either the (*S*,*S*)-enantiomer or the (*RR*,*SS*)-racemic mixture. Unfortunately, the limited scope of this text prevents discussion of the various aforementioned methodologies. An (*RR*,*SS*)-descriptor means that the compound is either (*R*,*R*)- or (*S*,*S*) in handedness.

6
Symmetry Comparison of Molecular Subunits: Symmetry in Nuclear Magnetic Resonance Spectroscopy and in Dynamic NMR

6.1
Symmetry in NMR Spectroscopy

Symmetry plays a central role in spectroscopy since it produces *degeneracies* of the spectral frequencies that arise from inherently symmetry-equivalent molecular subunits (i.e., *isochronicity,* from the Greek *isos* means "equal" + *chronos* "signals"). These signals from different parts of a molecule appear at *exactly the same frequency* in a spectrum and, hence, generate a correspondingly larger integrated peak area. Symmetry-*nonequivalent* proton nuclei (*i,j*) in ^{1}H Nuclear Magnetic Resonance (NMR) spectroscopy will afford a through-bond mutual $^{n}J_{ij}$ *spin–spin* coupling constant, where n = the number of covalent bonds linking nuclei *i* and *j.* The magnitude of the *J*-values and the NMR peak patterns resulting from *geminal* and *vicinal* coupling (i.e., $^{2}J_{\mathrm{HH}}$ and $^{3}J_{\mathrm{HH}}$, respectively) provide very useful information as to the angular disposition of the *i,j*-protons, as well as the number of proton neighbors located two or three bonds away. The *Karplus relationship* [73] (**107**) for *vicinal* protons in hydrocarbons predicts large magnitude (about 10–12 Hz) $^{3}J_{\mathrm{HH}}$ coupling constants for *synperiplanar* and *antiperiplanar* H(*i*)–C–C–H(*j*) dihedral angles due to efficient *orbital overlap* within the three covalent bond coplanar segment. This coplanar arrangement enables effective interactions involving the peripheral nuclear magnets via the intervening electron magnets within the covalent bonds (all atomic particles have spin-1/2) [73]. An *orthogonal* (about 90°) dihedral angular relationship readily disrupts the interactions between bonding electrons and results in about 0 Hz $^{3}J_{\mathrm{HH}}$ minimum value [73].

An analysis of the NMR spectrum in terms of the *quantity* of different proton NMR signals, their *shapes,* and *integrated peak areas*, followed by the deconvolution of their sometimes complex coupling patterns provides a very important foundation for the structure determination of solvated molecules. However, frequency degeneracies can reduce the information content of the spectrum to such an extent that the spectral data is insufficient to be structurally useful. This conundrum can be taken to its extreme when considering the solution-state

Symmetry, Spectroscopy, and Crystallography: The Structural Nexus, First Edition. Robert Glaser.

Companion Website: www.wiley.com/go/Glaser/Symmetry

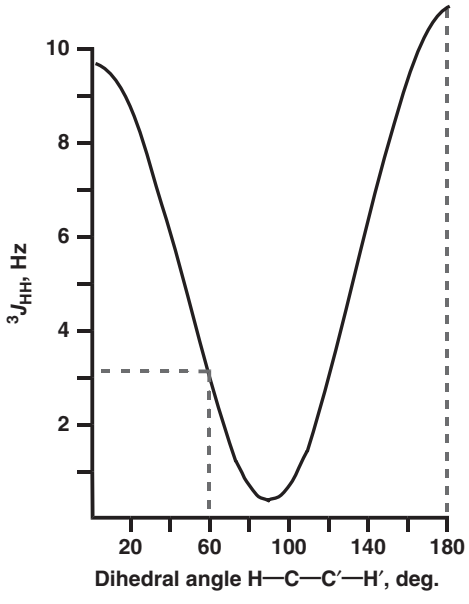

107

NMR spectra of two very high-symmetry hydrocarbons: cubane [74] **108** (C_8H_8, mp 132 °C, O_h symmetry of order 48, i.e., 48 symmetry operations) and dodecahedrane [3] **109** ($C_{20}H_{20}$, mp 430 ± 10 °C, I_h symmetry of order 120). Cubane has only a single ^1H ($CDCl_3$) resonance at δ_H 4.03 (singlet) and a single ^{13}C resonance at δ_C 47.74, while for dodecahedrane the corresponding signals are δ_H 3.38 (singlet) and a single ^{13}C resonance at δ_C 66.93. Clearly, there is a dearth of structural information to be gleaned from these spectra. Assuming that one also knows the molecular weight for each compound, then the primary conclusion is that they must have *very high symmetry.* The most important data from these spectra arises from the fact that their heteronuclear $^1J_{CH}$ direct coupling constants are markedly different: 155 Hz $^1J_{CH}$ (cubane) and 135 Hz $^1J_{CH}$ (dodecahedrane). Without performing the actual hybridization index (x) calculations [47] for the C–H bond's carbon sp^x hybrid atomic orbital (AO) (*vide ultra*), the larger $^1J_{CH}$ value for cubane clearly points to a much higher *s*-character for the carbon hybrid AO compared to that in the corresponding C–H bond in dodecahedrane. A higher *s*-character of the C–H bonds means a lower than sp^3 25% *s*-character in the C–C bonds. In other words, the more strained cubane C–C bonds have a higher than 75% *p*-character (i.e., the so-called banana bond) compared to that found in less strained dodecahedrane. This assessment is in accord with

the 161 Hz $^{1}J_{CH}$ value for cyclopropane (well known for its C–C bent "banana" bonds).

Thus, the higher a molecule's symmetry, the less structural information is contained in the spectrum. Pierre Curie in 1894 recognized that it is necessary for certain elements of symmetry to be absent in order that a particular physical phenomenon can exist (e.g., the existence of heteronuclear $^{1}J_{CH}$ spin–spin coupling for **108** and **109** versus the absence of homonuclear $^{3}J_{HH}$ coupling). "C'est la dissymétrie qui crée le phénomène," that is, phenomenon are created by a reduction in symmetry [75, 76].

108

109

6.2
Symmetry Comparison of Molecular Subunits, Topicity Relationships

Symmetry also forms the basis of comparisons between molecular subunits. The basis of these comparisons is the presence or absence of symmetry equivalence between molecular subunits having the *same number* and *type of atoms.* If the comparison is between groups within the same molecule, then it is *internal*, while one between corresponding subunits within two or more molecules is *external.* For example, solvated dodecahedrane has no difficulty in exhibiting its I_h point group symmetry having 120 symmetry operations. Twenty nuclei of each atom type are all symmetry equivalent and, hence, afford degenerate signals (*isochronous*, where *isos* and *chronos* are "equal" and "signal" in Greek). The isochronicity is due to 60 operations of the First Kind (i.e., they produce *homotopic* [76, 77] subunits, where in Greek, *homos* means "same," *topos* "neighborhood" or "environment" or "region" in the molecule). The same 20 nuclei are

also symmetry equivalent via an additional 60 operations of the Second Kind (i.e., these engender *enantiotopic* [76, 77] subunits where *enantios* in Greek means "mirror image nonsuperimposable", and *topos* "location" or "neighborhood").

The methine H-atoms in solvated *meso*-oxirane **110** are enantiotopic (isochronous) in *i*-butanol-d_{10} since the local environments around the two halves are symmetry equivalent. However, if the same oxirane is dissolved in an enantiomerically pure chiral solvent, for example, secondary-butanol [(+)-*sec*-butanol-d_{10}], then the local environments around the two half molecules now become *diastereotopic* [77]. Why? The two half molecules must be considered to be solvated within their shells of invariant handedness (+)-solvent. One may symbolically note the solvated half-molecules as "$(R_{half} \cdots +_{\text{solvent}})$" and "$(S_{half} \cdots +_{\text{solvent}})$." These "$(R_{half} \cdots +_{\text{solvent}})$" and "$(S_{half} \cdots +_{\text{solvent}})$" solvated halves are now diastereotopic (i.e., different), see **111**. The magnetic environments of nuclei within one solvated half molecule will now just be "very very similar" but not "identical to" those of corresponding nuclei in the other solvated half molecule. This certainly does NOT imply that *meso*-oxirane will now exhibit a markedly different geometry when it exists in a chiral environment as opposed to one that is achiral (after all, the molecule is rigid). It just means that the molecular geometry in this new environment will now be "ever so slightly distorted" so that the entire molecule becomes chiral (asymmetric) rather than being *meso.* Changing the solvent to pure (−)-*sec*-butanol enantiomer will afford the enantiomerically distorted oxirane skeleton. For the half molecules to be enantiotopic, one would have to use a racemic solvent, for example, "$(R_{half} \cdots +_{\text{solvent}})$" and "$(S_{half} \cdots -_{\text{solvent}})$." Therefore, "what something is depends on where you put it." [76] In other words, the (+)-*sec*-butanol solvated nuclei in the (*R*,*S*)-halves reside within diastereotopic (different) magnetic environments compared to the corresponding nuclei in the other half. Hence, the corresponding pairs of nuclei are predicted to be *anisochronous* (in Greek *an*, *isos*, and *chronos*, respectively, mean "not," "equal," and "signal" – as in *chronometer*, a clock that strikes/signals the hour) since they can never ever produce degenerate signals. Moreover, one should not be surprised if a $^3J_{\text{HH}}$ *synperiplanar* magnitude coupling constant is now observed between the two methine protons. Question: does your NMR magnet have a strong enough field strength to resolve two diastereotopic signals exhibiting very close chemical shifts? This instrumental problem has nothing to do with the *inherently different* solvated half molecules. A very high basis set molecular orbital or density functional calculation for *meso*-**110** within an *i*-butanol-d_{10} achiral solvent box will show symmetry equivalence for the "$(R_{half} \cdots i$-butanol-$d_{10})$" and "$(S_{half} \cdots i$-butanol-$d_{10})$" solvated halves since pairs of orbitals or functionals are inherently symmetry equivalent. However, similar solvent shell calculations will show a loss of molecular orbital or density functional symmetry equivalence for the homochiral solvated halves of **111**.

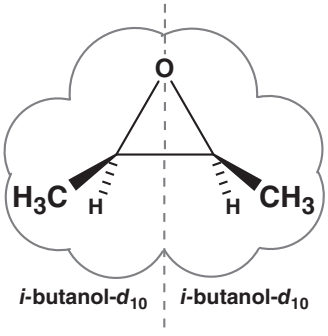

110

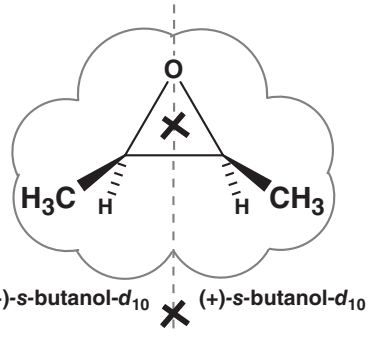

111

Finally, the constitutions of the two methyl groups in within the (+)-*sec*-butanol-d_{10} [$\underline{\boldsymbol{CD}_3}$CD(OD)CD$_2$$\underline{\boldsymbol{CD}_3}$] solvent itself are obviously different and thus symmetry nonequivalent. Therefore, their anisochronicity arises from the fact that they are *heterotopic.*

Diastereotopism in rigid molecules is readily visualized and understood. For example, there are five methylene carbons in the *N-cyc*-propylmethyl substituted amino-alcohol scopine moiety of scopolamine and its derivatives (e.g., the anti-cholinergic, spasmolytic agent **112**, Refcode CPRSBR [78]). The asymmetry of the molecule results in five sets of different methylene-proton geminal pairs. There are two diastereotopic pairs of methylene carbons: C(2)/C(4) and C(3′)/C(3″). Upon hydrolysis of the ester function, these pairs of carbons now will become *enantiotopic* due to the reemergence of the amino-alcohol's time-averaged σ-plane. Now, H(2*ax*)/H(4*ax*) are an enantiotopic set and are *diastereotopic* to their H(2 *eq*)/H(4 *eq*) homotopic geminal partners.

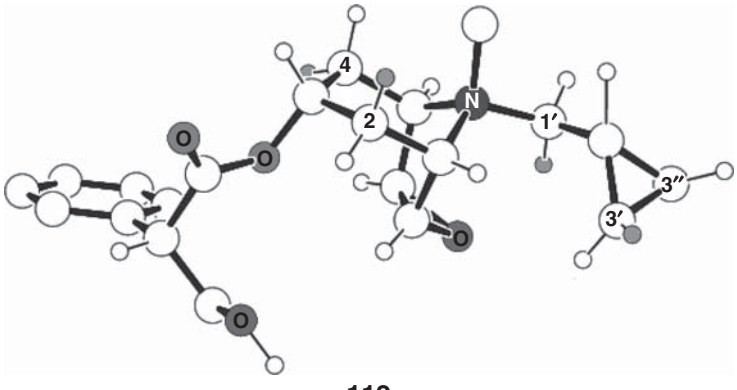

112

6.3
Dynamic Stereochemistry, Dynamic Nuclear Magnetic Resonance Spectroscopy (DNMR)

Dynamic stereochemistry concerns the *rapid equilibration* of two or more isomers/conformations/rotamers under conditions in which structural measurements are made. These measurements are weighted time-averages of those values from the individual symmetry-nonequivalent molecular constituents. Dynamic nuclear magnetic resonance (DNMR) is closely related to the aforementioned phenomenon. Variable-temperature NMR spectra are recorded in order to ascertain the energy of activation of the structural interconversion process. An important characteristic of NMR spectra made under these conditions is that the peak's linewidth (width-at-half-height, $W_{1/2}$) varies according to the temperature-dependent interconversion *kinetics.* NMR has a measurement "*timescale,*" which can be likened to a camera's shutter speed. For a set "shutter speed," *very slow* interconversion kinetic rates enable each of the two interconverting molecular species to be separately observed and their respective *narrow linewidth* peaks integrated. When the interconversion kinetics are *very fast* compared to the "shutter speed," only a single *narrow linewidth* weighted time-averaged peak is observed for the two interconverting peaks. DNMR concerns kinetic interconversion rate regimes that are intermediate to those of the two aforementioned extrema. In other words, the shutter speed and the process' half-time constant are of approximately the same order of magnitude. It is in this particular kinetics region that the peaks become broadened and change their shape and number. To make the variable temperature line-broadening phenomenon clearer, a series of very typical dynamic NMR plots between a ***generic*** exchanging pair of **H1** and **H2** labeled protons are presented in illustration **113.**

The average interaction distance between solvent-shell molecules and solvent-exposed nuclei is temperature dependent. Since solvent molecules also contain magnetic nuclei, the solvated molecule's chemical shift values will change slightly as a function of temperature. The kinetic regime in which two exchanging nuclei H(1) and H(2) change only their temperature-dependent δ-values while keeping their narrow line-shapes invariant is called the ***S**low **E**xchange **L**imit* or SEL. The NMR spectroscopist searches for low sample temperatures where the Larmor frequency difference between the exchanging nuclei, that is, $\Delta\nu_o = |\nu_{H1} - \nu_{H2}|$, appears to be constant. This seemingly invariant $\Delta\nu_o$ value is what characterizes the SEL. By the way, the experimental observation that nonsolvent exposed nuclei (e.g., those participating in internal hydrogen bonding) show considerably lower temperature dependence than solvent exposed nuclei is expected, logical, and true. Plots **113** were all measured at temperatures higher than the SEL.

The basic goal behind a series of variable-temperature NMR experiments is to determine the one particular temperature at which two diastereotopic anisochronous H(1) and H(2) signals first merge into one *very broad*

time-averaged H(1,2) signal. This is called the *coalescence temperature* (T_c). Within just a *one degree* temperature *increase* to T_c, the line-shapes dramatically change from a very high valley between two very broadened **H1** and **H2** peaks into a single broad *plateau-like* signal shape.

The lowest plot shows two very broadened peaks measured at 72.0 °C in the *slow magnetic site exchange broadening kinetics region.* Coalescence of the two signals occurs at $T_c = 75.0$ °C. Above this temperature, the plots of the single time-averaged *fast magnetic site exchange broadened* signal show progressively narrower $W_{1/2}$ values as the temperature is raised to 97.5 °C. The plot of the once-again narrow $W_{1/2}$ single averaged (***F**ast **E**xchange **L**imit*, FEL) signal also does not appear in illustration **113.**

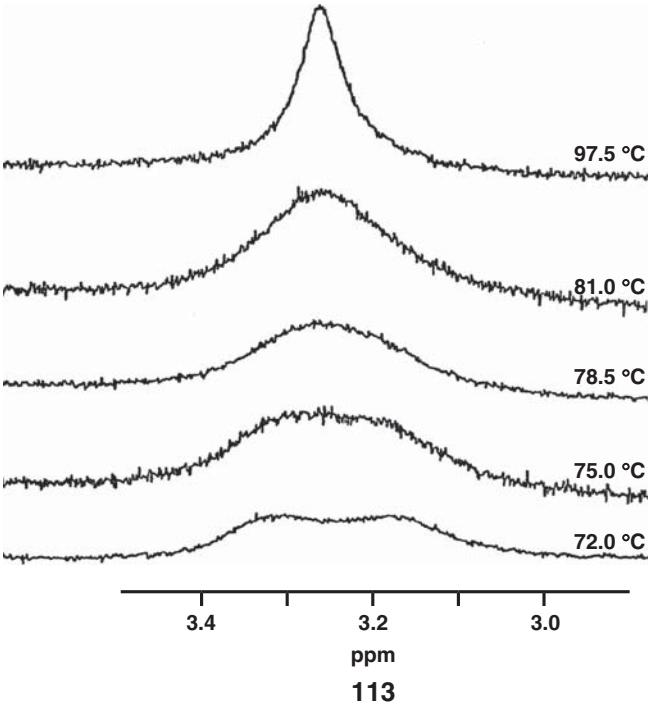

113

The variable-temperature DNMR experiments allows one to calculate k_{ex} (the kinetic exchange rate constant in s^{-1}) from the useful expression $k_{ex} = \pi\Delta\nu_o/\sqrt{2} = (2.22)(\Delta\nu_o)$ for the exchange process *at that particular T_c temperature* (283 K). From k_{ex}, the calculated $\Delta G^{\ddagger} = -RT_c \ln K_{ex}$ *energy of activation* for the exchange process is found. Later on, we will use DNMR measurements to determine $\Delta G^{\ddagger}$ for the exchange of two enantiomers. A method to determine

the exchange rates at temperatures *other than* T_c is based upon line-shape fitting algorithms.

6.4 Use of Permutations in DNMR for Topomerization-, Enantiomerization-, and Diastereomerization-Exchange Processes

We will propose a protocol to make it easier to follow the *dynamic interchange* of specific protons (e.g., **H1** and **H2** in generic achiral molecule **114**, see Figure 6.1). These protons reside in defined magnetic environments (e.g., ***a*** and ***b***) that change into *externally enantiotopic and diastereotopic* environments in rotamers ***I–III***. *Step 1:* label the methylene protons in rotamer *I* as **1** and **2.** *Step 2:* identify these same protons in rotamers *II* and *III*, and then label them also as **1** and **2**, to keep track of their structural identities. *Step 3:* inspect the original molecule (rotamer *I*) and decide if it is symmetrical (*yes*, *indeed it has* C_s*-symmetry*). *Step 4:* see if geminal protons **1,2** are symmetry equivalent (*yes*, *they are internally enantiotopic*). *Step 5:* label rotamer *I*'s *enantiotopic* magnetic environments with *enantiomeric* pairs of letters (***a*** and $\overline{\boldsymbol{a}}$). Crystallographers use barred letters and numbers to describe enantiomeric/enantiotopic molecules and subgroups. *Step 6:* inspect rotamer ***II***, and ascertain if it is a *homomer,* an *enantiomer*, or a *diastereomer* of rotamer ***I*** (*obviously*, *it is a diastereomeric rotamer*). *Step 7:* ascertain if rotamer *II* is symmetrical or not (*it is not*). *Step 8:* since it is an *asymmetric* diastereomer, then assign new *magnetic environment* letters to each unique region (***b*** and ***c***). *Step 9:* inspect rotamer ***III*** and ascertain if it is a *homomer,* an *enantiomer,* or a *diastereomer* of rotamers ***I***,***II*** (*it is the enantiomer*

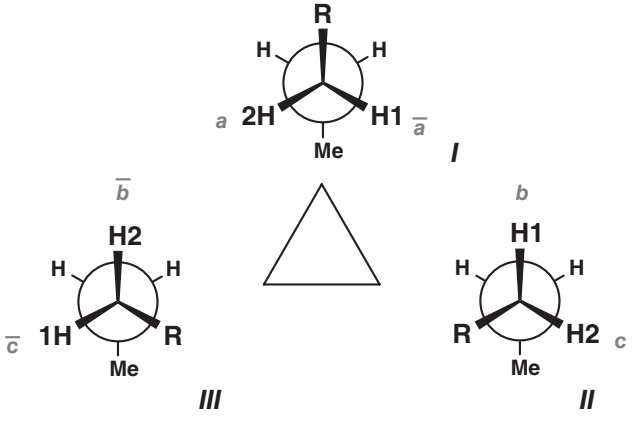

Figure 6.1 Interconversion of magnetic environments of *enantiotopic* geminal protons **H1**, **H2** in rotamers ***I–III*** of achiral molecule **114**.

*of rotamer **II***). *Step 10:* assign enantiomeric letters ($\overline{\boldsymbol{b}}$ and $\overline{\boldsymbol{c}}$) to the corresponding *externally enantiotopic* environments in ***III***.

Now that all the magnetic environment sites have been defined/labeled in rotamers ***I–III,*** start with H**1** and ascertain its *new* magnetic environment sites when it now resides within rotamer ***II*** (*it is in **b***). Next, in what environment is **H1** when in rotamer ***III***? (*it is in* $\overline{\boldsymbol{c}}$). The rotational exchange process for **H1** has caused it to dwell within three magnetic environments. A permutation for **H1**'s transit through these environments may be written mathematically as ($\overline{\boldsymbol{a}}, \boldsymbol{b}, \overline{\boldsymbol{c}}$). The meaning of this statement is: "$\overline{\boldsymbol{a}}$ becomes ***b***, then ***b*** becomes $\overline{\boldsymbol{c}}$, and finally $\overline{\boldsymbol{c}}$ reverts back to $\overline{\boldsymbol{a}}$" (since the parentheses make the exchange a *closed system*). *Step 9:* write down the site permutations for protons **H1** and **H2** in the three rotamers (($\overline{\boldsymbol{a}}, \boldsymbol{b}, \overline{\boldsymbol{c}}$) for **H1** and ($\boldsymbol{a}, \boldsymbol{c}, \overline{\boldsymbol{b}}$) for **H2**). Comparison of the two site permutations will show them to contain the same three enantiomeric pairs of site letters (and we are not concerned about their order of appearance). Thus, **H1** and **H2** in the freely rotating exchange of rotamers ***I–III*** are *dynamically enantiotopic*, that is, they are isochronous at the FEL. The exchange process for **H1**,**H2** is called a *topomerization* (exchange of place).

Next, consider the same geminal **H1**, **H2** pair within chiral molecule **115** (see Figure 6.2). Analyze the dynamic stereochemistry of these three rotamers in the same manner as for **114**. First of all, rotamers ***I–III*** are related to each other as three diastereomers. Secondly, they are all asymmetric. This means that their magnetic site environments are all different. As a result, three pairs of diastereomeric letters *a–b*, *c–d*, and *e–f* are used (one pair per rotamer). Now, follow the magnetic site exchange permutations as **H1** transits all three rotamers: (***a***,***c***,***e***) versus that for **H2:** (***b***,***d***,***f***). These pairs of weighted time-averaged magnetic environments are clearly different. Protons **H1** and **H2** are said to be *dynamically*

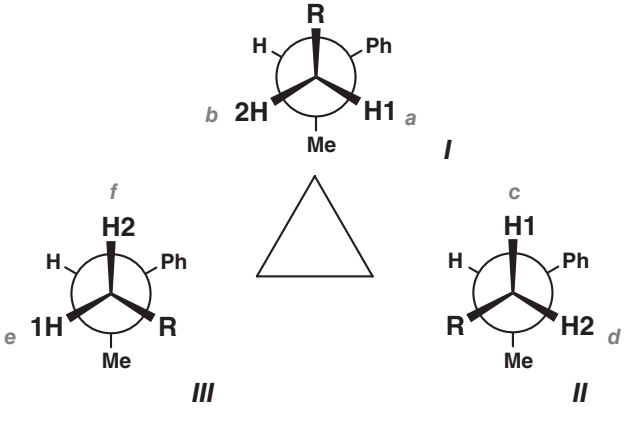

Figure 6.2 Interconversion of magnetic environments of *diastereotopic* geminal protons **H1**, **H2** in rotamers ***I–III*** of a chiral molecule **115**.

diastereotopic therein they travel through the cycle of three rotamers. Therefore, even under conditions of complete rotational freedom, the **H1** and **H2** averaged chemical shifts are anisochronous at the FEL.

Let us consider the very common process of cyclohexane ring-inversion. The pairs of ring-invertomers **116** and **117** are homomers, and the geminal protons *equatorial*-**H1** and *axial*-**H2** therein are diastereotopic. Using the same aforementioned protocol, the magnetic site permutations for the invertomer exchange are (***a***, ***b***) for **H1** and (***b***, ***a***) for **H2**. Thus, the exchanging protons in **116** and **117** are *dynamically homotopic.* They are isochronous at the FEL but anisochronous and of equal intensities at the SEL (since homomeric invertomers are involved). Again, this exchange process is also called a *topomerization*.

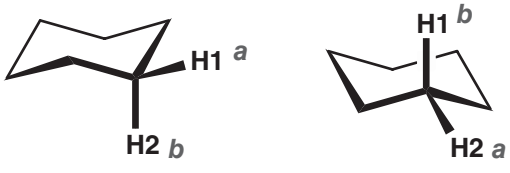

116 **117**

Next, we will consider **H1**, **H2** nuclei in the interconversion between the two enantiomeric *cis*-1,2-dichlorocyclohexane invertomers (**118**, **119** Refcode TARWAL [79], *cis*-1,2-dichlorocyclohexane solvate adduct). As before, since **H1**, **H2** are *internally diastereotopic,* we then use two new different site letters (e.g., ***a*** and ***b***). If the magnetic environment sites in **118** are labeled as ***a*** and ***b***, then the magnetic environment sites in **119** bear $\overline{\boldsymbol{a}}$ and $\overline{\boldsymbol{b}}$ notations. The permutation for **H1** is (***a***, $\overline{\boldsymbol{b}}$), while that for **H2** is (***b***, $\overline{\boldsymbol{a}}$). Notice that the same site letters are used in each set, but $\overline{\boldsymbol{a}}$ appears in one set and $\overline{\boldsymbol{b}}$ in the other. Thus, nuclei **H1**, **H2** are *dynamically enantiotopic* at the FEL. They are isochronous at the FEL but anisochronous and of equal intensities at the SEL. This ^{1}H *topomerization* exchange process has a special name (an *enantiomerization*).

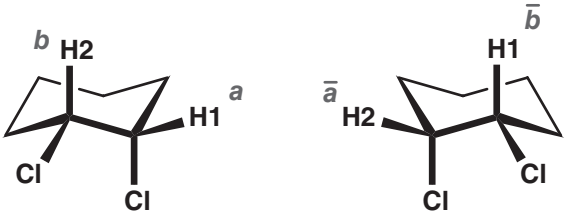

118 **119**

Now, the **H1**, **H2** nuclei will undergo exchange in two diastereomeric C_2-symmetrical *trans*-1,2-dichlorocyclohexane invertomers **120** and **121**. Each invertomer is chiral and contains two internally homotopic **H1**, **H2** nuclei. So, we use identical magnetic site letters (e.g., ***a***,***a*** for **120** and ***b***,***b*** for **121**). The

permutation for **H1** is (***a***, ***b***), while that for **H2** is also (***a***, ***b***). Thus, nuclei **H1**, **H2** are also *dynamically homotopic* at the FEL. They are isochronous at the FEL but anisochronous and of unequal intensities at the SEL. This **H1**, **H2** *topomerization* exchange process also has a special name (a *diastereomerization*).

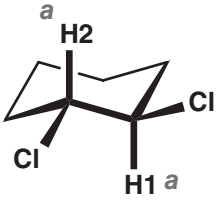

120

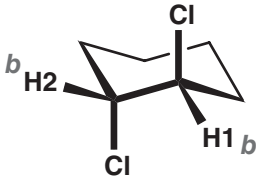

121

Recognition of *diastereotopism* is far more challenging when considering *flexible chiral molecules* having unconstrained C–C bond rotation. A typical case in point is the calcium channel blocker, cardio-vasodilator drug (2*S*,3*S*)-(+)-diltiazem·HCl (Refcode CEYHUJ01, **122**) [80]. The molecule is asymmetric and contains two stereogenic seven-membered ring adjacent methine-carbon atoms with a *cis*-arrangement of their protons. There is a simple symmetry argument that states that there can be absolutely no symmetry relationship between molecular subunits within an asymmetric molecular structure. Therefore, if we consider the

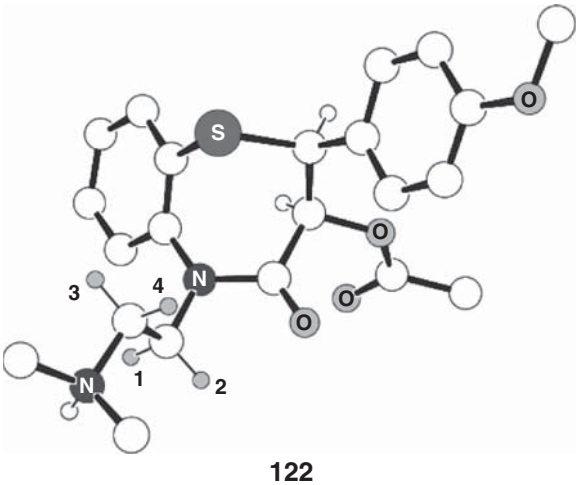

122

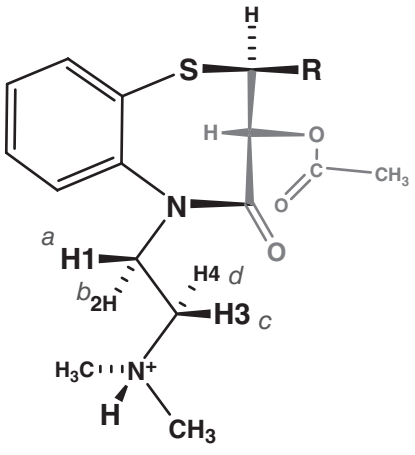

***exo*-123**

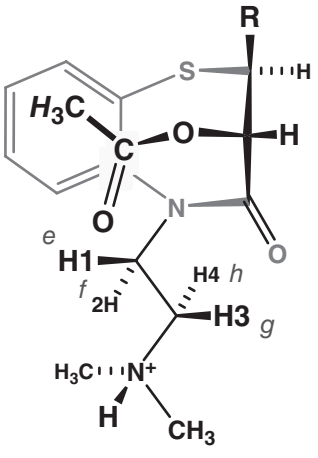

***endo*-124**

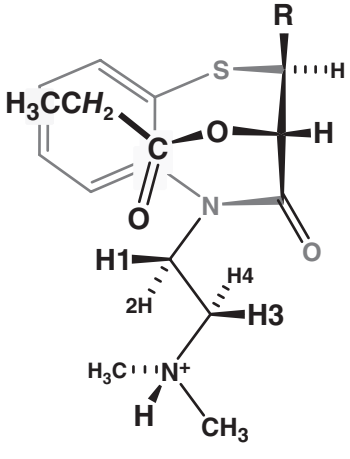

***endo*-125**

$NC\underline{\boldsymbol{H}}_2C\underline{\boldsymbol{H}}_2N^+(H)Me_2$ side chain in **122**, it should come as no surprise that *geminal* pairs of protons or methyl carbons are diastereotopic and, hence, exhibit *anisochronous* (unequal, i.e., different) NMR signals (δ, DMSO-d_6): 4.14 [*m*, 1H, $N_{amide}C\underline{\boldsymbol{H}}$] and 4.13 ppm [*m*, 1H, $N_{amide}C\underline{\boldsymbol{H}}'$], 3.45 [*m*, 1H, $N^+C\underline{\boldsymbol{H}}$], and 3.10 [*m*, 1H, $N^+C\underline{\boldsymbol{H}}'$] [81].

Unfortunately, the observed NMR anisochronism from *flexible chains* of diastereotopic geminal nuclei is often erroneously attributed to "sterically hindered bond-rotation." Thus, in discussing the ^{1}H NMR spectrum of

diltiazem·HCl (**122**) in DMSO-d_6 it was written: "*We propose hydrogen-bonding of the ammonium group to the Cl⁻, observed in the crystal, remains in solution and the slow rotation of the bulky side chains renders the two methyl groups magnetically non-equivalent.*" [80] This was argued despite the fact that DMSO is a very polar solvent so that the chloride anion is solvent separated. As said earlier, the geminal nuclei in **122** are anisochronous simply because they are *diastereotopic* (i.e., different)! The point is this, try as one may, no symmetry operation can be envisioned that will equivalence them. The fact that the side chain is completely rigid or very flexible to rotate/twist is *completely irrelevant* to this symmetry argument. If the side chain is flexible enough to show mobility, then each geminal proton transits through a *different* permutation cycle of averaged magnetic environments, and if this is *fast on the NMR timescale,* then we will observe *two different* (population) weighted time-averaged NMR signals.

After the aforementioned quote was published, Glaser and Sklarz [81] later showed that dissolution of *boat*-conformation crystals of diltiazem·HCl (**122**) afforded about 12 : 1 mixture of two diastereomeric solvated ring-invertomers (*exo*-acetyloxy **123**, crystal structure) and (*endo*-acetyloxy **124**), respectively, at ambient temperature SEL on the NMR timescale. The side chain magnetic site permutations are **(*a*,*e*)** for **H1**, **(*b*,*f*)** for **H2**, **(*c*,*g*)** for **H3**, and **(*d*,*h*)** for **H4**. From this it is clearly seen that geminal protons within each of the methylene groups are *dynamically diastereotopic* even under conditions of *fast* free rotation and *slow* invertomer exchange. This is all the explanation needed to explain their anisochronicity in the NMR spectrum.

Postulation of the –OC(=O)C$\underline{\boldsymbol{H}}_3$ proton's residence directly above the benzo-ring's shielding cone very adequately accounted for their 0.49 ppm shift closer to TMS for the *minor species* in the ^{1}H NMR spectrum. It was suggested that a *propionyloxy* [–OC(=O)Et] analogue of diltiazem be prepared to provide an additional proof. Based upon the ***endo*-124** molecular model, ethyl-group diastereotopic methylene-protons [–OC(=O)C$\underline{\boldsymbol{H}}_2CH_3$] would now be disposed above the shielding cone center but the terminal methyl group would suffer lowered shielding due to displacement toward the cone's side (see *boat axial*-OC(=O)Et-*invertomer* ***endo*-125** model). The prediction turned out to be correct since the diastereotopic methylene protons were indeed shifted 0.55 and 0.47 ppm toward TMS in propionyloxy ***endo*-125** while the methyl protons were shifted by a lesser 0.31 ppm amount, as predicted.

The aforementioned examples emphasize that enantiotopicity or diastereotopicity of *methylene-proton* NMR signals provides a very *sensitive probe for molecular chirality.* Mislow and coworkers [82] demonstrated the erroneous attribution of "restricted rotation" for an inherently diastereotopic geminal pair within an asymmetric molecule by preparing (2-(2-naphthyl))-5-methylhex-3-yn-2-ol **126**, and measuring anisochronous *i*-propyl methyl signals in both its ^{1}H and ^{13}C{^{1}H} NMR spectra, where {^{1}H} = broad-band ^{1}H decoupling. They showed, once and

for all, that the observed anisochronism arose from *intrinsic diastereotopism*, and had nothing to do with the kinetic rate of rotation about single bonds (or triple bonds in this case) [82].

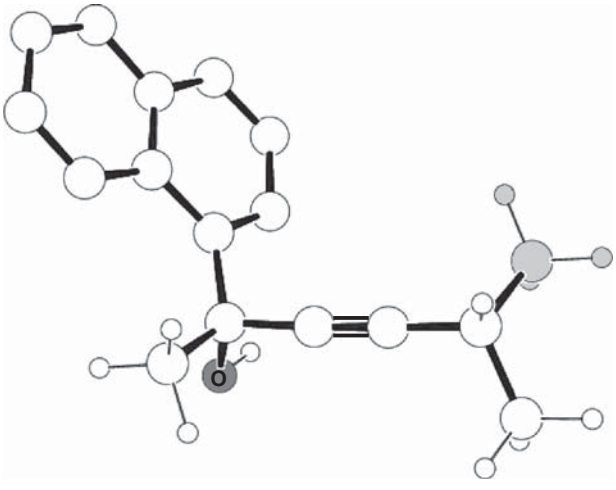

126

7
Prochirality, Asymmetric Hydrogenation Reactions, and the Curtin–Hammett Principle

7.1
Prochirality of Enantiotopic Subunits

Consider two methylene protons in a generic *achiral* RC***H***$_2$R′ molecule (where R ≠ R′ ≠ H, **127**) that undergoes a free radical–initiated bromination reaction using *N*-bromosuccinimide. Bromine substitution of one of the geminal proton pair will produce a *chiral* RCHBrR′ product, while substitution of the second proton partner will yield the enantiomer. These hydrogens are known as *prochiral* protons (since the parent achiral molecule is just one reaction away from being chiral). Each can be assigned a specific descriptor should we desire to unequivocally refer to one or to the other. In the case where the first atom in R has higher Cram, Ingold, Prelog (CIP) atomic number priority than that in R′, arbitrarily choose one of the two protons. The very act of choosing one of the two prochiral protons has increased its CIP priority over its chemically identical, but unselected, partner (see **128** and **129**). The assignment of *proR* or *proS* descriptors (**130**) is

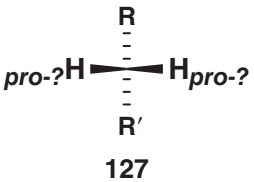

127

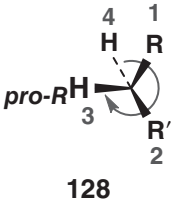

128

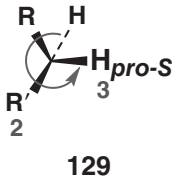

129

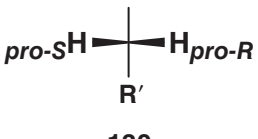

130

Symmetry, Spectroscopy, and Crystallography: The Structural Nexus, First Edition. Robert Glaser.

Companion Website: www.wiley.com/go/Glaser/Symmetry

then according to the accepted (*RS*) CIP priority method. These descriptors can also be applied in manuscripts if one simply desires to unequivocally specify one of two identical *G*-structural units in an achiral R–C($\underline{\boldsymbol{G}}_2$)–R′ molecule, for example, the two methyl groups in *i*-Pr-benzene.

Enantiotopic faces (but not homotopic faces) of carbonyls may also be assigned *prochiral* descriptors so that one can unequivocally specify one particular face over the other. Remember the tropicity of the spiral cloud patterns of tropical storms? If they appear to be anticlockwise when viewed from above by a weather satellite, then a ground observer will see them as clockwise. The same situation exists for a planar region of a molecule. Drawing **131** illustrates the assignment of a *re* (also for *rectus*) descriptor for butan-2-one's upper ketone-face (Refcode LASLAU [83] methylethylketone-C=O hydrogen-bonded to C$\underline{\boldsymbol{H}}_2Cl_2$ clathrate).

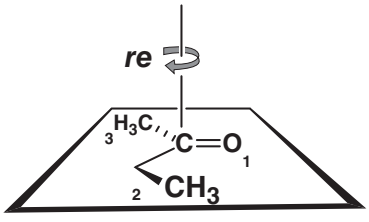

131

What about prochiral descriptors for double-bond faces? In the same manner as handling double and triple bonds in the CIP priority method, to define the top face of vinylic C(α) in **132** ((*Z*)-*N*-acetyldehydrophenylalanine dihydrate, Refcode BAHNED [84]), an extra carbon atom is affixed to the *nonselected* C(β) vinylic carbon since C(α) "*sees the C(β) atom twice*" (one for each of the two bonds within the double bond). Now, C(β) has four substituents ligated to it, in the same manner as the other two substituents on C(α). Using CIP priorities, the upper face of trigonal C(α) is designated as *re.* The process is now repeated for the C(β) neighbor (**133**), and it is assigned a *si* descriptor. But, what is the order of the two descriptors to be assigned to the upper face? Is it *re-si* or *si-re*? This is solved by searching for the highest CIP priority among total four *original* substituents ligated to the two vinylic carbon pairs. Obviously, C(α)'s nitrogen wins out over two carbons and one proton. Therefore, C(α)'s *re* descriptor takes precedence over the *si* for C(β), and the upper face is now defined as the *re-si* face (**134**).

Re, si descriptors can also be assigned to prochiral diastereotopic faces. In the case of the chiral natural product, (*S*)-camphor (**135**, Refcode UGAHUF [85]), such descriptors are unnecessary since the simpler *exo, endo* terms will suffice. However, they definitely are important for the (*R*)-phenethyl-*Z*-α-acetamidocinnamate ester **136**. The differential steric hindrance to **136**'s

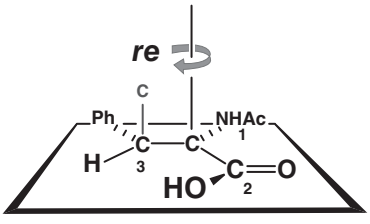

132

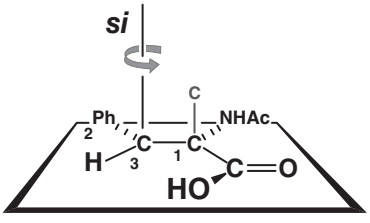

133

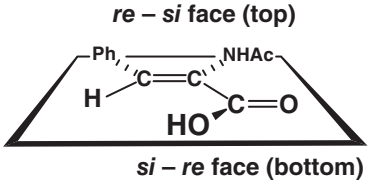

134

diastereotopic faces is not visually evident (since one does not know the preferred conformation of the chiral alkoxy group), but the faces are different.

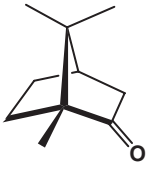

135

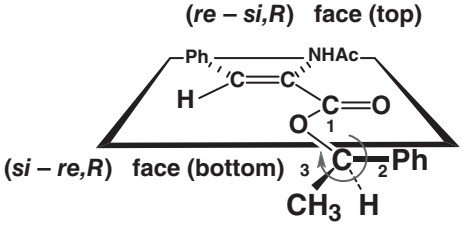

136

7.2
Homogeneous Hydrogenation by Rhodium^{I}/Achiral Diphosphine Catalysts Differentiates the Diastereotopic Prochiral Faces of Olefins

The accepted mechanism for $[Rh^{I}(DIPHOS)S_2]^{+}\cdot BF_4^{-}$ catalyzed hydrogenation of olefins is depicted in Figure 7.1, where DIPHOS = $Ph_2P(CH_2)_2PPh_2$ and S = solvent, for example, MeOH. For the purpose of stereochemical illustration, a *trans*-dideutero-olefin is bound to the active species in a π-complex (middle-right structure). The following step is dihydrogen activation to yield the dihydrido/Rh^{III}(π-complex). *This oxidative addition is the* ***slow step*** *of the catalytic cycle.* The next step is a hydride transfer to afford a σ-bonded

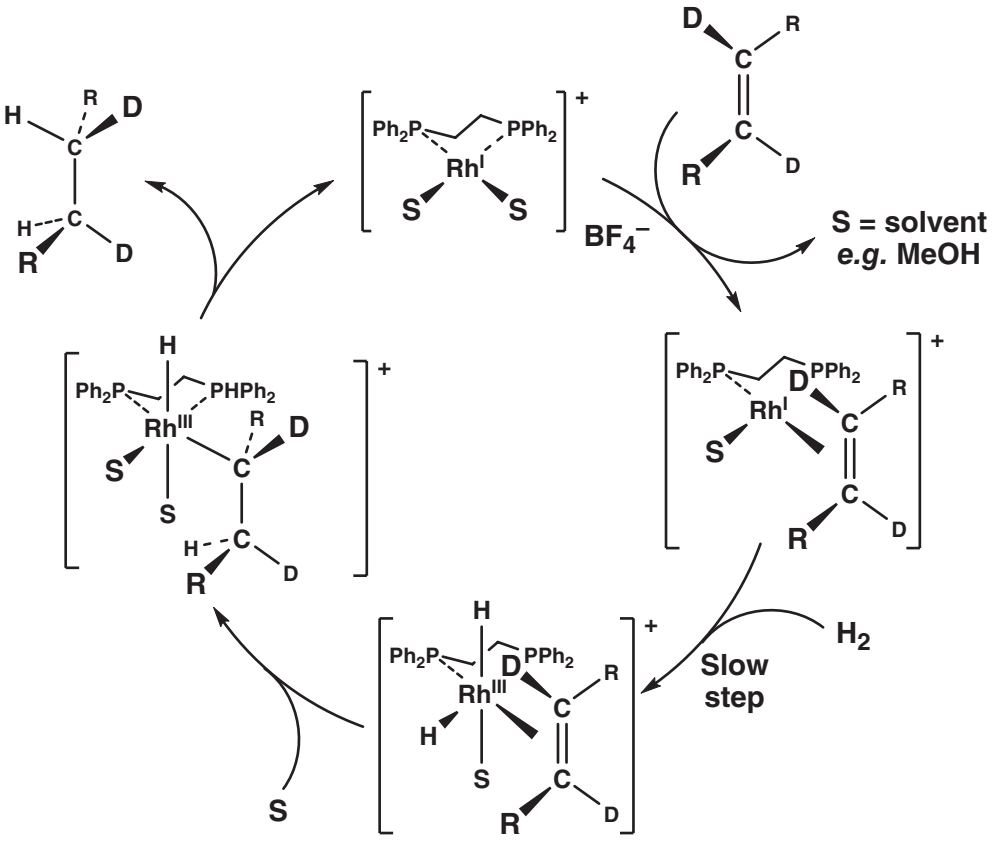

Figure 7.1 The catalytic cycle for the homogeneous *cis*-hydrogenation of the (*re-re*) enantiotopic face of a generic *trans*-olefin yields a *cis*-(*S,S*)-alkane-d_2 via a $[Rh^{I}/(diphosphine)]^{+}BF_4^{-}$ complex.

alkyl group/Rh^{III}(monohydride) intermediate (middle-left structure). *Reductive elimination* of the dideutero-alkane to reform the reactive species is the final step. A *cis*-reduction of the olefin is the net result of the process.

The catalytic cycle shown in Figure 7.1 arbitrarily depicts a π-complex of the olefin's (*re-re*)-enantiotopic face. However, the rate-determining oxidative addition step energy of activation is identical whether the (*re-re*)- or (*si-si*)-enantiotopic face is bound to the metal. Why? The two faces of the olefin are symmetry equivalent and, hence, exchangeable by reflection. The net result will be the production of an (*RS,RS*)-alkane *racemic mixture* product. Remember that the (*RS,RS*)-descriptor means that the compound either is (*R,R*) or (*S,S*) in handedness. Similarly, an (*RS,SR*)-descriptor means that the compound is either (*R,S*) or (*S,R*) in handedness.

Glaser *et al.* [86] demonstrated that diastereotopic prochiral faces in *Z*-α-acetamidocinnamate chiral esters of (−)-(1*R*,3*R*,4*S*)-*p*-menthan-3-ol (**137**) or (−)-(1*S*,2*R*,4*S*)-borneol (**138**) are differentiated by the achiral $[Rh^{I}/(DIPHOS)/(solvent)_2]^+$ active species since they form a pair of diastereomeric π-complexes in *thermodynamically controlled* unequal amounts, for example, $[Rh^{I}/(DIPHOS)/(re\text{-}si,2R\text{-}\pi\text{-eneamide ester})]^+$ and $[Rh^{I}/(DIPHOS)/(si\text{-}re,2R\text{-}\pi\text{-eneamide ester})]^+$. However, since the *kinetically controlled* slow step of the reaction is dihydrogen activation, unrelated unequal amounts of two *cis*-hydrogenated products, (***α*S**,2*R*)- and (***α*R**,2*R*)-α-acetamidophenylalanine diastereomeric esters, are also produced. The achiral diphosphine was part of a homologous series of $Ph_2P(CH_2)_nPPh_2$, that is, achiral diphosphines where $n = 3-6$. The (2*R*)-bornyl (***α*S**,2*R*)- and (***α*R**,2*R*)-diastereomeric reduction product mixtures were quantified by achiral gas chromatography and showed *diastereomeric excesses* of 4.9% (***α*S**,2*R*) ($n = 3$), 9.1% (***α*R**,2*R*) ($n = 4$), 13.6% (***α*R**,2*R*) ($n = 5$), and 12.0% (***α*R**,2*R*) ($n = 6$). Note the change in handedness for the major reduction product with $Ph_2P(CH_2)_3PPh_2$. What does the term *12% diastereomeric excess* signify? Answer: a 56.0% (***α*R**,2*R*) and 44.0% (***α*S**,2*R*) diastereomer ratio ($n = 6$). Is this result predictable? Not really, unless we know or guess the structures of the ephemeral transition states.

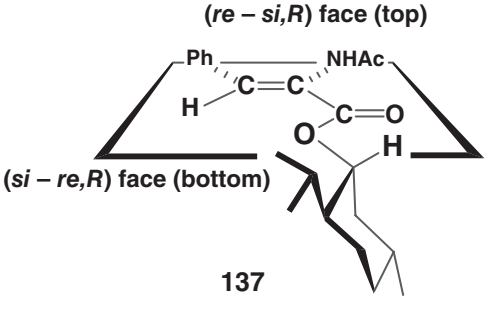

137

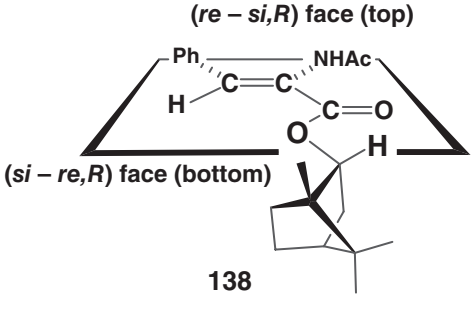

138

7.3 Homogeneous Hydrogenation by Rhodium^{I}/(Chiral Diphosphine) Catalysts Differentiates the Enantiotopic Prochiral Faces of Olefins: The Curtin–Hammett Principle

Asymmetric hydrogenations with a C_2-symmetry chiral diphosphine-bearing *stereogenic carbons* (DIOP, **139**) were reported in 1971–1972 by Kagan and coworkers [87–89], see structure of [Rh^{I}H/(*S*,*S*-DIOP)$_2$] complex (Refcode HOXLRH [90]). In 1975, Knowles *et al.* [91] developed DIPAMP (**140**), a C_2-symmetry chiral diphosphine with *stereogenic phosphorus* atoms, see [Rh^{I}/*R*,*R*-DIPAMP/η^4-cycloocta-1,5-diene] complex (Refcode IBOZAB [92]). Knowles along with Ryoji Noyori and K. Barry Sharpless shared the 2001 Nobel Prize in Chemistry for their seminal work in asymmetric catalysis. Earlier that same year, Henri Kagan along with Ryoji Noyori and K. Barry Sharpless were awarded the 2001 Wolf Prize in Chemistry in Jerusalem. These diphosphines, respectively, form seven- and five-membered chelating rings with a [Rh^{I}/(μ-Cl)/(COD)]$_2$ precursor, where COD = cycloocta-1,5-diene. DIOP's advantage is that it was based upon readily available (+) or (−)-tartaric acid *synthons,* but its disadvantage is the formation of a less rigid seven-membered chelating ring.

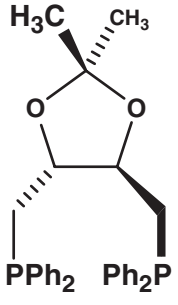

139

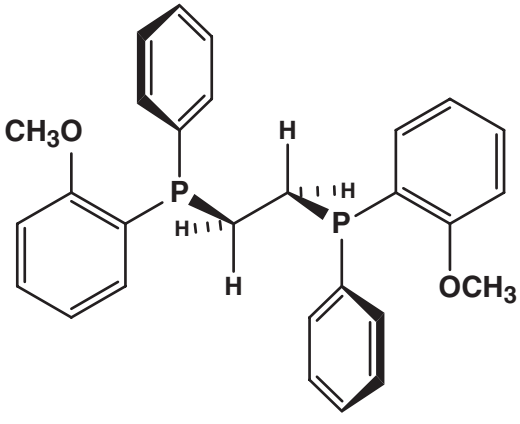

140

The aforementioned (−)-menthyl (**137**) or (−)-bornyl (**138**) chiral ester substrates were hydrogenated with either (+)- or (−)-DIOP (**139**) to observe the effect of *constructive* (match) or *destructive* (mismatch) steric fit involving the chiral interactions of both substrate and catalyst. With the (−)-(3*R*)-menthyl *Z*-α-acetamidocinnamate ester substrate, (+)-DIOP gave *diastereomeric excesses* of 77% (***αS***,2*R*), and with (−)-DIOP: 53% excess of (2*R*)-menthyl *N*-acetyl-(***R***)-phenylalanine ester reduction product [86]. The finding of different

diastereomeric excesses upon inverting the chiral catalyst's handedness is a predictable outcome, what is unpredictable is knowing which catalyst will provide the better result.

A series of (*R*,*R*)-*trans*-1,2-cycloalkyl analogues (**141**–**143**) of DIOP were synthesized and resolved by Glaser *et al.* [93, 94] See crystal structures Refcode BZCBRH [95] [Rh^{I}/*R*,*R*-**141**/η^6-C_6D_6]$^+$·ClO_4^-, and Refcode SIGKID [96] [$Pd^{II}Cl_2$/±-**143**]$^+$·$CHCl_3$ solvate. The cyclopropyl analogue (**144**) was later prepared by Molander *et al.* [97], see Refcode HAKJEJ [$Ni^{II}Br_2$/*R*,*R*-**144**] The goal was to rigidize DIOP's seven-membered chelating ring by increasing the P**C**H_2–**C**–**C**–**C**H_2P torsion angle as the carbocycle's ring size decreased: 73° (cyclohexyl-**143**), 94° (cyclobutyl-**141**), and 133° (cyclopropyl-**144**). Using *Z*-PhCH=C(NHAc)CO_2H (**134**), the proof of concept was seen by *in situ* [Rh(*R*,*R*-**141**–**143**)] catalyzed reduction product enantiomeric excesses that varied from 86% (*R*) (with cyclobutyl **141**), 63% (*R*) (cyclopentyl-**142**), to 35% (*R*) (cyclohexyl-**143**) [98]. For those not familiar with the term *enantiomeric excess*,

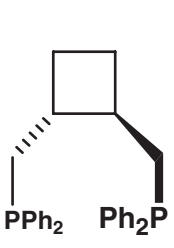

141

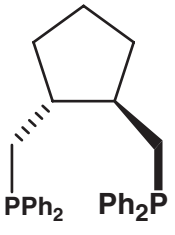

142

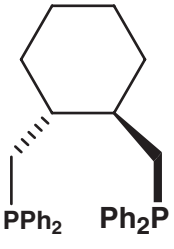

143

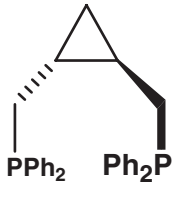

144

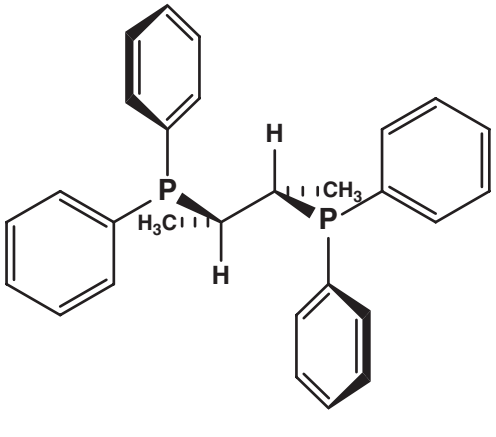

145

it is the |(*R*)%−(*S*)%| absolute difference and quantifies an asymmetric reaction's *enantioselectivity.* Nonselective reactions afford a 50 : 50 product mixture.

In 1978, Brown and Chaloner [99] using $^{31}P\ \{^{1}H\}$ NMR (301 K) reported that *Z*-α-benzamidocinnamic acid formed a pair of configurationally unassigned diastereomeric π-complexes with $[Rh^{I}/(S,S\text{-DIPAMP})/(solvent)_2]^{+}\cdot BF_4^{-}$ under argon in the ratio of about 7 : 1. They went on to show that subsequent hydrogenation of the solution gave an enantiomeric excess of 94% *N*-benzamido-(*S*)-phenylalanine. MeOH solutions under argon of diastereomeric π-complexes of the [Rh^{I}/(*RR*-cyclobutyl DIOP-type diphosphine **141**)/(RCH=C(NR′C=OR″)COOR‴) [100–103]]$^{+}\cdot BF_4^{-}$ were characterized by Brown, Glaser, and coworkers [104] using $^{31}P\{^{1}H\}$ NMR spectroscopy. These then underwent hydrogenation upon replacement of argon by hydrogen. Low temperatures had to be used in many cases in order to reduce the *slow magnetic site-exchange* line-broadening between complexes that varied by their π-complexed prochiral faces. As expected, decreasing temperatures reduced the linewidths and increased the quantity of the predominant solution-state species in accordance with *thermodynamic control.*

These NMR and hydrogenation studies were performed in Oxford during the summer of 1978, 2 years prior to the 1980 publication by Jack Halpern and coworkers of the [Rh^{I}/(*S,S*-CHIRAPHOS **145**)/(ethyl *Z*-α-acetamidocinnamate π-complex)]$^{+}\cdot ClO_4^{-}$ crystal structure, Refcode CHPSRH [105]. A later report (2004) presented the crystal structure of the analogous [Rh^{I}/(*S,S*-DIPAMP **140**)/(methyl *Z-m,p*-dimethoxy-α-acetamidocinnamate π-complex)]$^{+}\cdot BF_4^{-}$ complex, Refcode IBOYUU [106] see **146**. As an aid to structural analysis of **146**, substructures within the complex are also presented as a side view of the Rh^{I}/(*S,S*-DIPAMP) chelate fragment **147** and as a head-on orientation of the π-complexed prochiral substrate **148**.

The binding interactions in X-ray determined structure **146** deserve some comment. The +48° (+)-*synclinal* P–C–C–P torsion angle of (*S,S*)-DIPAMP affords a *Δ*-twisted conformation five-membered chelating ring **146**. A (+)- or (−)-*synclinal* P–C–C–P puckering angle of the five-member chelate defines the ring's respective *Δ,Λ*-twist sense. The *re-si* prochiral face of methyl α-acetamidocinnamate is π-complexed to Rh^{I}, and the acetamido oxygen is also ligated to Rh^{I} (see **148**). In addition, a DIPAMP phenyl ring undergoes an *edge-to-face* aromatic–aromatic interaction in which the phenyl and the *m,p*-dimethoxyphenyl centroids are only 5.2 Å apart (see the left arrow in lower right **146**). Inspection of the two aromatic rings to the left of the lower arrow shows that the H ⟶ C(aromatic) dipole's positive end in the *lower-right* DIPAMP phenyl points toward the partially negative interior of the cinnamate's dimethoxyphenyl ring (remember that the OMe groups were omitted in the drawing). Finally, the methyl ester's partially positively charged $C_{methoxy} \longrightarrow O_{alkoxy}$ dipole is aligned so that the methyl carbon is 3.97 Å above the *upper-left* DIPAMP phenyl ring-face (see right-arrow in upper left **146**).

All four host–guest interaction modes, together with an auspicious fit, make the **146** π-complex intermediate thermodynamically stable. It should be mentioned that some of these interactions result from an intimate *induced fit* between aryl group twist-orientations of the $[Rh^{I}/(S,S\text{-DIPAMP})/(solvent)_2]^{+}\cdot BF_4^{-}$ host and the steric/electronic requirements of the methyl *Z*-α-acetamidocinnamate guest.

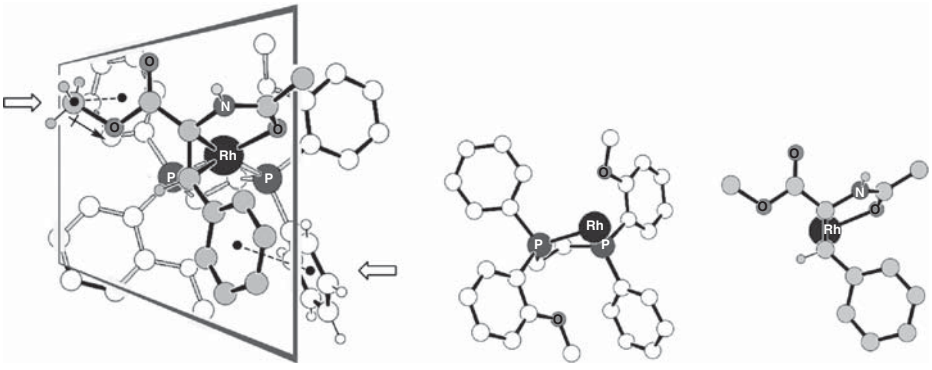

146 **147** **148**

$^{31}P\{^{1}H\}$ NMR (241 K) spectra of methyl (top) and *t*-butyl (bottom) *Z*-α-acetamidocinnamate esters π-complexed/acetamido bound to $[Rh^{I}/(R,R)$-cyclobutyl-DIOP **141**$)/(MeOH)_2]^{+}\cdot BF_4^{-}$ are depicted in plot **149** [104]. Today, we have the advantage of having a crystal structure of one of the intermediates (which was unknown when our experiments were performed and the article was written) [104]. δ39.6(1) and δ12(2) mean that chemical shifts in both spectra can now be assigned to P(1) and P(2) phosphorus nuclei, respectively, *trans* and *cis* to the acetamido-oxygen of diastereomer no. 1. In a similar manner, δ30(2) and δ14.5(3) mean that chemical shifts can also be assigned to P(1) and P(2) phosphorus nuclei, respectively, *trans* and *cis* to the acetamido-oxygen of diastereomer no. 2. Each phosphorus multiplet is a four-line doublet-of-doublets that arise from smaller 46(3) Hz $^{2}J(P_1-P_2)$ and larger 155(4) ^{1}J(Rh–P) mean coupling values. P(1) and P(2) relative assignments are in agreement with a ^{31}P spectrum of a similar complex in which the vinylic C(α) was 50% ^{13}C labeled and 20.5 Hz ^{2}J(CP) *cis*-geminal coupling was now observed in the δ ∼ 13 equal-intensity 8-line P(2) multiplet [107]. The ratios of the two diastereomers may be estimated by integration. The ratio of diastereomers 1 : 2 is 93 : 7 for the methyl ester and 21 : 79 for the *t*-butyl ester [104].

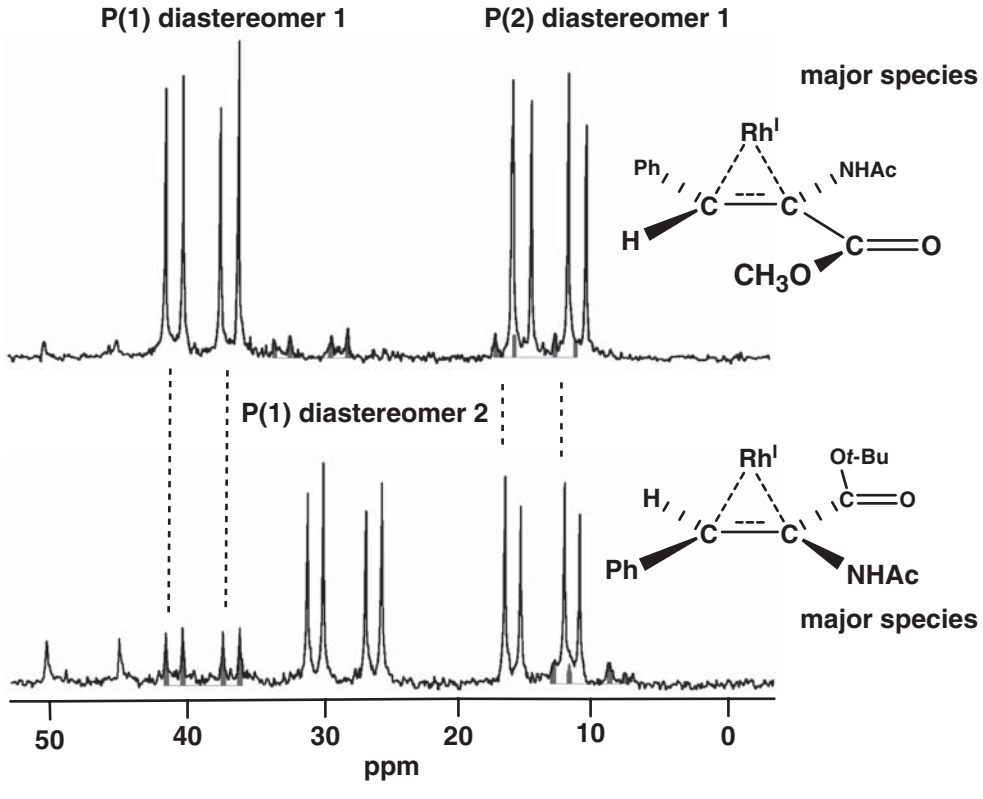

149

Can these results be rationalized? They now can with today's knowledge of crystal structures. The close contact interaction of the $\underline{C}H_3OC(=O)=$ methoxy carbon due to the interaction of the C ⟶ O dipole and the nearby partially negative DIPAMP phenyl ring interior was already commented upon. Exchanging a methoxy-carbonyl for a more spatially demanding $(CH_3)_3COC(=O)$-*t*-butyloxycarbonyl would likely result in unfavorable steric problems. This strongly suggests that increased ester steric bulk changed the predominate π-complexed prochiral face from *re-si* (MeO substrate) to *si-re* (*t*-BuO substrate). However, there was absolutely no correlation between the thermodynamically controlled intermediate's π-complexed face and that which eventually underwent *kinetically controlled cis*-hydrogenation. The enantiomeric excess for the *N*-acetylphenylalanine methyl ester product was 35% (*R*, MeO) and 52% (*R*, *t*-BuO) for the *t*-butyl analogue using the (*R*,*R*)-cyclobutyl-DIOP catalyst **141** [104]. When the chiral diphosphine was changed to (*S*,*S*)-DIPAMP **140**, then the same two esters gave diastereomer-(no. 1 : 2) π-complex ratios (305 K) of 93 : 7 (MeO) and 80 : 20

(*t*-BuO). Thus, the thermodynamically predominant diastereomeric intermediate has the same prochiral face π-complexed to the metal using the (*S*,*S*)-DIPAMP catalyst [104]. But, the hydrogenation product's enantiomeric excess was a larger 95% (*S*) (MeO) and 92% (*S*) (*t*-BuO) [104].

The temptation to assign prochiral face *re-si/si-re* descriptors to the NMR observed π-complexes *based solely* upon the reduction product's handedness should be resisted. Why? NMR observes thermodynamic ratios of intermediates that exist prior to the kinetically controlled rate determining step of dihydrogen activation. The well known Curtin–Hammett principle [108, 109] specifically states that the relative *thermodynamic stabilities of intermediates* are not relevant to the product distribution of kinetically controlled reactions involving *diastereomeric transition states*. By the time the Oxford NMR studies were done, one had to have a lot of faith in the Curtin–Hammett principle to state that a ca. 90 : 10 ratio of π-complex intermediates with DIPAMP (governed by ΔG^0) could produce an inverted ca. 10 : 90 ratio of enantiomeric products (controlled by $\Delta G^{\ddagger}$). A few months later, this indeed was shown to be true.

Two X-ray crystallographic studies of DIPHOS chelated to Rh^I (a molecular oxygen complex $[Rh^I/(DIPHOS)_2/O_2]^+ \cdot PF_6^-$, Refcode RHEPPO10 [110] and a $[Rh^I/(DIPHOS)_2]^+ \cdot ClO_4^-$ complex, Refcode PPERHC) [111] were already in the Cambridge Structural Database (CSD) in 1978. Another important crystal structure at the time the NMR studies were being run in 1978 was the *absolute configuration and structure* of the $[Rh^I/(S,S\text{-CHIRAPHOS})/(COD)]^+ \cdot ClO_4^-$ complex, Refcode OCPBRH [112] (**150**) published by Ball and Payne in 1977. (*S*,*S*)-CHIRAPHOS [113] (**145**) and (*R*,*R*)-DIPAMP [91] (**140**) were the two most efficient and successful chiral diphosphines for asymmetric hydrogenation at that time, and both yielded (*R*)-*N*-acetylphenylalanine. Visually, it is clearly seen that both of these chiral diphosphines have the same (+)-*synclinal* P–C–C–P twist to their five-membered *Δ*-chelating rings with Rh^I, and all exhibited *axial*-phenyls with *antiperiplanar* $C(ipso)_{phenyl}–P–C_{chelate}–H$ relationships. Fryzuk and Bosnich [113] hydrogenated *Z*-α-benzamidocinnamic acid in THF using their $[Rh^I/(\boldsymbol{S},\boldsymbol{S}\text{-CHIRAPHOS})/(NBD)]^+ \cdot ClO_4^-$ catalyst (where NBD = norbornadiene) and obtained an amazing 99% enantiomeric excess of *N*-benzamido-(***R***)-phenylalanine. Since both the (*S*,*S*)-absolute configuration of CHIRAPHOS, the P–C–C–P *Δ*-twist, the skew of the geminal phenyl rings, plus the (*R*)-handedness of the α-acylamino acid hydrogenation products were now known, those working in the field would muse about the (*re-si*)/(*si-re*) identity of the substrate's thermodynamically preferred prochiral face that was π-complexed to the Rh^I intermediates observed in our $^{31}P\{^1H\}$ NMR spectra.

Molecular modeling studies in Autumn 1978 strongly suggested that the best host–guest fit would have the *wrong* π-complexed/acylamido (*re-si*)-face bound to the *Δ*-twisted five-membered chelated $[Rh^I/(S,S\text{-CHIRAPHOS})/(solvent)_2]^+ \cdot ClO_4^-$ complex compared to that required to produce the major

chiral reduction product (R. Glaser, unpublished results). In other words, *cis*-hydrogenation of this face would produce *N*-acyl-(***S***)-amino acids, while (***S***,***S***)-CHIRAPHOS (**145**) was known to generate the (***R***)-enantiomers [113]. The proof of this hypothesis was found in the last of the six bimonthly issues of *Inorganica Chimica Acta* for 1979. Halpern and coworkers [107] published a crystal structure (**151**) molecular graphic of methyl *Z*-α-acetamidocinnamate bound to a $[Rh^{I}/(DIPHOS)]^{+}\cdot BF_4^{-}$ π-complex, Refcode DPEMRH (unfortunately, no coordinates were deposited in the CSD). Both molecular graphics-type representations of Rh^{I} complexes of (*S*,*S*)-CHIRAPHOS (**150**) and DIPHOS (**151**, Halpern molecular graphic with atom coloring by the author) showed common *Δ*-twisted-diphenylphosphino $Ph_2PCCPPh_2$ spatial dispositions for the [Rh^{I}/(DIPHOS and *S*,*S*-CHIRAPHOS)] chelating moiety. What was striking was that the published *Δ*-twisted-**151** molecular graphic indeed had the *wrong* methyl *Z*-α-acetamidocinnamate (*re-si*)-face bound to the Rh^{I}/(***S***,***S***)-*Δ*-twisted diphosphine and would yield the *incorrect* (*R*)-configuration *cis*-hydrogenation product. Surprisingly, this very important conclusion was not mentioned in the communication. But, by the time the author had this proof, the Brown *et al.* [104] paper had already gone to press.

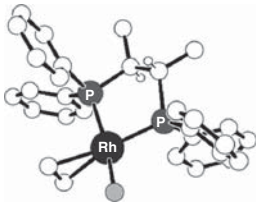

Δ-twisted-150

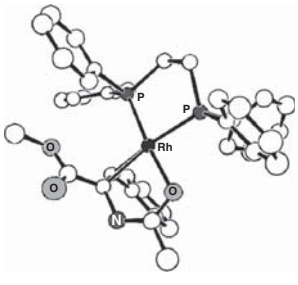

Δ-twisted-151

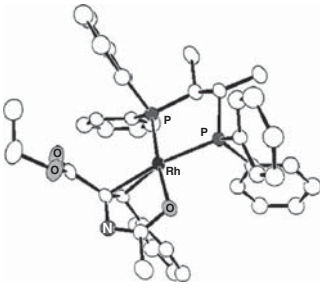

Δ-twisted-152

Just 2 years later, Halpern's group published the [Rh^{I}(*S*,*S*-CHIRAPHOS)(*re-si*) ethyl *Z*-α-acetamidocinnamate]$^{+}\cdot ClO_4^{-}$ crystal structure (Refcode CHPSRH [105], again without coordinates). However, the publication's *Δ*-twisted-**152** molecular graphic (atoms colored by the author) indeed showed the wrong π-complexed/α-acetamido (*re-si*)-face bound to the [Rh^{I}(*S*,*S*-CHIRAPHOS)] moiety. This intermediate was then subjected to solution-state $^{31}P\{^{1}H\}$ NMR analysis, and *only one diastereomer* could be detected. A hydrogenation was then performed giving >95% enantiomeric excess of the *N*-acetyl-(*R*)-phenylalanine ethyl ester product. This product had to arise from a (*si-re*)-bound intermediate

that was unobserved (i.e., a so-called *hidden partner*) in the $^{31}P\{^{1}H\}$ NMR spectrum. The Halpern group's findings unequivocally proved that the enantioselective asymmetric hydrogenation pathways were indeed governed by the Curtin–Hammett principle (i.e., the major reduction product was produced from the minor intermediate).

8
Stereogenic Elements, Chirotopicity, Permutational Isomers, and Gear-Like Correlated Motion of Molecular Subunits

8.1
Stereogenicity, Stereogenic Elements, Chirotopicity, and the Ambiguity of Some Stereochemical Terms

There are stereochemical terms based on symmetry whose meaning is ambiguous or unclear or even oxymoronic. For example, the terms "chiral or asymmetric *center*," and "chiral *plane*" are strange since the adjective "chiral" cannot logically modify symmetry elements of the Second Kind. On the other hand, "chiral *axis*" is reasonable since it does not refer to a bent axis but rather to a rotational symmetry element in a nonasymmetric C_n-symmetry point group molecule (i.e., one where $n \neq 1$). However, many chemists use the term "chiral axis" to refer to chirality of an axis through the three C=C=C carbons in the *d*,*l*-allene MeCH=C=CHMe. This axis is not even a rotational symmetry axis at all since the methyl groups are disposed *orthogonally* to each other.

An even more problematic example is the term "*asymmetric*" carbon atom. Most chemists usually understand what is meant by an "*asymmetric*" carbon atom, that is, the ability to generate another isomer (an enantiomer) by exchanging the locations of a pair of different ligands on a tetrahedral atom bearing four different substituents (a so-called *maximally stereochemically labeled* tetrahedral carbon). This atom is the most common example of a *stereogenic element.* Stereogenic elements are structural features in a molecule that give rise to a new isomer when changed to the second of two possibilities. Interchanging any two of the four ligands on this particular stereogenic element produces a new isomer. The case of a tetrahedral bonding geometry is special since the new isomer is always an enantiomer no matter what pair of ligands is exchanged [76]. Ligand exchanges in other bonding geometries (e.g., maximally labeled octahedral atoms) may generate either enantiomers or diastereomers [76]. Examples of stereogenic elements include (*R*,*S*)-tetrahedral atoms, or (*P*,*M*)-screw sense (*helicity*) helices, or (Δ/Λ)-twists of five-membered chelating rings, or *tropicity* (directionality) of a substituent pattern on chiral ring conformations, or the relative tropicities of catenane rings, and so on. However,

Symmetry, Spectroscopy, and Crystallography: The Structural Nexus, First Edition. Robert Glaser.

Companion Website: www.wiley.com/go/Glaser/Symmetry

"asymmetric" can just as well apply to an atom's *local site symmetry* [114]. If a molecule is asymmetric (C_1-symmetry), then all of its subunits must also be asymmetric. By this, we mean that asymmetric molecules have no symmetrical building blocks since their asymmetric molecular orbitals generate asymmetric electron distributions around all atoms. Logically, one cannot imagine symmetry within an asymmetric environment (it is a *mismatch*). For example, there are no chiroptical properties arising from an inherently achiral carbonyl chromophore within an achiral molecule. However, if the same chromophore is embedded within a chiral molecule, then the asymmetric electron distribution around the carbonyl, for example, will make it an "*asymmetric carbon*" that will induce $n \rightarrow \pi$ circular dichroism. This ambiguity of meaning was perplexing from the very beginning of van't Hoff's use of the term "*asymmetric carbon atom*" in 1874. van't Hoff realized that *meso* molecules can be constructed from maximally labeled tetrahedral carbons $CR^1R^2R^3R^4$ in which two of them (R^3 and R^4) differ only in chirality (i.e., they are heterochiral, e.g., $R^3 = (R)$–$CH(Ph)CH_3$ and $R^4 = (S)$–$CH(Ph)CH_3$). However, in a tetrahedral bonding arrangement, these chiral R^3 and R^4 groups will be enantiotopic by reflection through a σ-plane bisecting all three R^1–C–R^2 atoms, for example, $R^1 = H$ and $R^2 = Cl$. Hence, the molecule is *meso* and naturally achiral, and yet exchanging the locations of R^1 and R^2 produces a second *meso* isomer. This is illustrated by the *meso*-cyclopropanes **153** and **154**, where the achirotopic stereogenic carbon is colored gray. A result of this logical dilemma was van't Hoff's assignment of the term "*pseudo*asymmetric" to the central carbon atom in these *meso* compounds. The existence of "asymmetric"/"*pseudo*asymmetric" carbon atoms (or "octant"/"*anti*octant" rules in chiroptical spectroscopy) clearly points to a logical flaw [114].

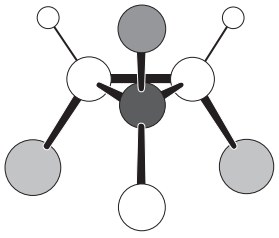

153

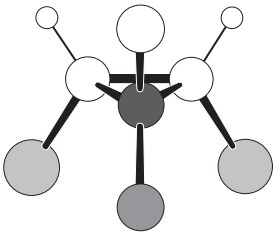

154

In 1984, Mislow and Siegel [114] reported a solution to the asymmetric/*pseudo*asymmetric problem by separating *stereogenicity/nonstereogenicity* from the concept of local site symmetry (*chirotopicity/achirotopicity*). In this new approach, the terms *chirotopic/achirotopic* are statements describing

the chirality/achirality of a particular *single* locale/site/point, as opposed to comparisons of symmetry equivalence between multiple subunit locales (*homotopic*, *enantiotopic*, etc.). Thus, a point (either occupied by an atom, or on a bond, or located in space around a molecule) is *chirotopic* if it exhibits *chiral local site symmetry*, that is, its site shows either identity or rotational symmetry. In other words, one may consider an *asymmetrically chirotopic point* or C_n*-symmetrically chirotopic* point ($n \geq 2$). Both *pseudo*asymmetric atoms in **153** and **154** can be described as being "*stereogenic and achirotopic*," whereby van't Hoff's conceptual ambiguity has now been corrected. The "commonly recognized" maximally labeled asymmetric carbon atom will now be "*stereogenic and chirotopic.*" In this manner, vinylic carbons in a *cis-/trans*-2-butene pair of diastereomers are "*stereogenic and achirotopic*," while the terminal methyl-carbons are "*nonstereogenic and achirotopic.*" Inspection of the achiral solvated oxirane **110** shows that all points in the molecule are chirotopic except those achirotopic points comprising the σ-plane or the midpoint of the C–C bond or the oxygen atom. On the other hand, all points in chiral solvated oxirane **111** are chirotopic since they have C_1 local site symmetry.

8.2 Triarylamine Propellers

P and *M* describe the twist sense of helices, propellers, and screws. We will see that all atoms in triphenylamine *(P,M)*-**155** (Refcode ZZZJCQ01, two sets of asymmetric *P*,*M*-symmetry independent molecules in the asymmetric unit) [115] are chirotopic since the entire molecule is chiral. The solvated molecules exhibit three-bladed right- or left-handed propeller-like geometries having dihedral D_3-symmetry. A C_3-axis passes through the trigonal nitrogen atom perpendicular to a *hub plane* defined by the three C(*ipso*) ring atoms while C_2-axes transit each of the three (*ipso-para*) carbon pairs. A least one C_2-axis through an N–C(*ipso*) bond guarantees that the trigonal nitrogen resides within the hub plane. A highly strained coplanar geometry of rings would permit extensive nonbonding electron-pair delocalization at the high expense of very short inter-ring H(ortho)···H(ortho) distances that are considerably less than the sum of the two van der Waals radii. On the other hand, a sterically free paddle-wheel arrangement (each phenyl is orthogonal to the hub plane) also places the nitrogen's nonbonding electron *p*-orbital orthogonal to the ring's π-orbitals and results in lone-pair localization. In the solid state, about 46(7)° propeller twist angles (relative to the hub plane) represent an effective compromise between the two stereochemical extreme molecular geometries. Since delocalization involving the nonbonding pair *p*-orbital and the aromatic π-orbitals is governed by a cosine relationship, propeller-like triarylamines are

still nonbasic even with a ~45° twist and run with the solvent front on a TLC silica plate. Perusal of the carpenter's plane hand tool depicted in **156** shows that only left-to-right movement can cut a sliver of wood. This is the same principle of a wood screw (or an airplane propeller), where by convention a clockwise torque on a screwdriver drives the screw into the plane of the wood. So, it is helpful to think of triphenylamine propellers as screws, for example, right-handed screw sense (*P*)-**155**. The chirotopic nitrogen and all the *ipso-para* carbon pairs reside at C_3 and C_2 rotational sites of symmetry, respectively, while all the *ortho-meta* carbons are "off-axis" and exhibit only identity (C_1) local site symmetries. Therefore, the propeller molecule's *chirotopic* sites are either *asymmetric* or *rotationally-symmetric.* Since the upper and lower sides of **155** are homotopic, they must exhibit the same screw sense when viewed from either side.

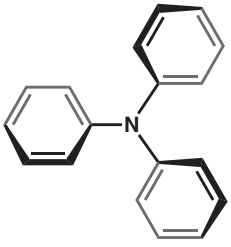

(*P*)-**155**

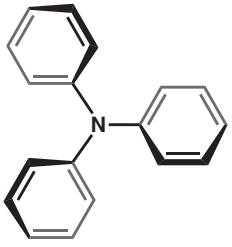

(*M*)-**155**

156

8.3
Dynamic Stereochemistry of Permutational Isomers: Correlated Motion in Triarylamines

Glaser *et al.* [116] have reported on *maximally stereochemically labeled* triarylamines composed of three aryl rings where each contains a different *o*-substituent (see **157** and **158**). Three stereogenic elements exist in these *permutational isomers* since *o*-substituents on each of the *three* different rings can be disposed either as "*up*" or "*down*" *vis-à-vis* a hub plane viewed from the same arbitrary vantage point. By this, we mean that if rings are described as "rings 1–3," then the **157**, **158** phenyl ring trio has $1 \rightarrow 2 \rightarrow 3$ *clockwise tropicity* arbitrarily defined as the "standard orientation". We have to always bear in mind that flat, enantiotopic, almost cyclic curved arrows change their tropicity when viewed from the other face (i.e., the hurricanes and cyclones). A fourth stereogenic element is the right-handed (*P*) or left-handed (*M*) *helicity* (screw sense) of the three-bladed propellers [116, 117]. The net result is that $2^4 = 16$ isomers are possible (i.e., eight *d*,*l*-pairs of diastereomers). These enantiomeric or diastereomeric molecules are denoted as *permutational isomers* since their *constitutions are always invariant.*

The nitrogen may not reside within the "*hub plane*" defined by the three aryl C(*ipso*) carbons, because three different aryl rings are ligated to the nitrogen central hub. Why? Only two geometrical conditions may enable the nitrogen to occupy the three-atom hub plane. One is that a reflection plane be passed through all four atoms, an impossibility due to the aryl-propeller's 45(8)° mean tilt to the hub plane. We already know that a second possibility exists if at least one C_2-axis can be passed through a N–C (*ipso*) bond. However, the different *ortho*-substituents of each ring are incompatible with C_2-symmetry. Therefore, nitrogen's very low 0.201(6) Å height above the hub plane shows that it is the apex of very shallow pyramid (quite different than the steeper nitrogen pyramid geometry of trialkylamines) [116]. This pyramidality is genuine and definitely not a result of crystal packing forces. Why? It is expected since the hub's two faces are diastereotopic and not symmetry equivalent. But, is the pyramidality *stereogenic*? In other words, do we have to consider 2^5 permutational (*R*)/(*S*)-isomers? Answer: only 2^4 isomers will suffice since the ground-state hub plane is *pseudo*planar solely due to symmetry constraint (and not structural constraint) since the inversion barrier of the pseudo-sp^2-nitrogen is less than RT calories [118].

When ring-1 = C_6H_4–*o*–C(=O)OCH_3, ring-2 = α-naphthyl, and ring-3 = biphenyl C_6H_4–*o*–Ph, then crystallization afforded *polymorphous* triarylamine crystals *in the same flask* (*rac*-**157** triclinic $P\bar{1}$ space group ***prisms*** (Refcode MANTHA,) and *rac*-**158** monoclinic $P2_1/n$ space group ***needles*** (Refcode MANTHB) [116]. Their readily observable differences in crystal *habit* (general external shape) enabled them to be hand-separated into two piles, see photo **159**. Despite the **157**, **158** pair's opposite (*P,M)-helicity*, they *cannot* be related as enantiomers since both exhibit invariant $1 \rightarrow 2 \rightarrow 3$ *clockwise hub tropicity* and "*up*"-labels for all *o*-substituents of rings 1–3. During the time the X-ray crystallographic work was being performed, Dr John Blount (head crystallographer at Hoffmann LaRoche Pharmaceuticals) telephoned Princeton and requested that the vial of needles be brought back up to Nutley, NJ, since he wanted to choose a "*fatter*" needle specimen. As a professional, he desired to report bond lengths with the customary third decimal place precision, but the original needle-type data crystal was just "too thin" for adequate signal/noise diffraction measurements. Crystallographers prefer to receive prisms since the crystal is "fat" in all three dimensions, "platelets" come next in favor, and thin "needles" bring up the rear. The following day, Dr Blount noted that the new (Refcode MANTHC, monoclinic $P2_1/a$) [116] needle is a *different needle* whose –C(=O)OCH_3 group was rotated by about 180°" to yield *exo*/*endo* rotamers. The visually similar *endo-carbonyl* **160** monoclinic $P2_1/a$ space group needle (Refcode MANTHC) [116] was a *conformational polymorph* of *exo-carbonyl* **158** [116]. For the purpose of the following stereochemical discussion, the *endo/exo-carbonyl* dispositions should be *neglected* and treated only as a secondary stereogenic element. Why? Nothing in the discussion

would be changed if trigonal $-C(=O)OCH_3$ is replaced by a conical bromo substituent.

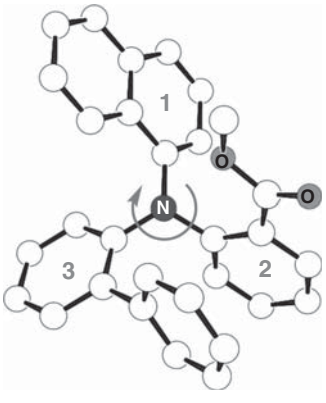

157

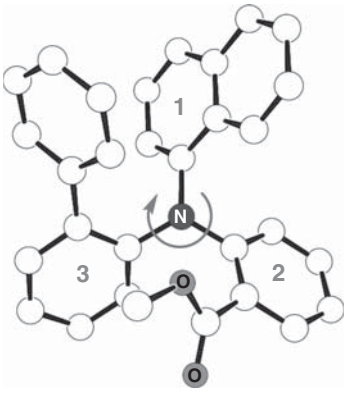

158

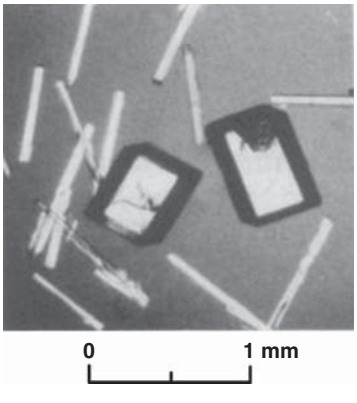

159

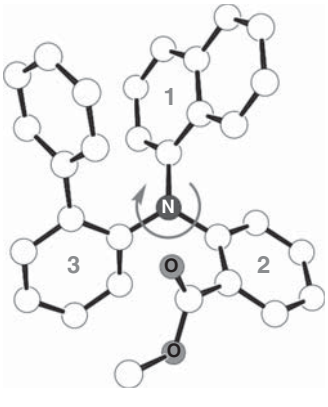

160

How does one keep track of the structural identities of so many similar looking isomers? Answer: by assignment of unique descriptors to each of the permutational isomers. A *binary* four-digit unique stereochemical descriptor may be affixed to each of the isomers, in which *helicity* is denoted as [w•••] (where "w" is 0 for *P* and 1 for *M*); and [•x••] x refers to ring-1's *o-substituent disposition* where 0 = *up* and 1 = *down* relative to the 1 → 2 → 3 *clockwise tropicity hub reference plane* [116]. A similar convention is utilized for ring-2's [••y•] and ring-3's [•••z] binary digits. Different binary [wxyz] descriptors readily inform us that (*M*)-*all up* [1000]-**158** is a diastereomer of (*P*)-*all up* [0000]-**157** and not an enantiomer. Why? The enantiomer of [0000]-**157** must have all of its

stereogenic descriptors inverted (i.e., [1111]) and not only just one. Why not just rotate [0000]-**157** 180° out-of-plane so that the substituents are *all-down*? Answer: it is forbidden since when viewed from above, the resulting anti*clockwise* (or levo) $1 \rightarrow 2 \rightarrow 3$ *tropicity hub plane* is simply *not* the "standard dextro reference orientation" used to define [0111], although the (*P*)-helicity would be the same.

We will now discuss the *correlated motional modes* responsible for helicity interconversion between all 16 permutational isomers. By *correlated motion*, one means that as one part of a molecule (e.g., a single aryl ring) starts to twist about its N–C(*ipso*) bond, it engenders a commitment *defined* motional response by the other two aryl rings. Each and every dynamic stereochemistry step interconverting these compounds always involves the two elements of (*P*,*M*)-*helicity inversion* accompanied by *ortho edge-label exchange*. Four mechanisms are possible [119]. The *three-ring* flip mechanism proceeds via a three *orthogonal-ring* hub transition state (see **161**). This diastereomerization mechanism interconverts [0000] on the left with *oppositely handed diastereomer* [1000] on the right, since the solid bold black top-edges signify "*up*" ortho-substituents and the unsubstituted "*down*" edges are gray.

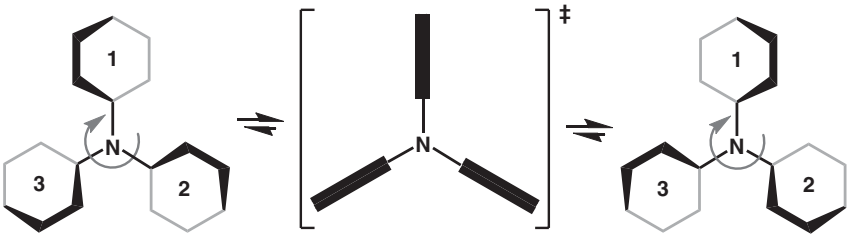

161

Isomer [0000] (on the left) is converted into oppositely handed diastereomer [1100] (on the right) via the *two-ring* flip diastereomerization mechanism **162**. Notice that the bold top-edge of [1100] ring-1 is white with black borders, while the "down" *ortho*-substituent is edge-labeled as bold solid gray. At the time the work was done, it was already established that (without known exception) the *two ring-flip* is the lowest energy mechanism for triarylamine helicity interconversion [120]. In this *threshold mechanism* (i.e., the *minimum energy process* when multiple processes are theoretically possible), one ring rotates through the hub plane via a *coplanar to hub-plane* transition state and then takes its *o*-substituent to the opposite face. The other two rings have orthogonal to the hub-plane

transition states. These two rings flip (like wind shield wipers) and keep the flipped *o*-substituents on the same hub-plane face during the helicity reversal.

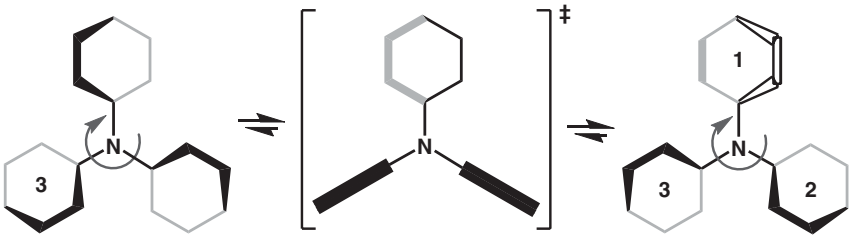

162

The *one-ring* flip diastereomerization mechanism (**163**) interchanges isomer [0000] (on the left) with the oppositely handed diastereomer [1101] (on the right). Finally, the *zero-ring* flip enantiomerization mechanism (**164**) interchanges isomer [0000] (on the left) with enantiomer [1111] on the right.

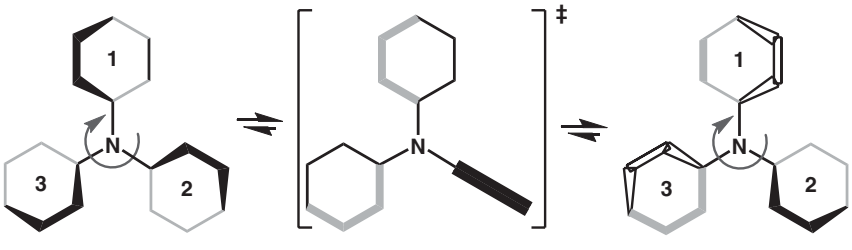

163

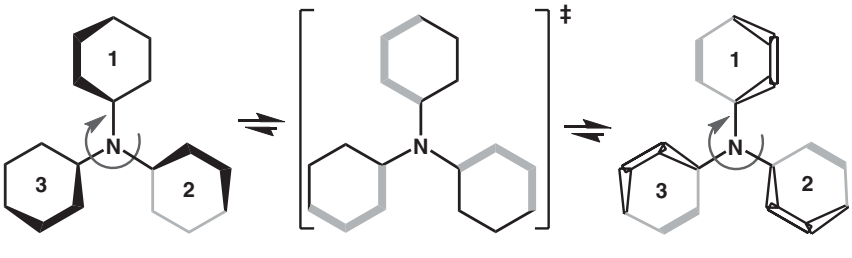

164

The triarylamine propeller's correlated motion enables it to be considered as a *molecular gear assembly* consisting of a cyclic system of three-primitive two-pronged gear-wheels. The simple fact that there is defined correlation motion means that it is a gear. Then why isn't helicity interchange occurring via constant rotation of all three interleaved aryl-rings? Answer: There is no limit to the number of interleaving gear wheels in a lateral gear train such as **165**. But, there is a mechanical constraint based upon the *parity* of *cyclic* gear-train interleaving gears, since pairs of gear wheels must undergo *disrotatory* relative motion as in the three-gear *lateral set* **165**. However, notice that this cannot happen in the three-gear *cyclic set* **166**, although there is certainly no difficulty with four-wheel cyclic set **167**. Removal of this mechanical constraint is the basis of the two-ring flip mechanism in which after each helicity interchange, another of the three aryl rings becomes the *nonflipping* partner for the next consecutive two-ring flip.

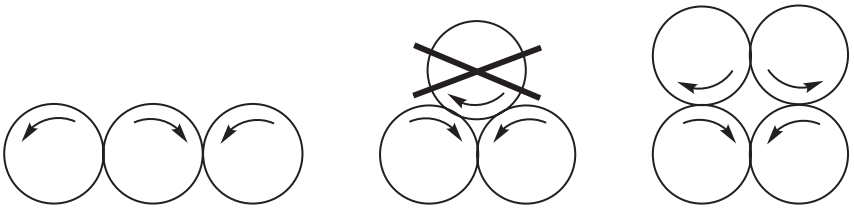

165 **166** **167**

Using *graph theory*, we may graph eight permutational isomers upon the vertices of a cube (**168**, a three-dimensional *Cayley* diagram). Each of the cube's eight sides symbolizes a two-ring flip interconversion. Enantiomeric pairs are graphed on the termini of the four diagonals through the cube's center. Starting with [0000], three different two-ring flips produce [1100], [1010], and [1001]. From [1100], two different two-ring flips yield new isomers [0110] and [0101].

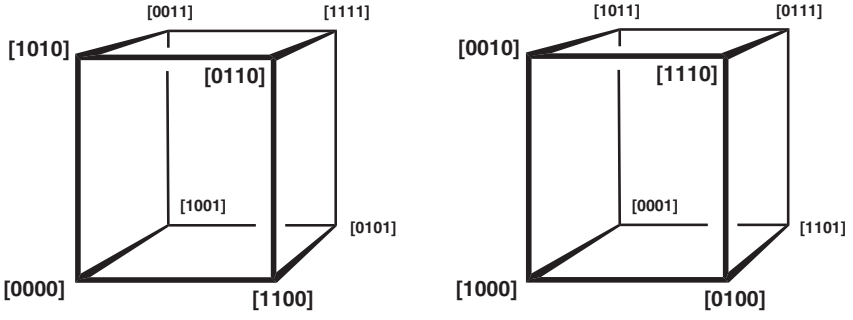

168 **169**

From [1001] comes new [0011]. Finally, all three isomers [0110], [0011], and [0101] afford the same new eighth isomer [1111].

Dissolving (±)-**157** [0000], [1111] crystals in an NMR tube filled with CD_2Cl_2 *precooled* in a dry ice/acetone bath and rapid insertion into a −40 °C precooled spectrometer probe enabled the initial measurement of a weighed time-averaged δ3.03 C$\underline{\boldsymbol{H}}_3$ singlet and a δ51.5 O$\underline{\boldsymbol{C}}H_3$ signal. Repeating the measurements on a cold solution of dissolved (±)-**158** [1000], [0111] crystals afforded *different* signals (δ3.38 and δ52.1) for corresponding nuclei. The reason for different chemical shifts is that the two ring-flip mechanism alone *cannot* interconvert all 16 permutational isomers (eight *d*,*l*-pairs) when this is the only available mechanism at very low temperature. The mechanism can interconvert only eight permutational isomers (eight *d*,*l*-pairs, see cube **168**) starting from (±)-**157** [0000], [1111] crystals. The second set of eight isomers (see cube **169**) is derived from the (±)-**158** [0000], [1111] crystals. At low temperature, the cubes represent two *disjoint* graphs, that is, they share no common topological point. A higher energy second mechanism (i.e., a nonthreshold energy mechanism) is required for complete dynamic interchange between the 16 permutational isomers in the two sets.

The −21 °C equilibration of both sets (via a higher energy one or three ring-flip mechanism) had a $\Delta G^{\ddagger} = 17.8\,\text{kcal mol}^{-1}$ barrier measured from either **157** or **158** crystal. The two ring-flip threshold mechanism's $\Delta G^{\ddagger}$ at −40 °C must be lower than $17.8\,\text{kcal mol}^{-1}$ since two *different* sets of weighted time-averaged NMR signals were observed from the rapid interconversion of each group of eight permutational isomers. Since these weighted time-averaged structures afforded anisochronous signals, the sets must be different in composition (i.e., *residual diastereomers*). Residual means that some measureable *diastereomeric character* remains for each NMR anisochronous set of rapidly averaged eight isomers in **168** versus that observed for **169**. Complex topics, such as this, can be mind boggling and are the reason why Mislow insists that stereochemical concepts must always be 100% logically correct.

8.4
Relative Stereochemical Descriptors: *Retro-Inverso* Isomers

The rate of increasing concentration in the blood stream upon dissolution of a tabletted drug is called *pharmacokinetics* (what the drug does to the body). Peptide pharmaceutical agents are usually administered by injection since they undergo rapid hydrolysis in our stomach/gastrointestinal track. This is called *pharmacodynamics* (what the body does to the drug). Some of these drug-administration liabilities can be considerably emolliated by *retro-inverso* (RI) peptide transformations. The concept is partially based upon inverting the specific ordering of amino acids in the historical, but arbitrarily chosen, N → C direction (characteristic of a naturally occurring *L*-peptide segment, e.g., **170**). RI peptide transformations

utilize D-amino acids (*inverso* configuration) whose order is reversed (i.e., *retro* ordering beginning from the C-terminus rather than the usual N-terminus); see **171.** There is a high probability that the spatial arrangement of the RI's pharmacologically important side chains will be quite similar to that in the native peptide. A salient review of this field has been written by Michael Chorev [121]. Peptide *bond direction reversal* coupled with *C(α) chirality inversion* generates diastereomeric peptides that are characterized by markedly increased resistance to rapid metabolism [121]. Furthermore, if needed, *gem*-diaminoalkyl and 2-alkyl-malonyl *amino acid surrogates* reposition the end groups to reintroduce their *original dispositions* relative to the N- and C-termini in **170** [121]. Murray Goodman's group pioneered the use of *partially modified retro-inverso* (PMRI) and *end group modified retro-inverso* (EGMRI) transformations to produce a wide variety of highly active long-lived peptide analogues. These modifications enable a limited segment of an L-peptide to be replaced by PMRI and EGMRI peptide surrogates. For example, β-endorphins are naturally produced pentapeptide opiates that were once thought to hold great promise as analgesics due to their endogenous origins. They are responsible for the so-called *runner's high.* However, they were therapeutically disappointing due to their extremely rapid metabolism upon injection. But, a 5 μg injection of one partial RI end group modified [Met^5] enkephalin-induced catatonic behavior in rats, which lasted 3 h [121]. A very happy rat indeed! Philosophically, one may muse that life without pain could produce deleterious effects (severely cutting our hands or leaving them in the fire).

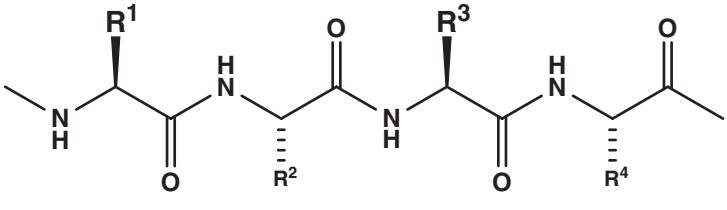

170

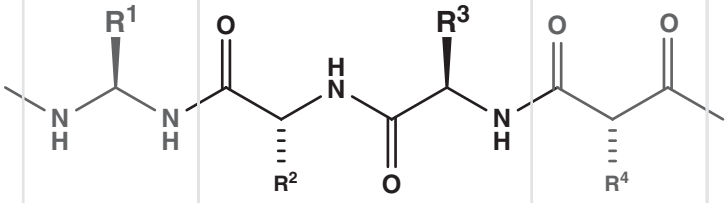

171

The natural L-configuration and N → C tropicity are readily recognizable RI reference standards for peptides. However, such reference standards are not apparent for many compounds, for example, substituted or labeled medium ring chiral conformations [122, 123]. The *boat–boat* conformation of the parent cyclooctene skeleton is chiral, see **172** (vinylic carbons colored gray). One enantiomer, for example, (*reference*)-**172**, is arbitrarily chosen to be the *ring-chirality* reference. Its enantiomer is ring-inverted and bears a (*inverso*)-**173** *relative configurational* descriptor.

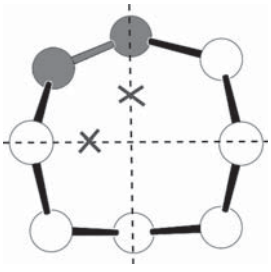

(*reference*)-**172**

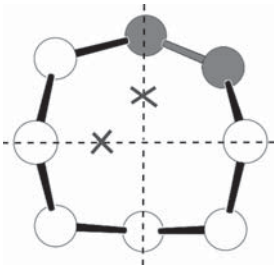

(*inverso*)-**173**

Addition of a second stereogenic element (e.g., an oxygen stereochemical label) gives rise to two *d*,*l*-pairs of *boat–boat* 4-oxacyclooctene diastereomers, **174–177**. The residence of oxygen in one of the two cyclooctene diastereotopic homoallylic positions results in the duplication of isomers. Again, the ring chirality and O → C=C label tropicity of one isomer is arbitrarily selected to be the *relative stereochemical reference* for both stereogenic elements, for example, (*reference*)-**174**. The enantiomer is assigned the *relative* configurational descriptor (*retroinverso*)-**175** because it has both *reversed* O → C=C tropicity and *inverted* ring chirality. The relative descriptors of the (*retro*)-**176** and (*inverso*)-**177** diastereomers denote only the single inverted stereogenic element in the *d*,*l*-pair (again relative to (*reference*-**174**).

Is there a practical use for this nomenclature in medium-ring stereochemistry? The answer is "yes," especially if you are planning to synthesize a series of structurally related compounds. "*Retro-inverso*" nomenclature provides a means of differentiating the substitution patterns in diastereomeric *d*,*l*-pairs. Even if only one medium ring is to be made, its structure should be compared to others in the literature. Consider again the nonnarcotic analgesic drug (±)-nefopam·HCl (**50**) [45]. Its (*reference*)-**178** and (*retroinverso*)-**179** enantiomeric *boat–boat* chiral conformation can be compared with different *boat–boat* conformations found

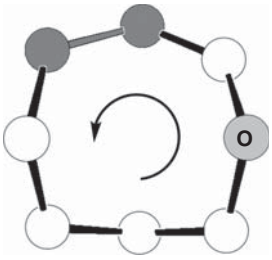

(*reference*)-**174**

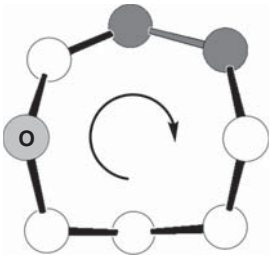

(*retro-inverso*)-**175**

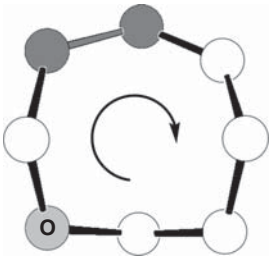

(*retro*)-**176**

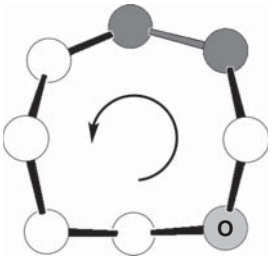

(*inverso*)-**177**

for the structurally similar crystalline (±)-thianefopam-cyanamide (*retro*)-**180** and (*inverso*)-**181** (Refcode **SUGJOV**, I. Ergaz and R. Glaser, unpublished data) [124]. One would have expected that simple sulfur substitution of nefopam's oxygen would have engendered a stereochemically similar product. Note the different *boat–boat* ring positions of the endocyclic nitrogens (<u>***N***</u>–CH_3/<u>***N***</u>–C≡N), phenyls, and oxygen/sulfur atoms. Structures **178–181** illustrate how RI nomenclature allows one to define both the *structural similarities* and *differences* between the *four boat–boat* medium rings. Obviously, we are dealing with two sets of nonisomers (i.e., *heteromers*), but here a structural chemist might be primarily interested in the *comparative stereochemistry* of the four different *boat–boat* ring skeletons and their heteroatom substitution patterns (**178–181**). The *boat–boat* rings of (*reference*)-**178** and (*retro*)-**180** are homochiral, but their phenyl → benzo tropicity is reversed *when viewed from the same convex (exo) side.* Similarly, the phenyl → benzo tropicity of (*reference*)-**178** and (*inverso*)-**181** is the same, but their *boat–boat* rings are heterochiral. Of course, in any discourse of this comparative stereochemistry, one is first obliged to explain how the relative descriptors are to be applied.

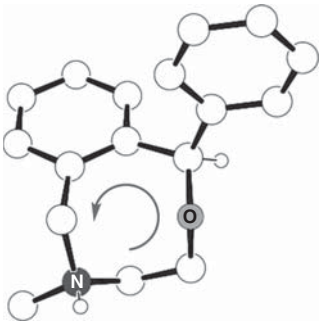

(*reference*)-**178**

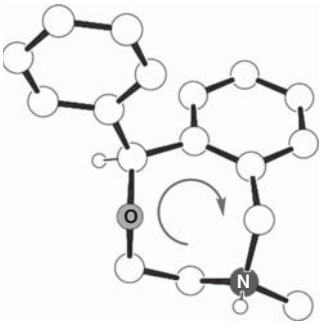

(*retro-inverso*)-**179**

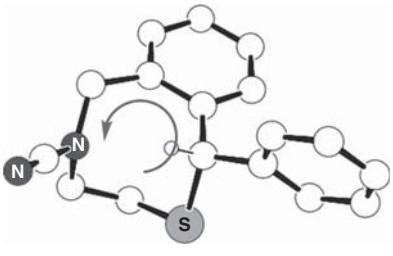

(*retro*)-**180**

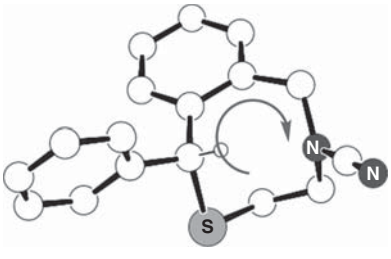

(*inverso*)-**181**

9
Symmetry in Extended Periodic Arrays of Molecular Crystals and the Relevance of Penrose Tiling Rules for Nonperiodic Quasicrystal Packing

9.1
Symmetry in Extended Arrays/Molecular Crystals

Space-filling symmetry within periodic extended arrays is described by *space groups. Chiral space groups* are those containing symmetry operations of only the First Kind. They lack all operations of the Second Kind (i.e., those that invert the handedness of symmetry-equivalent chiral objects: for example, *reflection, inversion, rotatory-reflection,* and *reflection-translation* or *glide-reflection*). *Achiral space groups* are those comprised of operations of both the First and Second Kinds. Illustration **182** depicts a *p*2*mm* 2D space group achiral array of M. C. Escher racemic chiral birds (**183**), which will be used as a heuristic device to explain some of the terminology of periodic extended arrays [125]. In this analogy, the Escher birds represent molecules.

A *unit cell* is the basic building block (repeat unit) of a *periodic crystal* and is duplicated up and down, sideways, and on the diagonal using only the *translation* symmetry operation. Later on, we will discuss *nonperiodic* crystals (i.e., *quasicrystals*). All periodic and nonperiodic crystals share a common attribute: they have *order.* Order in a periodic crystal is brought about by the mosaic of unit cells and the space group's symmetry operations. But, as a brief aside, order in nonperiodic crystals is induced by *tiling rules* that govern the placement of 36° or 72° oblique angle rhomboid tiles and thereby engender local fivefold symmetry within nonperiodic crystals. The nonperiodicity of *quasicrystals* and unit cells are mutually exclusive and will be discussed in detail later on.

Symmetry, Spectroscopy, and Crystallography: The Structural Nexus, First Edition. Robert Glaser.

Companion Website: www.wiley.com/go/Glaser/Symmetry

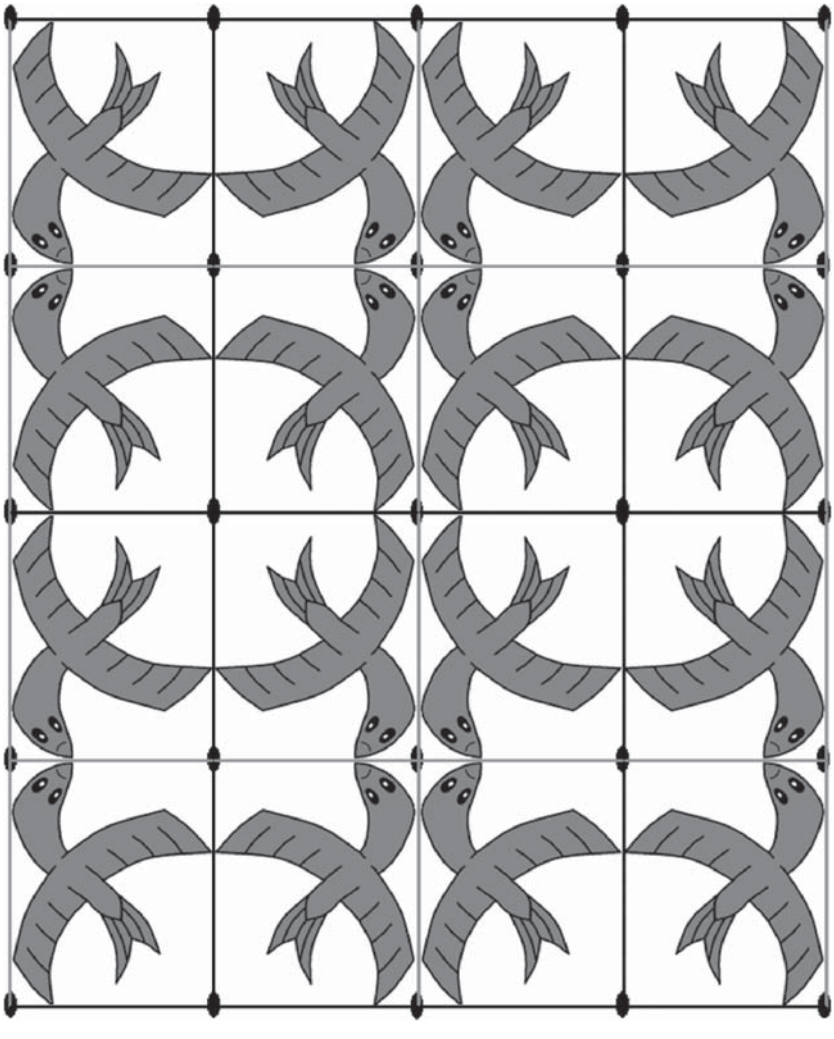

182

183

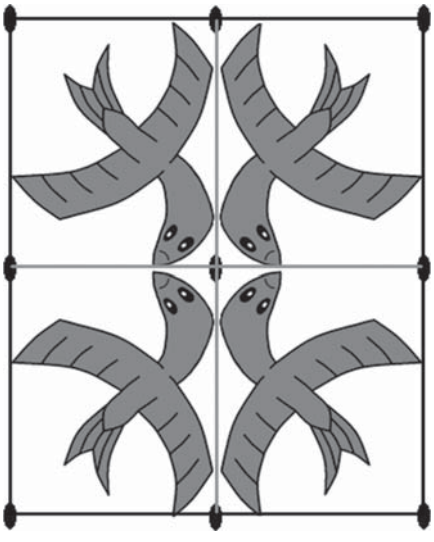

184

Since *identity* must always be present in every group, and *translation* must also be found in every space group, they are known as *trivial* operations (in the sense of being *commonplace* or *ordinary*). A one-bird *asymmetric unit* (**183**) contains the *minimal amount of structural information* required to generate the entire **184** unit cell utilizing all the space group's symmetry operations (e.g., σ_x, σ_y, and C_2) except *translation.* If only the two trivial operations comprise the space group, then the *asymmetric unit is the entire unit cell.* But, if additional operations are present as they are in **184**, then asymmetric unit **183** represents only one-quarter of unit cell **184**. In periodic lattices such as **182**, the $Z = 4$ parameter states the number of complete bird **183** graphical/molecular units (formula units) required to fill unit cell **184**, using the 2D *p2mm* space group's σ_x, σ_y, and C_2 symmetry operations. These operations generated two *d,l*-pairs of chiral birds. The crystals are achiral since these mirrors reflect left into right asymmetric units and vice-versa. The Z' parameter reports the fraction of an object/molecule (i.e., formula unit) that comprises the asymmetric unit. Since the chiral Escher bird **183** is also asymmetric, then $Z' = 1$.

There can be *no* symmetry elements within an asymmetric unit. By definition, all objects, molecules, and skewed birds residing within the bounds of the asymmetric unit are *chiral* and *asymmetric*. The lattice points in the asymmetric unit are called *general positions* of crystallographic symmetry. They are transformed from asymmetric unit to asymmetric unit by the space group's

symmetry operations. Where must the *symmetry elements* of a **184** unit cell be located? Answer: only on the asymmetric unit's boundaries and this is no accident. A symmetry element's locale of points will always remain invariant in space under its symmetry operation. As a result, this is probably the basis for referring them as being *special positions.* While all general positions are *asymmetrically chirotopic,* special positions can be either C_n-symmetrically chirotopic (where *n* is strictly *limited* to 2, 3, 4, and 6) or achirotopic (for all those of the Second Kind, excluding glide-reflection planes). Why is a glide-reflection plane not a special position? Answer: special positions are those that can be occupied by molecules having the exact same point group symmetry element. Symmetry operations based upon translation (pure translation, screw-rotation, and glide-reflection) are found only in space groups and, thus, can never be found in a molecule.

Characterization of general and special positions of symmetry need not be confined only to crystals [125]. The terms general and special positions of symmetry need not be confined only to extended arrays [125]. Let us consider the ^{31}P magnetic nuclei within **185** (Refcode DPTCIR [126], no coordinates deposited). They have symmetry-equivalent A- and X-partners due to the presence of molecular

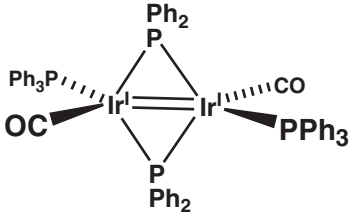

185

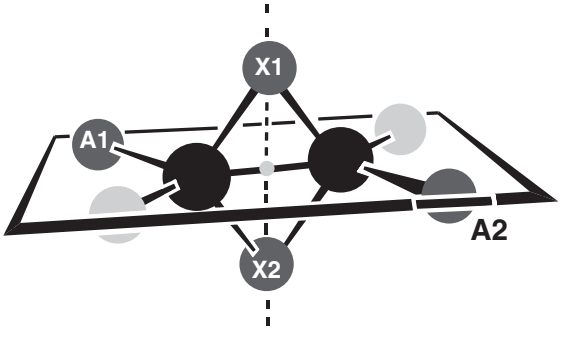

186

symmetry operations. Furthermore, consider a nonsymmetry-equivalent third nucleus X residing upon the same special position of *molecular symmetry* that relates the A-nuclei pair (see (- - -) C_2-symmetry element in **186**). If an X-nucleus vicinal coupling constant to one A-nucleus neighbor is $^3J_{AX}$, then there must be an *identical* $^3J_{AX}$ coupling to the second A-nucleus. In this case nuclear magnetic resonance (NMR) spectroscopists state that X is *isogamous* to each A-nucleus. *Isogamous* is the Greek *isos* ("equal") and *gamy* ("mating," as in mono*gamy*, bi*gamy*, poly*gamy*, etc.). In other words, not only are the two A-nuclei symmetry equivalent to each other, but we say that they are also *magnetically equivalent* to X. As a result, an A_2X_2 ^{31}P four-spin system's A_2 and X_2 2:4:2 transition-intensity simple triplets derive from *first-order splitting*, and the determination of δ_A and δ_X chemical shifts and their single mutual $^3J_{AX}$ coupling constant is a very simple task [125].

Next, consider the same symmetry-equivalent A_2 pair, but now X occupies a general position of molecular symmetry. Since the X-position is *asymmetrically chirotopic,* then X can never be equivalently spin–spin coupled to any pair of symmetry-equivalent neighbors (see **187** and **188**). X1 is *cis* to A1 and *trans* to A2. The crystal structure of **187** is found in Refcode BOPPEB20 [127]. Now, X is

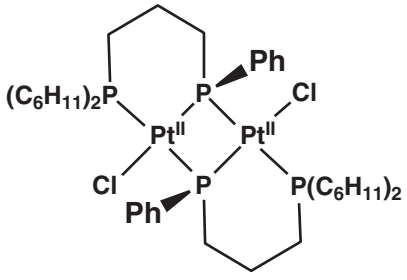

187

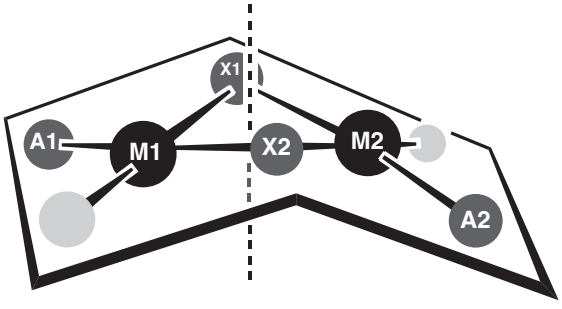

188

anisogamous to each A-nucleus, and the two A-nuclei are *not* magnetically equivalent to X. This situation leads to an extremely complicated $AA'XX'$ four-spin system. This *second-order* spin system is extremely complex since every nucleus is spin–spin coupled to every other nucleus in the system to afford $^3J_{AX}$, $^3J_{A'X}$, $^3J_{AA'}$, and $^3J_{XX'}$ couplings that require computer simulation to solve the unsymmetrical multiplet [125, 127]. We all remember that symmetry-equivalent nuclei do not spin-couple to each other in our *everyday* first-order spin systems.

9.2 Achiral Periodic Arrays of Chiral Objects and Racemic Compound Crystal Lattices

Crystallization of a racemic mixture will yield achiral crystals approximately 90% of the time. In this case, both enantiomeric birds reside in *equal amounts* and at *well-defined locations* in the achiral **184** unit cell. Such a crystal is called a solid-state *racemic compound*, since all of its physical and chemical properties that depend upon the solid-state packing arrangement will differ from those of a *chiral crystal* filled with only chiral compounds of *identical* handedness; see **189** (where $Z = 4$ and $Z' = 1$). In other words, the solid-state-dependent properties of a one enantiomer chiral crystal differ from those of the racemic compound crystal as if the latter were a different compound. Some of these properties of racemic compounds include X-ray diffraction (single crystal or powder), solid-state CPMAS (cross polarization magic angle spinning) NMR, circular birefringence (optical rotation), circular dichroism, solubility, rate of dissolution, melting point, density, storage stability, and so on. *Racemic modification* is the older term for racemic compound.

In many space groups, the choice of origin is set by historical convention, while in others, it is set by the crystallographer. In array **182**, any of the C_2 axes generated by the intersecting mirror planes in the achiral array is a logical locale to place the cell origin (i.e., between either the bird heads or the bird wings).

9.3 Chiral Periodic Arrays

Illustration **189** depicts a chiral periodic array of anticlockwise rotating birds. Both the **187** racemic compound and the chiral **189** unit cells have parameters $Z = 4$ and $Z' = 1$, since the four asymmetric birds have no choice but to occupy general positions. Crystallization of a racemic mixture of molecules affords *chiral crystals* only about 10% of the time. Pasteur's crystallization of about 20 different paratartrate (i.e., racemic acid, see introduction) salts and the parent diacid afforded only one example of a *spontaneous resolution* (sodium ammonium paratartrate).

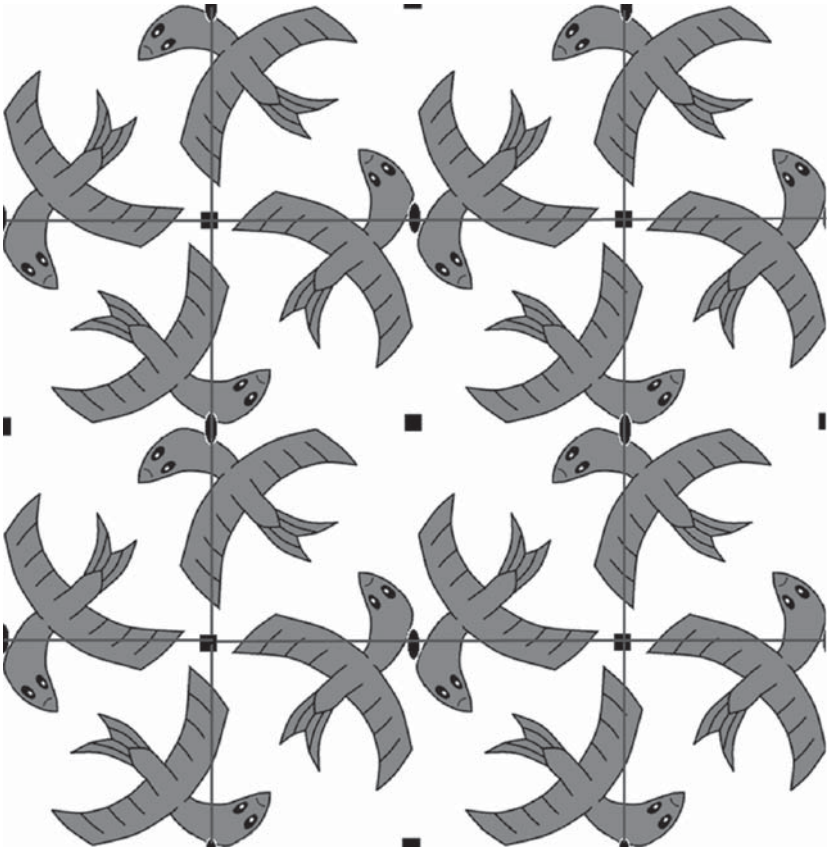

189

The chiral crystals formed via this process represent a *conglomerate* (a mechanical mixture, such as concrete's sand and cement) of (+)-**190** and (–)-**191** crystals. As in the landmark case of Pasteur, their outward appearance (*crystal habit*) *sometimes* may enable the naked eye to recognize them as a set of *enantiomorphous* crystals. But this visual perception of a chiral habit is not usually the norm. Space filling in chiral arrays/crystals is described by the 65 *Sohncke* space groups (space groups containing only symmetry operations of the First Kind). The Cambridge structural database (CSD) statistics on 3 January 2014 show that 15.7% of the database entries adopt Sohncke space groups. The CSD calls these space groups *chiral space groups* since they contain no operations of the Second Kind that can generate an enantiomer within the lattice. In other words, when the asymmetric

190

191

unit contains only one molecule ($Z' = 1$), then all the molecules within a single chiral crystal must have identical chirality since there are no operations within the group that can generate the enantiomer. The C_4- and C_2-axes preserve the rotation/twist sense of the birds in their *p4* 2D space group **190**, **191** unit cells.

If we compare the *racemic compound's* achiral **182** array with the *chiral crystal* **189** array, it is now clear why all solid-state packing-motif-dependent physical properties must be different by symmetry argument. Despite the presence of the *same chiral bird* in the two space-filling arrangements, the bird's neighbors are simply *different.* A left-handed bird in **182** is surrounded by four adjacent right-handed birds on all sides, but a left-handed bird in **189** is bordered by four left-handed birds. The pioneering solubility study by Berzelius showing 10-fold differences in the weight of water required to dissolve more soluble (+)-tartaric acid compared to less soluble paratartaric acid has already been discussed earlier in this book. Variation in physical properties, such as solubility noted in the previous section, shows the logic of using the noun "compound" in the term *racemic compound* crystal to differentiate it from an enantiomerically pure chiral crystal. Despite the fact that the two crystal forms differ only in enantiomeric neighbors for one and homomeric entities for the other, their solubility differences were so meaningfully disparate that Berzelius "might have thought" that crystals of two different compounds were being investigated.

Molecular structure is an obvious property that is dependent on disparate space filling in racemic compound and chiral crystal lattices. Artistic liberty has been taken by the author in using the "visually" identical left-handed chiral bird graphic for both achiral **182** and chiral **189** arrays. However, this analogy

is erroneous in the case of achiral and chiral crystalline arrays of molecules. It is highly probable that the molecular conformation in a racemic compound crystal is the *same* as that found for the molecule in the enantiomerically pure chiral crystal. One should not be surprised by this since Nature prefers low-energy spatial arrangements of molecular orbitals that dictate a particular 3D arrangement of bonds and atoms. However, it must be remembered that the concept of *same* conformation implies only a "similarity" and not an "identity." The crystallographer will find that the molecular conformations differ slightly in *all* their bonding parameters (bond lengths, bond angles, and torsion angles). Why? The answer is simple: identical structure requires a symmetry transformation to convert one environment into the other. But the absence of symmetry constraints obligates the two conformations to be nonidentical since their surroundings are different (i.e., their intermolecular interactions and forces have to differ to some extent). This point has already been discussed in regard to (±)-nefopam·HCl·anhydrate and (+)-nefopam·HCl·monohydrate *boat–boat* geometries.

There is a very high probability that a solvated symmetrical molecule will become ever so slightly distorted (i.e., desymmetrized) and become asymmetric as it enters a general position of symmetry in a crystal lattice. Why is this? Maintaining a molecule's solution-state symmetry is not Nature's primary goal in the crystallization process. Efficient space filling (minimum void space crystal packing) and the maximum of intermolecular interactions assume a greater importance toward the goal of attaining thermodynamically stable crystal packing. For this to come to pass, Nature often places the formerly symmetrical molecule at a general position of symmetry (i.e., one that is *asymmetrically chirotopic*). Doesn't asymmetric imply great distortion? Definitely not. In many cases, the crystal state molecular asymmetry often assumes *high-fidelity pseudo*symmetry whose distortions from ideality are not even visually perceived. For example, torsion and bond angles lose their ideal $360°/n$ integer values and exhibit noninteger values close to the ideal; bonding parameters (bond lengths, bond angles, and torsion angles) no longer show their symmetry equivalence. How do we know that the asymmetry exists if the solid-state molecule appears to us as symmetrical? By the same way we know that a solvated molecule is symmetrical. By observing or not observing multiple-intensity degenerate frequency signals in the solution-state NMR multiplets whose number is less than the ^{1}H or ^{13}C nuclei in the molecular formula. This slight change in solid-state geometry from the ideal is manifested by the loss of degeneracies in the diffracted X-rays so that different frequencies are now emitted from the formerly homo- and enantiotopic symmetry-equivalent subunits. In other words, the loss of ideal molecular geometry affords unique diffraction from the electron clouds around each and every atom in an asymmetric molecule. Avnir's algorithms [11, 12] provide a most useful tool for measuring the degree of distortion from ideal point group geometries.

9.4
Occupancy of Special Positions in Periodic Arrays

The commonly observed molecular occupancy of general positions (and subsequent attainment of molecular asymmetry) certainly should not imply that there can never be partial or even full retention of a solvated molecule's point group symmetry upon crystallization. A match between a solvated molecule's point group symmetry element and that of the special position in the lattice is a prerequisite (but not a sufficient condition) so that the two elements *may* coincide in the crystal. Contrarily, a mismatch of elements is a guarantee that the molecule will occupy a general position rather than a special one. First and foremost, the asymmetric unit must efficiently *tessellate* in three dimensions and concurrently benefit from auspicious intermolecular interactions.

Illustration **192** depicts a *p2mm* 2D achiral extended array of **193** achiral Escher birds. Notice that the achiral bird's σ-plane and the lattice's mirror plane

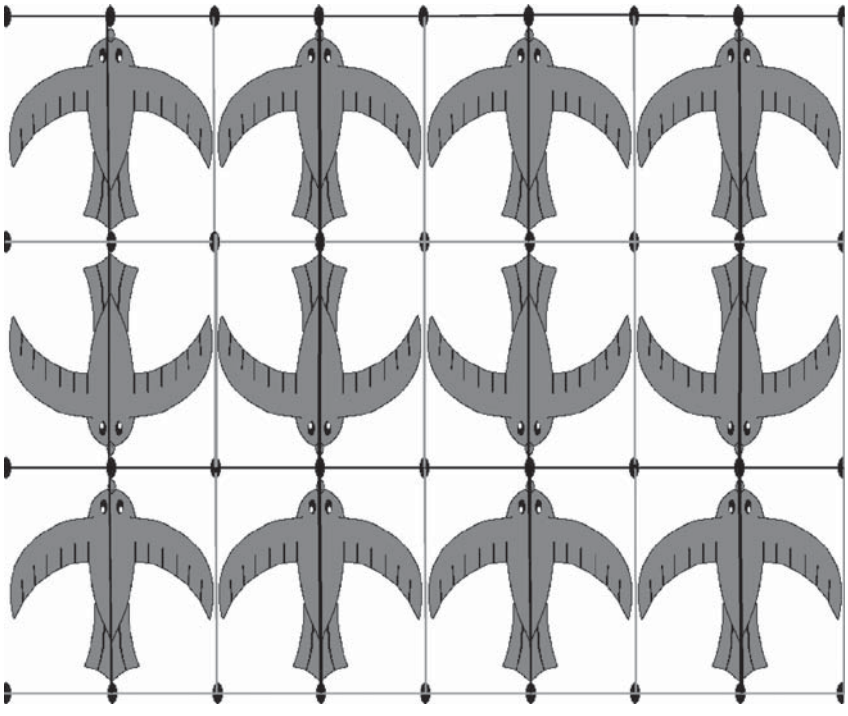

192

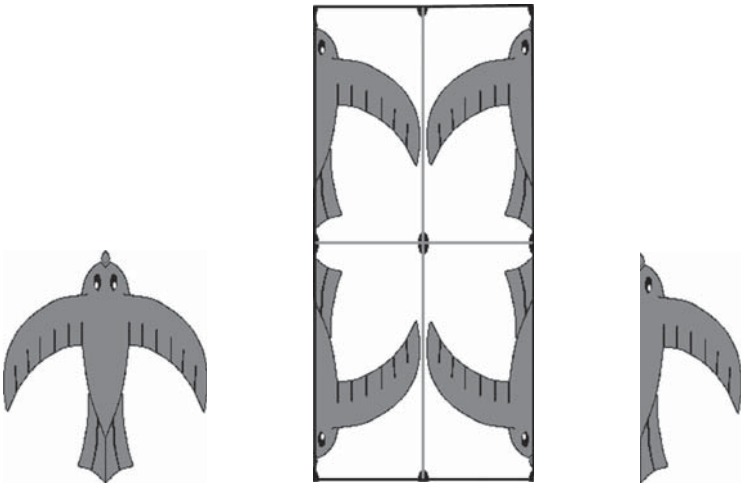

193 **194** **195**

coincide so that the unit cell volume is reduced to half of that for **184**. Now, the same *p2mm* σ_x, σ_y, and C_2 operations acting upon a *half-bird asymmetric unit* **195** generate two complete achiral birds within unit cell **194** (rather than the four complete chiral birds of unit cell **184**). In other words, the number of complete bird objects in the unit cell is $Z = 2$ rather than $Z = 4$ for the four full objects in unit cell **184.** The half-bird's asymmetric unit **195** affords $Z' = 0.5$ (rather than 1 for the complete **183** bird). However, $Z/Z' = 2/0.5 = 4$, that is, the same number of four asymmetric units in the **194** unit cell as that in unit cell **184** where $Z/Z' = 4/1 = 4$.

If the space group is known and the approximate volume of a molecule can be estimated, then determination of an appropriately reduced number of full molecules within the unit cell testifies to *occupancy of a special position* in the lattice (even before the molecular structure is known to the crystallographer). An example of this situation will be presented next. Two diplatinum^{II} complexes were synthesized by Glaser and Meek [127] as a mixture of two diastereomers (C_2-symmetry chiral (*rac*)-*cis*-**187** and C_i-symmetry achiral (*meso*)-*trans*-**196**) and then column-chromatographically separated. Their stereochemistry initially could not be ascertained by $^{31}P\{^1H\}$ NMR spectroscopy owning to the extremely complex $AA'XX'$ four-spin system, where $\{^1H\}$ = broadband ^1H decoupling. One of the fractions crystallized in the monoclinic $P2_1/c$ space group with $Z = 2$, $Z' = 0.5$ (rather than the general positioned case of $Z = 4$, $Z' = 1$). In less than one half hour, it was found that $Z' = 0.5$ since the unit cell's volume

was half that expected for the space group's symmetry operations when $Z' = 1$ complete molecule asymmetric unit. This fractional Z' value clearly showed that the molecule occupied a *special position* of symmetry in the unit cell. The call was simple since the sample had to be the *trans*-**196** diastereomer. Why? The only special position in that space group was inversion symmetry (compatible with both *point and space group symmetry*). Note: the 2_1-screw axis cannot be a special position occupied by a molecule's point group symmetry element, since screw-rotation symmetry is only compatible with space group symmetry. The power of this reasoning is that configurational assignment was made only a half hour after the sample was mounted on the diffractometer. Of course, for *good science*, this had to be later confirmed after data collection, and it was [127]. Diastereomer **196**'s residence at a special position of inversion symmetry is in accord with the remarkable CSD survey results by Pidcock *et al.* [128] reporting that 99% of the solvated C_i-symmetry molecules preserve that symmetry upon crystallization. Inversion arrangements between two enantiomers are very sterically favorable (rather than intermolecular mirror symmetry). Why? In an inversion relationship, the small substituent is opposite to the largest substituent of its symmetry-equivalent neighbor, that is, a (small–large) steric interaction. On the other hand, an intermolecular mirror relationship requires less favorable (small–small) and (large–large) dispositions. Other solution-state symmetries show a propensity to remain upon crystallization. For example, Brock and Dunitz [129] note that there is a strong preference for solvated molecules with C_3-axes to keep this symmetry by residing on special positions of threefold rotational symmetry when crystallized.

In addition to being able to make a rapid structural assignment, it was apparent from simple geometrical considerations that the presence of an inversion center in *trans*-diastereomer **196** obligated the four-membered [–Pt–P(phosphido)–Pt′–P′(phosphido)–] *core* **197** to be *ideally planar.* The crystal structure of **196** is found in Refcode CIBDAS10 [127]. A four-membered cycle of alternating A and B units will be coplanar only under certain geometrical conditions. The passage of a molecular reflection plane through all four units of the cycle was out of question, due to the chirotopic stereogenic phosphido-P atoms. Similarly, a C_2-axis through pairs of oppositely disposed A- or B-pairs could be ruled out for the same reason. The only other possibility is a center of inversion coincidental with the cycle's centroid, and this was certainly possible. The crystalline bimetallic complex was indeed found to be *meso* as initially predicted.

The *cis*-isomer occupied a general position of symmetry, which imposed no symmetry constraints at all upon the four-atom core geometry (indeed, it was shown to be bent by about 19°); see **188.** A consideration of the orbital-overlap consequences of *cis/trans* core geometries led to a reinspection of the already measured second-order *J*-couplings involving [130] Pt. A more careful comparison of the $^{195}Pt\{^1H\}$ NMR spectral parameters for both diastereomers showed two *Karplus-like* orbital geometry dependent *J*-coupling relationships.

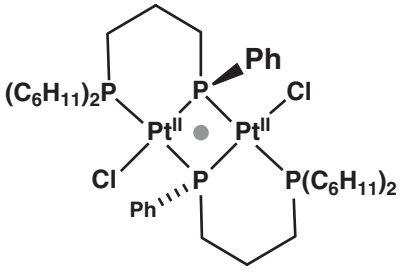

196

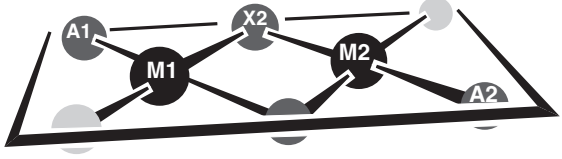

197

Greater orbital overlap in the *trans*-diastereomer's planar-core **197** versus reduced overlap within bent-core **188** manifested itself in a 2.5× higher 639 Hz ^{2}J(M1M2) and 6.6× higher 33 Hz ^{3}J(A2M1) values for *planar-core* **197** versus lower 259 and 5 Hz respective values for *bent-core* **188** [127].

9.5
The Bragg Law and X-Ray Diffraction

X-rays were discovered by the German physicist Wilhelm Conrad Röntgen in 1895. He was awarded the first Nobel Prize in Physics in 1901. At that time, they were assigned an "*X*" descriptor since the exact nature of the rays was unknown. The diffraction of X-rays by crystals was discovered in 1912 by Max von Laue, who described this phenomenon as diffraction from a three-dimensional grating. Gratings are ordered structures that are *periodic* (crystal lattice). Like Röntgen, who preceded him, von Laue was awarded the Nobel Prize in Physics in 1914. In 1913, William Lawrence Bragg (at the age of 23) noted a similarity between reflection and diffraction. He and his father, William Henry Bragg, were awarded the Nobel Prize in Physics in 1915.

In the single-crystal X-ray diffraction technique, a crystal (about one third the size of a sugar crystal) is chosen. Using a microscope and polarized light, periodic extinction upon crystal rotation is expected for noncubic *single crystals* (i.e.,

those that are not twinned or suffer from appended crystals). The crystal is affixed to a glass fiber with epoxy (two amorphous materials, i.e., nondiffracting) and then mounted in a *goniometer* (*gonia* Greek for "angle," a small metal holder with adjustable arcs to attain a particular orientation of the crystal facets relative to the incident X-ray beam). The crystal is then gradually rotated under bombardment by X-rays. An X-ray diffractogram (an *interferogram*) results from waves that are diffracted at discrete angles from electron density distributed periodically in the crystal lattice according to the *Bragg condition*. The Bragg law for diffraction states $2d \sin \theta = n\lambda$, where $d =$ interplanar spacing, $\theta =$ incident and emerging angle of rays with planes in the lattice, $n =$ an integer, and $\lambda =$ wavelength.

9.6 The Interferogram Phenomenon in Single-Crystal X-Ray Crystallography

X-rays are diffracted by the reflection planes of electron density (around atoms or covalently shared and nonbonded electrons) within the unit cell of a crystal and generate a *sphere of reflection*. Shorter X-ray wavelengths (e.g., 0.7105 Å, Mo K_α) enlarge the size of the reflection sphere, while longer wavelengths (e.g., 1.542 Å, Cu K_α) shrink the sphere. As the sphere grows, so will the number of reflections that will be observed by a detector.

If the crystal is both ordered and periodic, then the diffraction pattern consists of regularly spaced spots, see **198**. A detector measures intensities as a function of spatial location within the *interferogram* pattern. This data is in the form of intensity-squared reflections (I^2), and thus, the detector cannot differentiate between negative and positive intensities. One layer of an X-ray diffraction pattern is depicted in photograph **198** measured on film with a Buerger precession camera (not the latest technology). Note the periodicity of the spacings between dots. These spacings afford *reciprocal space* data that provide the *cell constants:* that is, the unit cell dimensions (a, b, c) and the angles (α between b and c axes, β between a and c axes, γ between a and b axes). What do we mean by reciprocal space? The larger are the uniform spacings between spots, the smaller is the real-space cell dimension. Thus, the vertical distances in **198** actually arise from a shorter cell axis, while horizontal distances are produced by a longer cell axis positioned 90° from the first axis.

Note the different I^2 intensities of the spots. A Fourier transformation of the interferogram's reflection intensities *plus addition of their phase relationships* will provide a three-dimensional model of electron density within the unit cell. The *atomic resolution* (in Å) in the model increases with diffractograms containing more *significant reflections* (i.e., those with $I_{net} > 2\sigma(I_{net})$, where $\sigma =$ average noise) measured at increasing angles from the pattern center. As with all interferograms in general, the intensity and phase of every reflection point contain information from all the electron densities periodically distributed

within the cell. The black hole in the center of the photo arises from nondiffracted rays passing straight through the crystal into a small lead cup behind the crystal and opposite the incident beam. Note the presence of lines of *white noise* near the center. Each reflection has noise intensity associated with it, which must be corrected prior to Fourier transformation of the data set. The crystal must be of a large-enough size and high quality so that very low intensity measurements will remain statistically meaningful after noise correction. As noted earlier for triarylamines, for good signal-to-noise measurements, crystallographers prefer prisms over platelets and platelets over needles. But too large a crystal runs the risk of lattice imperfections (e.g., layer slippage). Some interferogram film spots will show low intensities approaching zero, while others should exhibit integer-zero intensities due to specific space group symmetry (i.e., *systematic absences,* every *n-th* spot absent along a particular axis).

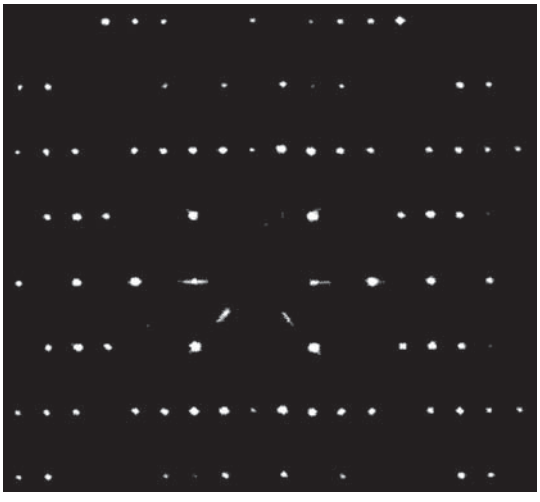

198

Great improvements have been made in terms of quantification accuracy and precision of these squared-intensity data measurements throughout the years. Initially, X-ray sensitive photographic film was used. Historically, the intensity quantification at various positions on the film was visually estimated via crude optical density comparisons with a "standard film set" produced by ever increasing X-ray irradiation times. This very time-consuming and subjective method was later replaced by more objective optical density scanners. It was then replaced by four-circle diffractometers with Geiger–Müller counters that were moved from position to position around the mounted crystal. These positions

were precalculated from the space group symmetry and the cell constants. Modern diffractometers now use *high dynamic-range* multipixel detector plates. These *charge-coupled device* (CCD) detectors afford high-resolution position-sensitive data.

Unfortunately, the I^2 data set lacks the *phase* information required to accurately characterize the sine-wave components of the interferogram. This is the origin of the so-called *phase problem* in X-ray crystallography. Determination of the phases for noncentrosymmetric crystals was once a very time-consuming task. However, *direct methods* were then developed for an initial estimation of phases for small molecules. Some of these *stochastic* (statistical) methods were based upon a first approximation assumption that the positions of atoms in the asymmetric unit are not totally random but rather have constraints due to bonding distances and van der Waals radii. The high importance and utility of the Karle–Hauptman *tangent formula* to provide these initial phases was recognized in 1985 by awarding the Nobel Prize in Physics to the developers, Jerome Karle and Herbert A. Hauptmann.

Both phase and intensity data are required to locate the spatial disposition of electron density in the unit cell. An iterative calculation process (called *refinement* by full-matrix least squares) relocates atomic positions of the initial *structure solution* until the calculated versus experimental unit cell electron density distribution converges. We may think of the reflection data as a large collection of simultaneous equations whose unknown variables include *atomic positional parameters* (e.g., [x, y, z] fractional coordinates), and atom-specific *thermal displacement parameters* that are either *isotropic* (for protons, one radius parameter for a sphere) or *anisotropic* (for nonproton atoms, six parameters defining ellipsoids of 50% probability), plus one overall scale factor parameter per structure. It is known that unique structural model hypotheses may not necessarily be found when the number of simultaneous equations (i.e., the nondegenerate *unique* statistically significant $I_{net} > 2\sigma(I_{net})$ reflection data) is only slightly greater than or equal to the number of unknown parameters. What makes the single-crystal X-ray diffraction structural model chemically accurate (i.e., refinement converging to a unique solution) is that the technique is *overparameterized* (i.e., unique significant reflection data is usually about 10 times the number of variables). In this event, the six anisotropic thermal displacement parameters can be readily calculated for the nonproton atoms. However, if this is not the case, then the number of variables must be decreased by considering only isotropic thermal displacement parameters for the nonproton atoms (one for each atom, rather than the six for each atom, for anisotropic thermal parameters) and neglecting the calculation of the inaccurate proton positions. Another method to increase the unique significant $I_{net} > 2\sigma(I_{net})$ reflection data is to reduce the thermal displacement by measuring a low-temperature data set. For *ambient-temperature* acquired data sets, refinement convergence usually occurs when the calculated model can account for more than 95% of

the electron density in the final map. In other words, less than 5% of the unit cell total electron density (the *final residual discrepancy index* or *R*-factor) remains unaccounted for by the model. Under these conditions, the residual positive and negative electron densities in the *final map* are typically ≤+1 and −1 electrons $Å^{-3}$.

Correct convergence to a chemically sensible structure during refinement requires consideration of the low electron densities for protons, as well as those readily measured for the higher electron densities of nonproton atoms. In principle, proton electron densities can be forthcoming from a *difference map*, where the calculated electron densities of the nonproton atoms are subtracted from the experimental electron density map for all atoms (nonproton atoms and protons). However, not only does the proton's single electron circle around the nuclear sphere, but it is also involved in covalent bonding. A common result is nonoptimum S/N in experimentally determined *low electron density measurements of protons.* Instead, protons are usually placed at geometrically calculated positions (based upon nonhydrogen X–X–X bond angles) and refined using the *riding method*. In this technique, constraints are applied to X–H bond lengths and H–X–H/H–X–Y bond angles, by setting them at certain fixed values. If the X-atom carrying the hydrogen moves under isotropic refinement, then the hydrogen atoms move with it keeping their bond lengths and angles constant. If we desire accurate positional measurement of protons, then neutrons will provide diffraction from the relatively more solid nuclei rather than from the "softer" more ephemeral electron clouds.

9.7
X-Ray Fiber Diffraction

One of the main differences between the A- and B-forms of DNA is that the bases are tilted on the axis in the former and perpendicular to it in the latter. Bundles of long fibers such as B-DNA can be held under tension in high humidity to afford partial ordering along their axes. This is sufficient for X-ray diffraction even if it involves order in only one dimension. However, in the direction perpendicular to the axis, there is disorder between the fibers composing the "bundle." This disorder is the reason why one only observes elongated streaks in diffractogram **199** rather a discrete spot pattern in **198.** This is a historic diffractogram taken by Rosalind Elsie Franklin's Ph.D. research student Raymond Gosling in May 1952 at King's College London in the Medical Research Council's (MRC) Biophysics Unit. The DNA fiber X-ray diffraction photographs taken by Franklin have been described by John Desmond Bernal (a pioneer in X-ray crystallography for molecular biology) as "amongst the most beautiful X-ray photographs of any substance ever taken."

The "cross" in the photo is characteristic of helical diffraction patterns described by *Bessel*-type mathematical functions. Layer lines are seen, since the helix is periodic along the axial direction. Two high-intensity curved streaks are located at the top and bottom termini of the vertical axis through the center and exhibit a large spacing. Remember, we are dealing with reciprocal space, so this large distance derives from the 3.4 Å base-pair stacking distance. The smaller distance between the lower intensity off-axis streaks, forming the cross, is the 34 Å axial distance of the helix required for one full turn (i.e., the repeat unit). The pitch of the helix can be calculated from these two data.

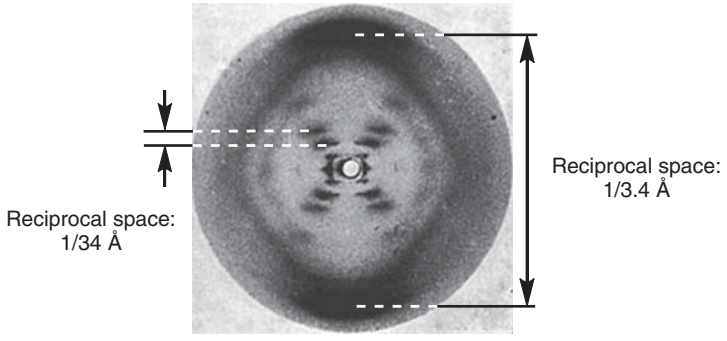

199

Franklin's 1952 photographs 51 (**199**) and 52 played a crucial role in the creation of DNA's double-helical theoretical model by biologist James D. Watson and physicist Francis Crick at the Cavendish Laboratory in Cambridge University. To understand what transpired, one has to recall that the situation of women scientists in prestigious universities of post-War Britain was not as it is today. In addition to having the disadvantage of being a woman in a man's world, Rosalind Franklin had a second stigma – she was also born into a very influential British Jewish family. Her father's uncle was Herbert Samuel (later the first Viscount Samuel) who was Home Secretary in 1916, the first practicing Jew to serve in the British cabinet and later the first High Commissioner of Palestine in 1920. Her paternal aunt was married to Norman de Mattos Bentwich who served as Senior Judicial Officer in the British Military Government of Palestine and later as Attorney-General of the civilian Palestine Mandatory Government until 1931.

In 1952, along with Gosling, her doctoral student, they applied a *Patterson Function* to their X-ray data to solve the "phase problem." In January 1953, Franklin had finished her research at King's College and was moving to a new position at the University of London's Birkbeck College. Unaware of Watson

and Crick's model-building endeavors, her experimental findings had already concluded that both the A- and B-forms of DNA had a double-helical structure and that *the phosphate groups were on the structure's periphery.* At that time Franklin was leaving her King's College laboratory to take up her new position at Birkbeck, Raymond Gosling (Rosalind Franklin's Ph.D. student) gave Maurice Wilkins (a Research Associate colleague also studying DNA structure at King's) a copy of photograph **199**. The reasons for Gosling doing so are unclear. Unfortunately, while at King's College, an intense personal animosity had already developed between Franklin and Wilkins, which was to exert its effect on future events. On 30 January 1953, Watson traveled down to King's and, after an altercation with Franklin, was shown photograph **199** by Wilkins without Franklin's permission or knowledge. During mid-February 1953, Max Perutz (Crick's research director) gave Crick a copy of a research report by Franklin containing many of her crystallographic calculations. It was this report that convinced Watson and Crick that the phosphate groups had to be on the outside backbone. Franklin had been asked to write the report in preparation for an impending MRC Biophysics Committee visit to King's in December of 1952 by Perutz and other committee members. On 7 March 1953 (1 day after Franklin's two Form-A submitted manuscripts reached *Acta Crystallographica*'s offices in Copenhagen), Watson and Crick finished their theoretical model of DNA. In 1962, 4 years after Rosalind Franklin had died of cancer, Watson, Crick, and Wilkins received the Nobel Prize in Medicine for the double-helical structure of DNA. For the sake of fairness and justice, it is indeed very regrettable that the Nobel Committee could not posthumously award the prize to Franklin. The lesson to be learned from this account is that science is performed by living human beings often inspired by great clarity of thought, ingenuity, and brilliance of insight, but these attributes of the spirit can also be tempered by flaws of character and competition. As a curiosity, Maurice Wilkins was the Ph.D. research director of Robert Langridge, the author's crystallographic postdoctoral mentor at Princeton.

9.8
Penrose Tiling Matching Rules, Quasicrystal Packing, and Dodecahedrane

It was earlier noted that C_n-rotational symmetry in a crystal lattice is constrained to be C_2, C_3, C_4, and C_6. These C_n-rotational symmetry limitations impose geometrical constraints upon the ability of C_5-symmetry objects/molecules to undergo efficient *tessellation* (the space filling of an infinite 3D-mosaic of congruent objects without gaps or overlaps within the lattice). Analogy may be drawn from 2D-space patterns of floor tiles. It is common to observe floor-tile repeat patterns constructed from triangles, as well as from squares/rectangles or hexagons. But, what about regular pentagons? They are considered by some to be

esthetically pleasing since the *cord* distance divided by a side is the golden ratio; see the dashed line in upper part of **200**. The problem is that regular pentagons cannot tile a floor without leaving some of the underlying subsurface exposed to view (see black color-coded subsurface in tiling pattern **200**). In other words, *five-membered rings just do not tessellate well.* However, *aperiodic* fully tessellated *ordered* arrays with local regions of fivefold symmetry can readily be constructed from 72° and 36° oblique angle rhomboid (2D) or rhombohedron (3D) building blocks if placed side by side according to *tile matching rule arrows,* see **201**.

The esthetically pleasing 2D arrays such as **201** are named after the English mathematician Roger Penrose, who shared the 1988 Wolf Prize with Stephen Hawking. It must be remembered that *order in crystal packing* is a prerequisite for all diffraction phenomena. We now understand that order is indeed present in a plethora of Penrose-type *aperiodic* 2D arrays of the aforementioned 72°/36° oblique angle rhomboids by means of the *tile matching rule arrows.* In these rules, single arrows must align with single arrows and double arrows with double arrows. With this constraint, 72°/36° oblique angle rhomboid building blocks can then be utilized to construct an ordered 2D arrangement that could be a representative model of that in *aperiodic* quasicrystal packing. Therefore, since the number 5 is a factor in aforementioned angular relationships ($360°/5 = 72°$ and $360°/(2 \times 5) = 36°$), it is obvious that these angles play a structural role in achieving local fivefold symmetry.

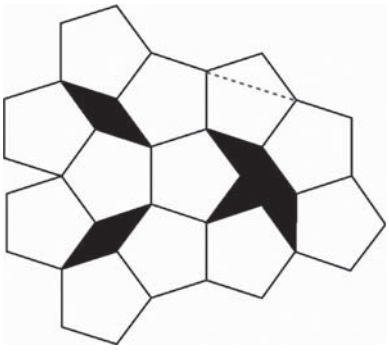

200

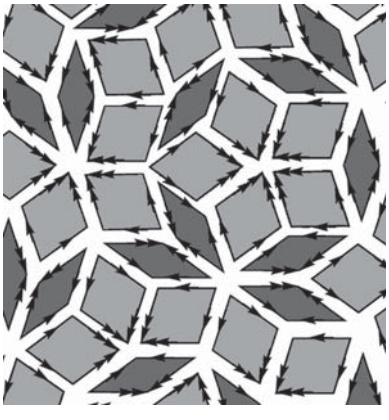

201

Prior to the discovery of fivefold symmetry in crystalline materials (now known as *quasicrystals*) by Daniel Shechtman at the Technion-Israel Institute of Technology (2011 Nobel Laureate in Chemistry), conventional wisdom was that all

crystals must be *both* periodic and ordered. A corollary to this was that the "laws of symmetry" mathematically stated that periodic arrays and fivefold symmetry were incompatible. Science has indeed come a long way since Gardner [131], the noted writer of recreational mathematics, wrote " … you will never find a pentagonal crystal." While "never" is usually just a very long time, the aforementioned statement was written in 1979, only 3 years prior to Shechtman's paradigm breaking discovery. It is reassuring to know that the laws of symmetry still reign supreme, since quasicrystals are aperiodic – so all is well. Quasicrystals are usually formed of metal alloys. Ho–Mg–Zn is the first rare earth containing quasicrystal structure and exhibits icosahedral morphology with fivefold symmetrical shinny metallic faces; see **202** [132].

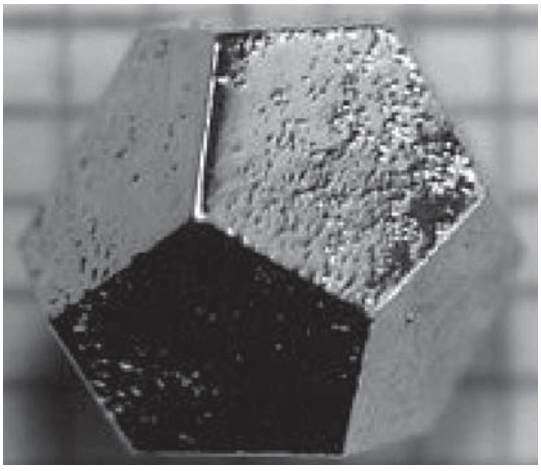

202

We have already discussed the spacings in diffractogram **198** of a periodic ordered crystal. Now, one can compare them to a different type of spacing in the electron diffraction pattern **203** of the Ho–Mg–Zn quasicrystal **202**. The spacing has been color-coded black on one of the fivefold axes. Instead of being multiples of 1, the spacings are multiples of the irrational number tau (τ, also called ϕ), that is, the *golden ratio*.

The observation of fivefold symmetry in crystalline materials by Shechtman was initially greeted with great skepticism and, even with derision, by some in the crystallographic community (especially the renowned crystallographer Linus Pauling) due to the dogma that said it was mathematically impossible. At one point, Pauling noted that "there is no such thing as bad science, only bad scientists."

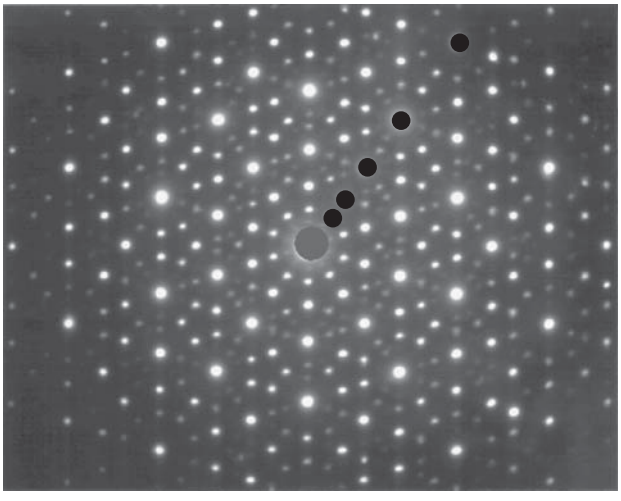

203

But, Shechtman was proven to be indeed correct, much to the chagrin of those who initially refused to accept his findings. As a result, the International Union of Crystallography in 1992 altered its definition of a crystal to be *an object having the ability of producing a clear-cut diffraction pattern whose ordering can be either periodic or aperiodic.*

10
Multiple Molecules in the Asymmetric Unit, "Faking It"; Pseudosymmetry Emulation of Achiral Higher Order Space Filling in Kryptoracemate Chiral Crystals

10.1
Multiple Molecules within an Asymmetric Unit

Desiraju [133] has noted that during the period of 1970–2006, the percentage of organic compounds in the Cambridge Structural Database (CSD) with more than one molecule in the asymmetric unit remained virtually constant at approximately 11%. Two molecules in the asymmetric unit ($Z' = 2$) occur when it is difficult, by symmetry alone, to simultaneously satisfy both the criteria of close packing and the requirements of optimal intermolecular interactions [134]. This situation enables the intriguing possibility of two molecules of either invariant or opposite handedness comprising the asymmetric units of chiral crystal structures. In most of those cases, asymmetric units consist of two molecules with the same handedness.

Gavezzotti [135] has investigated a large population of crystals with two molecules in the asymmetric unit ($Z' = 2$) and noted that with an asymmetry tolerance of 0.5 Å atom^{-1}, 83% of the nonsymmetry related intermolecular arrangements in the asymmetric unit revealed some kind of noncrystallographic symmetry beyond that of the true symmetry imposed by the space group. The presence of crystallographic *pseudosymmetry* emphasizes that the "… preconception that symmetry must rule exact and uninterrupted throughout proper crystals for best packing and for thermodynamic stability" sometimes is only achieved via multiple content ($Z' > 1$) [135].

In other words, why does Nature choose a packing arrangement with multiple molecules in the asymmetric unit ($Z' > 1$), when *almost all of the time,* a space group with only one molecule in the asymmetric unit ($Z' = 1$) nicely suffices for adequate spatial packing? Answer, there are times when $Z' > 1$ provides *more intermolecular interactions* and *reduced void space.* As an example, (±)-nefopam·methotetrafluoroborate quaternary ammonium salt (Refcode: SUGJIP)

Symmetry, Spectroscopy, and Crystallography: The Structural Nexus, First Edition. Robert Glaser.

Companion Website: www.wiley.com/go/Glaser/Symmetry

[124] (R. Glaser, R.A. Toscano, and I. Ergaz, unpublished data) crystallized in the *Cc* monoclinic space group ($Z = 12$, $Z' = 3$, $Z/Z' = 4$). The three (*R*)-symmetry cations of the asymmetric unit are aligned so that all their six aromatic moieties are oriented inward toward the center of a cluster of cations; see **204**. As a result, there are six intermolecular *edge-to-face* interactions (5.2(3) Å centroid–centroid mean distances, gray dashed lines) and one *face-to-face* π–π stacking interaction (4.1(1) Å centroid–centroid distance, black bold dashed line). Aromatic residues are said to have edge-to-face interactions if their inter-centroid distance is <7 Å (with 5 Å being most favored), and the optimum dihedral angle is about 90° [136]. The attractive force for a single Ar–Ar interaction is calculated to be weak (about −4 to −8 kJ mol^{-1}) [136], but there are a lot of them in the crystal.

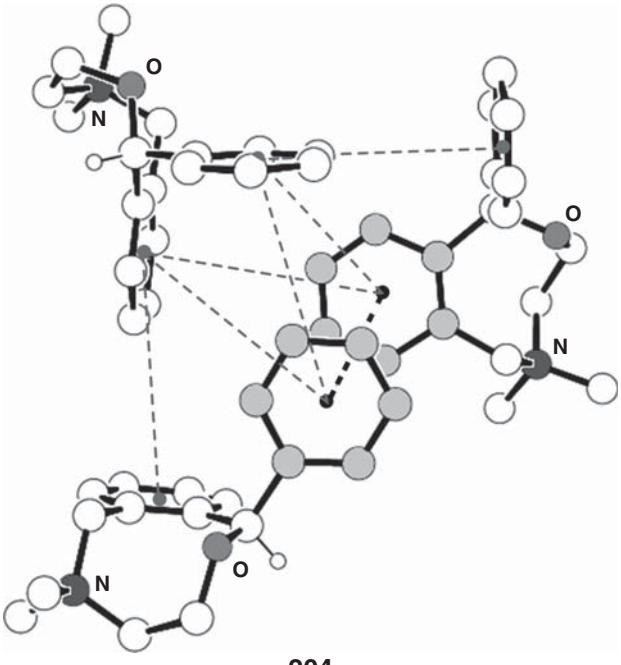

204

The more polar oxygens and nitrogens are disposed outward from the **204** asymmetric unit cluster, and the three charge-neutralizing tetrafluoroborate non-coordinating anions are located on the periphery of the cationic cluster forming a C_3-*pseudo*symmetric triangular array with "almost equilateral" 10.6(3) Å sides. This is in accord with Brock and Dunitz's observation that Nature has a propensity for C_3-symmetry packing [129]. There are no aromatic–aromatic interactions between the clusters. Glide reflection produces asymmetric unit clusters of three opposite (*S*)-handed molecules. The three (*R*)-symmetry homochiral molecules

within the asymmetric unit are structurally very similar, but they are indeed different. Welcome to the world of *pseudo*symmetry. They are diastereomers of the same handedness and all are bent into a *boat–chair* conformation of the eight-membered ring. *Pseudosymmetry* is enabling these molecules to emulate homomeric isomers. Why does it do this? Well, the *boat–chair* conformation of nefopam derivatives is found very frequently since the eight-membered ring can be inscribed upon the unstrained diamond lattice (*and nonprotonated* oxygen and planar $C(ispo)_{benzo}$ ring-atoms exhibit a minimum of transannular interactions); see nefopam·HCl **50**'s *iconic* representation. Since we are dealing with diastereomers, it is not surprising to measure slightly different bonding parameters, for example, N–C–C–O torsion angles of −49.8°, −48.6°, and −51.1°.

To measure just how structurally different the *pseudo*homomeric diastereomers are, we can superimpose all the eight-membered ring nonproton atoms, the two *N*-methyl carbons (in order to observe conformational differences), and also the phenyl carbons (to ascertain twist differences). It does not make sense to add the four benzo carbons to the superimposition, since we know that they are part of a *rigid appendage,* and their inclusion will only artificially improve the conformational RMS average fit (not a good idea statistically). Why not? We want to only superimpose those parts of the molecule that have possibilities of conformational and/or twist ambiguity. The RMS values of superimposition positional differences are quite low 0.073 Å (mol 1 on mol 2) and 0.038 Å (mol 1 on mol 3) values. Since both values are *less than* 0.1 Å, one can definitely state that the conformations and the phenyl twists of all the molecules in the asymmetric unit are the *same.* These RMS values provide an answer to the philosophical question: "How different can two symmetry- nonequivalent molecules be, and yet still have the *same structure*?" Once more we see that "same" is not a synonym for "identical." We have already discussed, the low 0.081 Å RMS for superimposition of (±)-nefopam·HCl·anhydrate (**50**) and monohydrate crystal structures. As a rule of thumb, one should expect symmetry-nonequivalent *isostructural* molecules (e.g., those in **204**) to show quite small ≤0.1 Å RMS superimposition values, since Nature prefers low-energy conformations, which arise from *chemical constraints* (i.e., stable conformations) and not from symmetry.

10.2 "Faking It": *Pseudo*symmetry Emulation of Achiral Higher-Order Space Filling in Kryptoracemate Chiral Crystals

*Pseudo*symmetry *relationships* between diastereomers at general positions of symmetry show a *continuum* of distortion from ideal symmetry. Glaser and coworkers [137] have reported algorithms to quantify the fidelity of *intermolecular pseudosymmetry*. Superior imitations imply higher *pseudo*symmetry fidelity

and concomitantly less distortion from ideal symmetry. Since intermolecular *pseudo*symmetry is Nature's most common crystallographic expression of this phenomenon, it should not be confused with structural differences between two *apparently randomly disposed* (Nature never does anything randomly) similar-structure isolated diastereomers that are *separately excised out* of the asymmetric unit and then superimposed.

A search of the CSD clearly shows that Nature will "fake" (or emulate) a symmetry relationship when she desires to be free of constraints of *symmetry equivalence* and *special position* in crystals and yet enjoy their important spatial benefits at the same time (a sort of "having your cake and eating it too"). She uses *pseudo*symmetry to perform this deception. Before we continue, it should be remembered that a sample of chiral molecules of the *same handedness* may crystallize ONLY in Sohncke space group crystals if there is one molecule in the asymmetric unit. Why? We know that these space groups lack symmetry operations of the Second Kind that are required to generate the enantiomer in a lattice.

But, what if there are *two molecules of opposite handedness* in the asymmetric unit of a Sohncke space group crystal? Think about it. These two oppositely handed molecules certainly *cannot be enantiomers,* since the space group lacks all symmetry operations of the Second Kind needed for the production of an enantiomer. Therefore, they must be *diastereomers of different handedness* since their connectivity is the same, and they are anisometric (corresponding diastereotopic atoms afford diffracted rays with nondegenerate frequencies since $Z' = 2$). Now, let us consider the following situation in the chiral crystal lattice: (i) the structural differences between the two diastereomers are so small that one visually perceives them to be enantiomers *and* (ii) they *appear* to be related by symmetry elements of the Second Kind. Once again, we return to the world of *pseudo*symmetry in what are known as *kryptoracemate* [138] (hidden racemate) chiral crystals. These crystals are produced by crystallization of a racemic mixture that yields a conglomerate of chiral crystals containing two molecules of opposite handedness in the asymmetric unit. In other words, the (+)-X and (−)-*pseudo*-X diastereomers reside within one chiral crystal, whereas (−)-X and (+)-*pseudo*-X occupy the other enantiomorphous crystal [138]. Kryptoracemate crystals have also been referred to as *false conglomerates* by Bishop and Scudder [139]. When kryptoracemate crystals are dissolved, the oppositely handed diastereomers are liberated from the lattice and revert once more into solvated enantiomers.

Fábián and Brock [138] undertook a very useful and extensive categorization of kryptoracemates and reported that only 0.1% of the entries in the CSD are kryptoracemates. Of this very small amount, about 60% of them exhibited *pseudo*symmetric relationships between the diastereomers [138]. The spatial arrangement of oppositely handed diastereomers in lower-order space group kryptoracemate unit cells often emulates space filling in *higher order achiral*

crystals [137, 138]. This is really quite reasonable. Why? Kryptoracemate space groups usually contain a nontrivial genuine symmetry operation (i.e., one that is neither identity nor pure translation). Approximate group theory can still be at work via *successive application* of a genuine operation followed by a *pseudo*symmetry *nonmathematical operation* (an oxymoron) to afford a third *pseudo*symmetry relationship. Consider a $P2_1$ kryptoracemate ($Z = 4$, $Z' = 2$) with obviously observable *pseudo*inversion symmetry as in *cis*-3,4-butano bridged *N*-desmethylnefopam·HCl $P2_1$ kryptoracemate (Refcode UTUNIH [137], **205**). A 2_1 screw rotation followed by a *pseudo*inversion engenders a *pseudo*glide reflection. All one has to do is to look for it in the unit cell packing. Moreover, of the approximately 200 or so examples in Fábián and Brock's [138] compilation of kryptoracemates, the largest number belonged to the $P2_1$ monoclinic chiral space group and exhibited *pseudo*inversion and *pseudo*glide relationships (see below). As a result, their unit cell space filling (with its two Second Kind *pseudo*symmetry operations) imitates packing in achiral $P2_1/c$ ($Z = 4$, $Z' = 1$) whose three nontrivial operations are all genuine [137]. Should we be surprised? Not really, since just based upon statistics alone, one should choose $P2_1/c$ to be the achiral space group that a kryptoracemate with *pseudo*symmetry would emulate.

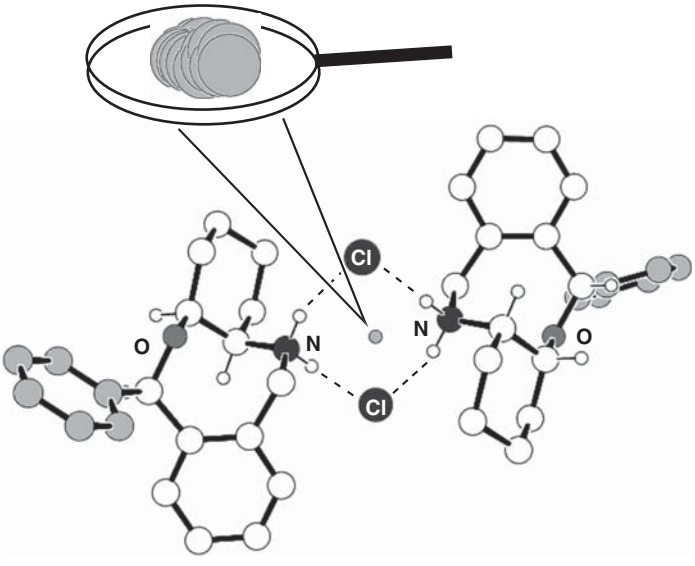

205

This mimicry is certainly not surprising since $P2_1/c$ is known as *Nature's favorite space group*. Approximately 36% of all the 750 000 or more organic molecules in the CSD crystallize in $P2_1/c$ (and its $P2_1/a$ and $P2_1/n$ variant settings), that

is, just one out of all the 230 possible space groups! The conclusion to be drawn from this interesting statistic is that despite myriad differences in molecular structure, shape, and chemical functionalities, the three nontrivial symmetry operations of $P2_1/c$ (2_1-screw rotation, inversion, and glide reflection) enable very efficient crystal space filling of diverse molecules with the minimum of wasted void space. The $P2_1/c$ space group choice for *efficient lattice packing* is evidently so beneficial, that Nature will even resort to *pseudo*symmetry to achieve this goal.

Before we proceed further, let us consider the geometrical consequences for arrays of midpoints *between all pairs of corresponding atoms* in two molecules related by one of the three symmetry operations of space group $P2_1/c$. It will be shown that these arrays are actually the *symmetry elements* that we are already familiar with. The midpoints of a 2_1-screw rotation generate an *ideally linear* array of points, while the midpoints of inversion related molecules all *coalesce to only one point.* Finally, the midpoints of glide-reflection molecules afford an *ideally planar* array that is perpendicular to one of the cell axes and parallel to one of the cell faces (e.g., by convention, it is perpendicular to the *b-axis* and parallel to the *ac*-face for $P2_1/c$).

The two oppositely handed molecules of kryptoracemate **205** interact via $^{+}$N–H$\cdots$Cl^{-} hydrogen bonds to generate a cyclic $R_4^2(8)$ graph set composed of two acceptors and four donors arranged within an eight-membered ring [137]. According to Bernstein *et al.* [140], an $R_4^2(8)$ graph set describes a ring hydrogen-bonding pattern (the "R" designator) with two acceptors (superscripted "2") and four donors (subscripted "4") and consists of an eight-atom cycle (degree = 8). *Edge-to-face* aromatic–aromatic interactions link the graph sets throughout the crystal. These Ar–Ar interactions can form since the two phenyl rings are *allowed by pseudo*symmetry *to be differently skewed* in the cyclic hydrogen-bonded unit! Due to C(alkyl, sp^3)–C(aryl, sp^2) ligation, one phenyl edge will be staggered between two bonds of its Csp^3 neighbor while the aryl's opposite edge eclipses the third Csp^3 bond. The (1*S*)-phenyl ring on the right-hand side of **205** shows the commonly observed Csp^2–Csp^3 arrangement where the smallest Csp^3 substituent, that is, benzylic-***H***(1) in the C–H bond, is eclipsed. On the other hand, the (1*R*)-phenyl ring on the left-hand side of the drawing eclipses a benzo-ring C(*ipso*) atom (less common, but often observed). We have now observed one of the important advantages of *pseudo*symmetry between the kryptoracemate pair of molecules, that is, chains of Ar–Ar interactions are engendered *since the phenyl rings in the oppositely handed partners are not obligated by a symmetry constraint* to be enantiotopically twisted (see **206**). Some of the aromatic moieties in these interactions are phenyl and others are benzo rings. The three edge-to-face interactions show auspicious 4.82(8) Å centroid–centroid distances. So, *pseudo*symmetry enables Nature to construct more intermolecular interactions by removing a symmetry constraint.

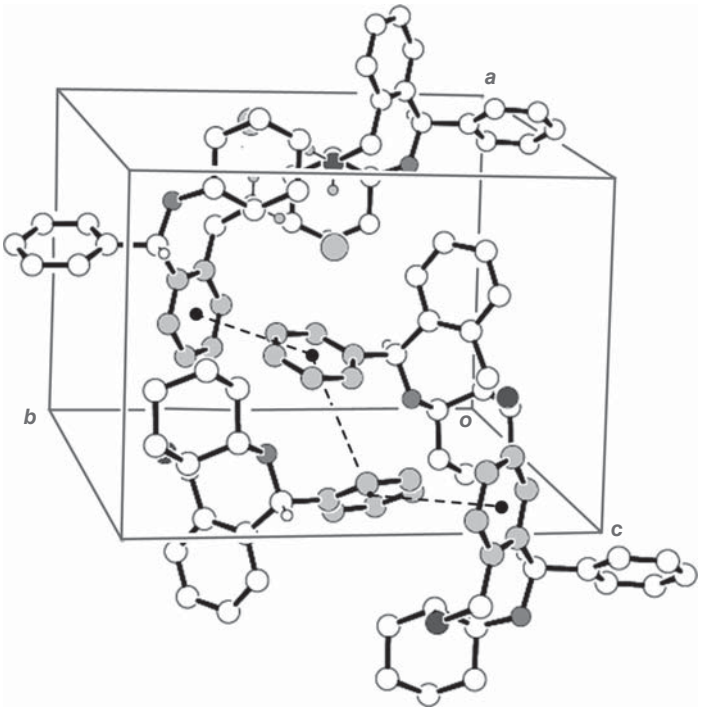

206

Note: When quantifying the fidelity of *intermolecular pseudo*symmetry via the algorithms noted earlier [137], obviously different orientations/locations of atoms or groups within the two molecules under study (e.g., the differently twisted phenyls in **205**) must be removed from the data set used in the calculation. For example, *rmS*(*i*) [137] can be defined to be a *pseudo*inversion *continuous fidelity (or distortion) measure* from an ideal *intermolecular i*-symmetry relationship. Using Cartesian coordinates of the **205** structure (without the phenyls) as the input file, the closest ideal inversion-symmetry *geometrical construct* is calculated using the Avnir *inv.exe* [141] program. The RMS difference in the superimposition of the ideal *i*-symmetry construct upon the actual pair of molecules is *rmS*(*i*). Its 0.088(1) Å low value testifies to *small deviations* from the ideal, which may or may not be visibly perceivable (i.e., good-fidelity *pseudo*inversion symmetry). It is only visually perceivable if one looks with a magnifying glass and notices the cluster of midpoints for **205**. The location of genuine symmetry elements at the interface (common border) of two adjacent asymmetric units has already been discussed earlier. However, this symmetry restriction is lifted in the case of intermolecular and intramolecular crystallographic *pseudo*symmetry *elements,* since they reside within the asymmetric unit itself.

Glaser and coworkers [137] have shown that the midpoints of *pseudo*inversion related molecules generate a *cluster of points* as in the *cis*-3,4-butano bridged *N*-desmethylnefopam·HCl $P2_1$ kryptoracemate (**205**). The root-mean-squared estimated standard deviation (esd) of these points from the $(x, y, z)_{mean}$-coordinate value is the *precision* of the *pseudo*inversion element. Similarly, the midpoints of *pseudo*glide related molecules afford an approximate plane. The statistical *best plane* can be calculated from these points, and the esd for all the points from the mean plane is the *precision* of the *pseudo*glide element (i.e., just how bumpy, or flat, is the "almost planar" array?).

Genuine symmetry elements are located at *special positions* of symmetry in the lattice by definition. This is another structural constraint that is lifted in kryptoracemates. *Pseudo*symmetry enables **205**'s general positioned inversion *pseudo*symmetry element to be located at a "near-to" statistical best-point (e.g. (0.779(3), 0.501(2), 0.249(4))) rather than "on" a predicted special position (e.g. (3/4, 1/2, 1/4)). The result is that the auspicious structural arrangement of molecules in the UTUNIH kryptoracemate lattice emulates the spatial arrangement found in genuine symmetry-based space filling. The *rmS*(dislocation) distance of the statistical "best point" from that of the predicted special position for a higher space group is the *accuracy* of the *pseudo*symmetry element. In the case of the kryptoracemate under discussion, the rather high 0.30(6) Å *rmS*(*inversion dislocation*) distance points to low accuracy. Therefore, since the intermolecular *rmS*(*inversion*) *pseudo*symmetry parameter just involves the diastereomeric molecules' spatial relationship (i.e., the cluster's *precision* or spread of midpoints), one must also consider the *rmS*(*inversion dislocation*) accuracy parameter when considering the chiral unit cells' achiral space filling fidelity as a whole.

The genuine 2_1-screw rotation between *cis*-3,4-butano bridged *N*-desmethylnefopam·HCl kryptoracemate molecules is depicted in unit cell **207**. The benzo ring and benzhydrylic ***CH*** unit have been colored-coded gray. As is commensurate with a 180° rotation and a translation by 1/2 the *b*-axis length, the phenyl rings in both molecules must point in the same direction (due to *translation*), while the benzhydrylic protons reside on opposite sides of the page (due to *rotation*). The 2_1-axis is parallel to the axis-*b* and passes through points (1/2, 0, 1/2) and (1/2, 1, 1/2) on the appropriate *ac-faces.*

The two molecules comprising the (0.779(3), 0.501(2), 0.249(4)) *pseudo*inversion pair in the *cis*-3,4-butano bridged *N*-desmethylnefopam·HCl kryptoracemate unit cell are illustrated in **208**. Such a relationship requires the benzhydrylic protons to appear about 180° disposed from each other (as in the 2_1-pair of molecules), but now the phenyl groups point in opposite directions. Similarly, cell **209** shows the kryptoracemate's two *n-glide reflection pseudo*symmetry related molecules. Both benzhydrylic protons now point toward the viewer (due to lateral *translation* toward the viewer), while the phenyls face in opposite directions (due to *reflection* across a plane approximately perpendicular to the page).

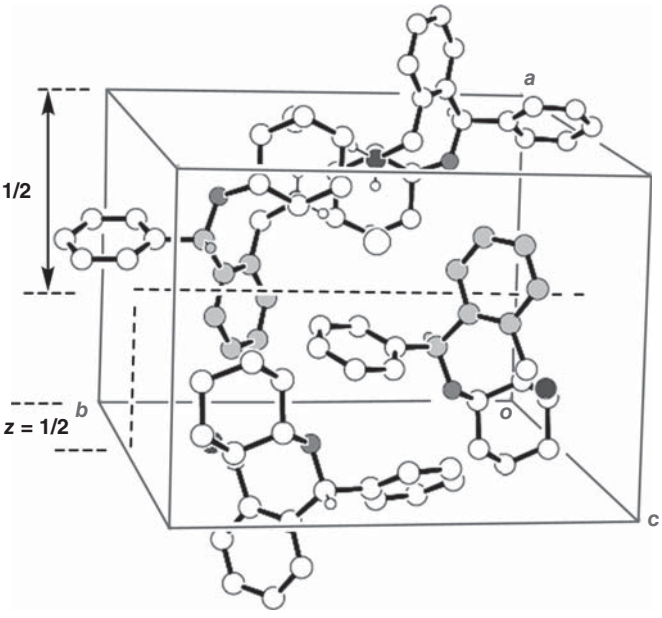

207

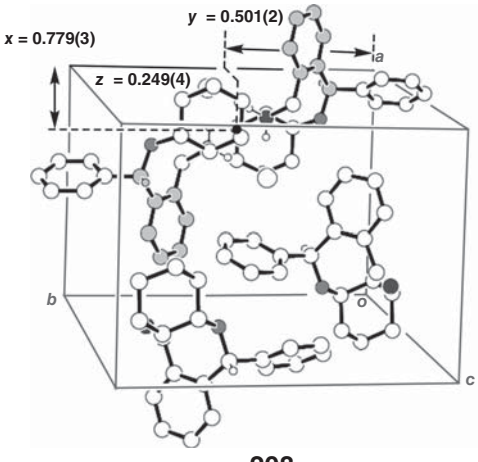

208

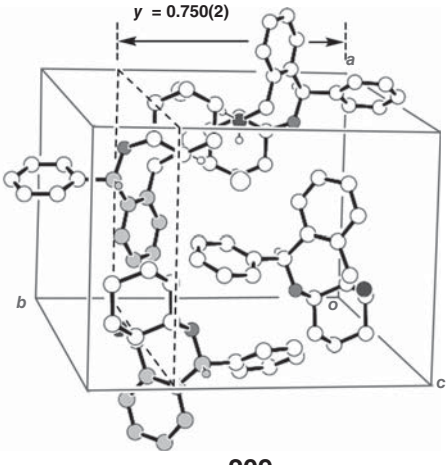

209

A clearer *pseudo*glide array of midpoints of 8-methoxy-1-oxacyclotetradeca-2,13-dione $P2_1$ kryptoracemate (Refcode NIWHUX) [142] is depicted in the edge-on view with translation of the more remote left molecule toward the viewer, **210.** The esd from the "best plane" for the set of 18 midpoints is only 0.04 Å and shows high precision. The 0.04(2) Å *rmS*(*glide dislocation*) *accuracy* from the ideal

$y = 1/4$ plane is quite good also. The low 0.09(9) Å $rmS(\sigma)_{glide}$ value testifies to a relatively high fidelity *pseudo*mirror relationship. Similarly, NIWHUX *rmS(i)* is only 0.05(3) Å, see **211**.

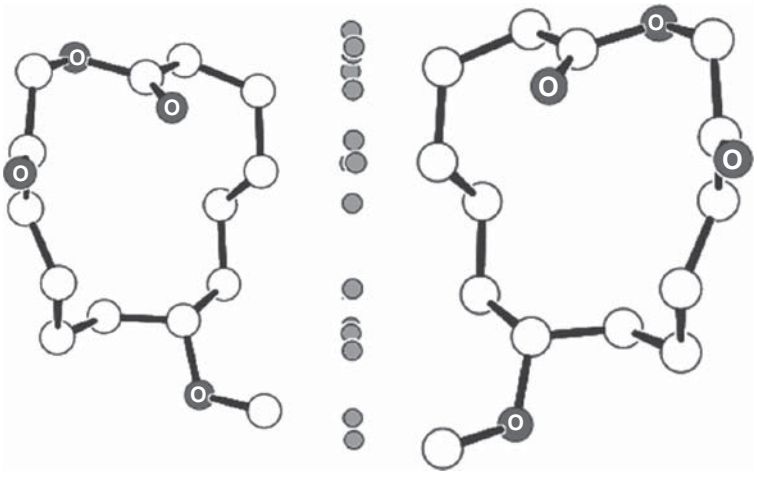

210

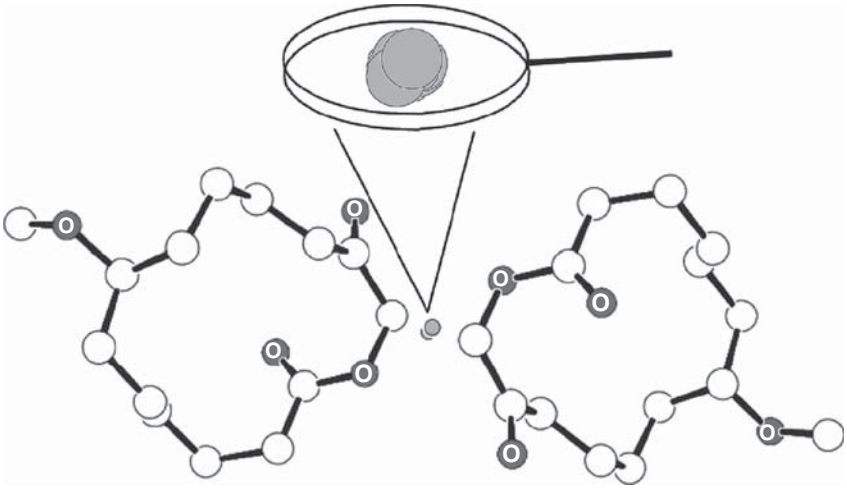

211

When one considers genuine glide-reflection 1/2-cell translation vectors within the parallel to *ac-faces* of the $P2_1/c$ space group (known as the *standard setting* for that space group) and similar vectors for the nonstandard $P2_1/a$ and $P2_1/n$ settings, we are reminded that *c-glide* vectors are parallel to the

c-axis; those for *a-glides* are parallel to the *a*-axis; and *n-glide* translations are parallel to the short diagonal between the *a*- and *c*-axes. The 1/2-cell translation distance is a symmetry constraint that is removed in *pseudo*glides. In the case of NIWHUX, the mean *x-translation* = 0.492(6) fractional *x*-units, while there is an additional *z-translation* = −0.028(4) fractional *z*-unit component. The finding of *x*- and *z-double components* for the *mean-pseudo*translation *vector* in NIWHUX is the norm in *pseudo*symmetry and signifies that the translation vector is *not ideally parallel to a cell axis!* In measuring about 40 examples of $P2_1$ kryptoracemates, the mean-translation vector was *never ideally parallel* to any cell axis as it is in genuine glide-translations (A. Steinberg and R. Glaser, unpublished data) [143]. Nor should it be expected to be so. What does this mean? The requirement that the *mean-pseudo*translation *vector* be parallel to a cell axis is another symmetry constraint that is lifted in translation *pseudo*symmetry relationships (i.e., *pseudo*glide or *pseudo*screw-rotation).

To conclude this discussion of $P2_1$ kryptoracemate crystal structures emulating higher order achiral $P2_1/c$ space filling, one should ask the question "why perform all these *rmS(X)* calculations of *X-pseudo*symmetry at all"? Answer: Some kryptoracemate emulation fidelities are better than others. These calculations provide structural insight as to just how well Nature has managed to "fake" symmetry to gain auspicious packing. Finally, the high-fidelity *rmS(i)* and *rmS(σ)* values reported earlier should really not be that surprising. Why? As said before, the *visual appearance* of a pair of *pseudo*enantiomeric molecules in the asymmetric unit is based on the same principles governing stable low-energy intermolecular arrangements between stable conformations. These arrangements are based upon either *pseudo*symmetry in kryptoracemates or genuine symmetry in achiral crystals.

Recently, Sunatsuki *et al.* [144] described the crystal structure of an iron(II) complex in a $P2_12_12_1$ ($Z = 8$, $Z' = 2$) kryptoracemate emulating higher order *P*bca *achiral* space filling. They also presented the first report of *chiroptical measurements* (solid-state KBr pellet circular dichroism, **212**) performed on selected kryptoracemate enantiomorphous *single crystals* [144]. If A and A′ are two oppositely handed diastereomers, then one chiral crystal contains (+)-A and (−)-A′ while (−)-A and (+)-A′ reside in the other crystal.

Finally, can *pseudo*symmetry act as a geometrical constraint to force a particular molecular geometry within the crystal lattice? The obvious answer is "yes." Diphenhydramine·HCl is a very well-known antihistaminic drug. It is structurally related to the skeletal muscle relaxant orphenadrine (an *o*-methylated diphenhydramine·HCl, Refcode JUVXIH) [145], and the nonnarcotic analgesic drug nefopam (a diphenhydramine cyclic analogue). Diphenhydramine·HCl (Refcode JEMJOA) [146] gave crystals belonging to the orthorhombic $Pn2_1a$ space group. A conformation having a *pseudo*mirror plane (**213**) enables a crystal that is lacking mirror symmetry to emulate higher order $Bb2_1m$ space

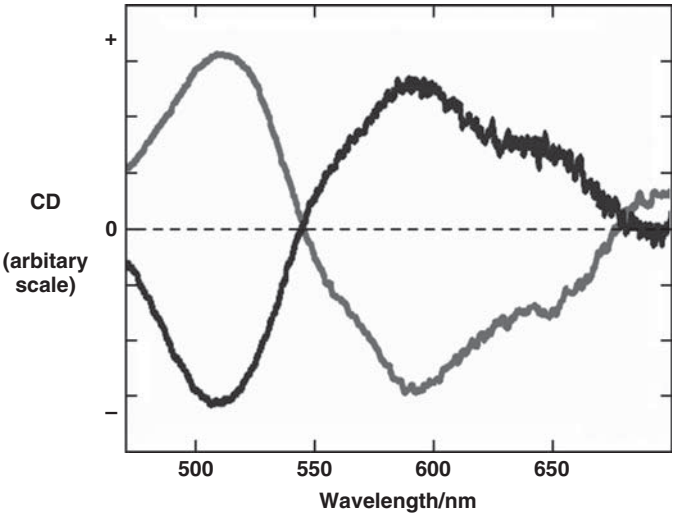

212

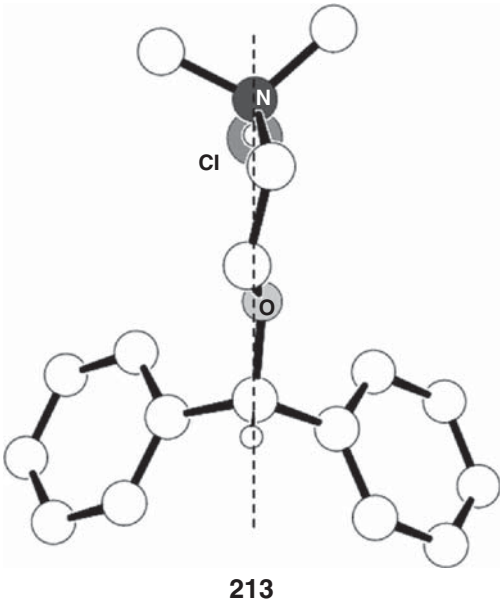

213

filling. An unusually low 37.5° O–C–C–N torsion angle is measured as the result of *pseudo*symmetry constraints in packing. This angle exhibits more normal 60(6)° *synclinal* values in nonsymmetry constrained crystals of diphenhydramine derivatives (e.g., Refcodes BEXHPA [147] and FIMTAW [148]).

10.3
Desymmetrization of Platonic-Solid Geometries Resulting from Crystallographic Symmetry Constraints

High symmetry point groups are defined as those that have *more than one rotation axis of C_3 or higher*. In solution, solvated cubane (**106**, C_8H_8) has no constraints to exhibit its inherent O_h high symmetry as seen by the isochronous δ 4.02 ^{1}H and δ 47.74 ^{13}C chemical shifts for its *eight* nuclei of the same type. However, crystalline cubane (Refcode CUBANE, $R\bar{3}$r space group) [149] does not exhibit O_h symmetry, although C_4-symmetry is permitted in periodic crystals. Instead, cubane only resides on single special positions of inversion and C_3-rotational symmetry (Refcode CUBANE). As a result, cubane's O_h high symmetry has decreased to the lower S_6 point group within the crystal. The asymmetric unit encompasses a H–C–C–H unit and $Z' = 0.17$ of the C_8H_8 formula unit. This means that two sets of symmetry- nonequivalent nuclei now exist in the solid state, that is, two gray *on-axis* nuclei and six white *off-axis* nuclei (**214**). Why is S_6-symmetry expressed and not C_4? Answer: Like the previous example, we can attribute this to *packing considerations.* Remember, it has already been noted that both inversion centers [128] and C_3-axes [129] in solvated molecules tend to be preserved upon entering the crystal lattice.

A symmetry point group's *order* is the number of symmetry operation *group elements* in its *symmetry set.* The S_6-point group is of *order* 6. These point group elements are S_6, $S_6^2 \equiv C_3$, $S_6^3 \equiv S_2 \equiv i$, $S_6^4 \equiv C_3^2$, S_6^5, $S_6^6 \equiv E$. This is quite a reduction in symmetry compared to the original O_h-point group *order* of 48. The O_h point group elements are E, i, $3(C_4, C_4^2 \equiv C_2, C_4^3, S_4, S_4^3)$, $4(C_3, C_3^2, S_6, S_6^5)$, $6C_2'$, $3\sigma_h$, and $6\sigma_v$, that is, $1 + 1 + (3 \times 5) + (4 \times 4) + 6 + 3 + 6 = 48$. One may ask "how much distortion can the O_h symmetry solvated cubane molecule (**106**) undergo by being desymmetrized from down to the S_6 point group when residing within the confines of the crystal's lattice?" The expected answer should be "not much" for such a small rigid skeleton.

A. Steinberg and R. Glaser (unpublished data) and Steinberg [143] used the Avnir Continuous Symmetry Measures (CSM) programs to calculate the distortion from ideal fourfold, threefold, and twofold rotational symmetry and found that $S(C_4) = 0.004$, $S(C_3) = 0.003$, and $S(C_2) = 0.002$ (where integer-zero is ideal symmetry and a value less than 0.01 testifies to *very negligible distortion*). When the molecular graphics portrayal of the crystal-state geometry is viewed, these distortions certainly cannot be noticed. However, it should be borne in mind that even this very slight distortion from ideality was enough for the crystallographer to readily observe diffracted rays from the electron clouds about atoms in two nonsymmetry equivalent C–H bonds with intensities in the ratio of 3 : 1. Therefore, X-ray crystallography is one of the *most sensitive* experimental tools to investigate symmetry and *pseudo*symmetry in ordered periodic molecular arrays.

Similarly, solvated dodecahedrane (**107**, $C_{20}H_{20}$) demonstrates is I_h high symmetry by a single δ 3.38 ^{1}H and δ 66.93 ^{13}C chemical shift for its 20 respective proton or carbon nuclei. The highest molecular point group is I_h group and is of order 120. These point group elements are E, i, 6(C_5, C_5^2, C_5^3, C_5^4, S_{10}^3, S_{10}^3, S_{10}^7, S_{10}^9), 10(C_3, C_3^2, S_6, S_6^5), 15C_2, and 15σ_h, that is, $1+1+(6\times8)+(10\times4)+15+15=120$. However, in the confines of the cubic $Fm\bar{3}$ space group crystal (Refcode DOPSIK01) [150] the I_h high symmetry of solvated dodecahedrane has decreased to the lower symmetry T_h point group of order 24 [150, 151]. Remember, C_5-axes are forbidden in periodic ordered lattices. The T_h-point group elements are E, i, 4(S_6, C_3, C_3^2, S_6^5), 3(C_2, σ_h), that is, $1+1+(4\times4)+(3\times2)=24$. Solvated dodecahedrane's I_h very high symmetry (120 operations, 60 of the First Kind, and 60 of the Second Kind) has been reduced to a crystal-state lower T_h high symmetry (lower order: only 24 operations). This was enabled due to the presence *of latent cubic symmetry* within the dodecahedrane skeleton [30]. A regular hexahedron (gray cube in **215**) within dodecahedrane is defined by eight gray carbon atoms. It is noted that T_h point group symmetry molecules are quite rare, while those with T_d-symmetry are obviously very common.

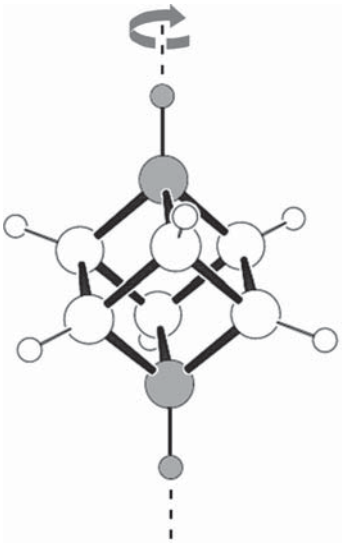

214

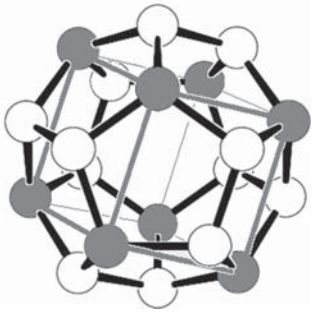

215

In the crystal, one C_3-positioned C–H bond (i.e., only 1/3 of each atom) and another σ-plane positioned C–H bond (i.e., only 1/2 of each atom) define the asymmetric unit comprising *4/100th* of the $C_{20}H_{20}$ molecule. The partial

desymmetrization breaks the degeneracies in the original set of 30 bonds so that 24 of them (gray-white bond termini in **215**) now form a symmetry-equivalent set. Six white–white bond termini engender a second symmetry-equivalent set. Therefore, disparate lengths for the C(gray)–C(white) and C(white)–C(white) bonds are expected since they reside in different sets. The new T_h-symmetry for crystalline **215** is the result of three mutually perpendicular pairs of coplanar white–white bonds. The partial desymmetrization preserves the latent cubic symmetry and enables the molecule to occupy *15 special positions of symmetry* within the lattice. *Bottom line:* symmetry is a structural constraint that may be lifted in its entirety, or partially, when a molecule's environment changes from enclosure within a solvent shell to residence inside a crystal lattice.

Just how distorted is the T_h-dodecahedrane skeleton from the ideal solution-state I_h-analogue? Very little, as expected, since it certainly has a rigid skeleton. The S(C_5) distortion index is only 0.0004, which is very negligible indeed (A. Steinberg and R. Glaser, unpublished data) [143]. Despite the molecule's very negligible distortion from ideal fivefold symmetry, it cannot be denied that the diffraction pattern arises from *two symmetry unrelated C–H bonds* rather than from only one.

We will see later on that the dodecahedron and icosahedron geometries are related as mathematical 'duals'. Therefore, not surprisingly, latent cubic symmetry is also found in crystalline icosahedron skeleton molecules, for example, dirubidium *closo*-dodecaborate (**216**, Refcode GALGUV01 [152]). This geometry is also found in isostructural Refcode FUYZOO01 [152] ($2K^+$ salt) and JINVAE [152] ($2NH_4^+$ salt). Inspection of the Rb^+ cations surrounding the icosahedron dianion shows them to be arranged in a perfect cube, 5.434 Å per side. Eight face-centered cations result in a desymmetrization of the solvated dianion's I_h point group down

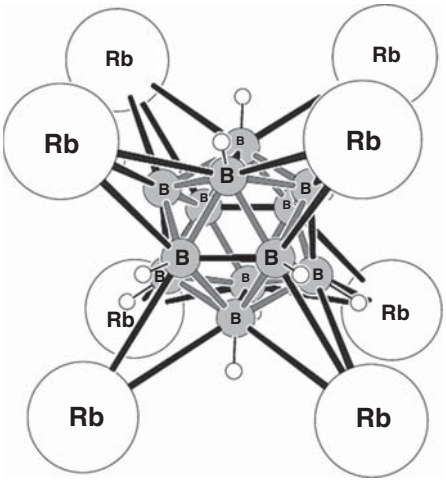

216

to T_h-point group symmetry in an $Fm\bar{3}$ space group crystal lattice. The four pairs of cations are arranged on opposite sides of the dodecaborate skeleton and define four C_3-axes that pass through the skeleton's inversion center. The 12 uncomplexed triangular faces are arranged as six pairs of fused 1.781 Å isosceles triangles sharing a 1.771 Å common side, through which three mutually perpendicular C_2-axes enter the midpoints of a black colored B–B bond, pass through the inversion center, and exit the B–B bond midpoint on the opposite face. Three pairs of parallel black B–B bonds on opposite sides of the dianion define the three mutually perpendicular σ_v-planes.

10.4
Mobility of Cubane and Dodecahedrane $(CH)_n$ Spherical Molecules within a Crystal Lattice

Crystallography is sensitive enough to probe even the negligible I_h geometry distortion of crystalline T_h-symmetries dodecahedrane **215** and $2Rb^+ \cdot$dodecaborate **216**. Can solid-state NMR spectroscopy do the same? If this is possible, then samples of crystalline T_h-symmetry dodecahedrane and S_6-symmetry cubane should exhibit Cross Polarization/Magic Angle Spinning (CP/MAS) solid-state NMR spectra with 3 : 2 and 3 : 1 respective ratios of diastereotopic anisochronous ^{13}C signals. Interestingly, solid-state NMR showed only one carbon signal for each crystalline solid. Does this mean that something is amiss in the solid-state NMR technique? The answer is "no." There simply are different measurement timescales for X-ray crystallography and solid-state NMR data collection (i.e., different "camera shutter" speeds). This section discusses why the expected number of signals (commensurate with their crystallographic point group symmetry) was *not found* in solid-state NMR.

Glaser *et al.* [153] recently observed only one signal in each of the corresponding ^1H and ^{13}C solid-state NMR spectra: δ 3.99 and δ 49.83 for cubane and δ 3.41 and δ 67.88 for dodecahedrane. These data were acquired with ^1H CRAMPS (COMBINED ROTATION AND MULTIPLE PULSE SEQUENCE, spectroscopists do have a sense of humor) and ^{13}C CP/MAS pulse sequences. The observed anisochronicity shows *fast topomerizations* of diastereotopic nuclei to afford isochronous time-averaged signals. These findings are clearly inconsistent with the S_6 and T_h point group symmetry for the crystalline samples.

What other NMR evidence is there for a fast topomerization of diastereotopic nuclei within these two molecules? First, there is the well-known precedent of spherical-like adamantane's mobility in the solid state. Mobility of adamantane enables it to be a standard sample for *solid-state* NMR magnetic field *shim* adjustment (adjustment of the superconducting static external magnetic field (H_0) to produce parallel magnetic lines of force, that is, a homogeneous magnetic field that enables detection of narrower linewidth signals).

To understand the other solid-state NMR evidence for mobility, we should consider additional aspects of the basic NMR experiment. A short microsecond pulse at a preset "o_1" megahertz *radio frequency* (RF) high-power electromagnetic energy H_1 field is broadcast in the $+X$ direction **217** so that its polarized magnetic-field oscillations are coplanar with the **218** conical base planes swept out by precessing $+\mu$ or $-\mu$ magnetic dipoles around the conal axis. This changes the initial *Boltzmann distribution* of nuclei whose ground α- and excited β-states nuclear populations were initially in $N_\alpha > N_\beta$ *thermal equilibrium.* The population change $N_\alpha = N_\beta$ occurs when the NMR broadcast magnetic-field o_1 oscillation frequency is in *resonance* with the μ-magnetic dipole vector's *Larmor* precession frequency ν_L (i.e., when $o_1 = \nu_L = \Delta E/h$ energy difference between α- and β-states, and h = Planck's constant, see **218**).

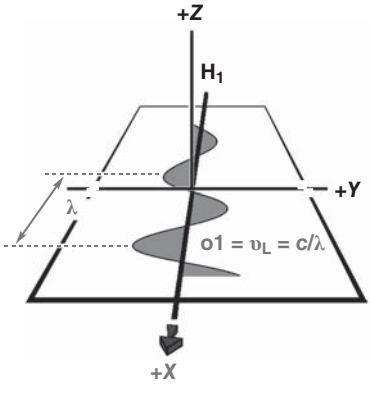

217

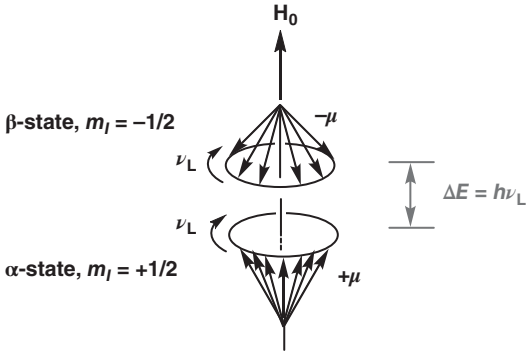

218

Cessation of the transmitter's RF-energy pulse then enables *relaxation mechanisms* to purge the spin-system of the excess (absorbed) energy. Their purpose is to rebuild the initial $N_\alpha > N_\beta$ thermal equilibrium population condition via stimulating emission of the β-state's excess energy. For this to come about, the emission is induced by mobile close-by ground-state *neighboring magnetic μ-dipoles* in nuclei whose local magnetic fields also fluctuate at the appropriate Larmor frequencies. In low viscosity solutions, *Brownian motion* of these ground-state *neighboring magnetic nuclei* generates a Gaussian distribution of fluctuating weak magnetic local fields (known as the "NMR-lattice" or "surroundings"). The $\beta \rightarrow \alpha$-state energy transfer process comes about by magnetic dipole–dipole interactions between the nuclei. As a result of the transfer, the energy-receiving α-neighbor's $+\mu$-magnetic dipole reorients more rapidly. The faster the rate at which the *relaxation* mechanism's donating nuclei revert to their $N_\alpha > N_\beta$ thermal equilibrium state population, the shorter is the *time constant* for this kinetic nonadiabatic process. Nuclei resident within very viscous solutions or

those within a solid matrix/crystal obviously cannot reorient at the required ν_L megahertz higher frequency magnetic field oscillations, and thus their time constants are very long. This time constant is called *time constant number one* (T_1) or the *spin-lattice time constant*. The almost immobility is the cause of the notoriously long T_1 times for nuclei in crystalline molecules (compared to their solution-state spatially mobile counterparts).

Immobile molecules have appendages that lock into a grid of preferred solid-state orientations due to intermolecular tessellation. However, within the category of crystalline molecules, there exists a subset of spherical molecules that undergo alternating periods of rapid flips about their preferred orientations, followed by rest for short time periods. Cubane **214** and dodecahedrane **215** are two of these spherical $(CH)_n$ crystalline molecules that undergo staccato-like *fast topomerization* in the lattice and enable the hydrocarbon's diastereotopic nuclei to afford weighted time-averaged chemical shifts. The mobility of these spherical molecules is what causes them to exhibit *considerably shorter* T1 values than immobile solid-state tessellated molecules. They are not continuously rotating, since if this was the case, then the resulting disorder would clearly be denoted in the crystal structure. These crystals with internal molecular mobility are referred to as "*plastic crystals*". We have recently measured cubane's T_1 to be 0.72 s and a longer 2.37 s value for dodecahedrane at 315 K [153]. Thus, larger and heavier spherical dodecahedrane appears to be less mobile than the smaller cubane hydrocarbon.

The broadcast pulse also induced *phase coherence* of the $+\mu$-magnetic dipole vectors that were previously randomly distributed (**218**) upon the conical surfaces at thermal equilibrium. Therefore, rebuilding the thermal equilibrium condition also requires a second process to randomize the phases of these vectors. The process is adiabatic since it is stimulated by very low frequency energy (i.e., that of thermally vibrating nuclear dipoles within the solid sample). The kinetics of this process proceeds at *time constant number two* (T_2), the *spin-spin time constant*. In low viscosity liquids, $T_1 = T_2$, and all the NMR signals are as narrow as they are ever going to be, that is, the *extreme signal narrowing condition.* The faster this T_2 process is, the shorter are the lifetimes of the nuclei in their excited states. These short lifetimes cause significant $\Delta\nu_L$ *inexactitude* when measuring the ν_L signal induced into the spectrometer's detector. The result is very wide $\nu_L \pm \Delta\nu_L$ nuclear dipole–dipole broadened signals in solid-state NMR.

Any more evidence? Yes, but one must become a tad more technical in presenting it. Solid-state CP/MAS experiments do not directly excite ^{13}C nuclei. Why? Long $5T_1$-based recycle times needed to repeat the experiment and thereby improve the very low signal-to-noise baselines found for low natural abundance ^{13}C nuclei. Instead, spatially close ^{1}H nuclei first absorb megahertz radio-frequency energy, and via some very cleaver physics, their energy is transferred through space to ^{13}C neighbors. The *contact time period* is the amount of time that ^{1}H nuclei make the transfer. This *cross polarization*

(CP) process proceeds with a T_{CH} *kinetic time constant. Less mobile molecules* afford a more rapid *CP-build up* rate to steady-state levels (i.e., the steeper the curves in plot **219** become, the shorter are the T_{CH} time constants). This plot measures the *minimum* $^1H \rightarrow {}^{13}C$ *contact period time* required to reach maximum ^{13}C signal intensity. The faster 28 ± 3 ms T_{CH} time constant for less mobile dodecahedrane can be compared to more mobile cubane's slower 1394 ± 68 ms value illustrated in plot **219** [153]. Therefore, both the T_1 and CP-buildup experimental results can be interpreted in the same manner (i.e., both molecules are mobile, but dodecahedrane is considerably less mobile than cubane) [153]. The known 4999 ± 877 ms T_{CH} value for spherical adamantane was measured as a check of the operator's skill in performing the experiment correctly. It must be added that mobility is not the only factor influencing T_{CH}. A ^{13}C-nucleus' T_{CH} value is also a function of the number of protons directly ligated to it. Therefore, the fact that adamantane has both methine and methylene carbons means that its T_{CH} values may not be compared with those of the *all methine carbon* Platonic-solid geometry hydrocarbons, $(CH)_n$ ($n = 8$ or 20).

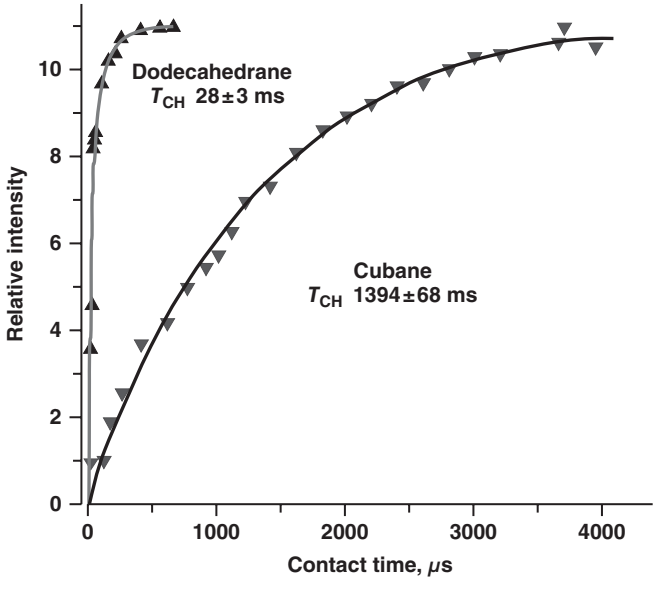

219

11
Platonic-Solid Geometry Molecules and Crystallographic Constraints upon Molecular Geometry, Symmetry Distortions from Ideality

11.1
Geometrical Considerations in High-Symmetry Molecules

It is difficult to predict when a symmetrical molecule will occupy a special position (although we did discuss the high preservation propensity for solvated inversion and C_3 symmetry elements) [128, 129]. However, we do know with certainty when a solution-state symmetry can never be expressed in a crystal lattice. Ideal fivefold rotation symmetry and any rotation axis whose order is greater than six will not be observed in any *periodic* crystal. This leaves the O_h-point group as the highest that can be expressed in a crystal. However, the O_h-point group's higher order (48) requires quite a lot of special positions to be occupied!

It is not unexpected then that high-symmetry solvated molecules have a particularly difficult time maintaining their *multiple symmetry elements* upon crystallization. There are two isostructural surprises however. Both the potassium and cesium salts of the hexaborate dianion $(B_6H_6)^{-2}$ (**220**) *maintain all 48* symmetry operations of their solvated octahedral O_h-point group geometry upon crystallization (Refcodes GIGRIX and GIGROD) [154], although crystalline cubane [149] does not. The asymmetric unit $Z' = 0.02$ includes K^+ (or Cs^+) and one B–H bond, while that for $Z' = 0.17$ cubane encompasses an H–C–C–H unit. Why do cubane and $(B_6H_6)^{-2}{\cdot}2K^+$ both exhibit O_h symmetry in solution and but only the latter does so in the solid state? When we look at both the dianion and its cations (**221**), the answer becomes apparent if one is trained to look for it. Eight cations are *face centered* in regard to the dianion. In other words, a cation resides above each of the regular octahedron's triangular faces, that is, they all occupy special positions of C_3-rotation symmetry. Why so many cations for only one hexaborate dianion? Answer: The cations are also shared by surrounding dianions so that neutrality of charge is maintained. A C_3-axis passes through K^+ and then enters the equilateral triangular B–B–B face beneath it. From there it transits the octahedron's center (a point of inversion) and then exits the other triangular B–B–B face with a K^+ beneath it. The eight cation super-arrangement affords a perfect cube. What this means is that each of the

Symmetry, Spectroscopy, and Crystallography: The Structural Nexus, First Edition. Robert Glaser.

Companion Website: www.wiley.com/go/Glaser/Symmetry

$(B_6H_6)^{-2}$ eight triangular faces bears a one-fourth negative charge, and each K^+ cation is surrounded by four tetrahedrally arranged dianion neighbors. This is the way one K^+ affords one-fourth positive charge to each of its spatially close dianion partners.

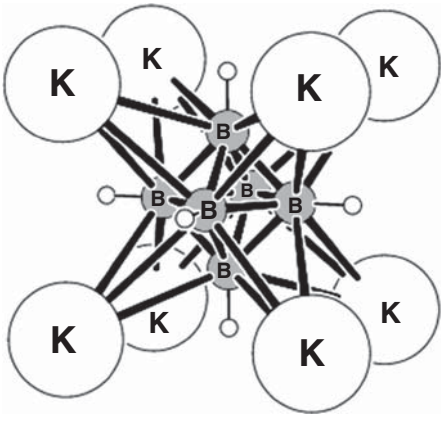

220

Arrangement **220** is not surprising if one knows about *duals* in solid geometry. The five convex Platonic solids have the esthetic property in which connection of each face's midpoint generates another perfect Platonic solid. Thus, the midpoints of each of the octahedron's eight triangular faces ("hedra" in Greek) generate a cube's eight vertices. Correspondingly, linking the midpoints of a cube's six square faces forms the octahedron's six vertices (see **221**). There are other examples. If we inscribe a midpoint within each of the 12 pentagonal faces of a dodecahedron, then we produce the icosahedron's 12 vertices. Finally, the 20 midpoints of the triangular faces of an icosahedron yield the dodecahedron's 20 vertices (see **222**).

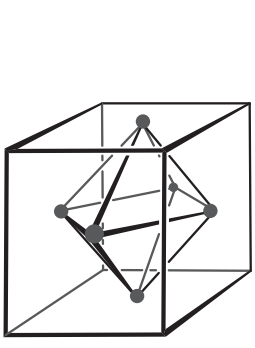

221

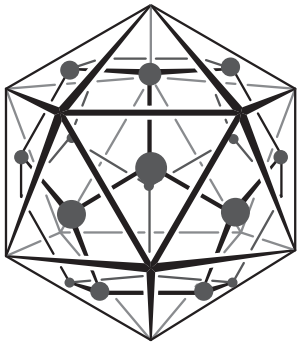

222

223

What about the tetrahedron (pyramid)? It is its own dual (see **223**). So, Nature does have a high esthetic sense of form and beauty.

Consider the octahedral O_h-symmetry of composite cube **224** that has been constructed from eight smaller cubes. Two pairs of adjacent cubes that share a common side (1,2 on top and 3,4 on the bottom) are then removed. This desymmetrization generates a T_d-symmetry tetrahedron from the centers of the four remaining cubes **225.** The desymmetrization to the T_d-point group has removed half the symmetry operations of the parent O_h-symmetry order 48 cube. The T_d-point group is of *order* 24. Its point group elements are $S_4^4 \equiv E$, $4(C_3, C_3^2)$, $3(S_4, S_4^2 \equiv C_2, S_4^3)$, and $6\sigma_d$, that is, $1 + (4 \times 2) + (3 \times 3) + 6 = 24$.

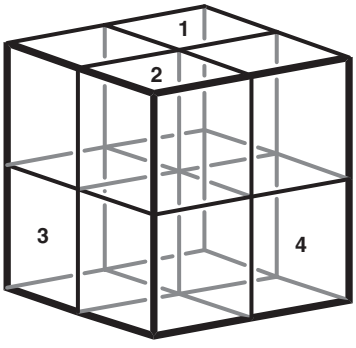

224

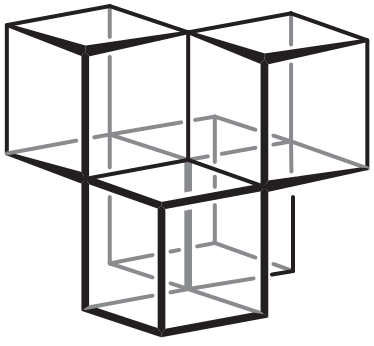

225

It has always been a challenge for chemists to synthesize molecules of high symmetry. The goal is even more difficult if it is desired to produce them with *high chiral symmetry.* Molecules with perfect T_d-, T_h-, and O_h-achiral symmetry are known. Obviously, methane and CCl_4 are common everyday examples of T_d-symmetry. We have already discussed two crystalline examples of the relatively rare T_h-point group symmetry (**215** and **216**). Now, we will discuss crystalline examples of the high T-symmetry chiral point group.

11.2
Syntheses Strategies of High-Symmetry Chiral Molecules

This section discusses a situation where researchers, referees, and the editors of two well-respected journals all fell into the trap of having an incomplete understanding of a particular unusual symmetry. Unfortunately, the result was an erroneous report of a *first synthesis* of a T-symmetry chiral organic molecule, when in fact the target compound only exhibited the more common

garden-variety D_2-symmetry. This first synthesis of a T-symmetry molecule was based upon a very simple premise [155, 156]. The idea was to convert T_d-symmetry adamantane's skeleton (**226**) into a 1,3,5,7-tetrakismethylol derivative, adamantane-1,3,5,7-$(CH_2OH)_4$. The next step involved taking an enantiomerically pure D_3-symmetry (−)-trishomocubane chiral skeleton (**227**) and elaborating it into the *supposedly C3-symmetry* (−)-trishomocubanyl-acetic acid. This was to be followed by linking it to the adamantyl-tetrakis-methylol to generate a chiral $-CH_2OC(=O)CH_2-$ linked tetraester derivative that was *supposed to have T-symmetry*. Can you spot the logical error? The synthesis strategy was that ligation of four chiral D_3-symmetry (−)-trishomocubanyl units to T_d-symmetry adamantane would remove all of the latter's σ-planes. And, indeed, this surmise was correct. However, at each stage of the multistep synthesis, the assumed symmetry was incorrect. Why? The D_{2d} and C_1 respective symmetries of adamantane-1,3,5,7-$(CH_2OH)_4$, and (−)-trishomocubane-1-$CH_2C(=O)OH$ were a mismatch with the former C_3-rotation axes *since the reactive groups were planar and not conical.* As a result, a further condensation reaction to yield the chiral tetraester product had a planar $-CH_2OC(=O)CH_2-$ (**228**) linkages, which now afforded only mundane D_2-symmetry (of which many examples already existed).

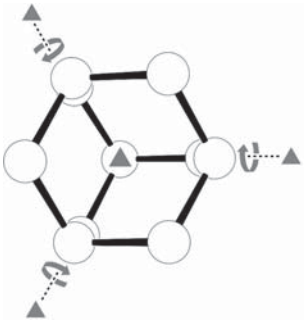

226

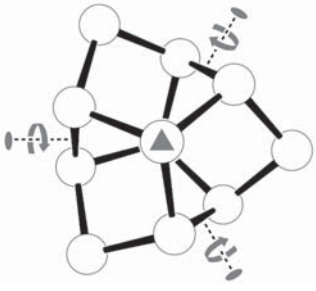

227

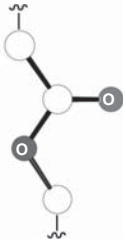

228

Reading this communication in the BGU library (R. Glaser, unpublished results), it was decided not to write a correction, since it was obvious that Kurt Mislow had undoubtedly seen it and had already written to *Chemical Communications* declaring that the tetraester's actual symmetry was only D_2. This assessment was indeed correct, and it was not long before the record was indeed set straight in a one-paragraph article [157]. Two years later, Nakazaki and coworkers [158] acknowledged Mislow's correction and reported a genuine T-symmetry adamantane molecule tetra-substituted by linear C_∞-symmetry

diacetylene (–C≡C–C≡C–) units ligated to (+)-trishomocubane termini. There was now no longer a symmetry mismatch since C_3 is a subgroup of the high-order C_∞-point group. However, the question has to be asked *why did the peer-review process break down*? Its purpose is to protect the author (and the journal) from publishing embarrassing errors. If there is a logical flaw, better to know about it prior to publication rather than afterward. Bottom line: referees who review manuscripts outside the scope of their expertise and editors who approve their reports due to work pressures can sometimes do a grave disservice to science. Mislow has been known to say: "once you write it, it is forever."

11.3
Ethano-Bridge Enantiomerization of *T*-Symmetry Molecules

In 1992, Vögtle and coworkers [159] set out to synthesize a nearly spherical hydrocarbon as a potential π-ligand with a largely (but not completely) closed surface and intramolecular cavity. While their goal was not to synthesize a *T*-symmetric organic molecule, nevertheless, this is indeed what they produced. The molecule crystallized in the rhombohedral *R3 chiral space group* and occupied a special position of C_3-symmetry perpendicular to the 1,3,5-trimethylphenyl ring center (Refcode PALWAA) [159]. Crystallization of a racemic mixture of chiral tetrahedral cage compounds afforded a *conglomerate* of chiral crystals. Since the unit cell contained only molecules of the same handedness, we see that the crystallization process afforded a *spontaneous resolution* providing that the molecules remained within the confines of the lattice. (*P*)- and (*M*)-enantiomers of C_3-symmetry tetrahedral cage structures of crystalline *spheriphane* **229** and **230**, respectively, exhibit high-fidelity

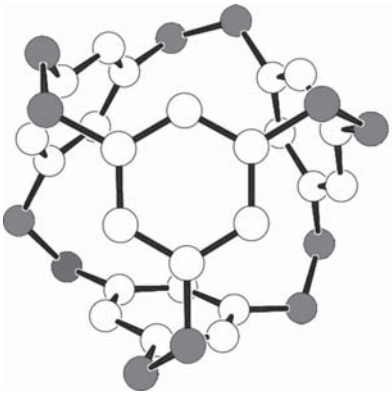

229

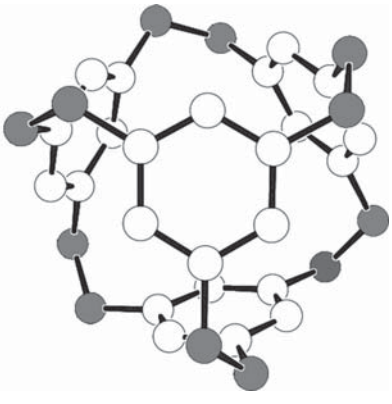

230

*T-pseudo*symmetry in the chiral crystals. The asymmetric unit comprises one-third of the C_3-symmetry molecule. Nevertheless, our eyes cannot discern the miniscule, but real, deformation that lowered the ideal symmetry from *T-* to C_3. We know this to be true since X-ray crystallography only showed a one-third molecule asymmetric unit. Dissolution of the crystals generates a rapidly interconverting racemic mixture of *genuine T-symmetry* enantiomers. The (+)- or (−)-*synclinal* twists of the gray color-coded ethano ($-CH_2-CH_2-$) bridges depicted in **231** are labile stereogenic units and are the source of chirality of the cage structure. During the construction of the structure, all the bridges are mechanically constrained to be *homochiral* due to the cage's compact geometry.

Crystalline **229** or **230** has only one genuine C_3-axis through a single 1,3,5-trisubstituted aromatic ring, while three other molecular axes are *high-fidelity* C_3-*pseudo*symmetry mimics. There are six ethano bridges, and three solid-state C_2-*pseudo*symmetry axes passing through the midpoints of pairs of opposite bridges. Inspection of an ethano bridge **231** drawn from crystal coordinates shows that our eyes really cannot differentiate between extremely high-fidelity C_2-*pseudo*symmetry and the genuine article.

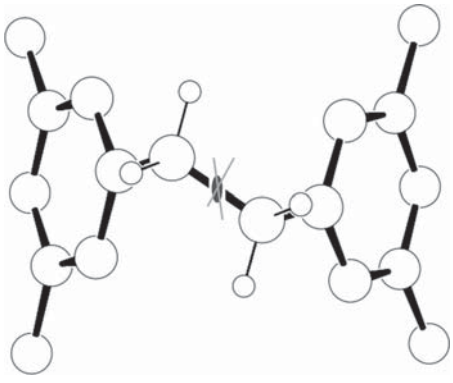

231

Enantiotopic nuclei become diastereotopic when residing within a chiral environment. We have seen earlier that the observation of anisochronous NMR signals for diastereotopic methylene geminal protons or isopropyl methyl groups provides a very useful probe for the existence of *molecular chirality*. However, while symmetry equivalence for pairs of nuclei is sufficient for isochronicity, it is not a necessary requirement since *fast topomerizations* of two or more diastereotopic nuclei (e.g., those in (+)-*synclinal* **232**) will also engender a single degenerate frequency time-averaged NMR signal. The (±)-*synclinal* twist angles

for the ethano bridge are *labile* stereogenic elements due to the low enantiomerization energy barrier for *disrotatory motion* about the single CH_2–CH_2 bond leading to an *eclipsed* transition state **233**.

Using the same atom and magnetic-site labeling protocol illustrated in Figure 6.1 for **114**-(***I–III***), we will follow the enantiomerization process of ^{1}H nuclei within (+)-*synclinal* **232** and (−)-*synclinal* **234**. The ethano-bridge protons are assigned atom labels (i.e., **H1**, **H2**, **H3**, and **H4**). Our observation of a C_2-axis (dashed line) results in two sets of symmetry-equivalent diastereotopic methylene protons: set 1 (*antiperiplanar* **H1** and **H3**) and set 2 ((−)-*synclinal* **H2** and **H4**). This means that there are also only two symmetry-equivalent magnetic sites (***a*** and ***b***) within **232**: ***a*** is assigned to both **H1** and **H3** and ***b*** to each of **H2** and **H4**. It is readily apparent that exchange partner (−)-*synclinal*-**234** also has C_2-symmetry and that it is the enantiomer of (+)-*synclinal*-**232**. Therefore, **234**'s *externally enantiotopic* magnetic sites are assigned as $\overline{\boldsymbol{b}}$ to each of **H1** and **H3** and $\overline{\boldsymbol{a}}$ to each of **H2** and **H4**. Finally, the permutation for set 1 **H1** and **H3** protons is determined to be ($\boldsymbol{a}, \overline{\boldsymbol{b}}$) while that for set 2 **H2** and **H4** is ($\boldsymbol{b}, \overline{\boldsymbol{a}}$). Since the two permutations contain the same site letters but differ in their respective "bar" notations, set 1 **H1**, **H3** and set 2 **H2**, **H4** are *dynamically enantiotopic* and hence isochronous at the fast exchange limit (FEL).

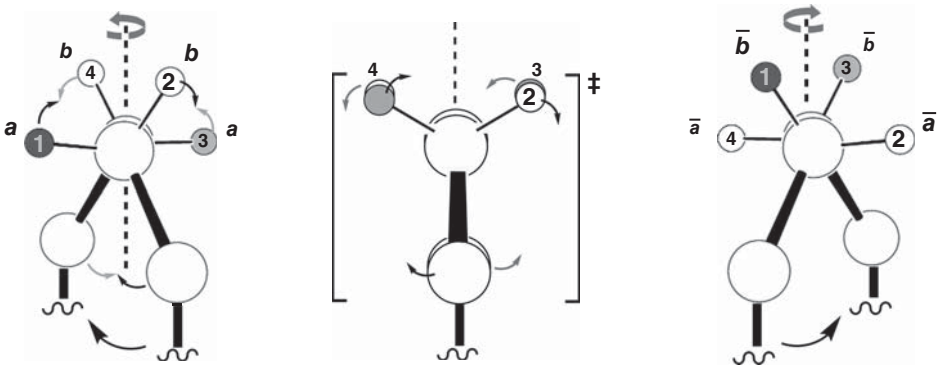

(+)-*synclinal*-**232** **233** (−)-*synclinal*-**234**

Vögtle and coworkers reported that "The high symmetry of spheriphane **229**, **230**, a tetramer of 1,3,5-trimethylenebenzene, is proved by spectroscopy. The ^{1}H NMR spectrum shows only one signal [each] for the aromatic and benzylic protons, respectively, and the ^{13}C NMR spectrum has only three signals." These are the methine and quaternary aromatic carbons and the aliphatic methylene carbons. They go on to state that "*Even at temperatures lower than −90 °C the molecular skeleton is flexible enough not to hinder the twisting of the ethano bridges about the [C_2-axes perpendicular to the] C_3-symmetry axes, so no splitting*

of the signals is observed." Clearly, they certainly were very well aware about the effects of molecular chirality upon the temperature-dependent dynamic nuclear magnetic resonance (DNMR) spectrum.

11.4 Self-Assembly of *T*-Symmetry Chiral Molecules

Chiral molecules exhibiting T-symmetry can be prepared in a "one-pot self-assembly" of four metal ions and six coordination-ligand linker units to yield tetrahedral tetranuclear tetra-anion clusters of chiral propellers [160, 161]. In 1990, Saalfrank *et al.* [161] reported T-symmetry tetrahedral chiral clusters (**235**) of four Co^{II} ions or four Mn^{II} ions, Refcodes SEVCEB and SEVCAX, respectively. Six tetradentate *atropisomeric* (not to be turned) C_2-symmetry *spacer ligands* **236** form the tetrahedron's edges and their termini link (or bridge) homochiral two C_3-symmetry octahedral metal propeller units **237** residing at the tetrahedron's apexes. Spacer twist angles for the $\delta,\delta,\delta,\delta$-enantiomer exhibit typical +70(8)° O(blade)–C_{quat}–C_{quat}–O(blade) *synclinal* torsion angles, while those of the propellers show +53(3)° O_{upper} – centroid$_{upper}$(on C_3-axis) – centroid$_{lower}$(on C_3-axis) – O_{lower} values. The R^1 and R^2 substituents on *o,o′-disubstituted atropisomer* linker units have all been removed to simplify drawing **235** (and others in this section). A listing of R^1 and R^2 propeller-blade substituents is given in **238**.

The very first T-symmetry geometry cluster with magnesium^{II} ions (Refcode GIJHAI, R^1 = C(=O)OEt, R^2 = OEt) was actually prepared by the Saalfrank [160] group 2 years earlier (1988), but like spheriphane, the authors did not recognize its symmetry. The 1988 paper stated "^{1}*H and* ^{13}*C NMR spectra are* ***impressively simple*** *[empirical formula … $C_{96}H_{120}O_{60}Mg_4(NH_4)_4$;* $\boldsymbol{T_d}$ *symmetry, eight (!)* ^{13}*C NMR signals] and thus provide* ***no detailed information*** *whatsoever about its structure."*

While solvated GIJHAI's ^{1}H NMR (500 MHz, $CDCl_3$, 32 °C) spectral plot **239** was published only in a later article (2002), the numerical data was presented in the 1988 paper. Considering the crystal structure's 10-hydrogens/blade ((6-C$\underline{H}_3$ and 4-C$\underline{H}_2$ protons)/blade) and 8-carbons/blade and an empirical formula of $C_{96}H_{120}O_{60}Mg_4(NH_4)_4$ clearly shows a basic asymmetric unit building-block unit of only 8/96 = 10/120 = 1/12 of the molecule. Despite the aforementioned statement to the contrary, solvated GIJHAI's detailed structure could be ascertained from its ^{1}H NMR spectrum. The cluster's 48 geminal protons can be subdivided into two heterotopic sets of 24 protons each: set 1 = 12 × **H1** + 12 × **H2** for $CH_3C\underline{\boldsymbol{H}}_2OC$ and set 2 = 12 × **H3** + 12 × **H4** for $CH_3C\underline{\boldsymbol{H}}_2OC(-O)C$. Only if both sets contain *diastereotopic* partners, all the geminal protons will be split into an AB-quartet pattern. Therefore, the observation of *four* overlapping AB-quartets at δ 3.95, 4.06, 4.17, and 4.27 can only be explained by concluding that *all* the methylene geminal proton pairs reside in chiral environments. Thus, it is apparent

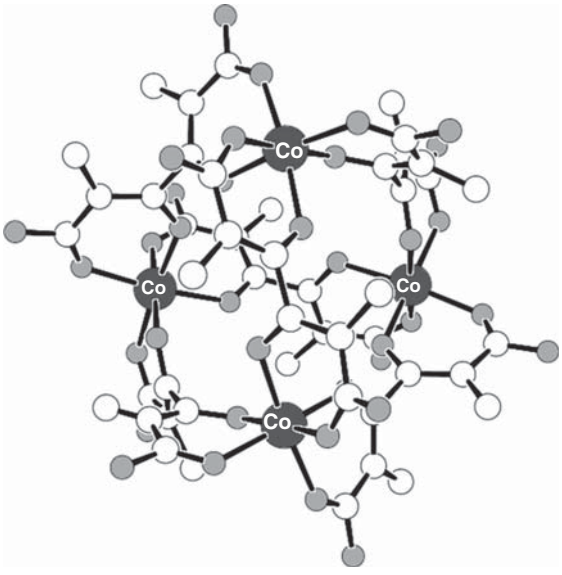

235

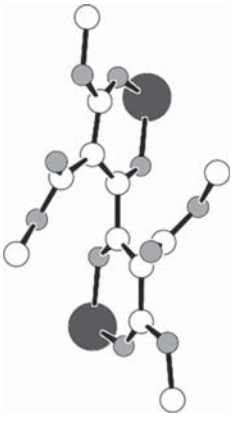

236

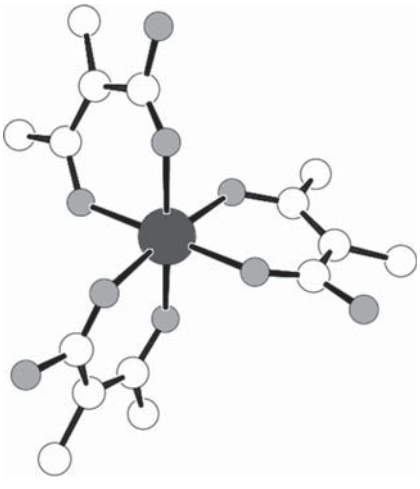

237

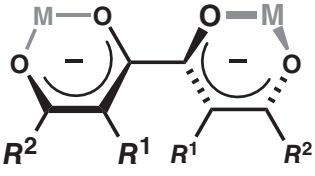

R^1 = H, C(=O)OMe, C(=O)OEt, C(=O)OBu^t
R^2 = OMe, OEt, OBu^t

238

that the one propeller-blade building-block unit was present in a T-symmetry *chiral cluster.* The *T-symmetry* point group is of order 12, and the 12-point group elements are E, $4(C_3, C_3^2)$, and $3C_2$. These are exactly half of that for achiral T_d and T_h since all of their 12 Second Kind chirality-inversion operations are absent.

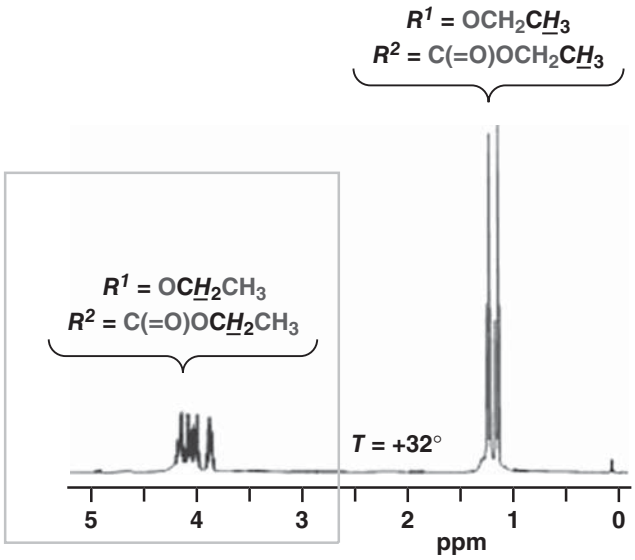

239

Three of the Saalfrank group's crystal structures showed perfect *crystallographic T-point group* symmetry (Refcode HERPEZ [162], $R^1 = C(C{=}O)OMe$, $R^2 = OMe$, $M = Fe^{II}$ and Refcode HERPID [162], $R^1 = C(C{=}O)OEt$, $R^2 = OEt$, $M = Fe^{II}$ both of which crystallized in the *Fd3* cubic system space group, and Refcode IFUHOG [163], $R^1 = H$, $R^2 = OEt$, $M = Mg^{II}$, which crystallized in the *F*d3*c* cubic system space group). Finding such a crystallographic high-symmetry point group structure *is a very big deal* to a structural chemist, and it can "make your day." Sadly, the good fortune of describing *perfect crystallographic T*-symmetry tetrahedral structures for these clusters was never specifically mentioned to this day. Other crystalline clusters exhibited C_3-, C_2-, and C_1-point group symmetry in the lattice and thereby only show high-fidelity *T-pseudo*symmetry to our eyes. But, ***all*** *clusters exhibit perfect T-symmetry when solvated*. So, what is the take-home message of this? The local environment's site symmetry at which a crystalline or solvated molecule resides dictates its molecular structure.

Some of the Saalfrank clusters showed ammonium ions ($^+NH_4$) or K^+ bound slightly *above* the centers of each triangular face (see **240**, **241**) [164]. They are called *exohedral* guests, and their Refcodes are MUYRIH, MUYSAA, MUYSEE, MUYRON, and MUYRUT. In these clusters, one observes that a tetrahedron is its own dual (**243**), compared to the different topologies of the cube/octahedron **221** or dodecahedron/icosahedron **222** pairs of duals. Again, this interesting geometrical finding was not commented upon in the original articles. These *face-bound T*-symmetry tetra-anionic crystalline clusters bear a striking similarity to the T_h-symmetry $2Rb^+ \cdot$icosahedral-$(B_{12}H_{12})^{-2}$ (**216**) and O_h-symmetry

$2K^{+}$·octahedral-$(B_6H_6)^{-2}$ (**220**) crystal structures, although only the latter has a dual. The esthetically pleasing inverted tetrahedron within the tetra-anionic tetrahedron's triangular faces (outlined by the dark bonds in **241**) is known as a "merkaba." It is sometimes called a "star tetrahedron" or a 3D Star of David, and some believe it to have healing and spiritual properties. There are those who consider its mystical properties to derive from Ezekiel's use of a merkavah (chariot in Hebrew) to *ascend to heaven.*

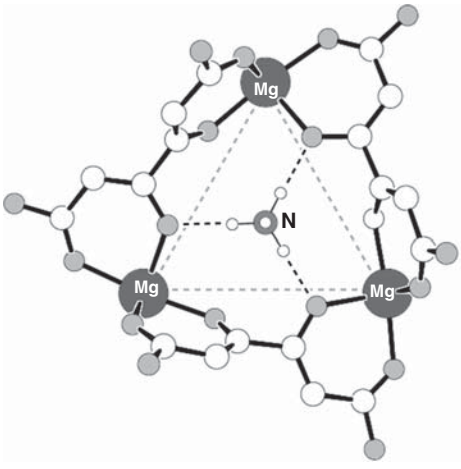

240

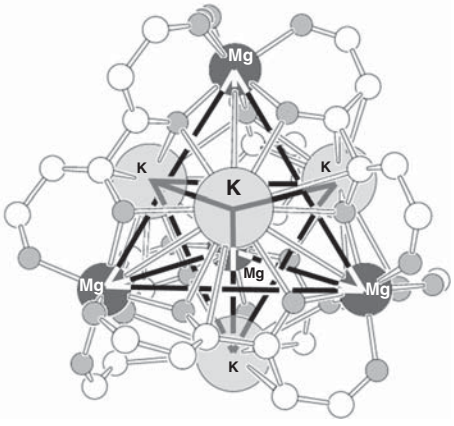

241

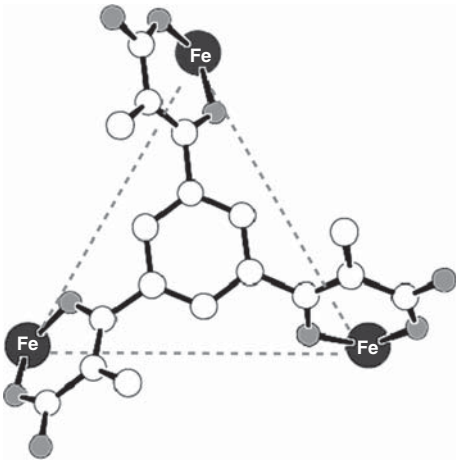

242

T-symmetry tetrahedral clusters can also be prepared from C_3-symmetry 1,3,5-trisubstituted phenyl hexadentate ligands [165]. In this case, the stereogenic spacer units now reside upon the cluster's equilateral triangular face centers (see dashed lines in **242**, Refcode ADODOM). The blade substituents of the tetranuclear Fe^{III} cluster were $R^1 = C(=O)OBu^t$, $R^2 = OBu^t$. Similar to the case of the C_2-symmetrical tetradentate ligands, the linkage unit is spatially compact enough to induce *homochirality* from one propeller into its partner as the cluster self-assembles.

11.5
Enantiomerization of T-Symmetry Clusters

During the self-assembly of edge-differentiated tetradentate-linked clusters, the induction of chirality from one propeller into its neighbor was mediated by the atropisomeric linking units. Clearly then, the two types of helicity are intimately correlated, and enantiomerization must proceed by a simultaneous change to both stereogenic building blocks. The *Λ*-propeller (**243**) undergoes a *Bailar Twist* via planar transition state (**244**) to become a Δ-enantiomer (**245**). At the same time, the (*M*)-atropisomer or *(−)-synclinal* tetradentate edge-linker in (**243**) must *concurrently* become the (*P*) or *(+)-synclinal* enantiomer (**245**) via the same transition state. The ($\Delta \leftrightarrow \Lambda$) enantiomerization process cannot occur without a concomitant ($P \leftrightarrow M$)-process, since the entire molecule enantiomerizes in a *concerted manner.* In a manner similar to the helicity interchange ring-flips discussed earlier (see **162**), the *syn* disposition of the atropisomeric linker's edge-substituents is maintained after a disrotatory passage through a combined two ring-flip/*Bailar Twist* coplanar transition state **244**.

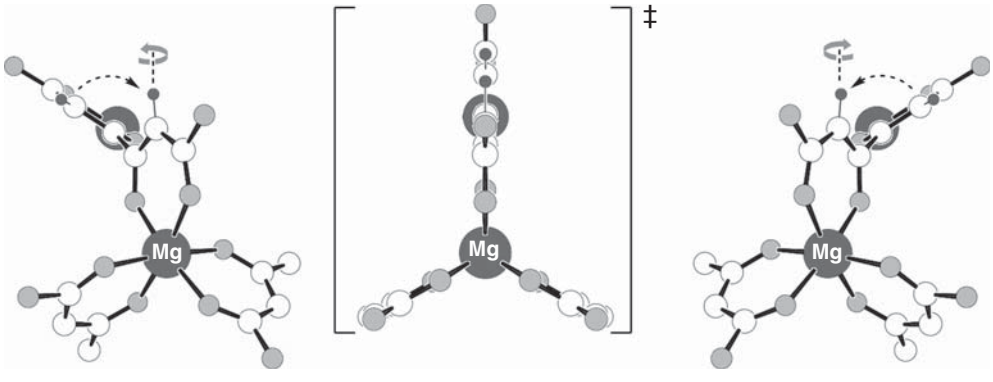

(*Λ*,*M*)-**243** **244** (Δ,*P*)-**245**

The Saalfrank [163] group performed some elegant DNMR experiments on the enantiomerization of the *T*-symmetry clusters. To do this, they prepared Mg^{II} clusters IFUHUM and IFUHOG with *very small sterically demanding* $\boldsymbol{R^1 = H}$ substituents (whereby a proton replaced the larger $R^1 = C(=O)OMe$ or C(=O)OEt unit) [163]. We will consider only the $(^+NH_3Et)_4$·tetranionic IFUHUM complex since it has *exohedral* Et-substituted ammonium nitrogens face-bound 1.40 Å above the Mg–Mg–Mg triangular faces. The impetus for preparing these particular $R^1 = H$ clusters was the desire to lower the energy of activation for the enantiomerization *coplanar transition state* (**244**) of abutting $R^1 \cdots R^1 = \mathbf{H} \cdots \mathbf{H}$ atoms in (*Λ*,*M*)-**243** and (*Δ*,*P*)-**245** interconverting clusters (and indeed it did).

We will again make use of the atom and magnetic-site label protocol to discuss the variable temperature ^1H NMR partial spectra inserts (recorded at 263, 273, 283 K) plotted above the 305 K full spectrum presented in **246**. Two heterotopic sets of geminal diastereotopic methylene protons can each probe enantiomerization of the *T*-symmetry cluster. These are the *δ* 2.23 diastereotopic **H1**, **H2** protons within the face-bound $^+NH_3C\underline{\boldsymbol{H}}_2CH_3$ group and the *δ* 4.09 diastereotopic **H3**, **H5** protons within $R^2 = OC\underline{\boldsymbol{H}}_2CH_3$ ligated to the stereogenic edge-linkers. Having said this, we may assign the magnetic-site letters as ***a*** to **H1** and ***b*** to **H2** for the face-bound $H_3N^+C\underline{\boldsymbol{H}}_2CH_3$ geminal pair, followed by ***c*** to **H3** and ***d*** to **H4** for the edge-bound $OC\underline{\boldsymbol{H}}_2CH_3$ geminal pair in *T*-symmetry cluster (*Λ*,*M*)-**243**. Similar to the example of the **232**, **234** enantiomeric pair, magnetic-site "enantiomeric" labels may be assigned for the **H1**, **H2**, **H3**, and **H4** externally enantiotopic protons within enantiomeric cluster (*Δ*,*P*)-**245**: that is, $\overline{\boldsymbol{b}}$ to **H1**, $\overline{\boldsymbol{a}}$ to **H2**, $\overline{\boldsymbol{d}}$ to **H3**, and $\overline{\boldsymbol{c}}$ to **H4**.

The next obvious thing to notice is that the NMR signals in plot **246** are *all appreciably broadened* in the entire series of temperature inserts. The absence of narrow lines means that no subspectrum was recorded under slow exchange limit (SEL) nor FEL exchange conditions. Each **H3** and **H4** $OC\underline{\boldsymbol{H}}_2CH_3$ proton signal has been recorded as a separate broadened peak at 263, 273, and 283 K clearly showing that they were recorded under ***S**low **M**agnetic **S**ite **E**xchange **B**roadening* temperature conditions that are above the SEL. Increasing temperature results in increased linewidths as the peaks move closer together. This is concomitant with an increasing valley height between the two broad peaks. On the other hand, the **H1**, **H2** $H_3N^+C\underline{\boldsymbol{H}}_2CH_3$ geminal pair appears as separate broad peaks at 263, 273 K and has coalesced as a *broad-plateau* at the 283 K T_c (coalescence temperature). Finally, geminal protons in both probes appear as different time-averaged single broadened peaks at 305 K showing that the protons are now undergoing exchange in the ***F**ast **M**agnetic **S**ite **E**xchange **B**roadening* temperature regime. The exchange permutations for the four protons can now be written: $(\boldsymbol{a}, \overline{\boldsymbol{b}})$ for **H1**, $(\boldsymbol{b}, \overline{\boldsymbol{a}})$ for its **H2** partner, $(\boldsymbol{c}, \overline{\boldsymbol{d}})$ for **H3**, and $(\boldsymbol{d}, \overline{\boldsymbol{c}})$ for its **H4** companion. Bottom line: there are two sets of *dynamically*

enantiotopic protons: **H1**, **H2** and **H3**, **H4**, that is, two anisochronous signals at the FEL.

From the $\Delta\nu_o = |\ \nu_{H1} - \nu_{H2}\ |$ and $\Delta\nu_o = |\ \nu_{H3} - \nu_{H4}\ |$ values found in the SEL spectrum (not shown in plot **246**), one can then calculate k_{ex} (the kinetic exchange rate constant in s^{-1}) from the useful expression $k_{ex} = \pi\Delta\nu_o/\sqrt{2} = (2.22)(\Delta\nu_o)$ for the exchange process *at that particular* T_c *temperature* (283 K). In this manner, the calculated $\Delta G^{\ddagger} = -RT_c \ln K_{ex}$ *energy of activation* for enantiomerization was found to be 13 kcal/mol. The high valley between the $OC\underline{\boldsymbol{H}}_2CH_3$ **H3**, **H4** broadened peaks shows a >283 K T_c value for this particular set.

Why are there two different T_c temperatures for $H_3N^+C\underline{\boldsymbol{H}}_2CH_3$ **H1**, **H2** and $OC\underline{\boldsymbol{H}}_2CH_3$ **H3**, **H4** signals? Answer: the SEL $\Delta\nu_o = |\ \nu_{H1} - \nu_{H2}\ |$ value is undoubtedly different than $\Delta\nu_o = |\ \nu_{H3} - \nu_{H4}\ |$. Is this reasonable? Of course. Why should the difference in magnetic sites for face-centered $H_3N^+C\underline{\boldsymbol{H}}_2CH_3$ **H1**, **H2** be identical to that for edge-centered $OC\underline{\boldsymbol{H}}_2CH_3$ **H3**, **H4**? After all, each set resides in a different region of the complex.

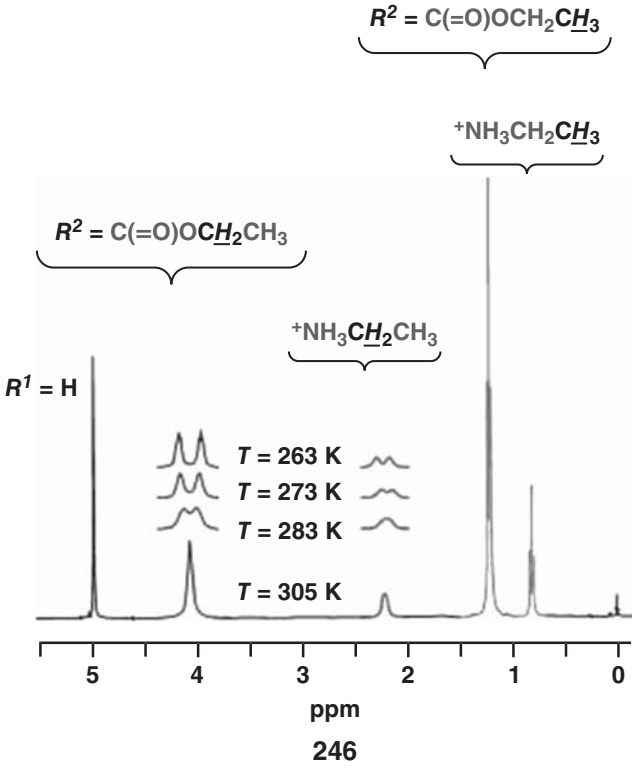

246

11.6
Tetradentate Edge-Linker Units Separated by a Spacer

The Saalfrank *et al.* [161] paper stated that "*The dissymmetry of this tetranuclear anion results from the* ***atropisomerism*** *of* [the] *ligands.*" While not untrue, the chiral propeller's important role was completely neglected in this explanation. The synergism between the two types of stereogenic units (propeller helicity and not just the atropisomerism of the edge-linkers alone) is actually the root of the cluster's homochirality. The fact of the matter is that the readily enantiomerizable $R^1 = H$ edge-linker discussed earlier would not really be categorized as atropisomeric if it was an isolated biphenyl molecule. In actuality, the barrier is due to *correlated motion* within a tetrahedral confined system of four simultaneous "two ring-flip like" *and* concomitant Bailar-twist transition states. Carrying this stereochemical argument one step further, one can hypothesize that if the propeller units were to be separated by a longer more flexible spacer, then the initial chirality of the first propeller need not be induced into that of its neighbors (i.e., loss of homochirality) as the complex self-assembled. A very warm e-mail of congratulations was written to Rolf Saalfrank in 1990, commending him for his achievement in preparing the esthetically beautiful *T*-symmetry complexes (R. Glaser, unpublished results). The possible role of short versus longer spacers was discussed (and their relative effect on the efficiency of induction of initial propeller chirality into the other metals as the self-assembly progressed). A 1,4-disubstituted phenyl unit spacer between adjacent bidentate propeller blades was suggested in this e-mail so that the prediction could be tested (R. Glaser, unpublished results).

Indeed, the following year, an S_4-symmetry *meso*-tetranuclear Fe^{III} cluster was produced by the Saalfrank [166] group using the 1,4-disubstituted phenyl spacer element. The Refcode PIDWAY cluster crystallized in the $P\bar{4}n2$ achiral tetragonal system space group in which the *meso*-molecule occupied a special position of fourfold rotatory-reflection (S_4) symmetry in the crystal lattice (see **247**). This

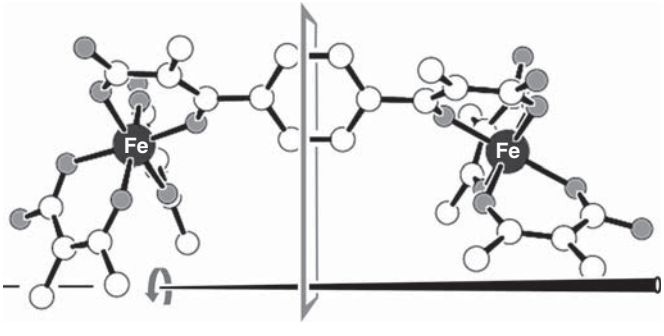

247

is another example showing that *meso* compounds do not only come about by reflection symmetry.

11.7
Self-Assembly of *O*-Symmetry Chiral Molecules

A similar principle has been recently used to self-assemble an *O*-symmetry chiral octahedron geometry cluster in which six C_4-symmetry square planar Pd^{II} metal/tetrakis 4-pyridinyl complexes form the apices of an octahedron, and 12 C_2-symmetry twisted 1,1-binaphthyl atropisomeric ligands generate the octahedron's sides; see **248** [167]. As opposed to the relatively labile atropisomeric ligands in Saalfrank's *T*-symmetry clusters, over-vigorous heating of the (*R*,*R*′)-8,8′-disubstituted-1,1′-binaphthyl stereogenic unit (where $R = R' = -OCH_2OCH_3$) will probably cause decomposition rather than enantiomerization. These units are C_2-symmetry edge-linkers ligating two Pd^{II} square-*pseudo*planar complexes and are shown in **249**. The twist of the 1,1′-binaphthyl unit in the density functional theory (DFT) model was measured to be an *orthogonal*-like 80° O*C*–C(quat)–C(quat)–*C*O value about the C–C central bond.

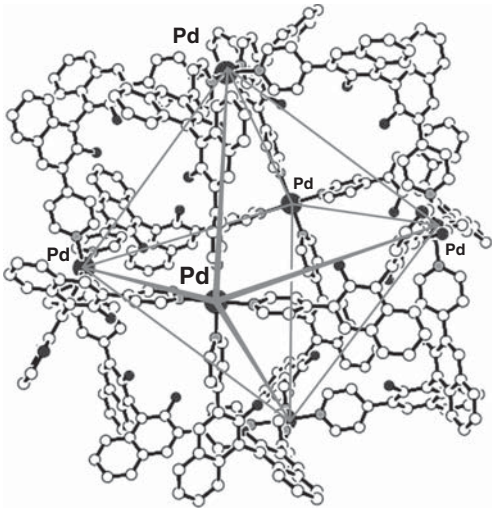

248

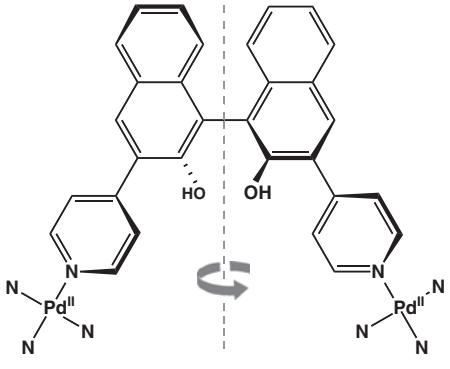

249

Although the cluster's crystals proved to be too thin for X-ray structure determination, the high *O*-symmetry was characterized by NMR, MS, dynamic light scattering (DLS), transmission electron microscopy (TEM), and electron

energy loss spectra (EELS) as well as electronic circular dichroism (ECD) [167]. Furthermore, experimental ECD data were in complete accord with the theoretical simulation.

The homochiral twists of the 12 atropisomeric edge-linkers result in a desymmetrization of the achiral O_h-symmetry point group of order 48 to yield the chiral O-symmetry point group of order 24. Similar to the case of the last desymmetrization, one-half of the O_h-symmetry group elements (i.e., those of the Second Kind) have been eliminated by incorporation of the chiral stereogenic units. The point group elements of the set are $C_4^4 \equiv E$, $3(C_4, C_4^2 \equiv C_2, C_4^3)$, $4(C_3, C_3^2)$, and $6C_2'$, that is, $1 + (3 \times 3) + (4 \times 2) + 6 = 24$.

11.8
O-Symmetry Ferritin Protein Octahedral Shell

Nature has provided us with an O-symmetry self-assembly called *ferritin* **250** (Protein Data Bank structure ID 1LB3) [168]. This $F432$ cubic system chiral space group protein consists of a mineralized core with an octahedral geometry protein shell made up of 24 identical subunits (obviously consisting of only L-amino acids) arranged in groups of three on the equilateral triangular faces of an octahedron. Ferritin is a ubiquitous intracellular protein that is produced by almost all living organisms. Its role is to concentrate intracellular iron and then release it in a controlled manner. It acts as buffer in humans against iron deficiency and iron overload.

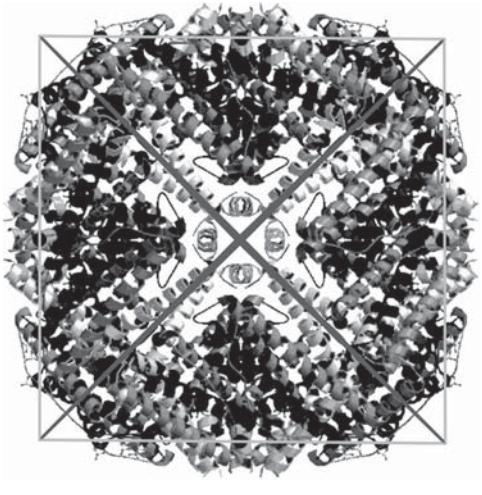

250

11.9 Desymmetrization Resulting from Symmetry and Chemical Constraints

Steinberg [143] (A. Steinberg and R. Glaser, unpublished data) has shown that the Platonic-solid geometry octa-*t*-butyl-octa*sila*-cubane, $Si_8(t\text{-}Bu)_8$ (Refcode YISJUF01 [169] **251**), and tetrakis(tri-*t*-butylsilyl)-tetra*sila*-tetrahedrane, $Si_4(Si\text{-}t\text{-}Bu_3)_4$ (Refcode PEMNEA [170], **252**) molecules offer an opportunity to probe the effects of threefold rotor steric bulk upon the coexistence of reflection and inversion *pseudo*symmetries in these crystalline regular *sila*polygons. Both molecules crystallized as *conglomerates of chiral crystals* in trigonal *R*32 and cubic $P2_13$ chiral space groups, respectively, and both have *skewed rotors* occupying a single special position of C_3-rotational symmetry within their respective lattices. Once again, this is in accord with the comment by Brock and Dunitz [129] that there is a propensity for threefold symmetry molecules to keep this symmetry upon crystallization.

Simple residence within a chiral space group lattice results in chiral molecular geometries for the two aforementioned molecules although the molecules could exhibit O_h and T_d *pseudo*symmetries. In principle, rotor substitution of all the regular polygon's vertices has the potential of accentuating rotor twist due to adjacent-rotor steric interactions as the molecule is assembled. These energy-demanding steric interactions are expected to be augmented by increased rotor size and geometrical factors such as decreased polygon-side bond lengths and bond angles between the side termini and the rotor central atom. For example, the Si(vertex)–Si(vertex)–Si(rotor) angle in the tetra*sila*-tetrahedrane is 144.3°, which decreases to 125.3° in crystalline octa*sila*-cubane and then would reduce to a very small 113.0° for a multirotor substituted *hypothetical* icosa*sila*-dodecahedrane. The larger the angle, the larger the rotor's size (bulk) can be. Therefore, it is reasonable that adjacent larger $-Si(t\text{-}Bu)_3$ rotors were found to be bound to the more spatially free tetra*sila*-tetrahedrane vertices, while smaller $-C(Me)_3$ rotors were ligated to the more spatially congested octa*sila*-cubane vertices and not *vice versa.* Carrying this one step further, placement of adjacent $-C(Me)_3$ rotors on an icosa*sila*-dodecahedrane skeleton is expected to generate unreasonably severe spatial angular constraints.

It is obvious that the genuine C_3-axis through the center of **251**'s cubane-like skeleton cannot interchange the *on-axis* white and dark gray $Si–C(Me)_3$ rotors. Only cubane-like **251** has symmetry-equivalent methyl groups (and these are within diastereotopic sets comprising the two *on-axis* rotors). Set 1 consists of the white methyls, and set 2 is composed of the dark gray methyls; see **253**. All the *off-axis t*-Bu groups are C_3-*pseudo*symmetric. The situation is even more complicated for tetrahedrane-like **252,** where all *t*-butyls now are *off-axis* and are only C_3-*pseudo*symmetric; see **254**. Note that all *t*-butyls contain three diastereotopic methyls. To simplify matters, we will not discuss the symmetry relationships between sets of methyl groups.

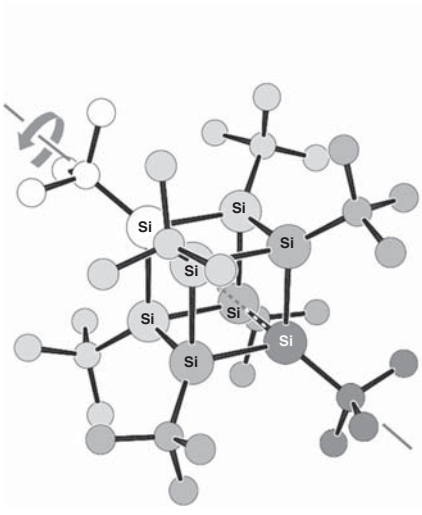

251

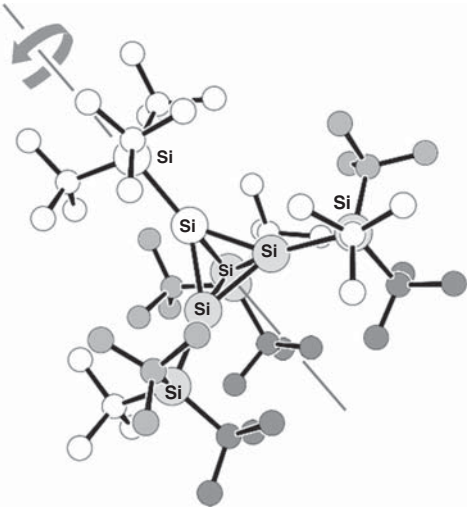

252

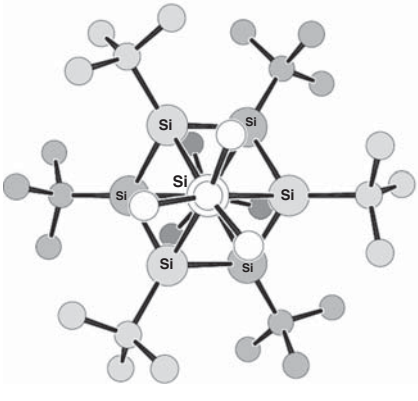

253

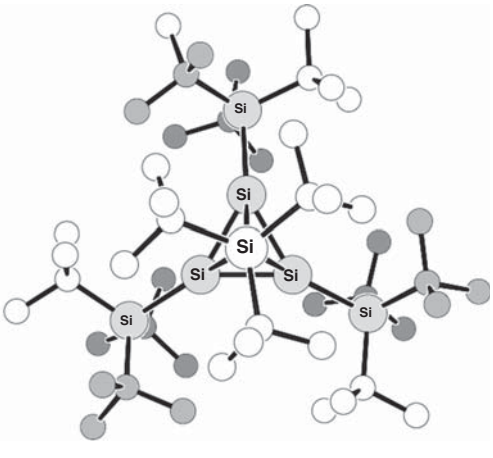

254

In these two Platonic-solid geometry compounds, do *all* the rotors exhibit the same sense and similar degrees of twist? The answer is yes. The deviations from an ideal staggered conformation for all three types of rotor were measured, and their twists were found to be homochirally skewed by approximately 10°.

Next, we can consider how the homochiral twists affect mirror and inversion *pseudo*symmetry in the chiral molecules. Steinberg [143] used the Avnir CSM distortion indices and measured relatively high 0.39(1) S(σ) and S(i) values commensurate with *chemically significant divergences* from ideal reflection and inversion symmetry in octa*sila*-cubane and an even higher 1.10 S(σ) distortion value indicating a readily perceived absence of reflection symmetry for tetra*sila*-tetrahedrane (A. Steinberg and R. Glaser, unpublished data) [143]. On the other hand, rotational *pseudo*symmetry fidelity markedly improved with increasing rotor size: octa*sila*-cubane 0.02–0.03 values for S(C_4), S(C_3), and S(C_2), and even lower tetra*sila*-tetrahedrane 0.002–0.014 values for S(C_3) and S(C_2) [143]. The latter indicated visually unperceivable deviations from solid-state *T-pseudo*symmetry. Bottom line: increasing rotor size effectively removed symmetry operations of the First Kind in the substituted Platonic-solid geometry molecules and caused them to assume an increasingly improved chiral high-symmetry *O*- and *T-pseudo*symmetry appearance [143].

12
Solid-State NMR Spectroscopic/X-Ray Crystallographic Investigation of Conformational Polymorphism/ Pseudopolymorphism in Crystalline Stable and Labile Hydrated Drugs

12.1
Divalent Anions Linking Conformationally Different Ammonium Cations

In this section, we discuss the use of *divalent* anions as counterions to conformationally different ammonium *mono*cations. The starting premise is if two conformations of a *mono*ammonium cation are observed in different crystals, then perhaps one may find them present within the same crystal when a divalent anion is used. (−)-Lobeline (**255**) is the active ingredient of Indian tobacco (*lobelia inflata*). Lobeline is both agonistic and antagonistic at acetylcholine receptors. Acetylcholine receptors may be subdivided into two subtypes. One subtype in the skeletal muscles is also activated by muscarine (**256**), while nicotine (**257**) can activate a different subtype in smooth muscles, glands, and central nervous system (CNS). The *diequatorial* arrangement of the *cis*-2,6-disubstituted piperidine ring favors a solid- and solution-state *axial N*-methyl diastereomer for the labile stereogenic nitrogen.

The solution- and solid-state stereochemistry of (−)-lobeline·HBr anhydrate (Refcode VUHFEJ) was studied by Glaser *et al.* [171] The crystalline-state conformation of the $-CH_2CH(O)$ fragment was found to have an *antiperiplanar* $H\underline{\boldsymbol{O}}-\underline{\boldsymbol{C}}H\cdots{}^{+}\underline{\boldsymbol{N}}H-\underline{\boldsymbol{C}}H_3$ torsion angle arrangement; see (composite)-**258** bottom. A hydrochloride monohydrate *pseudopolymorphic* crystal structure was found in the literature (Refcode ZZZSMK01) [172]. Since the molecular composition

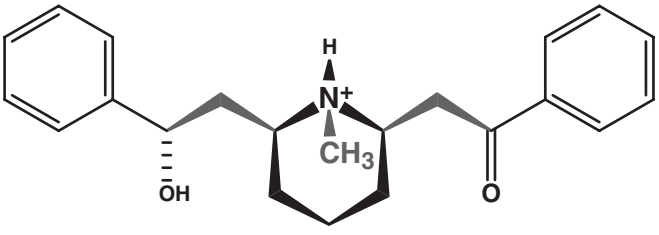

255

Symmetry, Spectroscopy, and Crystallography: The Structural Nexus, First Edition. Robert Glaser.

Companion Website: www.wiley.com/go/Glaser/Symmetry

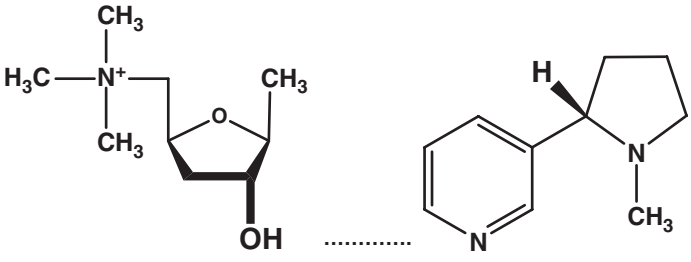

256 **257**

of the HBr·anhydrate and HCl·hydrate crystals differs, they are only related as *pseudopolymorphs* and not as true polymorphs. The hydrated structure exhibited a (+)-*synclinal* H***O***–***C***H···$^{+}$***N***H–***C***H_3 torsion angle conformation and an $R_3^3(7)$ graph set describes a ring hydrogen-bonding pattern; see (composite)-**258**-top. The observation of two conformations and hydrogen-bonding patterns within different crystal lattices strongly suggests that both structures represent different low-energy spatial arrangements (Nature does not look for challenges). One should always try one's luck and prepare a divalent anion crystal, that is, a sulfate, since it just may come to pass that the two monoammonium cations might show different conformations. Why? A divalent anion salt is a completely new crystalline entity compared to either the chloride anhydrate or bromide monohydrate salts. As such, there is no symmetry constraint that the two monoamine anhydrate/monohydrate conformations be either of those observed in any of the hydrohalide salts. In other words, it is impossible to predict if

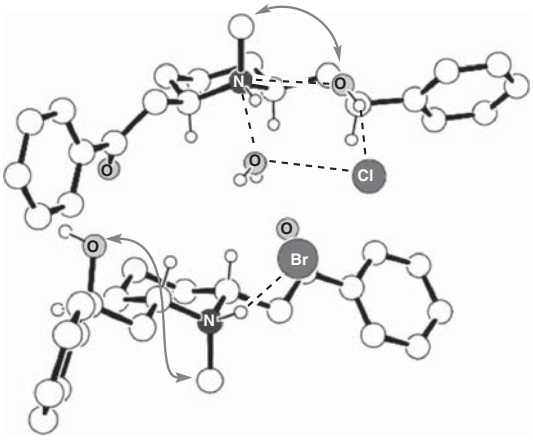

258

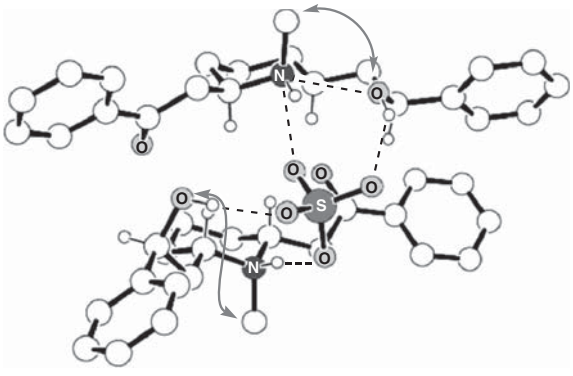

259

both monoammonium conformations will be those found for either of the two hydrohalides, or a combination of the two, or even a third (previously unobserved) structure. However, in the crystal structure analysis phase, there was a hint that two sulfate oxygen anions might replace the $R_3^3(7)$ water oxygen and chloride anion in **258** top and act as a *hydrogen-bonding template* while one or two of the remaining sulfate oxygens might substitute for the bromide anion of **258** bottom (or act as a second *hydrogen-bonding template*). Indeed, the mixed conformations found in structure **259** (Refcode SUGHOT) (R. Glaser and M. Drouin, unpublished results) clearly testify that the gamble paid off.

12.2
Cross Polarization/Magic Angle Spinning Solid-State NMR and X-Ray Crystallographic Studies on the Elusive "Trihydrate" Form of Scopolamine·Hydrobromide, an Anticholinergic Drug

The intimate relationship between molecular conformation and the surrounding environment can be demonstrated by the anticholinergic drugs (−)-Scopolamine·HBr·1.5H_2O (Refcode TIDPOL [173], **260**), and (−)-hyoscyamine·HCl (its structurally related deoxy-analogue lacking the oxiranyl oxygen). They are isolated from the perennial *herbaceous* (leaves and stems die in winter, but roots remain alive) *belladonna* plant or deadly nightshade. (−)-Hyoscyamine often racemizes during purification to yield racemic *atropine.* The compound is named after A*tropos Belladonna*, the third of the three Greek mythological Fates (three beautiful women who determine the fate of men). Clotho, the spinner, spins the *thread of life*; Lachesis, the measurer, chooses the lot in life one will have and measures off how long it will be; and finally, Atropos, she who cannot be turned, who at death cuts the thread of life with

her shears. In ancient times, there were some that desired to assist Atropos Belladonna in her holy endeavors and administered this drug in large doses to selected candidates. However, atropine and also its oxiranyl analogue scopolamine are antagonistic drugs, which, in the proper dosage, can actually save lives during a nerve gas attack by partially blocking some of the *parasympathetic* nervous system's muscarinic-type receptors so that the neuronal pathway will not be overexpressed. These neuropathways involve the neurotransmitter acetylcholine ($Me_3N^+CH_2CH_2OAc$) and regulate involuntary acts such as respiration. Organophosphorylating agents (i.e., nerve gases) irreversibly inactivate the acetylcholinesterase regulating hydrolase enzyme in the synapse by forming a covalent bond to the catalytically important active-site serine^{203}–OH group and thereby producing a stable phosphoric acid ester. The end result is that acetylcholine's synaptic concentration will quickly exceed healthy limits and death quickly follows. If atropine is administered in time, the postsynaptic membrane receptors will not be overactivated since the alkaloid competes with the high concentration of neurotransmitter within the synapse. In Israel, part of the arsenal for defense of the civilian population includes the distribution of self-injecting atropine syringes and gas masks.

The drug can be crystallized from D_2O to afford sesquihydrate ($1.5H_2O$) salt crystals (**260**) [173]. Single-crystal X-ray diffraction shows a *compact* conformation where the sesquihydrate's tropate ester phenyl ring resides underneath the scopine amino-alcohol bicyclic ring (13.9° O(oxirane)–O(alkoxy)–C(α)–C(ipso) torsion angle); see **260**. In contrast, crystallization of the same hydrobromide salt from ethanol under acetone vapor diffusion yields *conformationally pseudopolymorphic* anhydrate crystals (Refcode JAYZEO, **261**) [174]. The dispositions of the more- and less-polar subunits are reversed in this *extended* geometry conformation (141.5° O(oxirane)···O(alkoxy)···C(α)–C(*ipso*) torsion angle, **261**) [174]. Now, the more polar methylol is beneath the scopine bicycle.

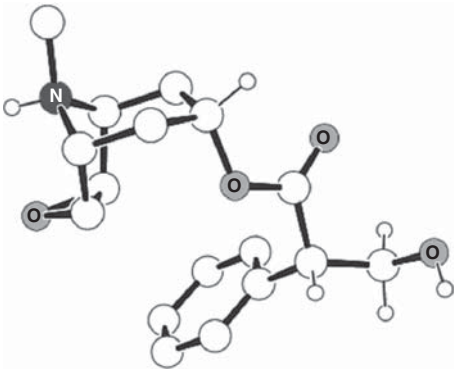

260

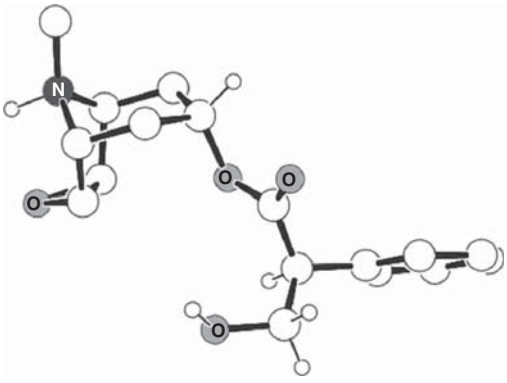

261

Cross polarization has already been discussed regarding solid-state CP/MAS (cross polarization/magic angle spinning) NMR of crystalline Platonic solid-geometry spherical hydrocarbons. A few words will now be provided to understand MAS. Quantum mechanical relationships regarding line-broadening involve a "geometrical factor" $(3\cos^2\theta - 1) = 0$ for $\arccos^2(1/3)$, that is, the $\theta = 54.73561°$ "*magic angle*" of physics. It is important since for solid-state NMR spectroscopy to afford useful relatively narrow linewidth signals, special techniques were developed to reduce (i) severe *dipolar line-broadening* originating from magnetic dipole–dipole interactions between neighboring magnetic nuclei and (ii) *chemical shift anisotropy (CSA) line-broadening* arising from different noneffectively averaged orientations of a magnetic nucleus relative to the spectrometer's magnet field. Brownian motion causes rapid isotropic molecular tumbling in nonviscous solutions to average out the geometric factor to zero. However, this is clearly not the case for solid samples. The aforementioned problems are "theoretically" solved when a 2 cm high-zirconia ceramic plastic turbine-capped rotor is dropped into the spectrometer's cushioned probe-head bottom and then mechanically tilted to magnetic field's magic angle. The fly in the ointment is that the magic angle orientation holds only for those relatively few nuclei *residing on the central axis* of about 1.6–4 mm diameter rotor. Since the vast majority of nuclei are *off-axis,* they have to be *positionally time-averaged* to this value via *rapid spinning* of the rotor on an *almost-frictionless* air-cushion. Unfortunately, state-of-the-art technology is unable to spin the rotor fast enough to effectively time-average out the dipolar interactions, although it does do a reasonable job on the CSA line-broadening. As we will see later on, the small degree residual friction between the spinning rotor and the antenna coils also contributes to the problem as well as heating the sample. Heteronuclear $X-{}^1H$ dipolar interactions are somewhat eliminated by high-power broadband proton

decoupling (if it is efficient enough). Unless very special techniques are used (e.g., CRAMPS (*C*ombined *R*ot*A*tion and *M*ultiple *P*ulse *S*equence) for ^{1}H), homonuclear X–X dipolar interactions are negated since we only observe either magnetic nuclei of very low natural abundance (e.g., the 1.1% ^{13}C nucleus) or those that usually lack homonuclear neighbors (i.e., solids with one ^{15}N, ^{31}P, ^{29}Si nucleus within the molecule).

Due to the spatial differences in the scopolamine·HBr·anhydrate and $1.5H_2O$ HO*C*H_2–*C*α–*C=O* segments, it is not a surprise that their ^{13}C CP/MAS solid-state NMR spectra are markedly different [175]. The *C*H_2OH methylol carbon signals are unequivocally assigned by use of the solid-state CPPI [176] (*C*ross *P*olarization/*P*olarization *I*nversion) *spectral editing* pulse-program. Comparison of the CPPI "methylene carbon only" *phase-inverted* **262** top plot (compact conformation) versus **263** top (extended conformation) shows a 4.0 ppm *closer-to-TMS* *C*H_2OH dark gray signal in the former *partial spectrum.* This enables a ready *C*H_2OH signal assignment in ^{13}C CP/MAS solid-state NMR aliphatic-C plots. The predictable change of chemical shift is the result of the 55.6° *synclinal* HO–*C*H_2–*C*α–*C=O* torsion angle (in *extended* conformation **261**) closing to a 15.7° *synperiplanar* value for *compact* conformation **260**. This well-known *γ-gauche effect* CP/MAS solid-state and solution-state ^{13}C NMR phenomenon involves a shift of $\delta_{C\gamma}$ and δ_{CX} closer-to-TMS upon closing torsion angle *C*$_\gamma$–*C*$_\beta$–*C*$_\alpha$–*C*$_X$. Note: liquid TMS is obviously *not* the internal spectral reference compound in solid-state ^{13}C CP/MAS NMR (it would leak out of the plastic turbine cap under *MAS* and damage the probe head's antenna coils). Instead, a secondary *external* (i.e., not in the sample) spectral reference glycine α-crystal form $\delta_{C=O}$ 173.06 signal is used for calibration.

Dissolution of either the anhydrate or $1.5H_2O$ salt in high or in low dielectric solvents (D_2O and CD_2Cl_2, respectively) shows a fast conformational equilibrium at the NMR FEL (fast exchange limit) timescale irrespective of solvent [177]. The disparate methylol solution-state DEPT-135 inverted-methylene ^{13}C chemical shifts compare nicely to the corresponding solid-state CPPI chemical shifts from samples of known conformational structure. Therefore, using solid-state δ_{CH_2OH} chemical shifts as conformational markers, one can deconvolute the solution-state *weighted time-averaged* δ_{CH_2OH} chemical shifts in terms of a particular solvent-dependent *preferred solvated conformation.* Changing from CD_2Cl_2 to D_2O affords a 4.2 ppm γ-gauche effect for the *axial N*-methyl diastereomers that is exactly the same as the 4.0 ppm value observed in solid-state CP/MAS aliphatic-C plots **262**, **263**. The scopine amino-alcohol's C(3) alkoxy δ 63.9(4) (solid-state) and δ 63.2(8) (solution-state) carbon peak is used as an internal reference for the comparisons. The solution-state δ_{CH_2OH} averaged values strongly suggest that the *extended* conformation predominates in CD_2Cl_2, while the *compact* conformation is favored in D_2O. This interpretation is quite reasonable since the *extended* conformation's more polar CH_2OH is tucked underneath the bicyclic moiety (i.e., making it less solvent-exposed), whereby the less polar

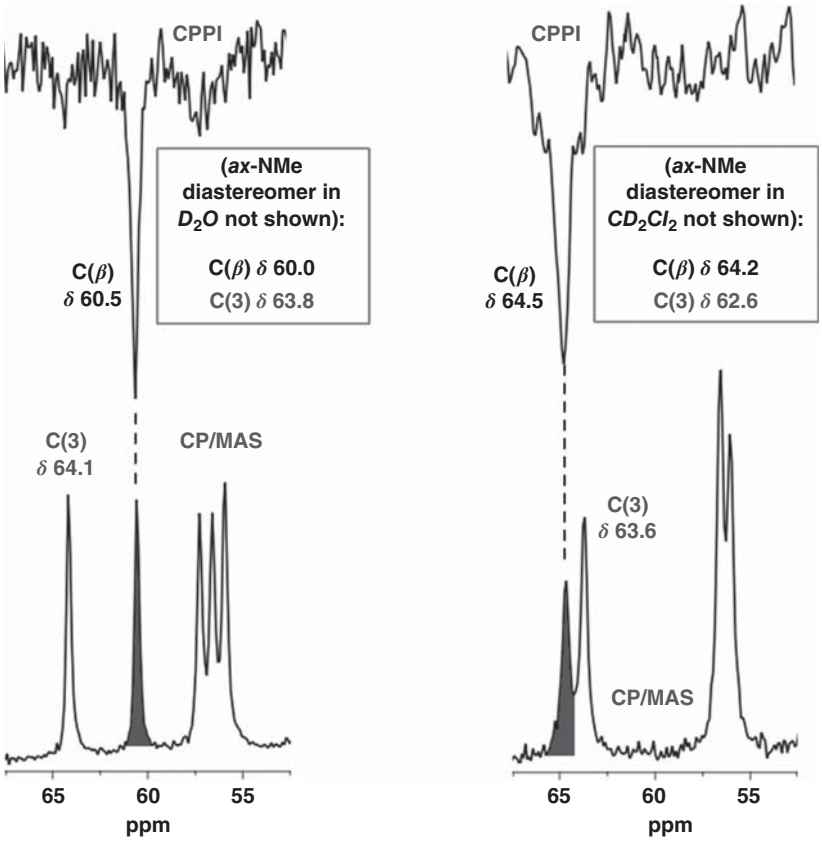

phenyl's two exposed sides are solvated by the *low* dielectric constant CD_2Cl_2 solvent [175]. Similarly, the *compact* conformation's less polar phenyl ring resides beneath the bicyclic entity so that only one side is solvent-exposed. As a result, the *higher* dielectric constant D_2O solvent can surround the polar CH_2OH hydroxyl. Location of less polar moieties within a molecule's interior while more polar groups reside on the periphery (so that they can be efficiently solvated) is a well-known structural phenomenon and is called a *hydrophobic collapse* in biochemistry. It is the reason why the less polar bases of polynucleotide duplexes are stacked in the interior while the phosphate anions are found on the double-helix's exterior.

There happens to be another important difference in the CP/MAS spectra of the two conformational pseudopolymorphic forms of scopolamine·HBr (see plot **264**) and HCl salts. The *compact* conformation's *aromatic ring immobility* within

the crystal lattice of HBr·1.5H_2O (and in that of the HCl·hydrate, and its methobromide anhydrate quaternary ammonium salt, Refcode KEYWEQ) is clearly implied by observation of signals from *all six phenyl carbon nuclei* [175]. On the other hand, only two sharp C(*ipso* or quat.) and C(*para*) carbon signals are found for *extended* conformations of HBr·anhydrate (see plot **265**), HCl anhydrate, and the *equatorial N-n*-butylbromide·methanol adduct (antispasmodic drug "Buscopan®, Refcode BHYOSM [178], see plot **266**). It is not an accident that the two sharp peaks involve nuclei on the C(*ipso*)–C(α) rotation axis (a nonsymmetry axis). The broadened hump for *off-axis* C(*ortho* and *meta*) in plots **265**, **266** results from a *π-flip* and clearly points to *mobile phenyl rings* in the *extended* conformation's crystal lattice. The temperature-dependent *π-flip* kinetic phenomenon involves a phenyl-ring *side-exchange* via a rapid 180° flip about the C(α)–C(*ipso*) axis, followed by a rest period, and then another rapid 180° flip, and so on. Obviously, the observation of phenyl ring mobility for only the extended conformation suggests that lattice constraints involving nearest neighbors have been relaxed in this packing arrangement. Are there structural features in the compact and extended conformations that can explain the absence or the presence of a *π-flip*? Yes, the distance between the aromatic rings and their nearest *intermolecular* proton neighbors differs in the two conformational arrangements (2.5 Å nearest neighbors in *all* the compact conformations versus ≥3.0 Å distances in all the *extended* conformations studied) [175]. The 2.5 Å *close contact* seems to be the cause of the compact conformation's immobile phenyl ring in the crystal lattice. On the other hand, a relatively small distance increment of only 0.5 Å between the *extended* conformation's aromatic ring face and its nearest proton neighbors appears to be enough to enable a *π-flip* to proceed at a solid-state NMR observable kinetic rate [175].

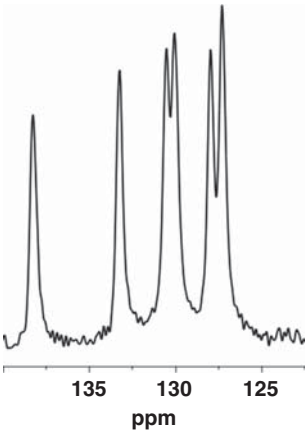

(*compact*•HBr)-**264**

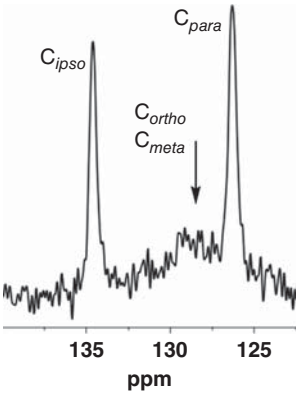

(*extended*•HBr)-**265**

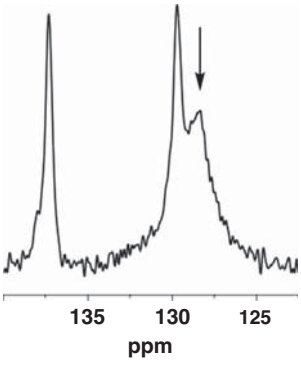

(*extended*•MeBr)-**266**

Why isn't the π-flip just a simple continuous rotation process as it is in solution? Answer: The nearest proton neighbors' minimum 3.0 Å distance is simply too short to enable it to occur. So, how then does a π-flip occur? Believe it or not, the extended conformation's crystal lattice is *dynamic* at ambient temperature. Periodically, it expands just enough to permit a phenyl ring to flip by 180° about the C(*α*)–C(ipso) bond before it closes up. The amazing thing is that a π-flip involves significant van der Waals contacts, highlighting the need for lattice deformations to permit ring dynamics. *This phenomenon is time-averaged over the entire volume of the crystal.* Riddel and Rogerson [179] found that the CP/MAS-observed π-flip free energy of activation at ambient temperature (293 K) was calculated to be about 10.0 kcal mol^{-1}.

Since an anhydrate and a sesquihydrate crystal form of (−)-scopolamine·HBr were found, *Glaser* et al. [175] next considered which of the two (if any) were approved by the *United States Pharmacopeia.* It was a surprise to see that a "trihydrate" form was listed for this drug. However, since the sesquihydrate was crystallized by *slow* water evaporation, it was an enigma to understand how more water could be incorporated into the lattice. One hypothesis could be that the "trihydrate" form was a kinetic crystal produced via a fast industrial crystallization, while the sesquihydrate was the thermodynamic form. A visit to the Bethesda, Maryland offices of the *United States Pharmacopeial Convention* did not bring much clarification. The USP (founded in 1820) is the *National Formulary* and is a nonprofit scientific organization originally set up by the industry to set standards for the identity, strength, quality, and purity of medicines, food ingredients, and dietary supplements manufactured, distributed, and consumed in the United States. The USP drug standards are enforced by the US Food and Drug Administration. Products proven to meet the high standards bear the words *USP-NF* on their labels.

When scopolamine·HBr was given as the reason for the visit, it was mentioned that both the US and British Pharmacopeia regulatory agencies knew it to be problematic since Karl Fischer titrations to quantify trace amounts of water in standard samples of scopolamine·HBr·$3H_2O$ show that the "trihydrate" contains less than three molecules of water. The water content varied according to the air's relative humidity after the sealed metal containers were opened. At the time of the visit, the USP water content [180] for scopolamine·HBr·$3H_2O$ was specified in terms of a maximum permissible weight loss of 13.0% of its weight after drying at 105 °C for 3 h, and no lower limits for weight loss were stated. A recent web search [181] shows that a preliminary drying stage (80 °C for 2 h) now precedes the drying at 105 °C for 3 h. A USP maximum weight loss of 13.0% signifies that the anhydrate, sesquihydrate, and trihydrate forms all meet the standard since the theoretical weight loss upon drying would be 0.0%, 6.6%, and 12.3%.

Glaser *et al.* [175] used solid-state CP/MAS ^{13}C NMR spectroscopy to show that scopolamine·HBr·$3H_2O$ samples from two manufacturers consisted of mixtures of *metastable* pseudopolymorphic hydrated forms with a three-component

ratio that varied from supplier to supplier. A 1 : 1 : 2 ratio of carbonyl signals of (−)-scopolamine·HBr·$3H_2O$ EUP (European Union Pharmacopeia) produced by Boehringer-Ingelheim GmbH, Germany, is depicted in the CP/MAS ^{13}C NMR, ***5.0 kHz*** **sample** ***spin-rate*** (***S***ide band ***EL***imination by ***T***emporary ***I***nterruption of the ***C***hemical ***S***hift (SELTICS)) **267** bottom plot versus the sole δ 171.8 ***C***=O signal found for the $1.5H_2O$ *crystal form* (inverted plot **267**-top). High-intensity spinning side bands (an annoyance in solid-state NMR spectra measured at low (e.g., 5.0 kHz) rotor spin-rates) are removed by the SELTICS pulse-program. At a 5.0 kHz spin-rate, the spin-air cools the rotor's outer surface by −1.8 °C compared to the 295 K temperature of a static rotor. Plot **268** bottom shows the same three carbonyl signals in a 1 : 1 : 1 ratio measured from a (−)-scopolamine·HBr·$3H_2O$ sample produced by Phytex PTY, Australia (with the Boehringer-Ingelheim sample as an inverted plot above it) [175].

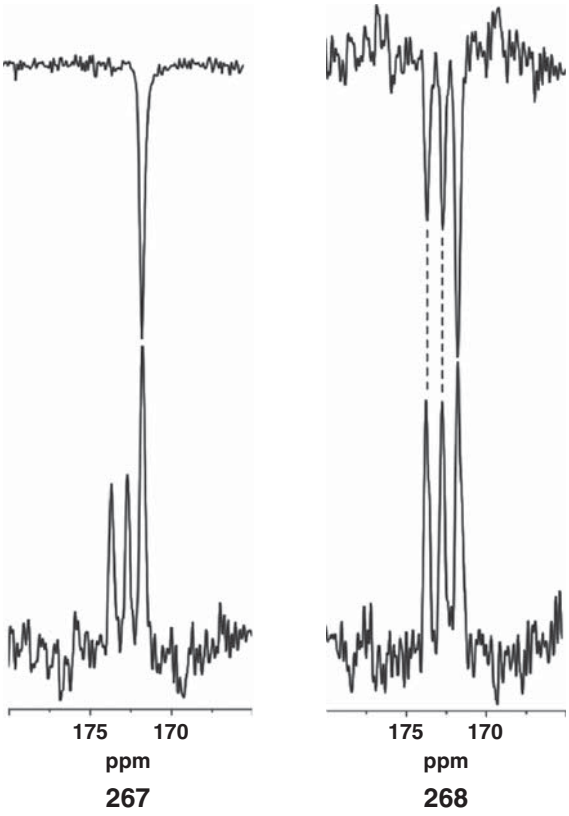

Spectra of the same two samples were then measured at an *increased rotor spin-rate* (11.5 kHz) by the ***V***ariable ***A***mplitude ***C***ross ***P***olarization (VACP) pulse-program. Surprisingly, intensities to the left of the δ 171.8 "*1.5H_2O*

crystal form peak" in the spectra decreased by about half to afford new ratios of 1 : 1 : 4 (plot **269**, Boehringer-Ingelheim) and 1 : 1 : 2 (plot **270**, Phytex). While only carbonyl region partial spectra have been illustrated to save space, it should be obvious that the remaining regions of the spectra also changed. Further increase of spin-rate to 13.5 kHz afforded only the δ 171.8 "$1.5H_2O$ crystal form's single ***C***=O peak for both Boehringer-Ingelheim (plot **271**) and Phytex (plot **272**) samples. These experiments testify to the fact that two of the components of (−)-scopolamine·HBr·$3H_3O$ appear to be *metastable hydrated crystals* while the third partner is the thermodynamically stable $1.5H_2O$ [175].

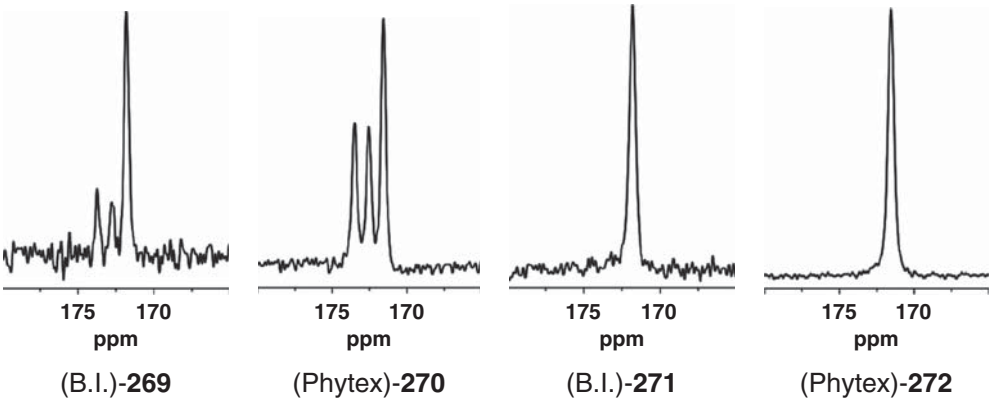

What would you do next? Probably, lower the spin-rate back down to 5.0 kHz to see if the three components are regenerated. An immediate decrease of spin-rate to 5.0 kHz affords spectra with signals from only the thermodynamically stable sesquihydrate form for both the Boehringer-Ingelheim (plot **273**) and Phytex (plot **274**) samples. Only $1.5H_2O$ signals were still seen after one full day of storage within the capped rotor. Forty-three days elapsed during which the samples were stored in their capped rotors at room temperature. The ternary mixture of pseudopolymorphic hydrated forms of (−)-scopolamine·HBr·$3H_2O$ was regenerated sometime during this storage period, for example, see the Boehringer-Ingelheim 43-day storage sample's plot **275.** Plot **276** shows a decrease in the two non-$1.5H_2O$ pseudopolymorphic hydrates after 17 months of ambient temperature storage in a half-*filled* 1 dram vial [175]. The partially filled vial was then left on a shelf in the Beer-Sheva laboratory for 3 years (in the relatively dry atmosphere of the Negev Desert). A rotor was filled, and the spectrum of the Boehringer-Ingelheim trihydrate sample was found to have signals arising from only the stable

sesquihydrate form of the drug. Negev ("Nakeb" in Arabic) means "to dry" in the Hebrew language, the same word root as "to wipe something dry."

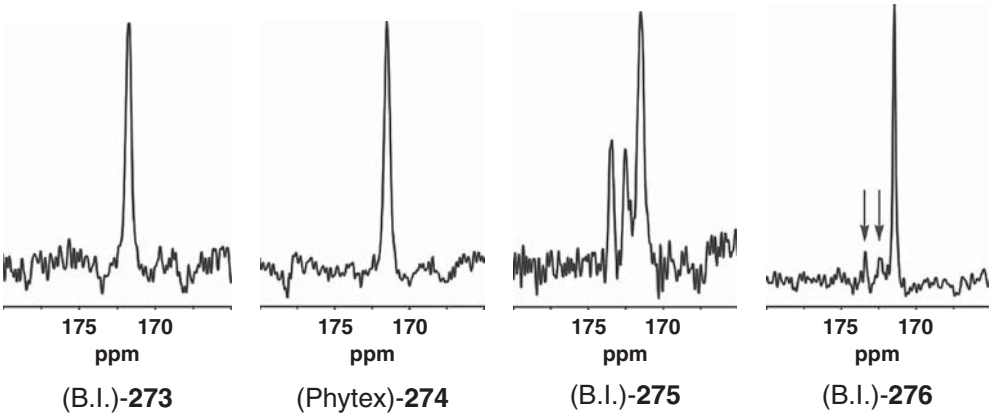

(B.I.)-**273** (Phytex)-**274** (B.I.)-**275** (B.I.)-**276**

It now remained to ascertain the mechanism for the disappearance of the two metastable hydrated pseudopolymorphic forms in the "trihydrate" mixture. The most likely explanation is that frictional heating of the rotor's walls overcame the cooling effect of the spin-air flow on the rotor surface. On the other hand, it is well known that opening sample-filled rotors that were previously spun at high spin-rates (12 – 14 kHz) always showed a vortex formed by centripetal force pushing the ground crystallites against the internal walls. This possible cause had to be eliminated. Using a lead-nitrate-filled rotor (the so-called lead nitrate thermometer due to the $\delta\ ^{207}$Pb linear dependence with temperature), the degree of internal sample heating at a spin-rate of 13.5 kHz was found to equal that of actually heating the rotor to 313 K. The final experiment was to keep the spin-rate at only 5.0 kHz (where the spin-air ordinarily cools the rotor surface to −1.8 °C lower than the temperature of a *static* rotor at 295 K) and then set the calibrated variable temperature unit to 313 K, see plot **277.**

It was now nicely illustrated that two of the trihydrate's metastable hydrated components disappear due to *frictional heating of the rotor* that overcomes the effect of spin-air cooling. This observation has important implications to spectroscopists performing CP/MAS NMR spectral analysis to characterize the polymorphic form of crystalline drugs as either the granular *API* (active pharmaceutical ingredient) or within tablets. At the time these experiments were undertaken, the rotors could be heated but not cooled. Luckily, this situation has now been rectified. Bottom line: if rotors spun at high spin-rates are not cooled to ambient temperature, the frictionally heated sample might not represent the actual material given in for analysis. In other words, the analyzed sample might turn out to be an artifact that has little in common with the true sample.

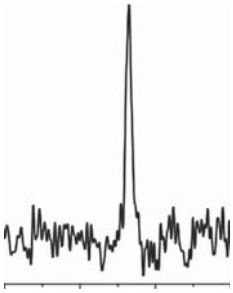

277

Structural insight into the problem of variable hydration was found by studying the analogous (−)-scopolamine·HCl salts, which also exist in the anhydrate and hydrated forms (like the HBr salts). As expected, the hydrochloride anhydrate salt was found to exist in the *extended conformation* (Refcode KEYSOW) while the pseudopolymorphic 1.67·hydrate shows the *compact* conformation (**278**, Refcode KEYTOX) [175]. A 1.67·hydrate means that statistically 33% of the eight asymmetric units of the tetragonal system $P42_12$ space group crystal consist of a dihydrate, while the remaining 66% contain a sesquihydrate in the asymmetric unit [175]. In other words, for every 3 unit cells there are 24 asymmetric units, and out of these, 8 statistically contain a *dihydrate* and 16 have a *sesquihydrate.*

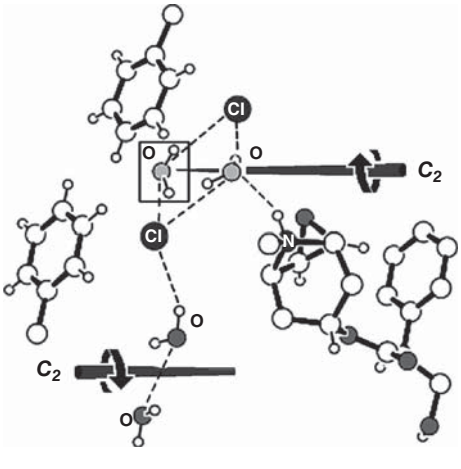

(HCl•1.67H_2O)-**278**

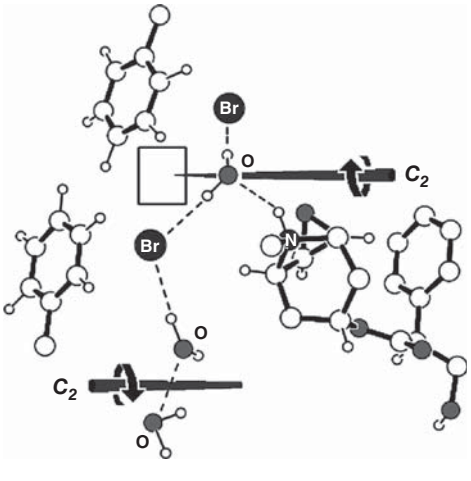

(HBr•1.5H_2O)-**279**

These two different asymmetric units are randomly distributed over all the unit cells in a 2 : 1 ratio. The net result is *crystallographic space averaging* to provide a statistical $1.67H_2O$ crystal.

Crystalline (−)-scopolamine·HBr·$1.5H_2O$ (**279**) is *isostructural* in space filling to the corresponding unit within the (−)-scopolamine·HCl·$1.67H_2O$ lattice. The same can also be said about the corresponding pair of anhydrate crystals. By this we mean that the molecular conformations and packing motifs are the same, but the crystal dimensions differ due to the larger size of the bromide versus chloride anions. Two water molecules in the HCl·$1.67H_2O$ structure occupy *special positions of twofold rotational symmetry,* see upper C_2 axis in **278.** The chloride anions participate in four hydrogen bonds as hydrogen-bond acceptors (a fourth hydrogen bond to a neighboring methylol hydroxyl-proton has been deleted in the drawing for simplicity). The water molecules appear in a diamond-shaped $R_4^2(8)$ ring hydrogen-bonding pattern graph set.

The thermodynamically stable HBr·$1.5H_2O$ crystal has two vacant hydrogen-bond acceptor sites on C_2-symmetry related bromide anions whose location and void space are appropriate to receive an additional water molecule; see empty box in **279.** One can rationalize the relative lability of an extra water molecule (with variable degrees of occupancy inside the box) since the bromide anions already participated in three hydrogen bonds mentioned earlier. Occupancy of a water molecule on a special position of C_2-rotational symmetry means that its stoichiometry is only one-half in the asymmetric unit. A word should be mentioned about the general positioned full water molecule and its symmetry related neighbor depicted on the bottom C_2 axis of the molecular graphic **278** and **279.** The general positioned oxygen is located 2.81 Å away from its C_2-symmetry related neighbor. Despite the fact that the intermolecular distance appears to be quite reasonable for a hydrogen bond between the two water molecules, the fact that the two donors are symmetry related would result in *both oxygen atoms simultaneously placing a proton* toward their neighboring oxygen acceptor. Since two protons cannot occupy the same space, it is obvious that this hydrogen bond is weak. *Isotropic and anisotropic displacement thermal parameters* describe the thermal motion of atoms in the crystal. At ambient temperature, the *isotropic equivalent displacement thermal parameter* (B_{eq}) of the full water oxygen's spherical thermal motion is about five times larger than the mean value of *all* the other 22 nonhydrogen atoms (i.e., C, N, and O) in the scopolamine cation skeleton [173]. In the original report of the *X-ray* crystal structure of (−)-scopolamine·HBr by Peter Pauling (son of Linus Pauling, 1954 Nobel Laureate in Chemistry) and Petcher [182], the crystal was reported as only a hemihydrate, most likely due to nonobservance of the large thermal motion oxygen atom in the off-axis water [173]. Michel *et al.* [173] used thermogravimetric analysis to show that weight loss for the HBr·$1.5H_2O$ crystal occurred in two stages: ∼4% at 90 °C ($1.0{\cdot}H_2O$ generally positioned molecule) plus an additional ∼2% at 102 °C ($0.5{\cdot}H_2O$ specially positioned molecule). As already

noted, the C_2-axis special positioned hemihydrate H_2O is much more tightly hydrogen-bonded in the lattice. Its two protons are hydrogen-bond donors to halide anions, while the oxygen is an acceptor to two $^{+}$N–H protons (the second symmetry related $^{+}$N–H–O bond has been deleted from **279** for simplicity). In conclusion, complete occupancy of the vacant site in **279** to produce the ring hydrogen-bonding pattern would afford a dihydrate·HBr crystal. It remains to be seen if adsorbed moisture is responsible for the hygroscopic dihydrate to appear to show a "trihydrate-like" water content.

A word should be said about the desolvation of a solvate adduct (e.g., a hydrate) crystal. The trihydrate samples (within tightly closed vials) were received as powders, which were carefully ground in a mortar and pestle. The desolvated trihydrate sample (i.e., now known to be the sesquihydrate) also consisted of a hard crystalline powder, which was ground prior to rotor filling. Therefore, the desolvated crystals kept their crystalline integrity. Sometimes solvated crystals turn into fluffy amorphous powders upon desolvation. There are channels and pores in the lattice that will enable the solvent to pass through despite the mirror-like appearance of the crystal's faces. As a result, it is recommended to keep problematic hydrated or solvate adduct single crystals under their mother liquor until the crystallographer mounts them on a glass fiber. If the crystals are not robust enough to keep their integrity when removed for a period of time from their mother liquor, then the crystal can be wedged inside a glass or quartz sealed capillary, together with a drop of mother liquor, and the orifice plugged with epoxy. The diffraction will only arise from the crystal since the glass and epoxy are amorphous. A second point to remember is that all crystalline solid-state NMR samples should be carefully and *gently* ground in a small agate mortar and pestle prior to filling the ceramic rotor to avoid local heating and possible sample change.

13
NMR Spectroscopic Differentiation of Diastereomeric Isomers Having Special Positions of Molecular Symmetry

13.1
NMR Anisochronism of Nuclei at Special Positions of Molecular Symmetry

Reinhoudt and coworkers [183] prepared supramolecular D_3-(D,L-pair, chiral) and C_{3h}-symmetry (*meso*, achiral) diastereomeric dynamic assemblies (**280** and **281**, respectively) consisting of six hydrogen-bonded barbiturates/cyanurates (color-coded white) utilizing three (C_2-symmetry **282** or C_s-symmetry **283**) color-coded gray dimelamine-substituted calix[4]arene building blocks.

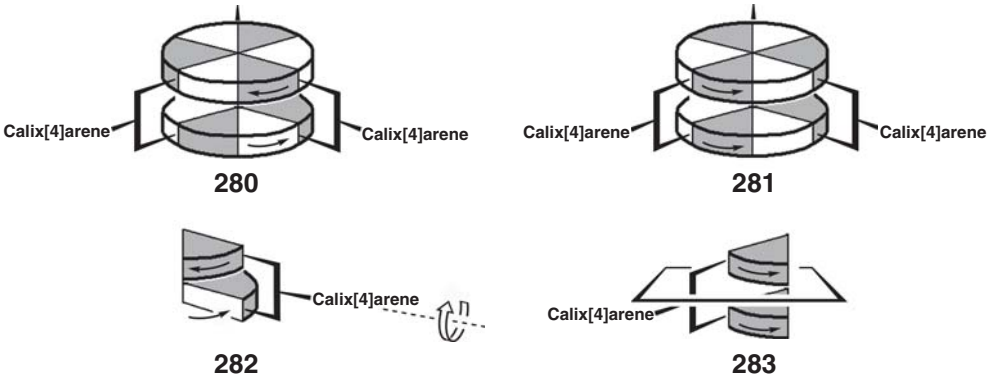

Reinhoudt referred to these esthetic self-assemblies as *rosettes.* The hydrogen-bond assembly of one layer is depicted as **284**, and its top-viewed R-group clockwise *tropicity* (directionality) of the stereogenic element is shown by curved arrows. Glaser (2000) (R. Glaser, unpublished results) has shown that it is possible to unequivocally differentiate between these D_3- and C_{3h}-symmetry diastereomeric solvated rosette assemblies by ^{13}C NMR spectroscopy based upon occupancy of either general or special positions of molecular symmetry. The D_3-symmetry chiral diastereomer had only pairs of nuclei occupying homotopic *general positions of molecular symmetry,* while the C_{3h}-symmetry rosette had

Symmetry, Spectroscopy, and Crystallography: The Structural Nexus, First Edition. Robert Glaser.

Companion Website: www.wiley.com/go/Glaser/Symmetry

nuclei residing in the special position of mirror symmetry, which is the source of the differentiation. For example, a C_2-rotation axis passes through the interior of chiral calix[4]arene **285** so that *homotopically related* (1,1′), (2,2′), and (3,3′) pairs of ^{13}C nuclei reside between the two hydrogen-bonding arrays. On the other hand, the two hydrogen-bonding arrays in the C_{3h}-symmetry *meso* diastereomer **286** are *enantiotopically related.* Thus, generally positioned nuclei in the upper array have a corresponding enantiotopic partner within lower one. But now, diastereotopic (1,4), (2,5), and (3,6) pairs of calix[4]arene nuclei reside upon the reflection special position itself. As a result, the $^{13}C\{^1H\}$ NMR spectrum *meso* compound contains more anisochronous signals than in that measured from the D,L-pair.

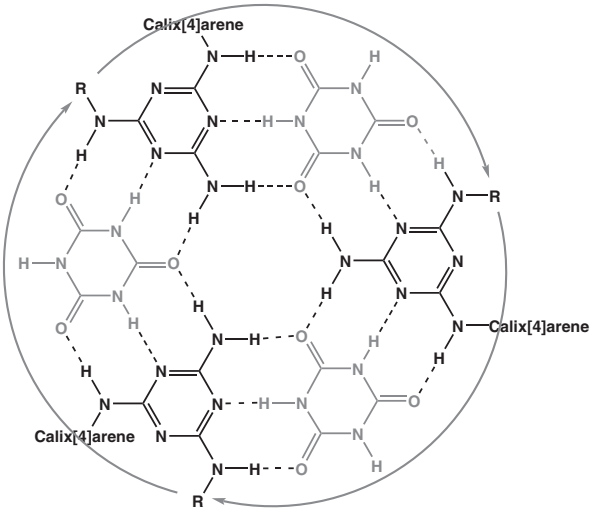

284

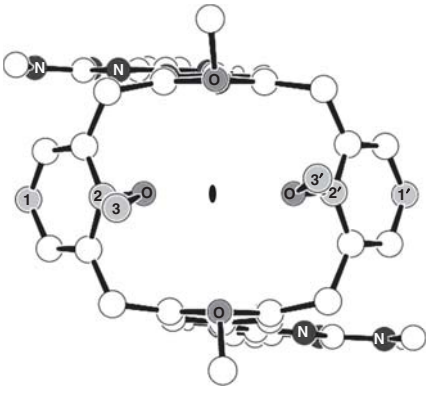

285

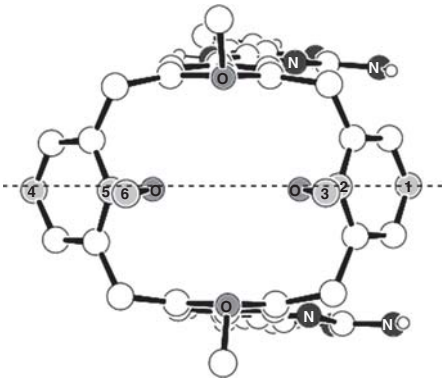

286

13.2
Pattern Recognition: A Graphical Approach to Deciphering Multiplet Patterns

The following method enables an NMR user to derive the proton–proton vicinal coupling constants ($^3J_{HH}$) in *complex multiplets* (R. Glaser, unpublished results). What is a complex multiplet? Complex multiplets are those that exhibit multiple-intensity peaks, which result in correspondingly less lines/multiplets than expected for the spin system. Sounds complicated, but this will be explained quite soon. But, first we should ask: "Why bother to decipher this multiplet pattern?" We could say, "it is fun to solve puzzles, and the harder, the better." But seriously, the answer is that the magnitudes of the vicinal coupling constants provide important information about the conformation of a solution-state molecular segment, see the Karplus relationship **107** [73]. We will later see that under some circumstances, the actual numerical value can be calculated for a dihedral angle in a solvated molecule (and thus we know its stereochemistry, i.e., local conformation).

Symmetry-equivalent nuclei do not exhibit signals showing mutual *J*-coupling. We have already seen that this is only true for two symmetry-equivalent nuclei that are *magnetically equivalent* (isogamous) to a third nucleus (see **185** and **186)**. However, fortunately, magnetic equivalence is usually not a problem in our spectra. Symmetry equivalence (or lack thereof) within the set of neighboring nuclei covalently bound to a particular nucleus plays an important role in the *J*-coupling patterns (multiplets) in NMR spectra. The most simple multiplets are composed of nonoverlapping peaks (all of which have the same unit-intensity value). It is a very trivial task to recognize the patterns in these multiplets and then measure the coupling constants numerous times. Why do we want to measure the coupling constants "numerous times"? Most of us work daily with instruments that produce numbers, and every scientist should know the *precision* of the numerical value, that is, the ***e***stimated ***s***tandard ***d***eviation of the last digit (*esd* or the number of *significant digits*). Why? We always should know when two "different" numbers are really statistically "the same." Don't be fooled by the number of digits of the chemical shift or frequency printout on the NMR spectrometer. It was probably arbitrarily set by the last operator.

Fortunately, analyzing complex multiplet patterns follows some simple and logical rules. These rules are based on the principles of *pattern recognition.* As the number of spins in a spin-system increases, the chance of observing *overlapping peaks* also increases. We will later see that these multiple-intensity peaks often arise by chance from the sum of two or more different coupling constants rather than from symmetry-equivalent nuclei. In addition, there is a *digital resolution* problem that can result in two close frequency *transitions* becoming either nonresolved or only partially resolved (and hence slightly broadened). In many articles and books, the reader will find deconvolution of a complex multiplet that is illustrated by a series of *inverted funnels* relating two nonadjacent transitions.

Understanding the construction of that multiplet becomes a trivial task due to these inverted funnels. But it is much more difficult to start with a complex multiplet of unknown pattern composition and to "figure things out from scratch." The more difficult the puzzle appears, the more satisfaction you will later derive when you finally "unravel the secret" by rational thought. Of course, there are NMR experiments we can perform to simplify complex multiplets. The most basic experiment to do is to perform a series of ***H***omonuclear ***D***ecoupling (HD) experiments of the nuclei in the sample. HD involves using an radio frequency (RF) transmitter during the data acquisition period of about $3T_1$ time periods. A nucleus in a *through-bond* spin system is irradiated to cause an equal population of its spin states. This effectively removes it from the spin system, and the other multiplets in the system become simplified. There are even very low-power ***n***uclear ***O***verhauser ***e***ffect (NOE) experiments that simplify overlapping multiplet signals from two heterotopic nuclei within different parts of the molecule. This is performed by very gently (extremely low power) irradiating only one of the terminal peaks of the overlapped system and then repeating the process on the other terminus.

For a one-spin system (i.e., no covalently bound neighbors), the number of transitions in the multiplet pattern is obviously only one (a *singlet*). For a two-spin system of covalently bound nuclei, the *number of transitions* is two for each multiplet (a *doublet*); for a three-spin system, it is four for each multiplet, and for a four-spin system, it is eight for each multiplet, and so on. Therefore, the addition of a new spin neighbor to an existing spin system *doubles* the number of transitions/multiplets. This is true since *the role of a coupling constant is to repeat the entire pattern generated by all the smaller magnitude coupling constants coming before it.* If neighbors are *symmetry equivalent,* then their respective coupling constants with a nonsymmetry-equivalent neighbor are *degenerate* (the identical or exact frequency). *J*-coupling degeneracies result in *ideal overlaps* of some of the transition frequencies arising from two or more *symmetry-equivalent J*-values. For example, consider a three-spin system in which the A-nucleus has two symmetry-equivalent X-neighbors (i.e., an AX_2 spin system). The two neighboring symmetry-equivalent X-nuclei generate two degenerate J_{AX} and $J_{AX'}$ coupling constants, one for each X-nucleus.. The role of the second $J_{AX}{}'$ coupling constant is to duplicate the arbitrarily chosen gray color-coded doublet pattern from the first J_{AX} splitting by starting at the *left-end of the gray doublet* shown in the A-multiplet pattern **287**. Using this arbitrary starting point means that transition **1** in the gray doublet is duplicated as new clear color-coded transition **3** located at transition **2**'s frequency that is *exactly* J_{AX} Hz from that of transition **1**. Since transition **2** is already resident at this frequency, there must be a *frequency degeneracy* for both transitions **2**, **3** (i.e., they exactly overlap to afford double-intensity *line 2*). The second J_{AX} coupling constant now duplicates transition **2** to become the new clear transition **4** that is located J_{AX} Hz away from transition **3**. It now becomes single-intensity *line 3* on the right-hand side

of the pattern. In this manner, the well-known 1 : 2 : 1 triplet intensity pattern is generated.

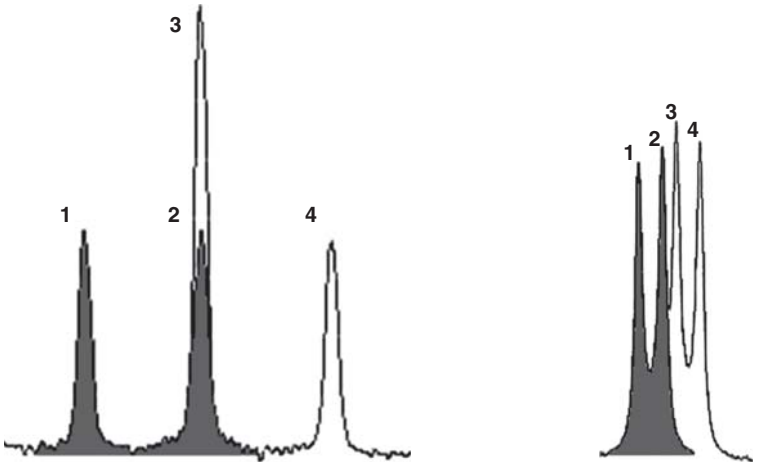

If the three-spin system has no symmetry-equivalent neighbors (i.e., *AMX*), then the degeneracy is lifted, and there are four *nonoverlapped* transition frequencies in a doublet-of-doublets four-line pattern (see **288**). Why? There are two different magnitude coupling constants ($J_{AM} \neq J_{AX}$) since the M- and X-nuclei are symmetry nonequivalent to nucleus-A. The *smaller* coupling constant (arbitrarily assigned as J_{AM}) generates transition **2** that is J_{AM} Hz from transition **1** to produce the gray doublet in **288**. Next, the *larger* J_{AX} duplicates transition **1** at a frequency of J_{AX} Hz away from **1** to become transition **3** of the second pattern. Nonsymmetry-equivalent coupling constants mean that there is no J_{AM} signal resident at this new frequency, and thus, there is no overlap by the new J_{AX} transition. Finally, J_{AX} duplicates transition **2** at a frequency of J_{AX} Hz away from **2** to become the last transition **4** of the second pattern. As a result, all four transitions of the pattern are observed with *unit intensities*, and each coupling constant can be measured twice (J_{AM}: $\nu_1 - \nu_2$ and $\nu_3 - \nu_4$; J_{AX}: $\nu_1 - \nu_3$ and $\nu_2 - \nu_4$), averaged, and the esd of each pair of values may be calculated.

Similarly, in a four-spin system of the AX_3 type, there are three degenerate J_{AX} coupling constants (one of each of the three symmetry-equivalent X-neighbors). As with the triplet, there is overlapping of transition frequencies [2, 3, 5] and also [4, 6, 7], so that the eight transitions now comprise only four lines in an intensity ratio of 1 : 3 : 3 : 1, that is, a *quartet.*

First-order multiplet patterns follow simple mathematical rules and are amenable to analysis without recourse to time-consuming computer-generated

iterated spectral simulations. One of the rules is that the $\nu(\alpha) - \nu(\omega)$ frequency difference of a multiplet pattern (i.e., the difference between the *first* $[\nu(\alpha)]$ and *last* $[\nu(\omega)]$ frequencies) must equal the *sum of all* the coupling constants that generate that particular coupling pattern.

Next, consider the case of an *AFMX* four-spin system in which all nuclei are symmetry nonequivalent. Three variants for the A-part of an *AFMX* multiplet pattern can be generated by three *different magnitude* coupling constants. We will first assume $J_{AX} > (J_{AM} + J_{AF})$ and $J_{AM} > J_{AF}$, variant **289**. Similar to the case of four-line pattern **288**, multiplet analysis is trivial since there are no overlapping transition frequencies. This analysis enables a structural chemist to use *J*-values to ascertain geometric information concerning the spatial disposition of the nuclei comprising the spin system: for example, dihedral angles between *vicinal* protons: H(A)–C(1)–C(2)–H(F), H(A)–C(1)–C(2)–H(M) in the solvated molecule (according to the Karplus relationship [73] **107**). The gray four-line pattern in **289** (similar to **288**) arises from J_{AF} and J_{AM}. A new transition **5** is generated by J_{AX} acting on transition **1** and places it at a distance of J_{AX} Hz from **1**. In a similar manner, transitions **2**, **3**, **4** consecutively are duplicated by J_{AX} as new transitions **6**, **7**, **8**. The ordering of the eight unit-intensity transitions is simply **1, 2, 3, 4, 5, 6, 7, 8**.

The second variant is that $J_{AX} \approx (J_{AM} + J_{AF})$ and $J_{AM} > J_{AF}$ (see **290**). This is *accidental* since there is no symmetry constraint for J_{AX} to be exactly equal to $(J_{AF} + J_{AM})$ and is only due to inadequate spectral resolution of two close frequency transitions by the spectrometer. As a result, there is an overlap of transition **4** from the gray four-line pattern with transition **5** of the new pattern. Careful

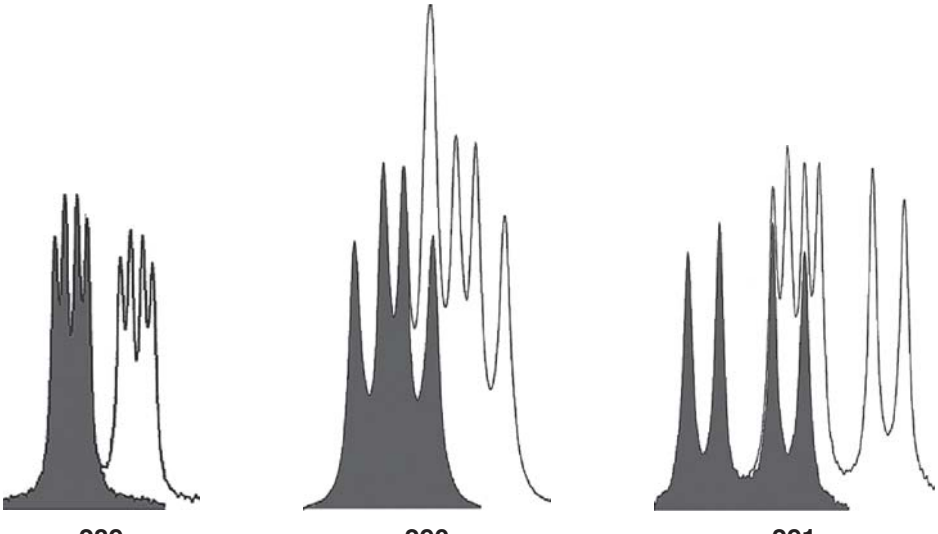

289 **290** **291**

inspection of the middle line (transitions **4**, **5**) will ascertain that it is broader and not really double the intensity of the other six lines. The order of the eight transitions in the seven lines is **1**, **2**, **3**, [4, 5], **6**, **7**, **8** and their intensity ratio is 1 : 1 : 1 : 2 : 1 : 1 : 1.

Finally, there is the possibility that $J_{AX} < (J_{AF} + J_{AM})$ and $J_{AM} > J_{AF}$; see **291**. Now, the eight- transition pattern will show an *inversion in the transition order* of the two middle transitions: **1**, **2**, **3**, ***5***, ***4***, **6**, **7**, **8**, since the second four-line pattern begins before the first gray pattern ends. Once again there will be eight transitions in eight lines of unit intensity.

14
Stereochemistry of Medium Ring Conformations

14.1
A Short Primer on Medium Ring Stereochemistry

As discussed earlier, medium rings (8–12 members) differ from the *common rings* (5–7) in that every saturated ring conformation suffers one or more close contacts between protons pointing into the cycle's interior (i.e., *transannular* interactions). These are removed when substituting a CH_2 with oxygen. The *butano-bridged* epimeric cyclononene derivatives *cis*-**296** *trans*-**297** (Refcodes SUGHUZ and SUGJEL) [124] (I. Ergaz and R. Glaser, unpublished data) have attractive (hydrogen-bonding) transannular interactions on one face and steric (between black-colored protons) interactions on the other. While diastereomer **296** has two possible *cis*-fused ring-invertomer possibilities, only the one with a gray *equatorial* CH_2 ligated to the starred epimeric carbon is stable. The *trans*-fusion in epimer **297** engenders a rigid ring system.

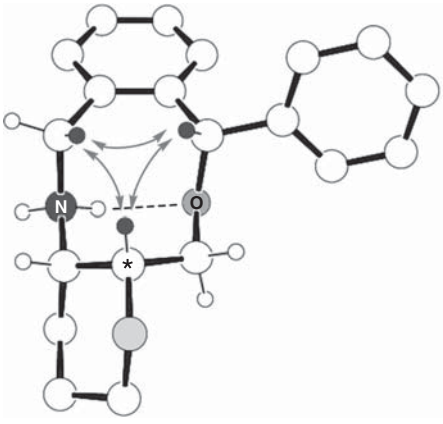

296

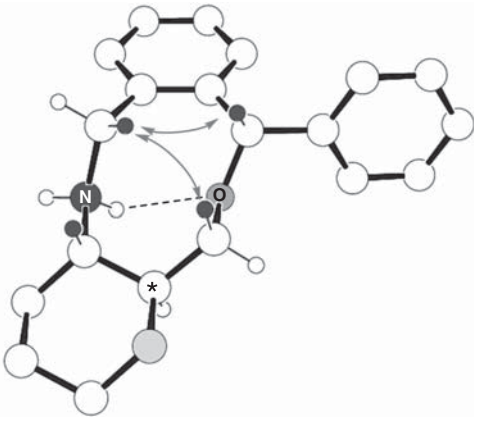

297

Symmetry, Spectroscopy, and Crystallography: The Structural Nexus, First Edition. Robert Glaser.

Companion Website: www.wiley.com/go/Glaser/Symmetry

Saturated medium rings are large enough for *synclinal* torsion angles to become *synperiplanar* angles in the corresponding *cis*-cycloalkenes *while causing minimal change to the other endocyclic angles.* What this means is that disregarding torsion angles on either side of the double bond (and, of course, the double bond itself), the twists of the other six bonds are minimally changed. Medium rings often contain more than one *synclinal* torsion angle, and thus, any of them is a possible candidate to be changed into a *cis* double bond (e.g., the *twist-chair–boat* TCB cyclononane conformation **292** has three adjacent about 60° endocyclic torsion angles). As a result, three different conformational types of TCB cyclononenes are possible (type I, type II, and type III). The *conformational families* of cyclononene and their relationships to those of their saturated parents were discussed by Glaser and coworkers [184]. Due to close similarity of saturated and unsaturated medium ring geometries, the same commonly used saturated ring conformational descriptors can also be assigned to the corresponding unsaturated rings [184].

The olefinic stereochemistry of cyclooctenes (the smallest of medium ring cycloalkenes) is naturally *cis*, since its ring size is incompatible with a *trans*-olefinic geometry (although *trans*-geometry transition states have been proposed). However, cyclononenes and higher medium rings may readily accommodate a *trans* double bond (since greater than 100° endocyclic torsion angles are a common feature in these larger medium rings). As a result, *anticlinal* (120°) torsion angles in cyclononane, and higher homologues, can become *antiperiplanar* angles in the corresponding stable *trans*-cycloalkenes while causing minimal change to the other endocyclic angles. These *trans*-cycloalkenes may also be assigned the same conformational descriptors as their saturated parents (G. Parvari and R. Glaser, unpublished results). The flexibility of medium rings also results in special stereochemical relationships. As opposed to cyclohexane, medium rings are large enough so that *partial ring-version* (i.e., an atom flip to be discussed later) may occur to only a segment of the ring while the remaining endocyclic torsion angles are very minimally changed.

14.2 Assignment of *Equatorial-/Axial*-Substituent Descriptors to Rings of Any Size

We will soon perform a solution-state NMR study of a medium ring compound whose structure has been determined by *X-ray* crystallography. Prior to this we should discuss some basic concepts of medium ring stereochemistry. Medium rings differ from the normal rings (five-, six-, and seven-member rings) in that they all suffer, to one extent or another, from *transannular* interactions (steric or electronic interactions) involving atoms across from each other in the ring. Why is this? Medium ring conformations have protons pointing into the ring's interior. Nine-membered rings with one *synperiplanar* torsion angle constraint (i.e., *cis*-cyclononenes) have 11 conformations and can be divided into seven archetypical

families, some of which have multiple subtype members [184]. Before we assign a solvated conformation based on solution-state ^{1}H NMR vicinal coupling constants, we should discuss Anet's general definition of *axial*, *equatorial*, and related terms for substituents of rings of any size [185].

The Anet [185] method is based only on the *local environment* around the ring atom to which the substituent is ligated. Using either a molecular model or one from *X-ray* crystallography, a midpoint (centroid, ***m***) is drawn between the two γ ring atoms on either side of the $\mathbf{R}^1$ or $\mathbf{R}^2$ substituent (e.g., $-\underline{C}H_2CH_2C\mathbf{R}^1\mathbf{R}^2CH_2\underline{C}H_2-$). The bond lengths C–$R^1$ and C–R^2 are both set to the *same* arbitrary value, for example, 1.1 Å, and the two nonbonded distances $\boldsymbol{m}-\mathbf{R}^1$ and $\boldsymbol{m}-\mathbf{R}^2$ are measured. *A ratio of* $\geq$*1* of the two nonbonded distances is calculated. If the ratio is *equal to integer-1* by symmetry since the two substituents are *homotopic,* then the two ring substituents are *isoclinal.* If the ratio is less than about 1.05 (but not integer-1 by symmetry), then the two substituents are *nearly isoclinal.* If the ratio is >0.05 but <1.1, then an *equatorial* or *axial* determination can only be made in the most general manner. In this general method, an *equatorial* or *almost equatorial* substituent has a longer $m-R^1$ or $m-R^2$ distance, while an *axial* or *almost axial* partner has the shorter distance. If the ratio is about 1.1–1.15, then the prefix *pseudo* should be affixed to the descriptors *equatorial* and *axial.* Finally, if the ratio is >1.2, then *equatorial* and *axial* descriptors can be assigned in the normally accepted manner.

To demonstrate Anet's method, let us start with the Density Functional Theory (B3LYP/6−31 + $G(d)$) model of a C_2-symmetry chiral *twist-chair–boat* (TCB) [184] cyclononane conformation. This is the lowest energy conformation for cyclononane. Inspect the *endo*cyclic torsion angles in **292**, and convince yourself that there is a C_2-axis. How do you know for sure? Answer: The torsion angles on the left-hand side are exactly the same as those on the right. How do you know where the C_2-axis is located? The lowest carbon atom has the same *adjacent* 65.6° angles, so this means that the corresponding bonds are *homotopic* and the axis bisects that atom. Now look at the −79.4° angle on the very top. The torsion angle involving these central C–C atoms is unique, that is, it is the only bond that does not have a homotopic partner, and therefore, the C_2-axis must pass through the bond's midpoint (see **293**). Now that you understand this, what would be the torsion angle sign relationship between pairs of *enantiotopic* bonds? Answer: Corresponding *same magnitude* bonds will have different signs.

Now look at structure **293**. The R^1- and R^2-substituents are both *isoclinal* (equally leaning or inclined) since the $d(m-R^1)/d(m-R^2) = 2.640$ Å/2.640 Å = integer-1, where d = distance. They are obviously *homotopic* symmetry-equivalent protons. Structure **294** is oriented with the C_2-axis directly pointing towards the viewer. Visually it is clear that we cannot differentiate between the two dark gray protons ligated to C(α) and C(δ). Now look at the geminal protons on C(γ), that is, light and intermediate gray. They certainly have different orientations relative to the ring. The intermediate-gray H(γ) points into the ring interior (*endo*) while the

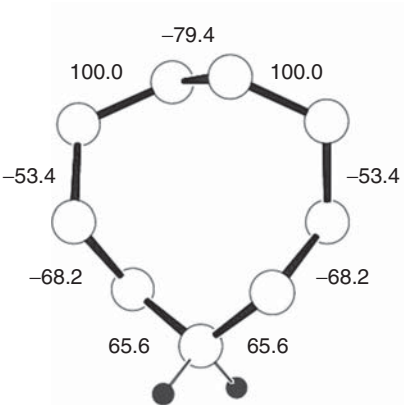

292

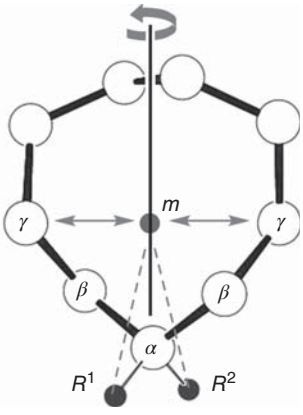

293

lightest-gray proton is *exo.* Notice something else: the intermediate-gray-colored protons on the two adjacent carbons have an *antiperiplanar* relationship, while the lightest-gray proton pair is (+)-*synclinal*. This already gives you a visual clue as to which one is *equatorial* and which is *axial.* Let us look at **295**. Now, $d(m-R^2)/d(m-R^1) = 2.581/1.485 = 1.74$, so R^1 is *equatorial,* while R^2 is *axial.*

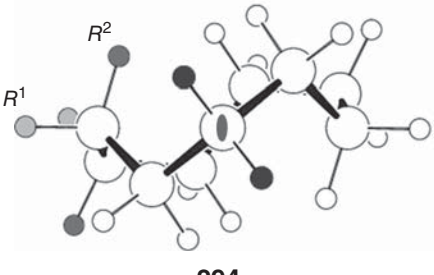

294

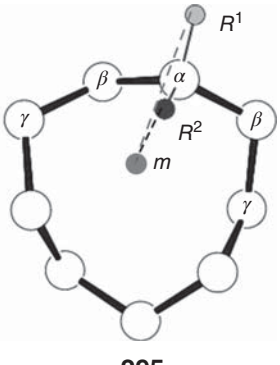

295

14.3
NMR Structure Determination of Medium-Ring Solution-State Conformations

We will illustrate a solution-state NMR structure determination of a *medium ring* (8–12 ring atoms) solvated structure since these cycles often have *more*

than one low-energy conformational possibility. Crystalline *N*-desmethyl-2,6-benzoxazonine·HCl (Refcode SUGJAH [124] (I. Ergaz and R. Glaser, unpublished data)) has a *TCB*(type-III) [184] conformation **298**. The diprotonated nitrogen makes it a partially useful heuristic example since ^{3}J(N***H***-C***H***) couplings (readily observed in CD_2Cl_2 solvent) provide a probe for the stereochemistry of the two attached bonds. The molecule is the nine-membered *N*-desmethyl analogue of the eight-membered nonnarcotic analgesic drug nefopam·HCl. The fact that the structural chemist already knows that a nine-member benzoxazonine is being studied means that he is not starting from zero when performing a solution-state structure determination. The first step is to perform a molecular mechanics *stochastic* (statistical) *conformational search* of the molecule. If there is an X-ray crystal structure, this is always good starting conformation to generate a series of models. A reader may ask "why bother with a solution-state structure determination if an X-ray crystal structure also exists?" Answer: The solvated molecule's environment is different than that in the solid state, and thus, its structure may differ. Thus, it is "good science" to prove that the solvated conformation is either the same or different from that in the crystal lattice.

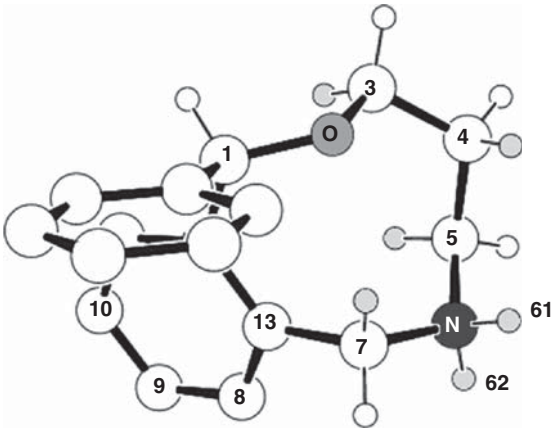

298

An assumption is made that a protocol of NMR experiments has been performed using a multitude of techniques: ^{1}H, $^{13}C\{^{1}H\}$ where $\{^{1}H\}$ means *broadband proton decoupled*, DEPT-90, DEPT-135 (a spectral editing technique to determine the number of protons ligated to each ^{13}C), COSY-90 ($^{1}H-^{1}H$ 2D correlation based upon J_{HH}-couplings), HMQC ($^{13}C_{protonated}-^{1}H$ 2D correlation based on direct $^{1}J_{CH}$-couplings), HMBC ($^{13}C_{quaternary}-^{1}H$ 2D correlation based upon vicinal $^{3}J_{CH}$-couplings), NOESY, and a series of homonuclear decoupling (HD) experiments for each proton. From this data set, the assignment of all ^{13}C

signals, ^{1}H multiplets, and *J*-couplings can unequivocally be made. In addition, it should be ascertained that the ^{3}*Jax-ax* and ^{3}*Jeq-eq* values have the expected about 11 and 2–3 Hz magnitudes characteristic of *antiperiplanar* and *synclinal* vicinal protons *at slow exchange*. In other words, we are looking to determine the predominant preferred conformation and not some unreal fast conformational equilibrium time-averaged structure which does not exist in reality. While the hybrid of a horse and a donkey is a mule, the appearance of a time-average metaphorical 'mule' structure is an experimental artifact which depends on the 'shutter speed', so to say, of the experiment. In other words, there is no 'mule' present in the equilibrium, only the metaphorical 'horse' and 'donkey'.

This structure determination is easier than it appears, since the presence of a double bond in our calculated models enables us to assign the same atom label descriptors to the nuclei as used for the crystalline-state 2,6-benzoxazonine compound **298**. If we were studying cyclononane, then it would not be obvious where to begin our numbering. The C(3)/C(7) carbon termini of the segment O(2)–***C***(***3***)–C(4)–C(5)–N(6)–***C***(***7***) are readily starting positions since the carbon and proton nuclei at these positions have chemical shifts characteristic of the electronegativities of their attached neighbors. The H(3), H(3′), H(7), and H(7′) protons each exhibit only two $^{3}J_{HH}$ couplings involving vicinal partners on only one side (as opposed to couplings with neighbors on both sides of each proton in the segment's interior).

From the data set, one finds that H(3*ax*) and H(7*ax*) have one *antiperiplanar* relationship to a vicinal neighbor and one large magnitude (−12 to −15 Hz) relationship to a geminal partner, while H(4*ax*) and H(5*ax*) each have two *antiperiplanar* relationships to their vicinal neighbors and one large magnitude coupling to their geminal counterparts. Finally, one of the N(6) geminal protons has an *antiperiplanar* relationship to its H(5*ax*) neighbor, while the other has an *antiperiplanar* relationship to its H(7*ax*) partner. Therefore, the N(6) protons are *isoclinal* and are assigned as 61 (*cis* to phenyl) and 62 (*trans* to phenyl) rather than *axial* or *equatorial* descriptors. These *axial* assignments (based upon the antiperiplanar coupling constants) are enough for us to examine our collection of calculated cyclononene structural models and eliminate all but one (or maximum two) conformational candidates. If there are two possibilities, these can usually be differentiated via a set of ***N***uclear ***O***verhauser ***E***ffect (NOE) experiments to determine spatially close *through-space* neighbors. From experience with medium ring stereochemistry, the intensity enhancements to particular multiplets will uniquely fit only one hypothetical cyclononene model. The *TCB* (Type III) [184] calculated cyclononene model nicely fits all the large magnitude *antiperiplanar* vicinal relationships suggested by the ^{3}J-couplings in Table 14.1 [124] (I. Ergaz and R. Glaser, unpublished data).

The next step is a more sophisticated double-check by Density Functional Theory (DFT) B3LYP/6−311 + *g*(2*d*,*p*) calculation of a geometry optimized model of *N*-desmethyl 2,6-homonefopam cation in the *TCB*(type III) conformation

and a vibrational frequency calculation to ascertain that all the frequencies are positive (i.e., an important check that the model is at the bottom of the potential energy well and not a nonsensical local minimum). Using the geometry optimized input coordinates, a second DFT B3LYP/6−311 + $g(2d,p)$ calculation affords calculated *total spin−spin* J_{HH} couplings. These should nicely agree with our experimental values, although the calculated chemical shift values usually leave a lot to be desired. Table 14.1 lists the J_{exptl} and J_{calcd} values for the C(3)–C(4)–C(5)–N(6)–C(7) covalent bond segment [124] (I. Ergaz and R. Glaser, unpublished data).

The agreement between the J_{exptl} and the J_{calcd} values from a *bona fide TCB* (type III) conformation calculated model is excellent, confirming that in this particular case, the solid- and CD_2Cl_2 solution-state conformations are indeed the same. However, since the two environments are not symmetry equivalent, we should determine the six *endocyclic dihedral angles* (θ) that characterize the solution-state structure by using Lambert's dihedral angle relationship arccos

Table 14.1 J_{exptl} and J_{calcd} for the CD_2Cl_2 solution-state *twist-chair–boat* (type III) conformation of the *N*-desmethyl 2,6-benzoxazonine analogue of homonefopam; estimated standard deviation (esd) of the values is 0.2 Hz [124] (I. Ergaz and R. Glaser, unpublished data). J_{calcd} comes from a DFT B3LYP/6-311 +g(2d,p) NMR=spin-spin calculation.

H–H	J_{exptl} (Hz)	J_{calcd} (Hz)
H(3*ax*–3*eq*)	−11.6	−11.4
(3*ax*–4*ax*)	10.1	10.8
(3*ax*–4*eq*)	2.0	2.1
(3*eq*–4*ax*)	3.0	3.8
(3*eq*–4*eq*)	4.5	2.1
(4*ax*–4*eq*)	−16.4	−16.3
(4*ax*–5*ax*)	10.0	10.5
(4*ax*–5*eq*)	2.1	1.2
(4*eq*–5*ax*)	<1	0.7
(4*eq*–5*eq*)	6	6.3
(5*ax*–5*eq*)	−12.8	−13.8
(5*ax*–61)	9.2	10.2
(5*ax*–62)	<1	0.7
(5*eq*–61)	2	0.8
(5*eq*–62)	6	5.6
(61–7*ax*)	5.0	6.0
(61–7*eq*)	1.2	0.3
(62–7*ax*)	8.7	7.1
(62–7*eq*)	5.6	6.6
(7*ax*–7*eq*)	−12.9	−11.8

$\theta = [3/(4R+2)]^{1/2}$, where $R = [^3J(5ax6ax) + {}^3J(5eq6eq)]/[^3J(5ax6eq) + {}^3J(5eq6ax)]$ [186]. Since the estimated standard deviation (esd) of the $\boldsymbol{J}_{\text{exptl}}$ values is 0.2 Hz, we will also calculate the esd of the $\theta_{\boldsymbol{J}\text{exptl}}$ solution-state values. This is done by calculating $R_{\max}$ to afford $\theta_{\boldsymbol{J}\text{exptl}}$max via addition of the 2×0.2 Hz esd to the numerator's ^3J value sum and subtraction of the 2×0.2 Hz esd values from the denominator's ^3J value sum. Similarly, one can calculate $R_{\min}$ to give $\theta_{\boldsymbol{J}\text{exptl}}$min (subtraction of the esd from the numerator's ^3J value sum, and addition of the esd values to the denominator's ^3J value sum). Table 14.2 provides a comparison of the $\theta_{\boldsymbol{J}\text{exptl}}$ solution-state, $\theta_{\text{X-ray}}$ *X-ray* crystallographic solid-state, $\theta_{\boldsymbol{J}\text{calcd}}$, and $\theta_{\boldsymbol{DFT}}$ values [124] (I. Ergaz and R. Glaser, unpublished data).

Therefore, despite different environmental conditions of the measurements, the NMR determined set of four adjacent solution-state $\theta_{\boldsymbol{J}\text{exptl}}$ dihedral angles is completely consistent with the $\theta_{\boldsymbol{X\text{-}ray}}$ values in the *TCB* (type III) conformational model of crystalline *N*-desmethyl 2,6-benzoxazonine as well as with those in the DFT calculated model. Are the $\theta_{\boldsymbol{X\text{-}ray}}$ values superior to $\theta_{\boldsymbol{J}\text{exptl}}$? No, since the molecule's surroundings differ from one model to another. One describes a solvated molecule, another is based upon a molecule resident within a crystal lattice, while the DFT calculations consider a nonvibrating isolated molecule at the bottom of a potential energy well. In summary, consider the power of Lambert's method. It enables us to ascertain conformationally characteristic dihedral angles *in solvated molecules!* Furthermore, NOE-difference experiments to probe *close-by through-space* nuclei also help to prove the structural hypothesis.

As we already asked, if we already know the *X-ray* determined crystal structure, then why bother to determine the solution-state conformation? Answer: There are many instances of conformational change when crystals are dissolved in solvents of one dielectric constant or another. For example, the *twist-boat–chair* (TBC) conformation was observed by *X-ray* crystallography for 2,6-benzoxazonine-di(*N*-methyl)·Iodide **299** or chloride·dihydrate quaternary ammonium salts

Table 14.2 Comparison of $\theta_{\boldsymbol{J}\text{exptl}}$ solution-state, $\theta_{\boldsymbol{X\text{-}ray}}$*X-ray* crystallographic solid-state, $\theta_{\boldsymbol{J}\text{DFTcalcd}}$, and $\theta_{\boldsymbol{DFT}}$ *dihedral angles* calculated for the *twist-chair–boat* (type III) conformation of *N*-desmethyl 2,6-benzoxazonine within different environments [124] (I. Ergaz and R. Glaser, unpublished data).

Dihedral angle, θ (°)	$\theta_{\boldsymbol{J}\text{exptl}}$	$\theta_{\boldsymbol{J}\text{DFTcalcd}}$	$\theta_{\boldsymbol{X\text{-}ray}}$	$\theta_{\boldsymbol{DFT}}$
O(2)–C(3)–C(4)–C(5)	62(2)	58	75	67
C(3)–C(4)–C(5)–N(6)	69(2)	74	88	81
C(4)–C(5)–N(6)–C(7)	69(2)	75	73	80
C(5)–N(6)–C(7)–C(13)	42(2)	34	42	32

analogues (Refcodes SUGHIN and SUGHEJ) [124] (I. Ergaz and R. Glaser, unpublished data). On the other hand, NMR structure determination of the two *solvated* molecules clearly shows both to exist in the same TCB-III conformation as that observed for solvated *N*-methyl tertiary ammonium hemitartrate salt (Refcode YIPSEV [187]) and the *N*-desmethyl secondary ammonium salt (**298**) discussed earlier. The 132° value for gray torsion C(1)–O–C(3)–C(4) angle in the TCB-III DFT model of solvated-**300** dramatically closes to 65° in crystalline-**299** and results in solid-state CP/MAS NMR showing a *very large* 11.4 ppm closer-to-TMS *γ-gauche effect* for benzhydrylic C(1) compared to that value in the solution-state spectrum. Further verification of the new solvated TCB-III structure comes from NOE intensity enhancements shown in **300**. Bottom line: dissolution of TBC **299** crystals enables them to undergo interconversion into a solvated TCB-III conformation via a series of consecutive (and nonconcerted) flips and twists [124] (I. Ergaz and R. Glaser, unpublished data). The reasons for this remain to be proved. Both conformations are low energy structures since this is what Nature prefers. Since the TCB-III of the quaternary ammonium salt is unequivocally found in solution, it thus appears that it is more efficiently solvated than the TBC conformation.

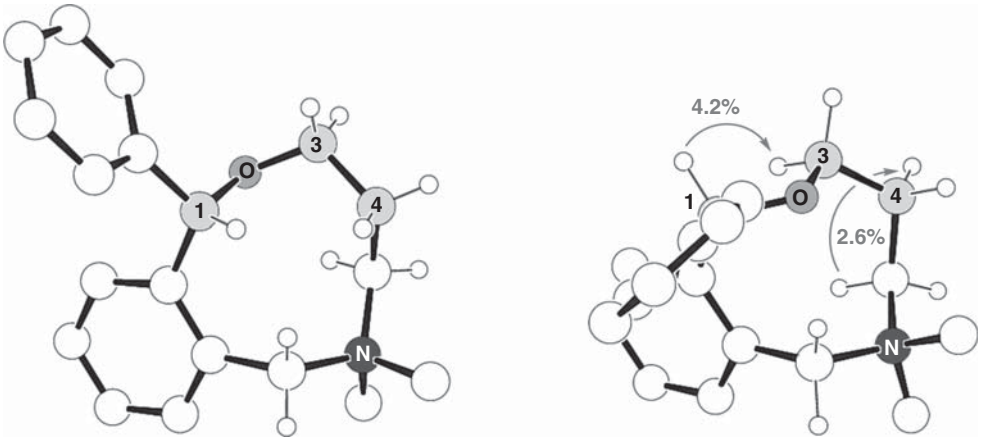

299 **300**

14.4
Dynamic Disorder in Crystals

We have already discussed *static disorder* in crystals. The partial occupancy of the additional water molecule in scopolamine·hydrochloride·1.67H_2O (**278**) was an example of this type of disorder. In this particular case, the void space was both large enough and nonspecific enough to enable a third water molecule to reside

at an additional site on the same twofold rotational symmetry special position as the more strongly bound hemihydrate water beneath it. Space filling at this extra site in the special position was stochastic (statistically random) since the total water content may vary from one data crystal to another. These partial occupancy crystals are usually *kinetic crystals* and suffer from lack of long-term stability since the third water molecule is very weakly held in this particular case.

We now consider a $P2_1/c$ space group crystal whose one asymmetric unit contains only one eight-membered ring molecule, but a segment of that ring structure continually undergoes a rapid atom flip (half ring-inversion) in the solid state. In this particular case to be discussed, methohalide quaternary ammonium salts of the nonnarcotic analgesic drug nefopam undergo a medium-ring *atom-flip* dynamic interconversion from a more compact *boat–boat* (BB, **300**) conformation to a slightly more extended *twist-chair–chair* (TCC, **301**) arrangement. This is a common conformational interconversion mechanism for medium rings.

It will be shown that intermolecular distances between two close adjacent 2_1-screw rotation-related rings are modulated by the volume of the Cl^- or Br^- or I^- spherical counter anions laterally pushing their two cationic neighbors apart. Therefore, since the BB/TCC conformations are close in energy, the occupancy factor of the *more extended* conformer is augmented as the halide anion's van der Waals radii increase from 1.80(5) Å [Cl^-], to 1.91(4) Å [Br^-] and then to 2.07(5) Å [I^-]. This lattice expansion is also observed as a function of increasing measurement temperature. In other words, the occupancy factors of two approximately equal energy interconverting diastereomeric conformations are lattice *void size dependent.*

In the case of primary, secondary, and tertiary ammonium ions, hydrogen bonds (e.g., $N^+–H–Cl^-$) *immobilize the N⁺–H bond's tropicity* since the N***H*** proton is disposed toward the anion. Interconversion of *axial, equatorial* $N^+–H$ bond orientations (commensurate with the atom-flip mechanism) cannot occur for *N*-protonated ammonium cations since the counter anion resides at a particular lattice location. Obviously, this directional constraint is absent in crystalline *gem-N,N*-dimethyl quaternary ammonium salts. Under the appropriate packing conditions, the resulting positional freedom enables the *N*-methyl and proton substituents two bonds away from the flipping atom to interchange their *axial*, *equatorial* orientations concomitant with the *conrotatory* twisting of methylene C(4) about its adjacent lateral C(3)–***C***(4) and ***C***(4)–$^+$N(5) bonds (compare the synchronous movements in **301** and **302**). The *axial*, *equatorial* dispositions of the flipping atom are also inverted. Notice that the H*ax*–H*ax* proton pair in **301** becomes a H*eq*–H*eq* pair in **302**. Should we be surprised? No, this is exactly what happens in cyclohexane ring-inversion, and medium ring atom flips are half ring-inversions. Atom flipping is a conformational change that occurs to ring segments of two *adjacent* oppositely signed *synclinal* torsion angles. A characteristic of medium ring atom flips is that adjacent (−)· · ·(+)-*synclinal* torsion angles are both inverted to (+)· · ·(−), while all other endocyclic torsion angles remain the

same. Should we be surprised? No, this is exactly what happens in cyclohexane ring-inversion, and medium-ring atom flips are simply half ring-inversions.

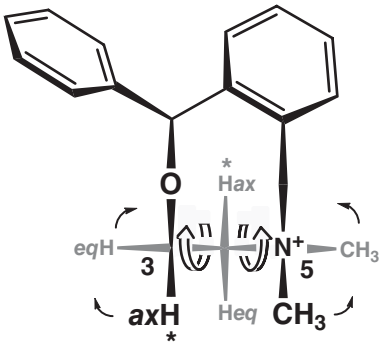

301

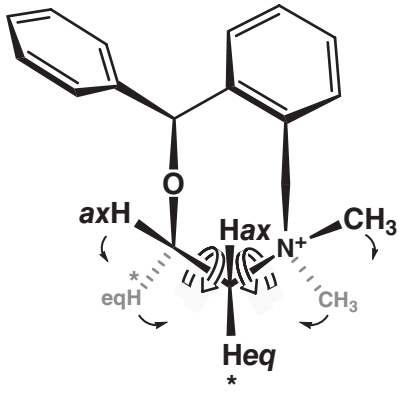

302

Fortuitously, nefopam methohalides, despite the different halide anions (Cl^-, Br^-, and I^-), all crystallized in the same $P2_1/c$ monoclinic system space group and with the same isostructural packing motif. While this observation is not uncommon, nevertheless it is not a given that it will occur once the anion is changed. When the anion is too large (e.g. tetrafluoroborate) the nefopam quaternary ammonium salt can crystallize in a new space group. Figure 14.1 illustrates 2_1 screw rotation-related nefopam methohalide quaternary ammonium ions separated by halide ions in crystal structures measured at 193 K. (a) Methiodide, (b) methobromide, and (c) methochloride. The halide's increasing van der Waals spherical volume laterally pushes 2_1-screw related adjacent cations further apart, whereby the $N^+ - N^+$ distance increases from 6.54 Å [Cl] to 6.87 Å [Br] and then to 7.35 Å [I]. These increasing $N^+ - N^+$ distances can be correlated with increasing TCC occupancy factors measured at 193 K: 0.000 [Cl^-], 0.039(5) [Br^-], and 0.343(5) [I^-], where the TCC occupancy factor is the mole fraction of electron density for that conformation in the lattice. From this it is apparent that the 6.54 Å $N^+ - N^+$ distance between the methochloride cations is just *too short* to accommodate the slightly more extended TCC conformation. The *dynamic nature* of this conformational disorder is readily apparent from the correlation of increasing TCC occupancy factors with elevated measurement temperatures *of the same data crystal:* 0.039(5) [193 K, Br^-], 0.220(5) [293 K, Br^-], 0.245(6) [343 K, Br^-], 0.343(5) [193 K, I^-], and 0.408(7) [293 K, I^-]. Clearly a dynamic process is occurring since a static disordered crystal's occupancy factors are temperature-invariant. It is important to stress that the same data crystal be used for the variable temperature measurements to show that the disorder is dynamic. Why? Since *static* conformationally disordered crystals are formed

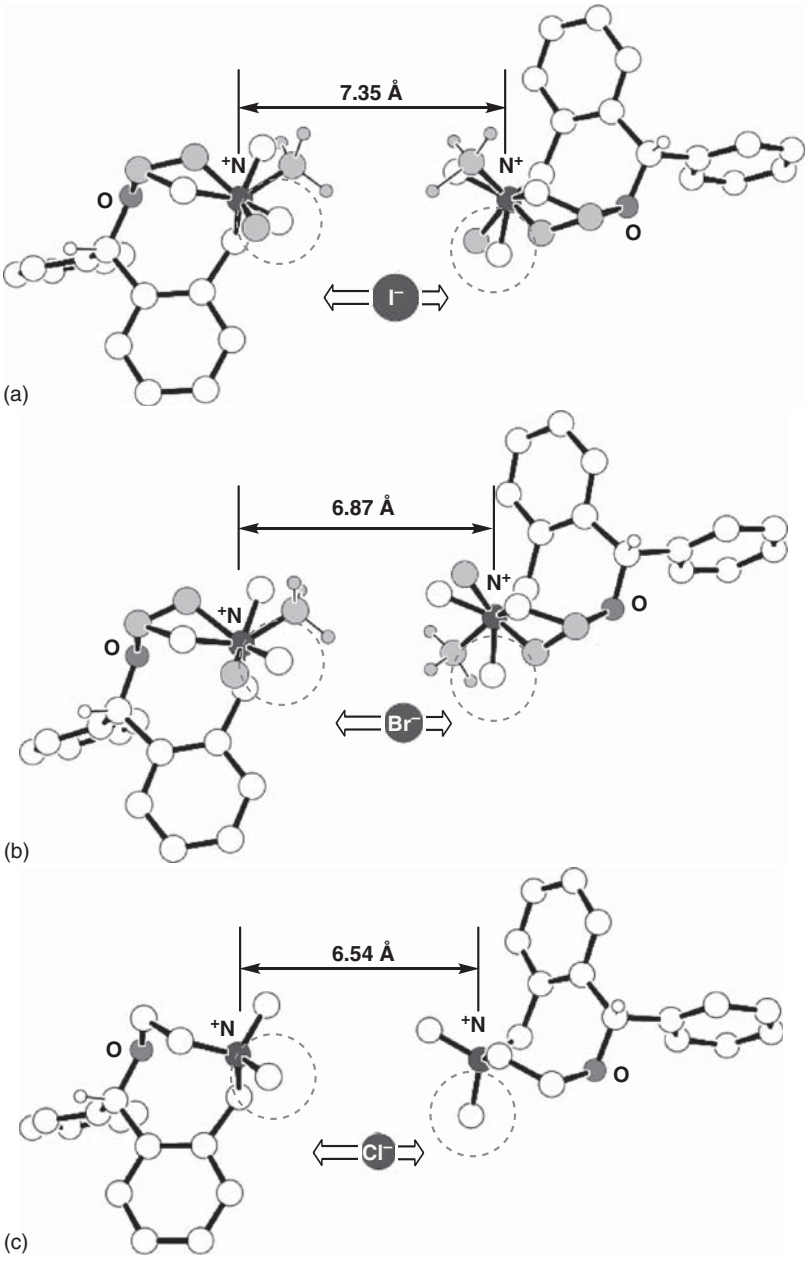

Figure 14.1 2_1 Screw rotation-related nefopam methohalide quaternary ammonium ions separated by halide ions in crystal structures measured at 193 K. (a) methiodide, (b) methobromide, and (c) methochloride.

as the result of kinetic growth processes, their occupancy factors could vary from crystal to crystal. One wants to negate the possibility that what looks like temperature dependence is actually the result of different kinetic crystals used for each temperature measurement.

It was hoped that an even larger counter-anion (e.g., BF_4^-) might spread the adjacent N^+-atoms even further apart than for the case of the methiodide crystal. However, the likelihood of this happening is low since Nature avoids large voids in a lattice. Not surprisingly then, the molecule crystallized in a completely different packing motif in the C*c* monoclinic system space group with three *boat*–*boat* conformation molecules in the **303** asymmetric unit (rather than have a larger void in a $P2_1/c$ lattice). Based upon our prior observation that greater than 6.54 Å

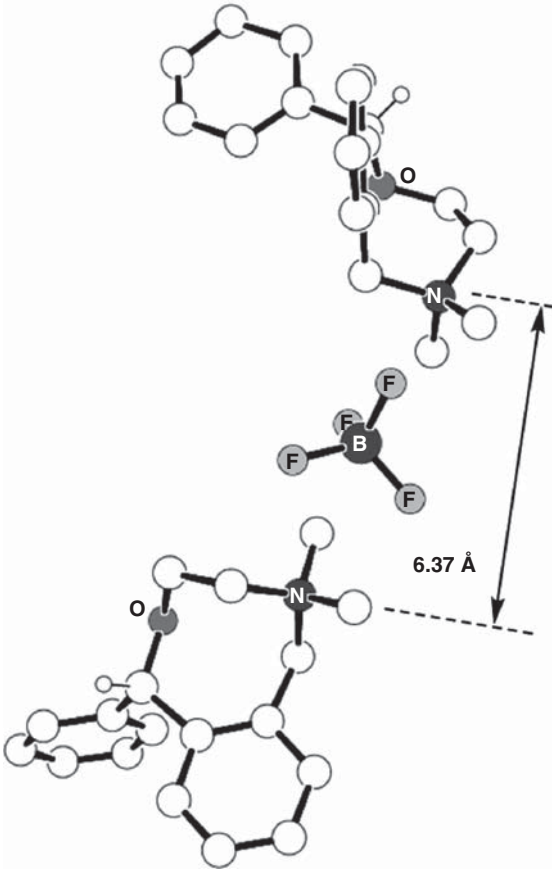

303

$N^+ - N^+$ distances are required for the *TCC* more extended conformation in the series of methohalide isostructural crystals, **303**'s corresponding 6.37 Å $N^+ \cdots N^+$ lateral distance is completely consistent with the sole appearance of the compact *boat–boat* conformation (see **303)**.

Plot **304**-bottom shows the aliphatic region of the solid-state CPMAS ^{13}C NMR spectrum of the nefopam *methochloride* immobile BB-conformation measured at 298 K. T_1 relaxation time constant values have been affixed to the peaks. Peak assignments in $^{13}C\{^1H\}$ *liquid-state* NMR spectra are usually trivial endeavors with the help of data from DEPT-135/90 and HMQC/HMBC 2D correlation pulse sequences. Fortunately, there exist some solid-state NMR variants of these useful spectral editing experiments. The previously mentioned "methylene carbon only" *spectral edited* CPPI [176] pulse program provides inverted phases for δ 67.52, 66.50, and 58.51 signals; see plot **304**-top (left). The artificially inverted spectral editing NQS (***N***on-***Q***uaternary and nonmethyl ***S***uppression) partial spectrum in plot **304**-top (right) shows peaks from nonefficiently dipolar-relaxed ^{13}C *methyl* and quaternary nuclei.

Therefore, the methyl, methylene, and methine proton-multiplicity of the carbons can readily be assigned in CP/MAS plot **304** on the basis of the aforementioned solid-state NMR spectral editing techniques. However, while the δ 58.51 chemical shift value is obviously consistent with the electronegativity of a $^{13}\underline{C}H_2N$ nucleus, one cannot unequivocally assign the close δ 67.52 and 66.50 peaks without recourse to additional experiment.

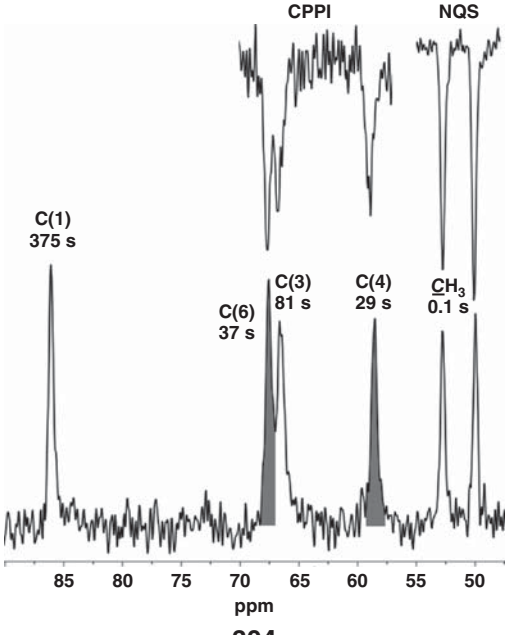

304

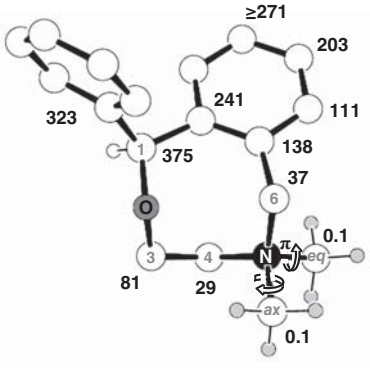

305

Fortunately, this is possible by performing spin-lattice relaxation time constant (T_1) measurement for each nucleus. Remember that T_1 is kinetic time constant number 1, and it measures the rebuilding rate of the Boltzmann distribution between the α- and β-spin state populations. We also discussed the fact that

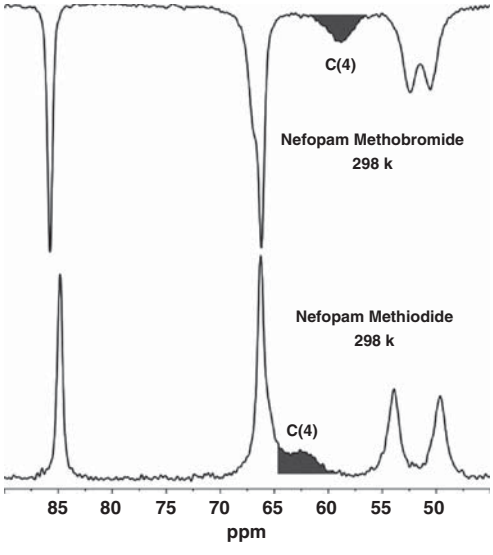

306

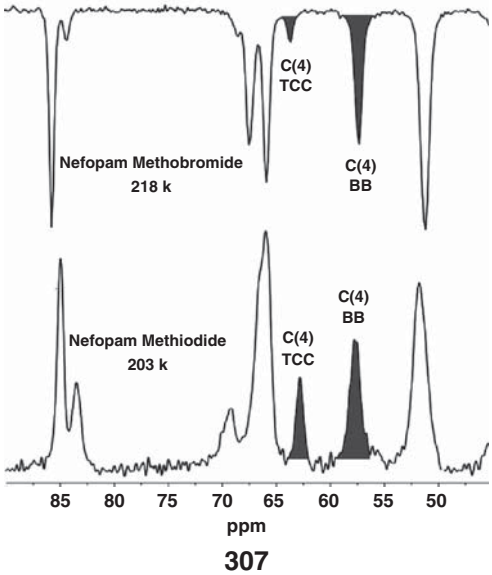

307

T_1 time constants are *notoriously long* in solid-state NMR due to ^{13}C's obvious inability to undergo thermal motion at their Larmor precession frequencies when resident within a crystal lattice (compared to facile Brownian motion at these frequencies in solution). On the other hand, methyl protons are not constrained by near neighbors in the lattice during their very rapid staccato-like 120° flips about the C–CH_3 bonds as they transit from one staggered conformation to another. These rotating protons generate *fluctuating local magnetic fields*, which relax nearby ^{13}C neighbors. The closer a ^{13}C-nucleus is from the spinning protons of the two geminal methyl groups, the shorter is its T_1 value. It is, therefore, no surprise that the carbons closest to the spinning protons are the very $^{13}C_{methyl}$ nuclei themselves. Their low about 0.1 s T_1 values are very characteristic of solid-state methyl carbons (see **305)**. The vicinal C(4) [δ 58.51] and C(6) [δ 67.52] carbons are the next closest to the spinning methyl protons (T_1 29 and 37 s, respectively). The 81 and 375 s T_1 values for the more distant methylene-C(3) [δ 66.50] and very remote methine-C(1) [δ 86.02] now enable an *unequivocal assignment for the two close peaks* (as well as for some of the benzo-carbons).

These assignments may now be utilized to interpret the following variable temperature CP/MAS spectra of crystalline nefopam methobromide and methiodide quaternary ammonium salts as further evidence for the crystallographically observed C(4) atom-flip BB/TCC dynamic conformational interconversion. Plot **306** depicts the nefopam methobromide (upper) and methiodide (lower) CP/MAS ^{13}C aliphatic region spectra recorded at 298 K. It is clear from the broadened the BB/TCC C(4) signals that the measurement temperature is within the *fast magnetic site exchange broadening* region. Lowering the temperature has resulted in *slow magnetic site exchange broadened* C(4) MeBr signals (BB:TCC about 5 : 1, 218 K) and MeI resolved signals (BB:TCC about 1.5 : 1, 203 K); see plot **307**. Spectra were recorded by the author at the Max Planck Institute for Polymer Chemistry, Mainz, Germany (R. Glaser, H.W. Speis, and G. Brunklaus, unpublished results).

15
The Pharmacophore Method for Computer Assisted Drug Design

15.1
The Pharmacophore, Neurotransmitters and Synapse

This section discusses two ***C***omputer-***A***ssisted ***M***olecular ***M***odeling (CAMM) techniques commonly used in the pharmaceutical industry for rational drug design. One is the *pharmacophore* method and the second is *crystal structure–based molecular design.* We discuss the first method now and the second one in a later chapter. Similar to the terms "chromophore," "fluorophore," and so on, a *pharmacophore* comprises those portions of the *active pharmaceutical ingredient* (API) responsible for its bioactivity. In other words, the pharmacophore is a specific *3D arrangement* of chemical groups common to active molecules and essential for their specific biological activity. An API's internal skeleton is usually *not exposed* to a receptor's interacting functional groups, and hence, the scaffold's prime function is to preposition the drug's *essential peripheral parts* for efficient interaction with the biological host. In this manner, *reuptake* sites (**308**), *receptors,* or enzyme *active sites* react to the drug's periphery and functionalities as if they were those of the natural (i.e., *endogenous,* "internally produced" within the body) *agonist* or substrate. One can conclude that a radical change of skeleton may be made, and if the important peripheral functionalities (e.g., ammonium ion, aromatic ring, carbonyl, carboxyl, keto, hydroxyl, etc.) still remain in their *bioactive conformation,* then there is a very high probability that the new compound will also be bioactive. Yet, since it exhibits a novel skeleton, patent authorities consider the new molecule to be *innovative* (i.e., a patentable invention).

To understand a neurotransmitter's elementary biochemistry, let us begin with an electric pulse traveling from right to left through neuron 1 (see schematic diagram **308**). It reaches the *transporter* site at the *presynaptic membrane* from which the neurotransmitter is released into the synapse. Many (but certainly not all) neurotransmitters are decarboxylated amino acids bearing hydroxylated aromatic rings. Neurotransmitters (the *endogenous agonists*) binding to the

Symmetry, Spectroscopy, and Crystallography: The Structural Nexus, First Edition. Robert Glaser.

Companion Website: www.wiley.com/go/Glaser/Symmetry

postsynaptic membrane receptors induce a conformational change from the *silent-* to the *active-state.* For example, this conformational change may open or close an "ion gate" in neuron 2 that generates a new pulse of electric charge. In addition, a quantity of neurotransmitter is reabsorbed back into *reuptake sites* on the presynaptic membrane. These two absorption phenomena establish Nature's desirable *steady-state* neurotransmitter equilibrium concentration within the synapse (see **308)**. The result is the appropriate level of neural kinetics required for our body's health and well-being.

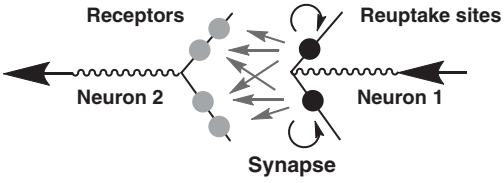

308

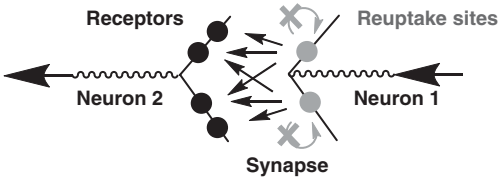

309

Due to disease, many neurological conditions cause either a *deficit* or a *surplus* of a particular neurotransmitter within the synapse. Patients suffering a neurotransmitter deficit will benefit from a *selective reuptake inhibitor* (SRI), since the blocked reuptake site causes a net increase in the neurotransmitter's synaptic concentration (see **309)**. Patients afflicted by an overproduction of a neurotransmitter will be aided by administration of a nonendogenous *antagonist*, for example, atropine (at the acetylcholine receptor) or naloxone (at an opiate receptor). Antagonists exhibit binding affinity to the receptor site but inhibit the receptor from flipping into its active conformation. This may arise from steric factors or improper charge distributions that differ from that of the agonist. The geometrical and chemical requisites for auspicious binding affinity at each site differ. Since neurotransmitters exist in multiple conformations, one low-energy conformer has been bioengineered to fit the receptor site while another one complements the reuptake site. Understanding the pharmacophore for each site enables the pharmaceutical industry to produce nonendogenous agonists,

antagonists, and reuptake blocker drugs, to treat an overproduction or deficit of a neurotransmitter.

15.2 The Pharmacophore Method for Computer Assisted Drug Design

The quest for the pharmacophore begins with five or more drugs known to exhibit high binding affinities and nanomolar concentration therapeutic activities at the *same biological site.* The more the skeletal diversity, the better it is for the molecular design process. A great deal will not be learned if the structures are too similar. One of the strengths of the pharmacophore method is that information about the site and mechanism of action is quite often completely unknown. The underlying premise is that drugs interacting at the *same site* must all be emulating a common *endogenous* agonist in terms of their peripheral geometries and functional groups required for site binding. The hypothesis that the drugs all interact at the same site is very important prerequisite in pharmacophore discovery. If this premise is untrue, then a quality answer will not be obtained, and the entire process will have to be repeated.

There are usually a number of structural requisites composing a pharmacophore. This is mentioned since a particular drug within the "learning set" need not mimic all of the biologically important pharmacophoric structural features. Some drugs may mimic different regions and others may mimic them all. This is why it is best that the set includes structurally and functionally diverse drugs when beginning the quest. These drugs either are in use (i.e., known pharmacotherapeutic agents for other diseases) or are selected from a library of proprietary and commercially purchased test compounds via screening methods for a particular medical condition. If the drugs in the study are rigid, then the task becomes relatively easy since it is now only up to the modeler to decide how to superimpose them (sometimes not a trivial choice).

The problem becomes challenging when the drugs are flexible. In this case, a computer-driven *conformational search* is performed to generate a set of *energy accessible* conformers of each drug. One has to always bear in mind that the lowest energy conformer (called the *global minimum* energy structure) is often not the *bioactive conformer*. Why is this so? The global minimum structure is usually "*in-silica*" (meaning resident within the computer's silicon chip, that is, at the bottom of the potential energy well and in the absence of neighbors). But the residence conditions for the bioactive conformation in the body are different. The guest's interactions with the host often offset the slightly higher energy (e.g., usually within a window of ≤ 3 kcal from the global minimum) required for correct juxtaposition between the guest and host. In this case, the binding energy that is released "pays the price" of molding the guest into a somewhat higher energy form.

On the other hand, there is a limit to just how high a price Nature is willing to pay for good space filling and interactions. As the molecule approaches the active site, long-range dipolar or electrostatic charge interaction forces will begin to shape the molecule into the required *bioactive conformation*. Concurrently, as the guest approaches the host, the host in turn will make some minor structural adjustments to better receive its guest. This is the *induced fit* concept of gentle structural perturbation between a *lock* and its *key.* As was said, it is the intermolecular interaction energy that pays for these perturbations. When the higher-energy guest complexes with the host, it is replenished in solution at the expense of the global minimum conformer (if the solution-state conformational equilibrium is rapid) until all the host's sites are populated. Once the pharmacophore is known, design of a rigid conformational analogue permanently in the bioactive conformation (i.e., a *rigid conformational analogue*) will markedly improve the drug candidate's potency.

Now that we have added the terms *bioactive conformation* and *global minimum* to our vocabulary, a word about the main thrust of this book should be said. The point to be stressed is that the solution-state NMR determined preferred conformations, the solid-state conformations (as found in *conformationally polymorphic* crystals), the bioactive conformations at a receptor or at a reuptake site, and the global minimum computed conformation are all influenced by the molecule's surrounding neighbors. So, one often does not know what to expect when predicting the conformation in a new environment based upon our prior knowledge of a known conformation within a different *milieu* (environment, setting, background, etc.).

Having said this, let us return to the pharmacophore quest and assume that the conformational search has generated (within a window of about 4–5 kcal mol^{-1} above the global minimum) a file of 45 reasonable (i.e., energy accessible, not super-strained) conformers of drug A, 61 for drug B, 83 for drug C, 29 for drug D, and 54 for drug E. This means that within each of these five files there exists *one common pharmacophoric bioactive arrangement*. In other words, each set will contain one conformer where all or part of the pharmacophoric functionalities are spatially the same in all five "learning set" drug candidates. How do we know this to be true? Well, the drugs were specifically chosen as they have high nanomolar activity at the same host site. This means that when these drugs are administered to the patient, the host site "assumes" that it is feeling the presence of its natural agonist. Algorithms exist to compare individual structures in one file with each and every structure in all the other files by artificial intelligence *superimposition* techniques. These are utilized to ascertain a common single bioactive conformation within each of the sets. When these programs are run, a centroid is located in the aromatic rings (if there are any), and this is used in the superimposition. If there are N*H* protons present (potential hydrogen-bonding donors), then a dummy acceptor atom is

calculated in a straight line from the N–H bond and 1.8 Å away from the N*H* proton.

15.3 Determination of the Dopamine Reuptake Site Pharmacophore

The determination of a first generation dopamine (DA) reuptake site pharmacophore will be illustrated in this section. (*R*)-(−)-Apomorphine (**310**, Refcode FIKFIP) [188] and an *N*-methyl ergoline alkaloid skeletal nucleus (**311**, as in ergotamine Refcode HICCUR) [189] are two known DA reuptake site inhibitors (i.e., in other words, they increase the DA agonistic activity at the receptor). The ergoline nucleus is the same rigid skeleton as found in the psychedelic drug, lysergic acid diethylamide (LSD). These rigid molecules provide an easy entry for elucidation of a DA reuptake inhibition first-generation pharmacophore. Superimposition of the nitrogen atoms, *N*-methyl groups, and the aromatic ring *centroids* in apomorphine **310** and *N*-methyl ergoline **327** provide a simple pharmacophore (starred atoms in **312**) for DA reuptake site inhibition. All nonstarred atoms on the right-hand side of the molecules represent putative (assumed) nonpharmacologically significant skeletal regions with spatial freedom and can be altered. Note: the *empty space* to the left of each molecule in superimposition **312** is considered to be a possible *steric barrier* in the host.

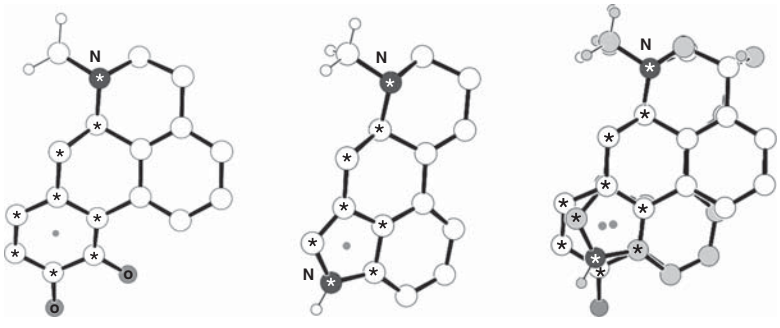

310 **311** **312**

The DA reuptake inhibitor pharmacophore hypothesis can be further elaborated and refined as new information is acquired, and new highly active drug molecules are incorporated into the structural hypothesis. In addition to the 5.0(2) Å $d(N^+\cdots Ar_{centroid})$ and 0.7(3) Å $d(N^+\cdots Ar_{mean\text{-}plane})$ distances, important structural features of this initial pharmacophore also include the 12(7)°

C(*ipso*)–$Ar_{centroid}$–N^+ angle and ±176.6(7)° N^+–C(α)–C(β)–$Ar_{centroid}$ torsion angle (see **313**). An ammonium proton in both **310** and **311** suggests the existence of a putative acceptor site *x* that may have hydrogen-bonding importance. Site *x* is defined by three measurements: 2.8 Å *d*(N^+–*x*), 98(4)° $Ar_{centroid}$–N^+–*x* angle and 50(12)° x^+–N^+–C(α)–$Ar_{centroid}$ torsion angle (see **314**).

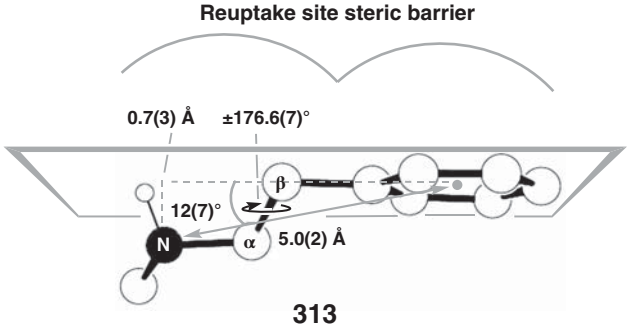

313

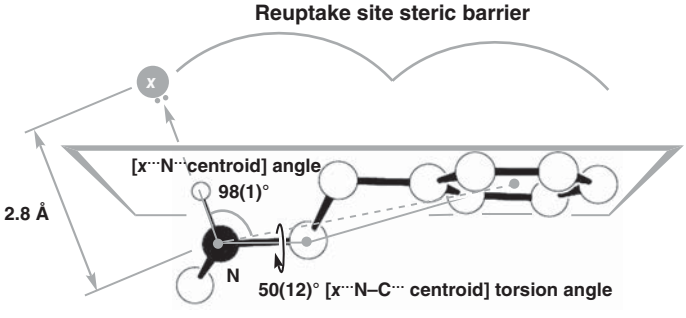

314

Conformational searches play an important role in the pharmacophore method. The *grid search* method is systematic (it finds every possible conformation). It is based on the number of theoretical conformational possibilities for single, double, and triple bonds, for example, three staggered rotamers per Csp^3–Csp^3 single-bond, three single-bond rotamers for Csp^3–Csp^2(*ortho-meta* = *ortho'-meta'* edges), and six single-bond rotamers for Csp^3–Csp^2(*ortho-meta* ≠ *ortho'-meta'* edges), and so on. However, increasing the number of bonds exponentially increases the number of calculated structures, that is, this method soon becomes too computationally intensive in terms of computer time. The more common method is the *stochastic* (statistical) conformational search, which works with a

random number generator to choose which bonds to rotate, which ring bonds to break (followed by rotating the broken segment and then reforming the bond), and so on. The premise is that if it does not find all the conformations at least once, then at least it searched for them in a spatially unbiased manner (i.e., it did not start from a preset particular end of the molecule and then run out of time as it works toward the other end). The search works by the very fast molecular mechanics approach and can generate hundreds (if not thousands) of conformations per hour on a fast modern desktop multicore computer. The energy minimization does not even have to reach the bottom of the potential energy well, since a preset number of (let us say) 100 geometry optimization steps for each structure will also suffice. Upper limits for calculated energy have to be specified for a conformation's inclusion into the learning set. Search termination criteria are set by the operator, that is, a specified number of calculations, or finding the same conformation "x" times, and so on. The idea behind the latter criterion is that if the same conformation is discovered a preset number times, then almost all the conformations should have been found at least once. The output file is ordered in terms of increasing energy structures, and enantiomeric duplicates can be removed if so desired. At a second stage, the energy of the remaining structures in the previous output file is completely minimized, and all those above a preset energy cut-off upper limit are removed. Another function of the second energy minimization is to remove all structures that are *local minima,* that is, artifacts, shallow "wells" on the potential energy surface. A final candidate energy minimized molecule should be subjected to a *vibrational frequency* calculation. One negative frequency is enough to invalidate the structure as a nonsensical local minimum.

15.4
Methylphenidate (Ritalin·HCl) and (—)-Cocaine·HCl

While in a crowded room, have you ever been able to concentrate on a relatively faraway conversation in spite of all the background noise and din around you? Many of us have developed the knack for doing this. How does it work? We all have been bioengineered to *filter out extraneous noise,* for example, the air conditioner fan, children's play, baby crying, outside traffic noise, and so on. This trait works reasonably well when we are healthy. What is that? Some of "that" has to do with having the correct (bioengineered) neurotransmitter concentrations in the synapses of our nervous system. Before we progress with this topic, let us go back to bioengineering in the human body.

Let us face it, the world around us is anything but sterile. As a matter of fact, if we examine our skin under a strong microscope we would undoubtedly be shocked to see the *creepy crawlies* merry living in cohabitation with us (and on us). Yet, most of us are healthy individuals despite the bacteria and germs around us. Why? We have been bioengineered over the eons to possess an *effective immune system* to efficiently cope with our nonsterile environment. However, sometimes the immune system temporarily or permanently breaks down, and then the bacteria get us. Well, it is the same with our central nervous system and mind. When the neurotransmitters are present at their bioengineered concentrations of *not too much* nor *not too little*, then we can take disappointment and stress (up to reasonable amounts), the passing of loved ones, the filtering of background noise, and so on, without *jumping off the deep end.* However, if a medical condition develops where there is too much or too little of a neurotransmitter, then our troubles begin. Not enough serotonin (**315**, also called 5-hydroxytryptamine, 5HT, Refcode SERHOX [190]) and stress can sometimes trigger deep depression. I am not talking about the ordinary sadness and the grief of losing a loved one (which will eventually pass to some extent when the survivor eventually realizes that *life must go on*). I am talking about anxiety, constant pounding of the heart, deep depression, lack of will to do anything, and so on. And yet, taking a selective serotonin reuptake inhibitor (SSRI) drug can increase the amount of serotonin in the synapse by blocking its reuptake into vesicles (reuptake sites) on the *presynaptic* membrane. Some well-known SSRIs are Prozac® (fluoxetine, **316** Refcode FUDCOW [130]), Zoloft® (*S*,*S*-sertraline, **317**, conformational polymorphs Refcodes CAVVUO [191] and WAKYEN [192]-predominant solution-state conformation [193]), Cipralex® (*S*-escitalopram, **318** Refcode SETVUJ [194]), and so on. Now, a patient

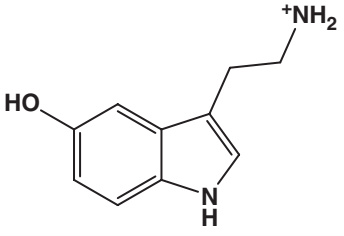

315

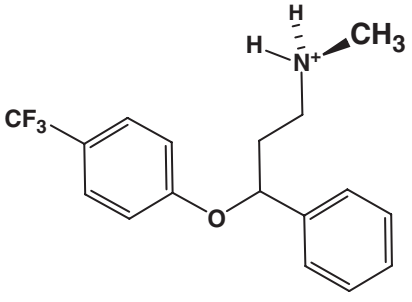

316

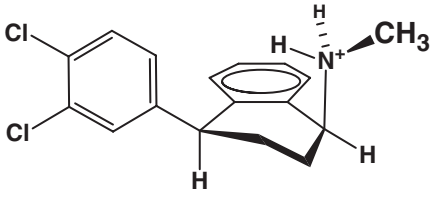

317

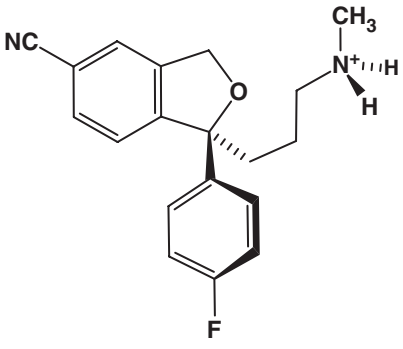

318

who suffers from a serotonin deficit will have more of the neurotransmitter in the synapse to activate the receptors on the postsynaptic membrane. This SSRI therapy may bring the patient back to good mental health at faster rate, and with much less expense to themselves and society, than costly Freudian psychoanalysis by a psychiatrist who really does not have the great amount of time required to help us solve our problems. In addition, this psychotherapy requires the patient to possess a certain degree of mental sophistication. However, a combination of SSRI pharmacotherapy together with less expensive psychotherapy, provided by a trained psychiatric nurse or psychologist, will be very synergistic than just the drug alone.

Our generation is more cognizant of ***A***ttention ***D***eficit ***D***isorder (ADD) and ***A***ttention ***D***eficit ***H***yperactivity ***D***isorder (ADHD) than those that preceded us, although, without a doubt, these health problems did not suddenly develop overnight in today's society. They were there before, and the sufferers were just known as "problem children" or "underachievers." The primary pharmacological activity of ritalin·HCl (**319**, the active (2*R*,3*R*)-(+)-enantiomer of *threo*-methylphenidate, Refcode WOGQAK [195] *ethyl*phenidate·HCl) is to block the reuptake of both DA (**320** Refcode DOPAMN01 [196]) and norepinephrine (NE, **321** Refcode NADRHC [197]) at their respective presynaptic membrane sites and thus increase the amount of these two neurotransmitters in the synapse. Ritalin is also a *psychostimulant* since it increases the synaptic concentration of DA. The result of this pharmacotherapy can be quite startling in its marked benefit to the patient, although there is a penchant to overprescribe the medication, and it recently has shown a tendency for abuse at exam time.

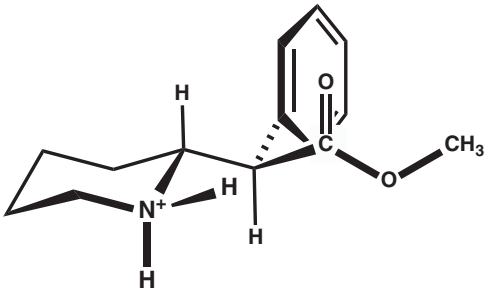

319

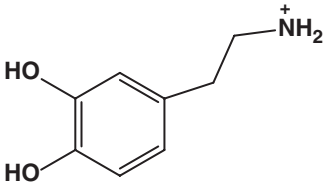

320

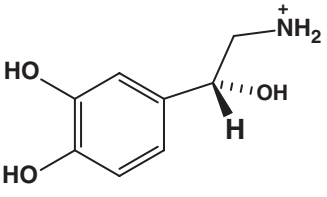

321

A second-generation DA reuptake inhibition pharmacophore (**322**, **323**) is illustrated for ritalin. It should be mentioned that while ritalin blocks the DA reuptake site, for it to be ADD/ADHD active, *it must also block the NE reuptake site* (albeit to a lesser extent). In 1995, Froimowitz and coworkers [198] performed conformational analyses on a series of potent DA reuptake blockers, including (2*R*,3*R*)-methylphenidate and (–)-(2*R*,3*S*)-cocaine (the natural enantiomer, **324**, Refcode COCHCL01 [199]). The laudable overlap of the methoxycarbonyl ester functions of both molecules enabled them to be incorporated into the pharmacophore (see superimposition **325**, where methylphenidate is colored gray and cocaine white) [198]. Methylphenidate's methoxycarbonyl ester plane intersects the aromatic plane at a dihedral angle of 106°.

15.5
Ritalin versus Cocaine: Binding Affinity and Inhibitory Concentration

It is important to stress that pharmacotherapeutic activity of many drugs (e.g., ritalin) results from the sum total of their concomitant interactions at more than

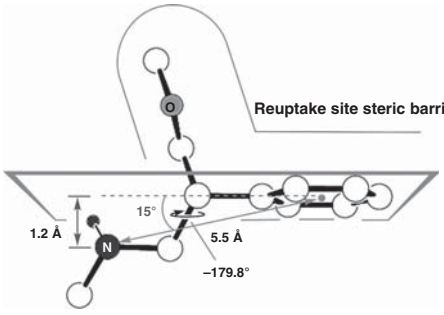

322

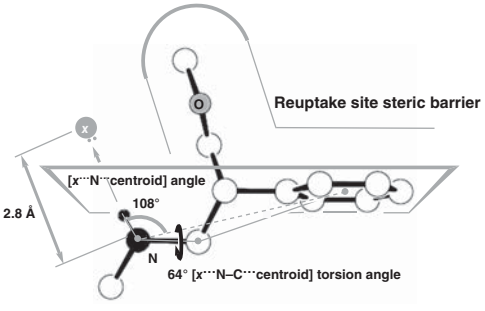

323

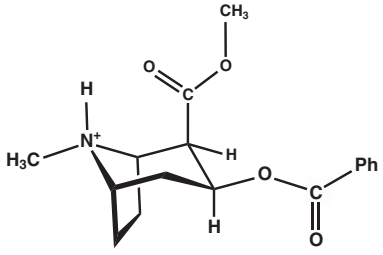

324

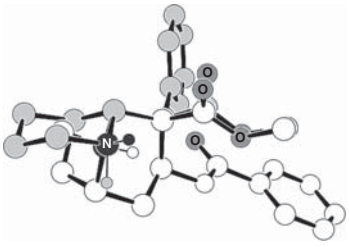

325

one receptor (or reuptake sites in this case). The K_i concentration (nM) is a measure of a test compound's *binding affinity* to a particular biological site (i.e., the presynaptic neurotransmitter's reuptake sites in this case). In a reuptake competition experiment, K_i is the concentration of a competing test ligand required to displace a radioactive-labeled ligand bound to the reuptake site. The radioligand in these assays is [^{125}I]RTI-55 (**326**), an ^{125}I-labeled cocaine-like psychostimulant and a standard test ligand for reuptake site binding affinity studies. The IC_{50} (*half maximal inhibitory concentration,* nanomolar) is an *in-vitro* measure of a test compound's effectiveness to cause 50% inhibition of a particular *biological or biochemical function* (e.g., a reuptake site bound [^{3}H]-labeled neurotransmitter, [^{3}H]DA or [^{3}H]NE). The lower the IC_{50} value, the lower the nanomolar concentration of the competing test ligand (i.e., the drug candidate) required to displace 50% of the reuptake site bound [^{3}H]-labeled neurotransmitter. It is comparable to the EC_{50}, that is, *effective dose* of an *agonist* that results in half-maximal activation of a receptor. Having said this, let us compare ritalin with cocaine (and a third drug candidate, which we will discuss later on); see Table 15.1. In our comparison, we will use the following abbreviations: DA = dopamine, NE = norepinephrine, [^{125}I]RTI-55 = **326**.

Table 15.1 Different pharmacotherapeutic profiles of (±)-*threo*-ritalin and (−)-cocaine.

Drug	DA K_i [^{125}I]RTI-55 binding (nM)	NE K_i [^{125}I]RTI-55 binding (nM)	DA IC_{50} [^{3}H]DA uptake (nM)	NE IC_{50} [^{3}H]NE uptake (nM)
Ritalin	110 ± 9	660 ± 50	79 ± 16	61 ± 14
Cocaine	500 ± 65	500 ± 90	240 ± 15	210 ± 30
*i*Bu4ClRit	7.8 ± 1.1	230 ± 30	8.2 ± 2.1	120 ± 40

Data taken from Ref. [200].

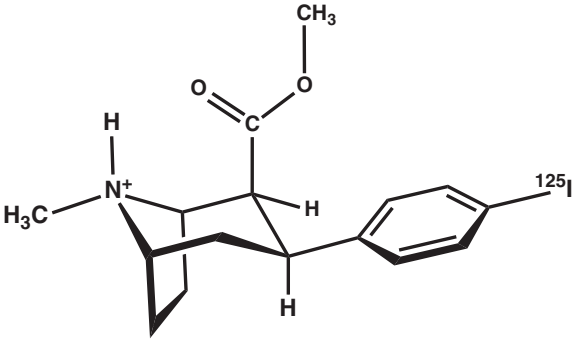

326

Remember, the lower the K_i concentration value, the higher is a test compound's *binding affinity* to the DA reuptake site, and the lower the IC_{50} value, the more effective is its inhibition of [^{3}H]-DA reuptake at 50% of the reuptake sites. Analysis of the tabular data shows that methylphenidate's *binding affinity* to the DA reuptake site is 6× higher than it is to the respective NE reuptake site [200]. Since ritalin's affinity to the DA site is 590× higher than to the serotonin (5-HT) reuptake site (data not shown in the table), the comparison shows that ritalin's *binding affinity is primarily to the DA and NE reuptake sites,* with a higher selectivity for the DA site. Cocaine's binding affinity to the DA reuptake site is the same as it is to the NE reuptake site. A comparison of *ritalin versus cocaine* shows that ritalin's *relative binding* affinity to the DA reuptake site is 4.5× higher than that of cocaine and 0.75× that of cocaine to the NE reuptake site. Thus, ritalin shows *higher binding affinity* than cocaine for the DA reuptake site, but slightly lower affinity than cocaine for the NE site. By comparison, the DA binding affinity of an *i*Bu-*para*Cl·ritalin (*i*Bu4ClRit) analogue is 14.1× than ritalin. In addition, this

new analogue exhibits more selective binding to the DA site than ritalin (29.5×) stronger to DA than to NE. This new analogue will be discussed later on in more detail.

Ritalin's concentration for *50% inhibition of DA reuptake* is 1.3× higher than that for NE reuptake. Therefore, ritalin's inhibition of DA reuptake is slightly less efficient than for NE reuptake. On the other hand, cocaine's concentration for *50% inhibition of DA reuptake* is only 1.14× higher than that for NE reuptake. Comparing the two drugs together we see that ritalin's *relative* ability to inhibit DA reuptake is 3.0× higher than that of cocaine and is 3.4× higher than cocaine for NE reuptake. Thus, cocaine inhibits both DA and NE reuptake to approximately the same lower extent than ritalin. By comparison, DA reuptake inhibition by the *i*Bu4ClRit analogue is 9.5× than ritalin. In addition, this analogue exhibits more selective reuptake inhibition at the DA site than ritalin (14.6× stronger to DA than to NE and 59.8× stronger to DA than to 5-HT). This data shows that the *i*Bu4ClRit analogue has a *different pharmacological profile* than either ritalin itself or cocaine. It shows a higher binding affinity, reuptake inhibition efficiency, and selectivity to the DA reuptake site than do ritalin and cocaine. More will be said about this interesting compound later on.

There are two reasons why the data are presented in this chapter. One will be given now and the other later. Nowadays, there is a great deal of discussion about the use/misuse of ritalin. Since we are discussing DA reuptake geometry requirements of both ritalin and cocaine at the same time, it is important that the reader realize that ritalin is NOT a cocaine mimic in its pharmacological activity. The given table clearly shows that the binding profile and pharmacotherapeutic activities of both drugs are very different. In other words, cocaine will *not* alleviate the symptoms of ADD and ADHD only methylphenidate will do the job. Bottom line: if our children are prescribed ritalin, then we do not have to be concerned that their behavior will be similar to that resulting from cocaine intake.

The pharmacophorically important groups of (−)-(2*R*,3*S*)-cocaine docked within the DA reuptake pharmacophore are shown in **327**. The fact that the aromatic ring centroid of cocaine is 7.76 Å distant from the ammonium nitrogen (instead of ritalin's 5.2 Å) may account for the about 4.5× lower binding affinity and 3.0× higher IC_{50} values for cocaine at the DA reuptake site, compared to corresponding values for ritalin. It is generally known that the more sites occupied by a drug candidate in a pharmacophoric model (and in the natural receptor or reuptake site), the more effective it will be and the lower dosage that will be required for therapeutic activity. An important goal of the pharmaceutical industry is to find a compound with nanomolar activity and *very high specificity* to the site where it interacts. Why does decreased site-specificity result in increased deleterious side effects? The natural agonist and receptor have been bioengineered for a particularly good mutual fit. Nature often uses a basic

low-energy structural motif (e.g., the seven transmembrane G-protein family of receptors) and imparts specificity by incorporating minor changes into the overall structure. The result is that families of receptors, enzymes, and so on, that, while different, do share many common features. Since drugs are foreign entities, as far as our bodies are concerned, they often fit into multiple sites with varying degrees of success. Remember, Nature did not specifically bioengineer a receptor for ritalin, cocaine, or for that matter tetrahydrocannabinol (cannabis), and so on.

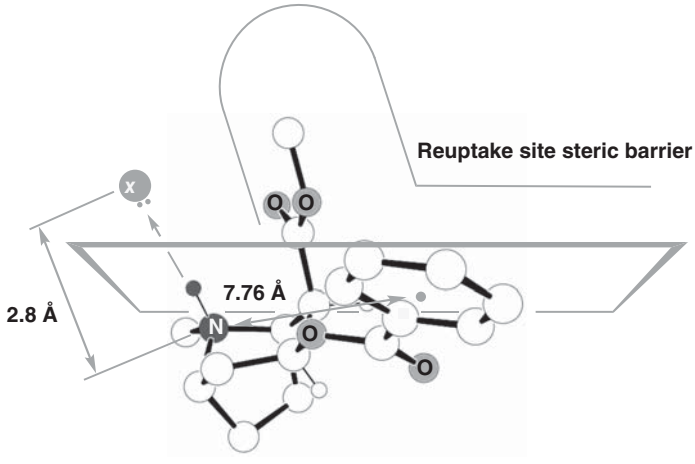

327

15.6
Second Generation Pharmacophore: The Orientation of the NH Proton

Froimowitz and coworkers [198] proposed that the orientation of the ammonium N***H*** proton played an important role in the pharmacophore on the basis of the superimposition of methylphenidate and cocaine. They stated that DA reuptake inhibition required an *equatorial* N***H*** proton disposition for methylphenidate and an *axial* orientation for tropane skeletal analogues such as cocaine. The next step in extending the DA reuptake inhibitor pharmacophore was played by Kozikowski and coworkers [201, 202] when they experimentally confirmed the ammonium-proton's role in the inhibitory process using a pair of N***H*** *configurationally rigid* cocaine-like analogues: *equatorial* N***H*** "front-bridged" **328** (Refcode PUNZAZ [201]) and *axial* N***H*** "back-bridged" **329** (Refcode VAZKIQ [202]). The front-bridged **328** molecule with the fixed *equatorial* N*H* proton tropane analogue was assayed as either the pure (+)- or (−)-enantiomer, and [^{3}H]DA reuptake inhibition

was found to be, respectively, 3.7× and 7× stronger than cocaine's inhibition of DA reuptake. This assay showed only a twofold difference in activity between the (−)-*eutomer* (more active enantiomer) and (+)-*distomer* (less active enantiomer).

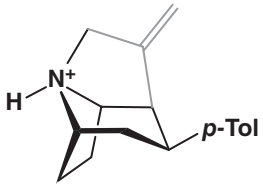

328

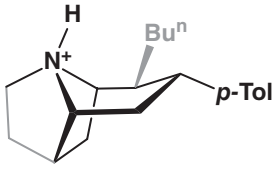

329

The real breakthrough for DA reuptake inhibition specificity versus the 5-HT and NE sites came from the *axial* N*H back-bridged* analogue (**329**), which showed 190× (for DA) and 28× (for NE) *relative inhibition* activities *versus that produced by cocaine.* Not only did these observations prove the importance of an *axial* N***H*** proton for the tropane nucleus, and an *equatorial* N–H proton for the piperidine ring of methylphenidate, but they also showed the *auspicious presence of an n-butyl group*; see pharmacophore model **330**. Interestingly, the Kozikowski group never mentioned the role of this function, which is almost an *isostere* (approximately the same steric volume) of methylphenidate's $C(=O)OCH_3$ ester function (see **329**). Later on, the presence of the *n*-butyl group was to play a central role in the development of highly *specific dopamine reuptake inhibitors* (SDRIs) for

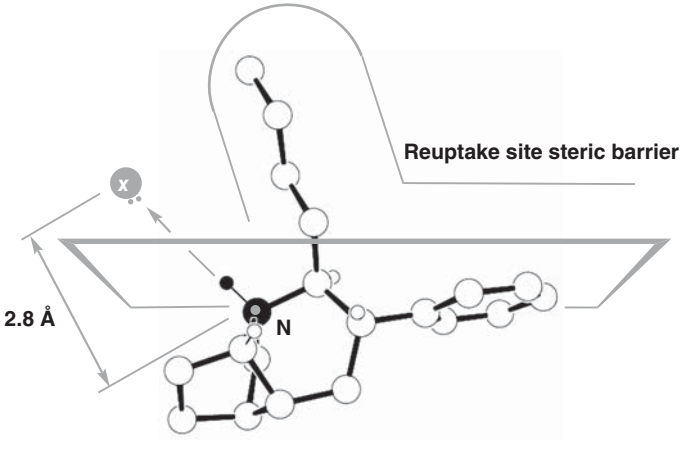

330

potential use as pharmacotherapeutic agents for the treatment of cocaine abuse. An important point coming from the Kozikowski paper was their observations that the DA reuptake site was blocked more by the *axial* N*H* back-bridged tropane **329** than by the *equatorial* N*H* front-bridged **328**, and that NE reuptake site inhibition was about the same for both **328** and **329**. This finding of inhibitory strength differentiation as a function of *axial/equatorial* N–H orientation was an important step on the road to design an SDRI.

15.7 Avoidance of Adjacent Gauche$^+$ Gauche$^-$ Interactions

Froimowitz *et al.* [195] predicted on the basis of their second generation pharmacophore **322**, **323** that *N*-methylated methylphenidate would be less active than the unsubstituted parent. They reasoned that the *N*-methyl would prefer a less sterically demanding *equatorial* disposition and thus cause the N*H* to be *axial* (i.e., the same unfavorable *equatorial*-position as in the front-bridged tropane **328**). As such, it would be unable to point toward the putative hydrogen-bonding acceptor site.

Using solution-state ^{1}H and ^{13}C NMR, Glaser, Deutsch, Froimowitz, and coworkers [203] demonstrated the presence of two solvated *N*-methyl diastereomers at the slow exchange limit (SEL) in both high (D_2O) and low (CD_2Cl_2) dielectric solutions. The two *threo*-methylphenidate *N*-methyl diastereomers in solution were found to be the *equatorial N*-methyl *species* (**331**) and its *N*-configurationally different *axial N*-methyl *epimeric* partner (**332**). While an *equatorial N*-methyl group in **331** is sterically favored for the parent *N*-methyl piperidine skeleton, the presence of the nearby *equatorial* –CH(Ph)CO_2CH_3 function gives rise to sterically unfavorable opposite signed (+)-*gauche* C(2)–C(3)–N(4)–C(methyl) and (−)-*gauche* C(carboxyl)–C(2)–C(3)–N(4) (g^+g^-) torsion angles about the adjacent C(3)–C(4) and C(2)–C(3) bonds in **331**. Why? The N–C(methyl) and C(methine)–C(carbonyl) bonds are *coplanar* (i.e., they eclipse each other), and hence, the C(methyl)*H* and C(carbonyl) atoms are spatially close.

The avoidance of these g^+g^- steric interactions is a well-known structural constraint utilized by Nature in natural product side chains to induce *preferred conformations.* This subject has been nicely reviewed and explained by Rheinhard Hoffmann [204]. For example, the well-known sterically unfavorable *cis*-1,3-*diaxial* interactions in disubstituted cyclohexanes result from adjacent opposite-signed *synclinal* torsion angles (g^+g^-). Notice how symmetry enters into these unfavorable g^+g^- interactions, for example, an *enantiotopic* R, $\overline{R}$ substituent pair on straight chain segment **333**. Note the (+)-*synclinal* R–C(1)–C(2)–C(3) and (−)-*synclinal* C(1)–C(2)–C(3)–$\overline{R}$ torsion angles (i.e., g^+g^-). Now, observe the *homotopic* R,R′ pair of substituents on straight chain segment **334**. In this

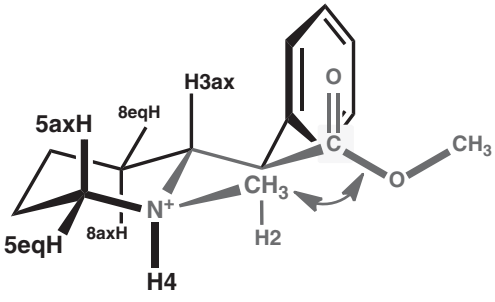

331

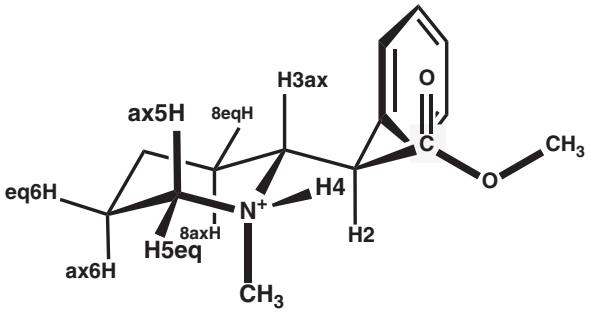

332

more favorable arrangement, the presence of (+)-*synclinal* R–C(1)–C(2)–C(3) and (+)-*synclinal* C(1)–C(2)–C(3)–R′ torsion angles (i.e., g^+g^+) avoids the $R \cdots \overline{R}$ close contacts present in **333**. This is the reason why it is relatively rare to find molecules in the crystal lattice occupying special positions of mirror symmetry unless they are rigid (e.g., *cis*-1,2-disubstituted oxirane **88**). Thus, while mirror symmetry is commonly found *between* molecules in a crystal lattice, it is rarely observed *within eclipsed* conformations.

An (*eq-N*-Me g^+g^-, **331**):(*ax-N*-Me g^+g^+/g^-g^-, **332**) diastereomeric ratio was found to be 87 : 13 in less polar CD_2Cl_2 and 44 : 56 in the biologically relevant more polar D_2O. Can you figure out why what appears to be a less sterically favorable g^+g^- geometry is present in the CD_2Cl_2 87% major species, and why does its concentration drop down to 44% in D_2O? To figure this out, you should ask yourself two questions. First, "what positive feature results from an *equatorial* disposition for the *N*-methyl that enables it to be the major species in CD_2Cl_2 with a dielectric constant of ca. 9?" The second question is "why does its concentration decrease to 44% in D_2O (with a 9× higher dielectric constant of 80)?" The first thing to

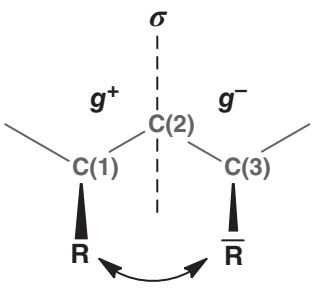

333

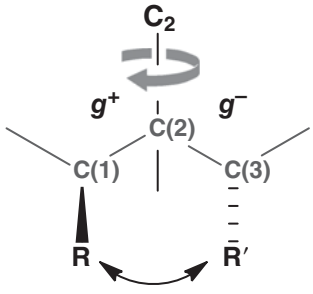

334

consider from the outlook of the piperidine ring's *axial* protons is that an *equatorial N*-methyl is preferable to an *axial* epimer as was realized by the Froimowitz group (for obvious reasons, as in the cyclohexanes) [200]. But there is the nearby ester function to also consider. Look at the geometry of the carbonyl Csp^2 facing the methyl protons. The carbonyl is *flat*, and that is very important. What do you think would happen if that carbon's hybridization was changed to a more bulky sp^3? Later on we will illustrate and discuss this further. OK, the next question to ask is what do you know about the polarity of the carboxylate group? It's relatively polar, isn't it? Which of the two solvents will *more intimately* solvate the carboxylate *on both faces*, CD_2Cl_2 or D_2O? Hint: consider the net solvated volume around both faces of the flat carbonyl. So, now you figured it out. The carboxyl carbon *appears* to have two water solvated faces, while the less polar CD_2Cl_2 is happy to primarily solvate the *anti*-to methyl face and let the methyl group block the *syn*-face. This is another type of *hydrophobic collapse* phenomenon seen in globular proteins.

15.8
Static Disorder in *N*-Methyl Ritalin Crystals

Static disorders have been discussed before (e.g., scopolamine·HCl·1.5H_2O and scopolamine·HCl·2H_2O statistically occupying the same asymmetric unit position in a 2 : 1 ratio in the lattice to give a scopolamine·HCl·1.67H_2O kinetic crystal **278**). In the *N*-methyl ritalin·HCl case, there is a *static disorder* between two diastereotopic piperidine rings both comprising the same asymmetric unit position of $P2_1$ monoclinic system space group chiral crystals (Refcode NODBIR) [203]. Crystallization of *N*-methyl ritalin·HCl engenders a lattice void whose spatial constraints enable one of two conformationally and *N*-configurationally *different* molecules to reside within (see **335**). Notice that the sterically demanding $-C_\alpha$HPh–C(=O)OMe unit is located in one specific location. However, the

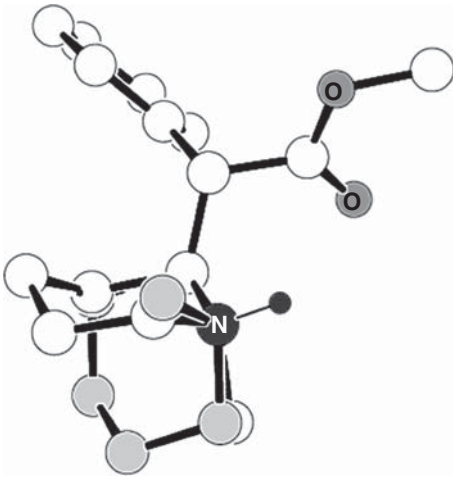

335

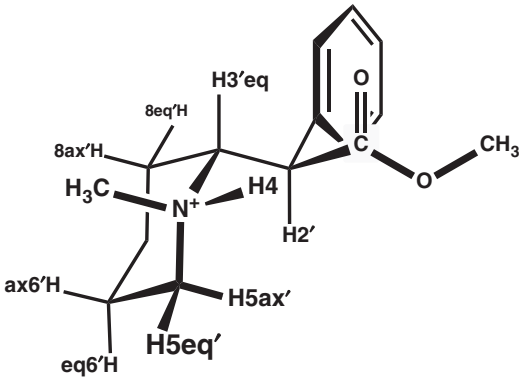

336

five piperidinyl carbon atoms and the *N*-methyl carbon in the white-colored *axial N*-methyl/*equatorial*-CHPh–C(=O)OMe *more extended* molecule **332** occupy 25% of the asymmetric units, while the light gray corresponding six atoms in the *axial N*-methyl/*axial*-CHPh–C(=O)OMe *more compact* epimeric diastereomer **336** reside in the other 75%. In other words, since there are only two asymmetric units within a $P2_1$ unit cell, for every two unit cells of the kinetic crystal, one asymmetric unit contains **332** and three contain **336**. As we have seen in the scopolamine·HCl·1.67$H_2$0 case, occupancy of different molecules in the

asymmetric units gives rise to *space averaging* (i.e., a *static disorder*). Why static in this case and not dynamic as for the nefopam methohalides of Figure 14.1? The disorder is static because the stereogenic N^+ requires bond breaking and bond making in order to exchange, while the nefopam methohalides exchange just involves a conformational interchange. In all disorders, the occupancy ratio of the resident molecules in the asymmetric unit is governed by the void's overall geometry and the packing requirements of the guest. Notice also that the superimposed piperidinyl rings approximate a ball-like entity (similar to adamantane in some respects).

By what mechanism does solvated **332** interconvert to **336** and *vice versa*? Figure 15.1 shows that piperidine *ring-inversion* (middle-left to the uppermost structure) followed by a *prototropic shift/nitrogen inversion* (or performed in reverse order) converts **332** (within solid rectangle) into **336** (inside dashed rectangle).

Now that a discussion of the stereochemistry of these methylphenidate *N*-methyl diastereomers (**331**, **332**, **336**) has been presented, let us consider their abilities to fit the DA reuptake inhibitor pharmacophore. Solution-state **331** (44% in D_2O, 87% in CD_2Cl_2) is a nonviable candidate for binding to the DA reuptake inhibitor model due to its *axial* N*H* [205]. The *equatorial* N*H* minor species (**332** or **336**) in D_2O allows it to be incorporated into the pharmacophore (see **337**). However, as Froimowitz *et al.* [200] predicted, the concentration of the *equatorial* N*H* proton species is not 100% but rather only 56% in D_2O (as determined by NMR) [205]. This could explain the NMe's *six times lower* activity (IC_{50} 500 ± 25 nM), compared to methylphenidate (IC_{50} 83 ± 8 nM), in

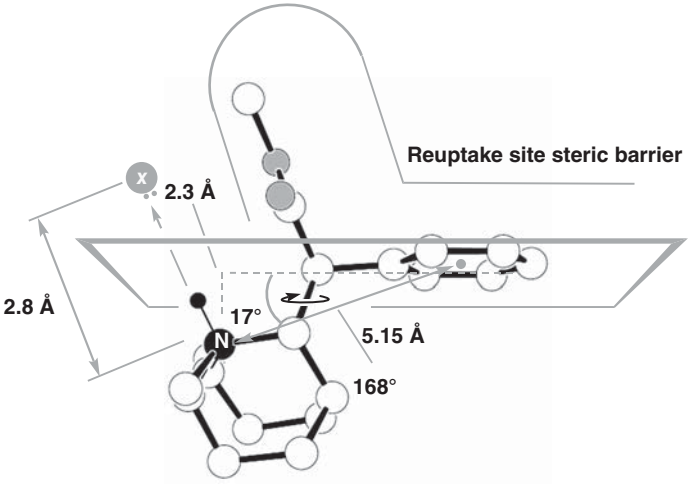

337

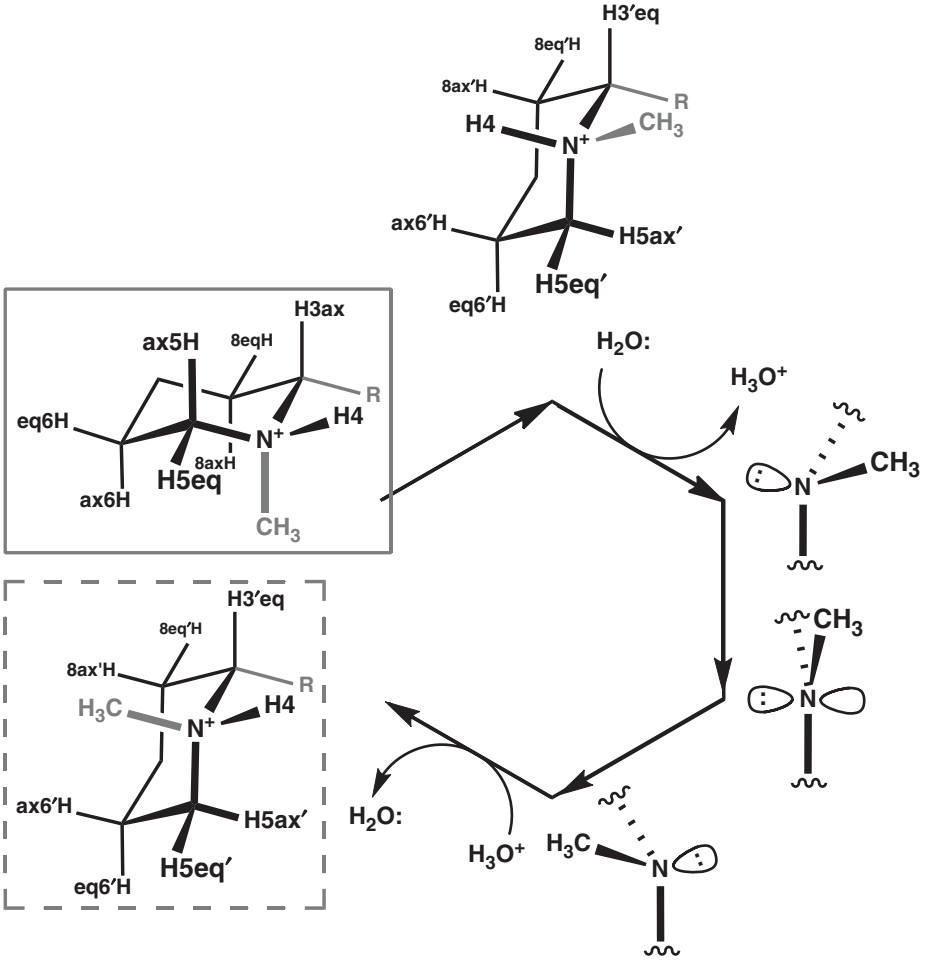

Figure 15.1 R = CH(C=O)OMe. Ring inversion interconverts **332** (inside solid-rectangle) with its *ring invertomer* (topmost structure) while keeping the *N*-configuration invariant. The ring invertomer is then converted to **336** (within the dashed rectangle) via an overall *prototropic shift/nitrogen inversion* mechanism.

competitive displacement of [^{3}H]-β-CFT (Refcode QUHZIC) [199] at the DA reuptake site, where β-CFT is the fluorine analogue of *p*-^{125}I-RBI-55 (**326**) [205].

15.9 Development of Specific Dopamine Reuptake Inhibitors (SDRI)

We have seen that substitution of the C(=O)OMe moiety by an appropriate length alkyl group (e.g., *n*-Bu) in the *back-bridged* tropane derivative **329** preserved its cocaine-like activity. This was the impetus for Froimowitz *et al.* [200] to prepare an extensive series of C_α-alkyl "*methylphenidate-like*" surrogates and investigate their reuptake inhibition activities at DA and NE sites. These compounds are ritalin analogues where alkyl groups have replaced the hydrolytically labile C(=O)OCH$_3$ ester function. Before discussing this topic further, we should mention that mono- and dichloro-substituents on ritalin's phenyl ring markedly increased both the binding affinity and the inhibition efficiency at the DA reuptake site. The K_i binding affinity of *m,p*-dichloro- and *p*-chloroaryl methylphenidate are, respectively, 79× and 4× that of the unsubstituted-phenyl control, while the IC_{50} inhibition efficiencies are, respectively, 7× and 3× that of the control. These findings suggest that the pharmacophore's aromatic ring interacts with an electron-rich binding region in the DA reuptake site.

Due to the consistently higher activities from *p*-Cl aromatic ring substitution, a series of C_αH(*p*-ClAr)R-alkyl decarboxylated-ritalin analogues were prepared where *R* = Me, Et, *n*-Pr, *n*-Bu, *n*-Pnt. Their binding affinities to the DA reuptake site were found to increase with longer straight-chain lengths and peaked at *n*-Bu (3.20× higher than the *p*-Cl-methylphenidate control) [200]. On the other hand, their binding affinities to the NE reuptake site were fairly insensitive to chain length, and even at its best, the *n*-Pnt alkyl-compound was only 0.68× that of *p*-Cl-methylphenidate. These results were very promising since they suggested binding affinity *selectivity to the DA reuptake* site over its NE counterpart. Moreover, what was really impressive was the DA/NE *relative binding affinity* of the *n*-Bu test compound (29.48× higher than that demonstrated by the control) [200].

The IC_{50} efficiency of DA reuptake site inhibition relative to *p*-Cl-methylphenidate was found to be relatively insensitive to the straight-chain length with a maximum at 1.49× (for *n*-Pr) and 1.34× (for *n*-Bu) [200]. But very fortuitously, the corresponding values for NE reuptake site inhibition efficiency were all much lower: 0.22× (*n*-Pr) and 0.42× (*n*-Bu) [200]. The *relative efficiency* for DA inhibition compared to NE peaked at 9.13× for Et and then decreased to 6.76× (*n*-Pr) and 3.17× (*n*-Bu) [200]. Therefore, it seems that the greatest effect of the straight-chain alkyl groups is their *higher binding affinity to the DA reuptake site* versus attraction to the NE counterpart.

The next step was to compare a series of branched chain C_{α}-alkyl groups methylated at the first, second, or third carbons. The K_i binding affinity to the DA reuptake site reached a maximum of **6.94**× (for *i*-Pnt) compared to that of the *p*-Cl-methylphenidate control [200]. Once again, the binding affinity of the methyl branched-chain analogues to the NE reuptake site was constantly about 0.13× lower than that for the $C(=O)OCH_3$ moiety in the methylphenidate control [200]. As we saw with the alkyl straight-chain compounds, these alkyl branched-chain results demonstrated a very useful trend: *increased DA reuptake site binding affinity* for the appropriate length branched-chain alkyl (i.e., *i*-Pnt) test compound versus the control. But now, even better, the affinities to the NE site were found to be both *iso*-alkyl group positionally invariant *and consistently lower than ritalin.* Bottom line: the results are extremely impressive when considering the *i*-Pnt test compound's **230.6**× *relative binding affinity to the DA versus NE reuptake sites* (compared to methylphenidate's **6**× relative selectivity for the same two sites) [200]. To increase DA versus NE reuptake site selectivity requires the laudable attributes of both an increase in DA binding affinity and concomitant decrease for that to NE.

The IC_{50} efficiency of DA reuptake site inhibition relative to that for *p*-Cl-methylphenidate increased to a maximum of **39.6**× for *i*-Pnt [200]. Once more, another important observation for DA selectivity was the *extremely poor* NE reuptake site inhibition for positionally invariant *i*-alkyl groups, for example, 0.05× for *i*-Pnt [200]. From the high *binding affinity* to the DA reuptake site versus its markedly lower attraction to the NE site, one can already predict an auspicious DA *reuptake site inhibition* specificity for the *i*-Pnt test compound. This is readily seen by the **15.0**× (*i*-Pnt) *DA relative reuptake inhibition versus that for NE* compared to that demonstrated by the *p*-Cl-ritalin control [200].

The aforementioned *in vitro* results from three branched-chain α-alkyl analogues of methylphenidate (e.g., *i*-Bu, $-CH_2$cyc–Pnt, and especially *i*-Pnt) showed *impressive augmentation of DA reuptake site specificity, in terms of both binding* affinity and increased *DA inhibition efficiency.* Clearly, these new compounds exhibit very different pharmaceutical profiles compared to that of ritalin·HCl. It should be stressed that they are *not* improved pharmacotherapeutic agents for the treatment of ADHD, since ritalin must inhibit two reuptake sites (the primary DA site and the secondary NE site).

Both CH_2*cyc*Pnt and *i*-Bu groups are *isosteric replacements* (occupy the same space) for $C(=O)OCH_3$. Hydrolytically labile cocaine (as opposed to the *i*-Bu analogue) suffers from the liability of the ester function's rapid metabolism to the inactive acid [206]. Larger doses of cocaine have to be administered in order to overcome this. The rapid increase in cocaine concentration to high levels in the blood stream is said to produce the "*rush*" described by addicts. Locomotor assays of the *i*-Bu analogue showed it to exhibit the favorable therapeutic attributes of both *slow onset* and *long duration* [200]. Since lower doses of the *i*-alkyl

analogue need be given, its DA reuptake inhibition effect builds up at a slower rate and then metabolically decreases at a markedly lower rate than measured for cocaine. There is evidence that cocaine abuse is linked to its *fast onset* and *short duration* of action. Thus, a compound with the opposite pharmacokinetic profile would be expected to have *reduced abuse potential,* which might allow it to be a useful substitution pharmacotherapy for the treatment of cocaine abuse. Preliminary animal studies suggest that the *i*-Bu analogue indeed has a lower abuse potential.

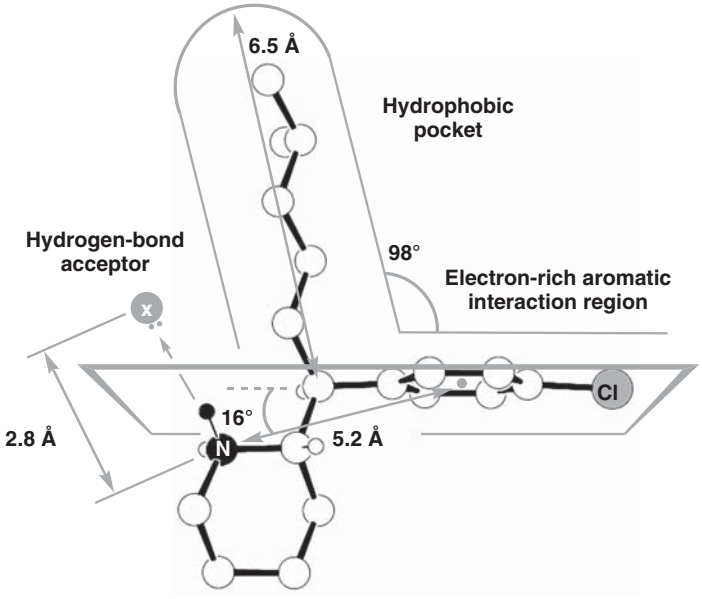

338

These studies have now enabled the construction of a more detailed third-generation DA reuptake pharmacophore. Incorporation of the α-*iso*-pentyl methylphenidate-surrogate into the DA reuptake site inhibition pharmacophore now enables the definition of three important sites: an electron-rich aromatic interaction region, a hydrogen-bond acceptor about 2.8 Å from a piperidine nitrogen donor with an *equatorial* N–H bond, as well as the presence of an approximately 6.5 Å deep hydrophobic pocket (see **338)**.

Glaser, Froimowitz, and coworkers [207] reported the solution-state and solid-state stereochemistry of a series of active (*RR*,*SS*)-*p*-Cl–Ar,C(*α*)-alkyl analogues (e.g. Refcode PIDGEO) and inactive (*RS*,*SR*)-C(α)-alkyl "ritalin surrogate" epimers with and without *N*-methylation. The active (*RR*,*SS*)-3,4-dichloro-*N*-methyl-*i*-Bu ritalin-like analogue afforded 2.4× the DA binding affinity and 0.66× the inhibition of DA reuptake relative to that of the non-*N*-methylated compound [200].

The X-ray structures of the active (*RR*,*SS*)-α-alkyl methylphenidate-substitutes all exhibited a gray color-coded *antiperiplanar* H–H conformation as in **339** (Refcode PICRAW) [207]. About half of the inactive (*RS*,*RS*)-α-alkyl analogues exhibited a *different* solid-state gray color-coded *synclinal* H–H conformation as shown in the *equatorial N*-methyl diastereomer **340** (Refcode PICREA) [207]. The $-CH_2CHMe_2$ conformation and *axial/equatorial* N*Me* orientations are all in accord with avoidance of oppositely signed sterically unfavorable g^+g^- interactions noted earlier. The same solid-state N*Me* configurational and *i*-Bu conformational geometries were found for the corresponding *major* solution-state species in both D_2O and CD_2Cl_2 [207]. It remains to be proved that this H–H *antiperiplanar*/*synclinal* conformational difference has biological significance.

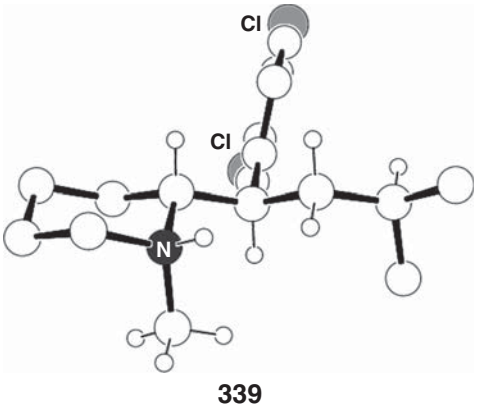

339

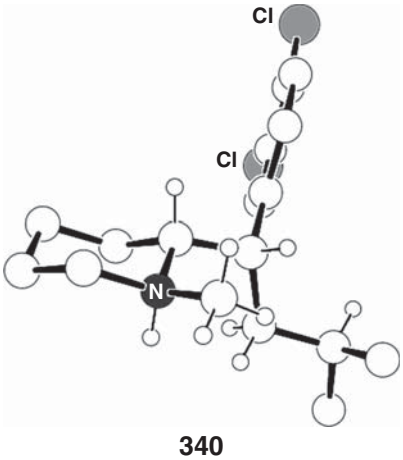

340

16
The X-Ray Structure–Based Method of Rational Design

16.1
X-Ray Crystallographic Structure–Based Molecular Design

We have seen that the pharmacophore method enables the design of new drugs even when the exact location and structure of the host are unknown. But, on the other hand, there are many cases where X-ray crystallographic structures exist and depict a guest molecule residing within its host. This provides the ability to observe the actual interactions between the intimately docked partners. Once these are understood, the next step is to look for *unused* potential binding sites within the host's cavity. With this in mind, the goal is to design a new guest containing *additional interaction functions* that can be auspiciously located to take advantage of the unused site (and hence increase the guest's binding affinity). An apt example of the use of the structure-based technique was the rational design of the current world record holder (2014) for the *strongest known noncovalently bound* host and its guest: $K_a = 7.2 \times 10^{17}\,\mathrm{M}^{-1}$; $K_d = 1.4 \times 10^{-18}\,\mathrm{M}$ (*attomolar*), D_2O, 25 °C [208]. To put such a large number like $7.2 \times 10^{17}\,\mathrm{M}^{-1}$ into perspective, it was about 45 000× the US Gross National Debt as of April 2014. It is also approximately 1400× stronger than Nature's best effort ($K_d \approx 10^{-15}\,\mathrm{M}$) for the

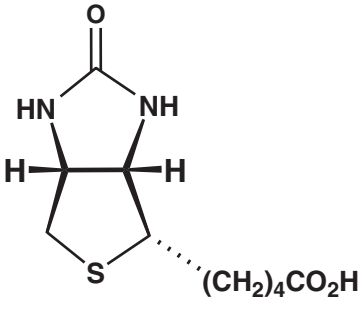

341

Symmetry, Spectroscopy, and Crystallography: The Structural Nexus, First Edition. Robert Glaser.

Companion Website: www.wiley.com/go/Glaser/Symmetry

dissociation of the biotin cofactor (**341**) from avidin (its protein host comprising about 0.05% of the total protein in chicken egg whites).

The ultrahigh binding is between a cucurbit[7]uril host (**342**) and *N,N,N,N′,N′,N′*-hexamethyl-diamantane-4,9-diaminium diiodide (diam-4,9-di(NMe_3I), **343**), a bisquaternary ammonium guest. *Cucurbit* is a gourd-shaped pumpkin-like object, for example, the bottom of an *alembic* (**344**, derived from the Arabic "*al anbiq*" meaning *the still,* a glass vessel fitted with a long tapered tube air-cooled condenser used by alchemists and early chemists for distillation). Before we discuss the design method, some background should be provided for these remarkable macrocyclic water-soluble *molecular containers.*

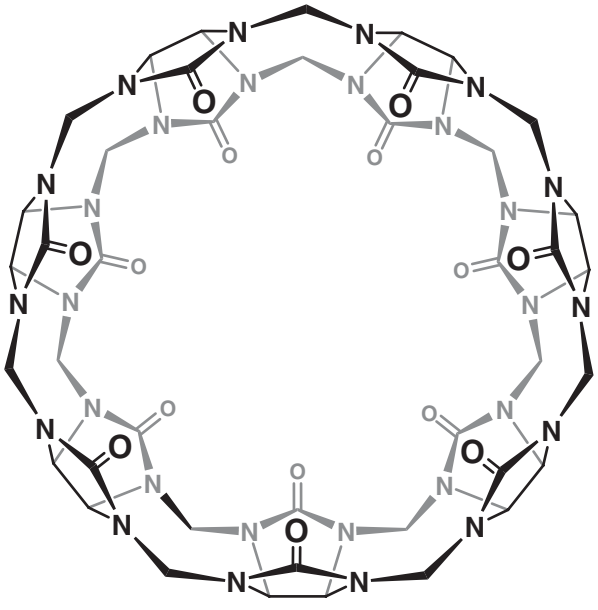

342

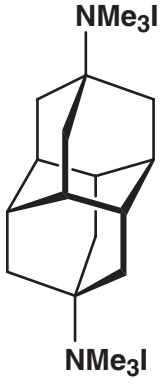

343

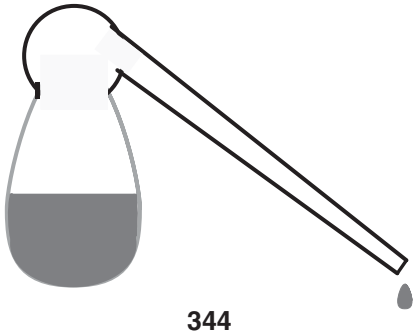

344

Cucurbit[*n*]urils (**345**) are synthesized via reaction between urea and dialdehyde (2 : 1 ratio) to afford the intermediate glycoluril (**346**). This is followed by condensation with formaldehyde to give a mixture of cucurbit[*n*]uril macrocyclic products.

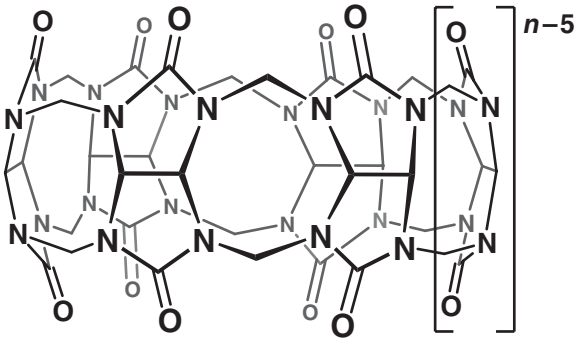

CB[*n*] (*n* = 5, 6, 7, 8, 10)

345

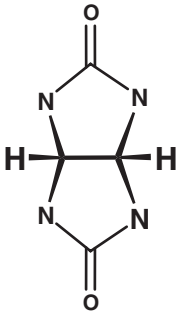

346

Over the past decade, the cucurbit[n]uril (CB[*n*], $n = 5$, 6, 7, 8, 10) family of molecular containers has emerged as a very popular platform for basic and applied studies of molecular recognition in water. The CB[*n*] hosts feature two symmetry-equivalent *partially negatively charged* ureidyl carbonyl portals, which guard the entrance to a hydrophobic cavity. Mock and Shih [209] showed that guests with both cationic and hydrophobic regions bind with micromolar affinity, and good selectivity, toward CB[6] in acidic aqueous solution. For example, a variant of CB[6] binds to the oligoamine spermine with $K_a = 3.4 \times 10^{12}\,M^{-1}$ (*in pure water*) by a combination of hydrogen-bonding ($^{+}N–\underline{H}^{\delta+}\cdots{}^{\delta-}\underline{O}{=}C$), electrostatic interactions ($^{+}NC_{methylene}\underline{H}^{\delta+}\cdots{}^{\delta-}\underline{O}{=}C$), and the hydrophobic effect (Refcode XUBYUP) [210]. This hexacyclohexyl-type variant has *exo*-3,4-butano bridges replacing the methine protons in the equatorial C**H**–C**H** units. In 2005, Isaacs and coworkers discovered, by ^{1}H NMR competition experiments, that CB[7] exhibits very high affinity toward adamantane-1-NH_3Cl (**347**), adamantane-1-NMe_3Cl (**348**), ferrocene-1-CH_2NMe_3I **349**, and ferrocene-1,1′-di(CH_2NMe_3I) **350** (e.g., CB[7]·**347** $K_a = 4.23 \times 10^{12}\,M^{-1}$; CB[7]·**348** $K_a = 1.71 \times 10^{12}\,M^{-1}$; and CB[7]·**349** $K_a = 3.31 \times 10^{11}\,M^{-1}$, *all in 50 mM NaOAc buffered* D_2O at pH 4.74) [211]. In 2007, it was reported that the affinity of the CB[7]·**350** complex ($K_a = 3 \times 10^{15}\,M^{-1}$ in *pure unbuffered* H_2O, and $K_a = 1.9 \times 10^{13}\,M^{-1}$ in *50 mM NaOAc buffered* D_2O at pH 4.74) rivaled that of the avidin·biotin complex [212]. The reduction in K_a for CB[7]·**350** in 50 mM NaOAc-d_3 buffer is fully consistent with the known ability of Na^+ ions to bind at the $C{=}O^{\delta-}$ portals of CB[*n*], and thereby reduce the observed values of K_a by competition [213, 214]. The

advantage of the sodium acetate-*d*3 buffer is that it provides a standard pD solution that is independent of the ammonium salt's pK_a.

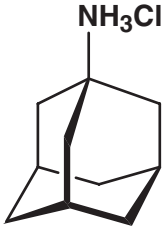

347

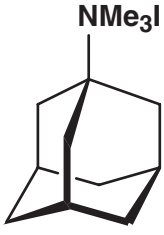

348

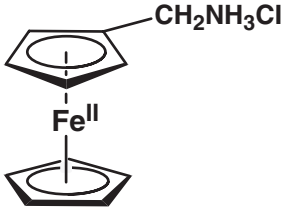

349

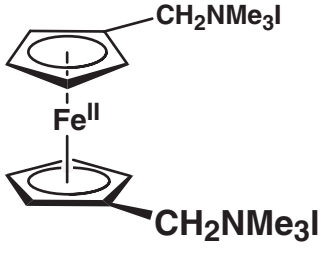

350

A tripartite collaboration between Beer-Sheva, Croatia, and the United States was formed 4 years ago to undertake a systematic study of adamantane-based diammonium guests in order to decipher the structural requisites for ultrahigh binding. This section discusses the *Structure-Based Molecular Design* technique with crystal structures of CB[7]/CB[8] hosts binding adamantane guests. Two published structures and six in-house (yet to be published) [215] structures were compared in the learning set. Binding studies had shown that quaternary ammonium salts had stronger affinity to the CB-hosts than their primary ammonium analogues, and one of the project's goals was to ascertain the reason why this was so.

16.2
The Different Primary Ammonium and Quaternary Aminium Binding Modes

With a learning set of eight CB-hosts, containing adamantane mono- and diamine guests, two markedly different binding motifs became apparent, that is, those for primary- versus quaternary-ammonium salts [208]. The first structure to be discussed is 3,5-dimethyladamantane-1-NH_3Cl, (**351**, memantine – a monoamine

guest). Memantine is a clinically useful drug for the treatment of many neurological disorders, including Alzheimer's disease. A capped sticks/space filling side view of the CB[7]·**351** complex (Refcode SULZIJ mol A/mol B) [216] is shown in **352** and top view **353**. In order to engender a hydrogen bonding distance, the primary ammonium nitrogen tilts 30° from the host's axis toward two adjacent C=$O^{\delta-}$ oxygen atoms on the portal rim in order to engender a hydrogen bond. (L. Isaacs, R. Glaser, K. Majerski, and coworkers, unpublished results). The 2.77 and 2.86 Å $^{+}$N–$\underline{H}^{\delta+}\cdots{}^{\delta-}\underline{O}$=C hydrogen bonds are depicted in **353**. The nitrogen atom is only 0.18 Å above the mean portal plane defined by the seven oxygen atoms.

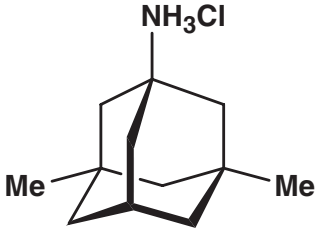

351

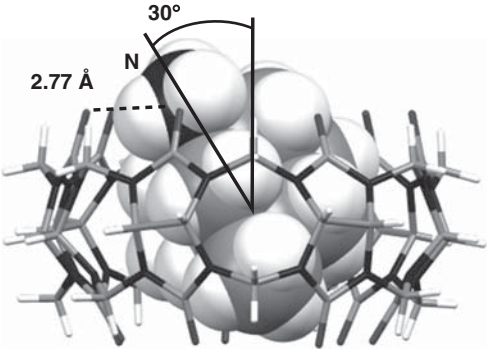

352

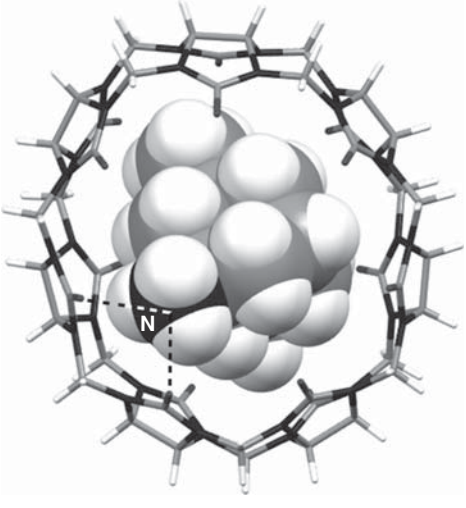

353

The combination of two methyl groups abutting the cavity's interior walls and the ammonium ion tilt of **352** results in an energy demanding elliptical deformation of the narrow CB[7] host, $K_a = 2.50 \times 10^4$ [211] (see **353)**. The molecule

occupies a *general position of symmetry* in the $P2_1/c$ crystal lattice so that its visually apparent C_7-rotational symmetry is only *pseudo*symmetry. The Avnir S(C_7) parameter [11, 12] was used to measure the degree of distortion from ideal C_7-rotational symmetry. The distortion indexes of the seven portal oxygens from ideal symmetry increased from the hydrogen-bonded top portal (0.14(6) S(C_7)), to the equator (0.24(4) S(C_7)), and then to the more elliptically deformed empty bottom portal (2.7(2) S(C_7)) (R. Glaser and A. Steinberg, unpublished results). To put these S(C_7) values into perspective, the *top* portal and equatorial plane S(C_7)-values of 0.14–0.24 correspond to visibly perceivable *small deviations* from the ideal (i.e., moderate-fidelity C_7 *pseudo*symmetry). Whereas *bottom* portal's very high 2.7(4) value (due to abutting methyls) testifies to important distortions that are large enough so that the absence of a particular *pseudo*symmetry element within an object is visually perceived (i.e., extremely *low-fidelity pseudo*symmetry).

A better fit should be expected for residence of **351** within the larger diameter CB[8] container ($K_a = 4.33 \times 10^{11}\,M^{-1}$) [208]. This was indeed so, a remarkable $2.11 \times 10^{7}\,M^{-1}$ *increase in binding affinity*, and a slightly larger 36° tilt in order to form a single 2.82 Å hydrogen bond, see **354** (L. Isaacs and P.Y. Zavialij, unpublished results). Due to the larger tilt, the nitrogen atom is only 0.01 Å above the mean portal plane defined by the eight oxygen atoms. The larger diameter CB[8] host suffers a lower degree of energy-demanding elliptical deformation (see **355**). The 0.15 S(C_8) values for both portals now show a very small magnitude structurally significant deviation from the ideal symmetry that can still be visually perceived (R. Glaser and A. Steinberg, unpublished results). However, this value is very misleading. Why? The CB[8] host occupies a special position of inversion symmetry in the $I4_1/a$ tetragonal space group lattice (L. Isaacs and P.Y. Zavialij, unpublished results), while two *static disordered* asymmetric **351** guests occupy the unit cell's 16 asymmetric units. This means that eight of the unit cell's asymmetric units have the monoammonium guest interacting with the top portal while the other eight have it disposed toward the opposite orifice (R. Glaser and A. Steinberg, unpublished results). The two C_1-symmetry space averaged superimposed guests depict a statistical *i*-symmetry disordered composite (**354**). As a result, the *apparently* enantiotopic portals in the X-ray crystallography determined complex **355**, **356** are really a *hybrid* of two unobserved diastereotopic faces (one hydrogen-bonds the guest while the other does not) (R. Glaser and A. Steinberg, unpublished results). There is a clear lesson to be learned here. To many chemists, a crystal structure represents *the* definitive representation of structural reality. But it is clear that this is not necessarily so. Does this mean that crystal structures **355** and **356** are useless? Of course not! They do give us insight into how the complex looks *on the average.* One just has to be aware of exactly what the structure is telling us. This is where a computational model produced with a very high level of density functional theory (DFT) (e.g.,

BLYP-D/def2-SVP/COSMO=dft triple−zeta + polarization empirical dispersion, and COSMO implicit solvent) can help fill in the gaps in our knowledge.

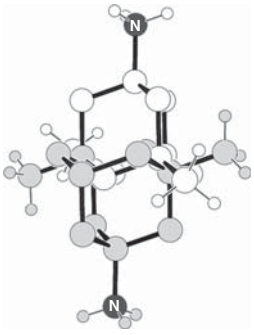

354

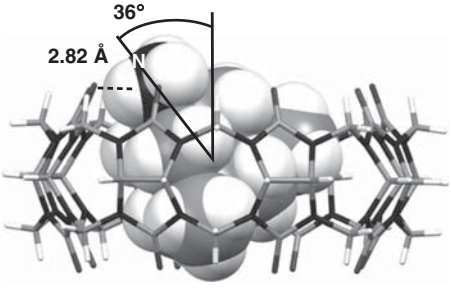

355

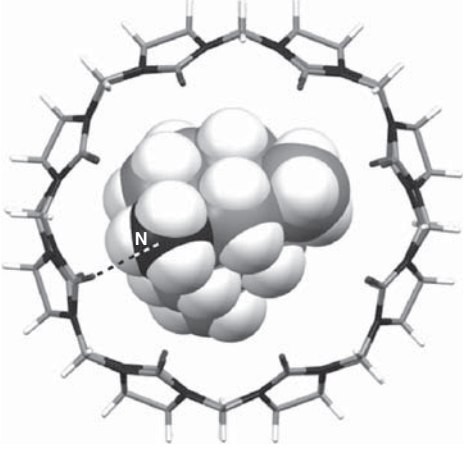

356

The larger diameter CB[8] host complexed with *N,N,N,N′,N′,N′*-hexamethyladamantane-1,3-di(NMe_3I) **357** (Refcode SAXKEI [211], **358, 359**) is representative of the quaternary ammonium salt binding motif. In this arrangement, the C(ada)–N bond is almost perpendicular to the top mean plane of the portal oxygens, and the nitrogen atom juts out about 0.51 Å above the top plane. The second NMe_3 group is not properly placed to do this. Instead, it is pushed against the cavity's interior wall and its nitrogen is 2.30 Å *above* the bottom portal mean plane. Five of the carbonyl oxygen atoms on the top portal undergo *strong electrostatic* $^{+}NC_{methyl}\underline{\boldsymbol{H}}^{\delta+}\cdots{}^{\delta-}\underline{O}{=}C$ Coulombic interactions as evidenced by the mean 4.35(8) Å $^{+}N\cdots{}^{\delta-}\underline{O}{=}C$ distances for four oxygens and

an only very slightly longer 4.74 Å distance for a fifth one (see **359**). These interactions and distances are very similar to those $^{+}N-$Aromatic(centroid)$^{\delta-}$ interactions and distances between acetylcholine's quaternary $^{+}N(CH_3)_3$ group and the surrounding partially negatively charged aromatic ring interiors lining acetylcholinesterase's tunnel [217, 218].

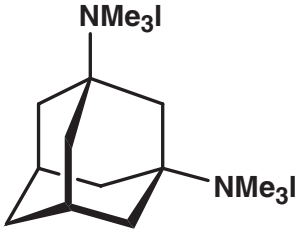

357

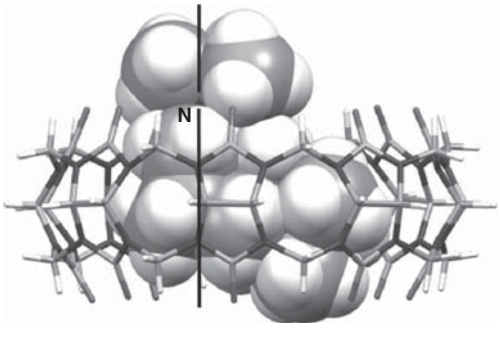

358

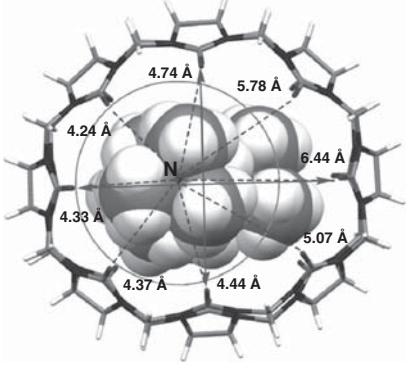

359

The steric fit between adamantane-1,3-di(NMe_3I) **357** and its CB[8] host is vastly improved over that for the smaller diameter CB[7] host. This is clearly seen in the 1.7×10^6 larger K_a value of $1.11 \times 10^{11}\,M^{-1}$ for CB[8] versus only $6.42 \times 10^4\,M^{-1}$ for CB[7]. The Avnir 0.83(2) S(C_8) mean distortion parameter for the *top* portals (with perturbing $^{+}NMe_3$) of the two symmetry-independent molecules points to a visually observed *structurally significant deviation* from ideal C_8 symmetry (see **359**) compared to the lower 0.25(9) mean value for the *bottom* portal (R. Glaser and A. Steinberg, unpublished results). Why should this be when the sterically challenged lower NMe_3 group exhibits a 2.56 Å close contact with a lower portal oxygen (i.e.,

$^{+}NC_{methyl}\underline{H}^{\delta+}\cdots{}^{\delta-}\underline{O}$=C) as evidenced by the 2.74 Å sum of O and H van der Waal's radii? The reason is the top portal's five strong $^{+}NC_{methyl}\underline{H}^{\delta+}\cdots{}^{\delta-}\underline{O}$=C and $^{+}NCC_{methylene}\underline{H}^{\delta+}\cdots{}^{\delta-}\underline{O}$=C electrostatic interactions (R. Glaser and A. Steinberg, unpublished results). What does this mean? These strong attractive attractions result in an *almost semicircular arrangement* of five top portal oxygens that appear to be pulled toward the N^{+}. The net result is that the *top* elliptical portal becomes *slightly pinched* (crimped) in the middle of its long axis (see top view **359**). This is seen in the larger disparate *top* portal's O–O 8.90 and 10.72 Å respective short and long elliptical axes' lengths versus the bottom empty portal's closer values of 9.40 and 10.32 Å. Detailed crystal structure analyses like these lie at the heart of the *Crystal Structure–Based Rational Design* method. A modeler cannot adequately suggest a new potentially bioactive molecule without understanding the bonding and nonbonding interactions in his learning set.

While a lot has been mentioned about host–guest bonding and nonbonding interactions, almost nothing has been said, as yet, of the space-filling aspects of these complexes. The interior's hydrophobic cavity has a propensity for maximal space filling by the guest's hydrocarbon skeleton concomitant with nondistortion of the host's interior walls by laterally protruding substituents (i.e., a type of hand-in-glove arrangement). Intimate space-filling interactions result from *dispersion forces* (the term used by computational chemists) between host and guest. Moreover, maximization of these forces engenders the most efficient liberation of all water molecules from the hydrophobic cavity (a very obvious important driving force for strong binding) (L. Isaacs, R. Glaser, K. Majerski, and coworkers, unpublished results).

16.3
Search for Unused Binding Sites

Now that the bonding and nonbonding forces have been ascertained from our learning set of crystal structures, we are ready to finish the initial stage of the technique and start looking for potential unused binding sites. Can you find any? Of course you can, since all of these structures (and other unpublished structures in our learning set) utilize only *one of the two portal faces.* OK, but what skeleton should we use? The $(2-4)\times10^{12}\,M^{-1}$ *teramolar* association constants of CB[7] with adamantane-1-NH_3Cl (**347**) and the corresponding quaternary-NMe_3 salt (**348**) make these guests an attractive starting point. Moreover, these high values suggest that the adamantane-1-NMe_3I guest's rigid skeletal framework already possesses the "bioactive conformation" BLYP-D/def2-SVP/COSMO=dft triple-zeta + polarization empirical dispersion, and COSMO implicit solvent geometry optimized models (P. Hobza, J. Hostaš, L. Isaacs, K. Mlinarić-Majerski, and R. Glaser, unpublished results.) of adamantyl primary (**360**) and quaternary (**361**)

cations residing within a CB[7] cavity clearly confirm that adamantane-1-NMe_3's cylindrical skeleton makes it an attractive candidate to begin the design of a new and improved guest.

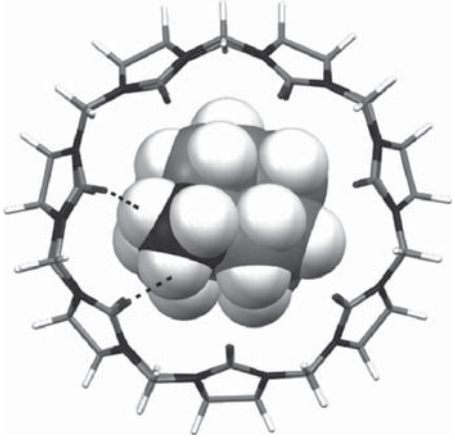

360

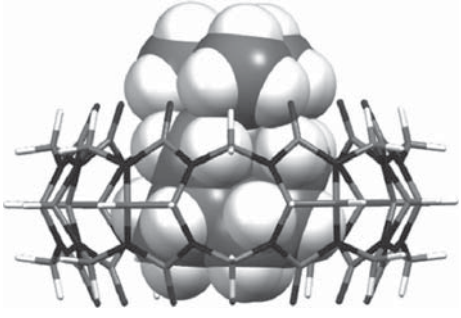

361

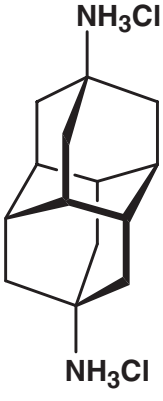

362

The *i*-symmetry disordered 3,5-diMe-Ada-1-NH_3Cl composite (**354**) provides the clue for the next design step. The obvious strategy should be to *utilize both portals* and thereby increase the binding affinity of our new guest. This approach is seen in the straight-chain primary ammonium versus alkane-α,ω-di(NH_3Cl) diammonium salts studied with CB[6] by Kim *et al*. [210] (see Refcode XUBYUP

structure). Space-averaged composite **354** gives an illusion of two-portal binding capability as expected for a diamantane skeleton with ammonium-groups at the 4,9-bridgeheads (R. Glaser and A. Steinberg, unpublished results). However, it must still be decided whether the bis-primary or bis-quaternary binding modes will be used in the design. The bis-quaternary binding mode wins out since it has the potential of both *above-portal* $^{+}NC_{methyl}\underline{\boldsymbol{H}}^{\delta+}\cdots{}^{\delta-}\underline{O}$=C and *below portal* $^{+}NCC_{methylene}\underline{\boldsymbol{H}}^{\delta+}\cdots{}^{\delta-}\underline{O}$=C interactions with *all* $2\times7=14$ portal oxygen atoms, while a bis-primary diammonium candidate can only hydrogen-bond to a limited number of 2–4 oxygen sites. The centroid of adamantane's *bottom six-member ring* (perpendicular to the C_3-axis) is 3.97 Å from N^+ in quaternary ammonium model **361** (P. Hobza, J. Hostaš, L. Isaacs, K. Mlinarić-Majerski, and R. Glaser, unpublished results). Adamantane is the archetypical member of the diamondoid family of molecules. Fusing a bottom six-membered ring in adamantane-1-amine with the corresponding ring in an inverted structure generates D_3d-symmetry diamantane-4,9-di(NH_3Cl) **362**, and diamantane-4,9-di(NMe_3I) **343**, whose $2\times3.97=7.94$ Å N^+-N^+ putative distance is able to span the 6.2 Å high inter-portal void [219]. This distance is very similar to that measured for composite **354**. Since the cross-sectional diameters of adamantane-1-NMe_3 **348** and diamantane-4,9-di(NMe_3) **343** are the same, the new guest should encounter little difficulty upon CB[7] portal entry. The mean $S(C_7)$ index of distortion from ideal C_7-symmetry for the two sets of seven portal oxygen atoms in DFT model **361** was found to be only 0.009(3), which testifies to an *extremely high* C_7 pseudosymmetry fidelity and gives assurance of a *nonelliptical very negligibly distorted complex.* (R. Glaser and A. Steinberg, unpublished results). Finally, the inversion center of the new guest should engender an auspicious juxtaposition of the two $^{+}NMe_3$ moieties above the portal planes to simultaneously enable $^{+}NC_{methyl}\underline{\boldsymbol{H}}^{\delta+}\cdots{}^{\delta-}\underline{O}$=C and $^{+}NCC_{methylene}\underline{\boldsymbol{H}}^{\delta+}\cdots{}^{\delta-}\underline{O}$=C interactions with *all* 14 C=$\underline{O}^{\delta-}$ units.

16.4
Primary Ammonium and Quaternary Aminium Binding Modes in CB[7 and 8] Complexes of Diamantane-4,9-Substituted Guests

Before we move on, let us take a close look at the crystal structures of CB[7]·diamantane-4,9-di(NMe_3I) **363**, and CB[8]·diamantane-4,9-di(NH_3Cl) **364**, Refcodes FITBIV and FITBAN [208], respectively. Our analyses of the CB[7]/CB[8] learning set complexes discussed earlier enabled the prediction that multiple $^{+}NC_{methyl}\underline{\boldsymbol{H}}^{\delta+}\cdots{}^{\delta-}\underline{O}$=C/$^{+}NCC_{methylene}\underline{\boldsymbol{H}}^{\delta+}\cdots{}^{\delta-}\underline{O}$=C electrostatic attractive interactions would be observed with appropriately spaced $^{+}NMe_3$ groups perpendicularly disposed above and below each portal plane and whose $^{+}N\cdots N^{+}$ C_3-symmetry axes would be collinear with the host's C_7 axis [208]. Fourteen $^{+}NC_{methyl}\underline{\boldsymbol{H}}^{\delta+}\cdots{}^{\delta-}$O=C interactions were indeed observed as evidenced by the

typical 4.38(7) Å $^{+}$N$\cdots$ O=C mean distances measured on both portals of **363**. The 90(7)° $^{+}$N$\cdots$ centroid(portal plane) $\cdots$ O=C mean angles testify to a perpendicular disposition of the C(4)–N^{+}/C(9)–N^{+} bonds to the portal planes. Similarly, as predicted by our structural analyses, the CB[8]·diamantane-4,9-di(NH_3Cl) **364** bis-primary ammonium nitrogens were indeed tilted by 36° from the pseudo C_8 axis.

How much are an additional set of interactions at a second portal worth in terms of K_a measured in 50 nm NaOAc-d_3 buffer (pD 4.74) for complexes comprising the appropriate *optimum diameter* CB[7] or CB[8] host? The answer should be different for multiple interactions involving the quaternary $^{+}NC_{methyl}H^{\delta+}\cdots{}^{\delta-}O$=C versus primary $^{+}$N–$H^{\delta+}\cdots{}^{\delta-}O$=C binding modes. The CB[7]·diamantane-4,9-di(NMe_3I) **363** complex's $1.9\times10^{15}\,M^{-1}$ K_a value [208] in buffer is *1110 times larger* than that of CB[7]·adamantane-1-NMe_3I (K_a $1.71\times10^{12}\,M^{-1}$) [211] **361**. This comparison is for *optimum space-filling* of diamantane-4,9-di(NMe_3I) within complex **363**. What happens if a larger-than-optimum host (e.g., CB[8]) is used for the comparison? The CB[8]·diamantane-4,9-di(NMe_3I) complex's K_a $2.0\times10^{12}\,M^{-1}$ value [208] in buffer is now only *21 times larger* than that of the CB[8]·adamantane-1-NMe_3I $9.7\times10^{10}\,M^{-1}$ K_a measurement [211].

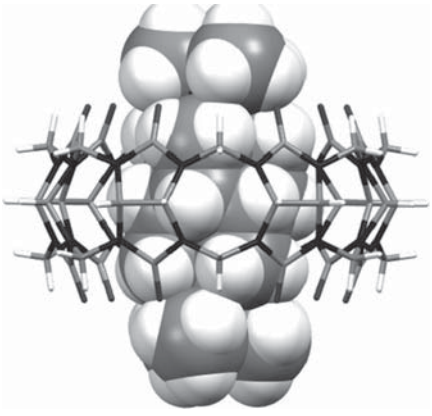

363

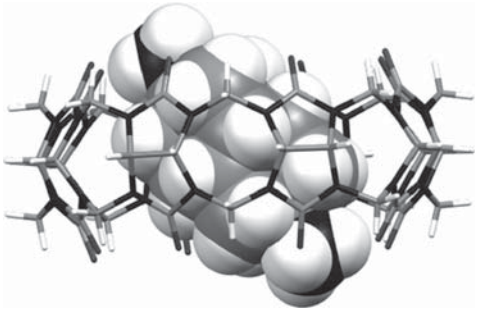

364

On the other hand, the CB[7] host's diameter is *too narrow* to enable the CB[7]·diamantane-4,9-di(NH_3Cl) complex's bis-primary guest to successfully tilt for *two-portal* hydrogen-bond formation. The resulting $1.3\times10^{11}\,M^{-1}$ K_a value [208] is actually *0.03 times smaller* than that of the CB[7]·adamantane-1-NH_3Cl **360** ($4.23\times10^{12}\,M^{-1}$) [211] K_a determination. However, if the host's diameter is then increased as in CB[8]·diamantane-4,9-di(NH_3Cl) **364**, then tilting for two-portal hydrogen-bonding is less constrained, and the K_a $8.3\times10^{11}\,M^{-1}$

value [208] becomes *1030 times* larger than that for the CB[8]·adamantane-1-NH_3Cl ($8.19 \times 10^8\,M^{-1}$) [211] K_a measurement. Bottom line: in the case of the diamantane guests in this study, each of the two binding modes has its own specific optimum host size for maximum rim C=$\underline{O}^{\delta-}$ interactions. When this proviso is met, then diamantane diammonium guest K_a values are about *1000* times larger than those for adamantane monoammonium binding to a single orifice irrespective of the binding mode.

The C_7 pseudosymmetry of the seven portal carbonyl oxygens is not distorted by the vertically disposed diamantane-4,9-di(NMe_3I) complexed within CB[7] (**363**) (R. Glaser and A. Steinberg, unpublished results). The multiple $^{+}NC_{methyl}\underline{\boldsymbol{H}}^{\delta+}\cdots{}^{\delta-}\underline{O}$=C and $^{+}NCC_{methylene}\underline{\boldsymbol{H}}^{\delta+}\cdots{}^{\delta-}\underline{O}$=C electrostatic attractive interactions actually introduce increased sevenfold rotational *order* into each portal, that is, an *induced fit.* How do we know this to be true? Certainly, it cannot be done by means of visual inspection. Three empty CB[7] molecular containers were arbitrarily chosen from the Cambridge Structural Database (CSD) (Refcodes FUYHIR [220] and IJINIZ (J.C. Berthet, P. Thuery, and M. Ephritikhine (2009) Private communication to the Cambridge Structural Database) mol A and B), and a 1.0(7) Avnir S(C_7) parameter was calculated for the seven oxygen atoms on each portal rim (R. Glaser and A. Steinberg, unpublished results). This large 1.0(7) S(C_7) parameter value for these empty complexes testifies to *structurally significant deviations* from an ideal C_7-symmetry rim oxygen arrangement, compared to a *38 times lower* 0.026(7) S(C_7) distortion parameter value for the filled CB[7]·diamantane-4,9-di(NMe_3I) complex **363** (R. Glaser and A. Steinberg, unpublished results). What does this really mean? Answer: in the absence of a guest, CB[7] rim oxygen atoms exhibit *very low fidelity* C_7-pseudosymmetry since they possess *positional freedom* (i.e., they exhibit a degree of flexibility due to lack of a strong cylindrical constraint within the cavity). It is likely that this flexibility aids diamantane-4,9-di(NMe_3I) **343** as it enters the CB[7] cavity under the attraction of electrostatic forces. A combination of seven $^{+}NC_{methyl}\underline{\boldsymbol{H}}^{\delta+}\cdots{}^{\delta-}\underline{O}$=C attractive interactions above the portal plane together with six $^{+}NCC_{methylene}\underline{\boldsymbol{H}}$ partially positively charged protons (0.95(2) Å below the portal plane) induce *nonstressing* 2.6(1) Å $^{+}NCC_{methylene}\underline{\boldsymbol{H}}^{\delta+}\cdots{}^{\delta-}\underline{O}$=C *short contacts* (see dark gray protons in **365**). These short contacts are only 0.1 Å shorter than the sum of their van der Waals radii and, hence, are quite gentle compared to lateral methyl groups rammed into the cavity interior walls in **352**, **353**, and **357**. On the other hand, the about 36° $^{+}N-{}^{+}N$ axis tilt required for optimum $^{+}N-\underline{H}^{\delta+}\cdots{}^{\delta-}\underline{O}$=C hydrogen-bonding distances causes the diamantane-4,9-di(NH_3Cl) **362** to elliptically *distort both portals* of the CB[8] host (i.e., 0.293 S(C_7)) testifying to *structurally significant deviations from the ideal,* see **364** (R. Glaser and A. Steinberg, unpublished results).

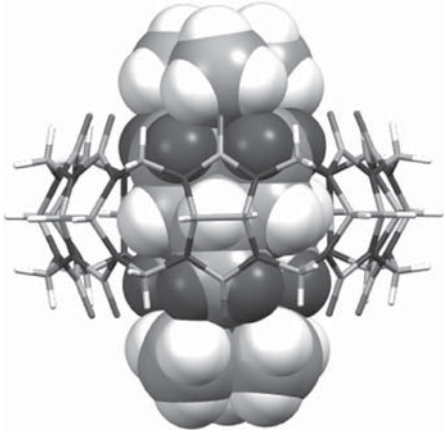

365

17
Helical Stereochemistry

17.1
Helical Stereochemistry

We have already seen that helicity, like tetrahedral atoms with four different ligands, is a *stereogenic element.* Of the eight symmetry operations, screw-rotation (rotatory-translation) is unique in that its "helical pathway" *usually* has a chiral sense (we will later see that achiral helical pathways are a very special case). This helical chirality is *always completely independent* of the chirality of the molecule (or unit) that undergoes the helical transformation from place to place. For example, *B*-DNA [221] (**366**) is a duplex of *right-handed antiparallel* chains (10 homochiral D-sugar·base units/1 complete turn of the helix), while *Z*-DNA [222] (**367)** is an *antiparallel left-handed* duplex formed in high salt concentrations (yet, the backbones of both contain the *same* D-2-deoxyribose sugar residues)!

Screw-rotation descriptors denote the handedness of the transformation (or lack of handedness in very special cases). Screw-rotation n_1 helix descriptors (e.g., 3_1, 4_1, 5_1, etc.) always define *right-handed* rotatory-translation operations with *clockwise-rotated tropicities* when viewed down the axis from close to far (from either end). Their screw sense is also designated as (*P* or +)-helicity. As noted earlier, screw displacement is a combined operation involving the components of *translation* and *rotation*. The n_1 right-handed descriptor means that the object is rotated clockwise by 360°/*n* and translated by the descriptor's inverse (i.e., "*1/n*"-th) times the unit cell length parallel to the screw axis. The unit cell length is one complete turn of the helical pathway (also known as the

Symmetry, Spectroscopy, and Crystallography: The Structural Nexus, First Edition. Robert Glaser.

Companion Website: www.wiley.com/go/Glaser/Symmetry

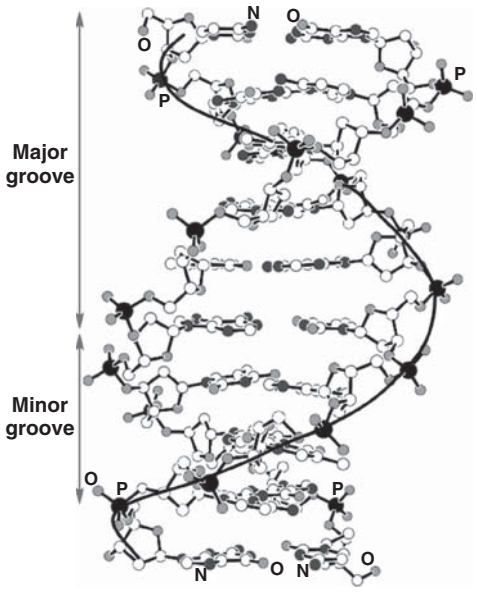

366

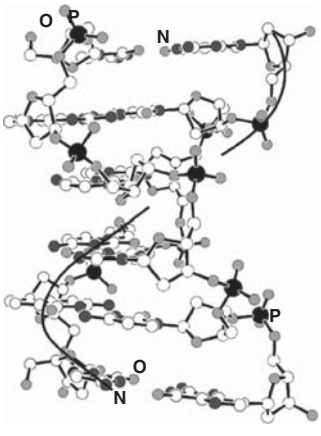

367

pitch height of the helix, *h* in drawing **368**). A triangle would be formed if one complete turn of a helix was excised out of the infinite array and then unrolled laterally. The *pitch* of the helix is arctan((pitch height)/(2 × helix diameter)).

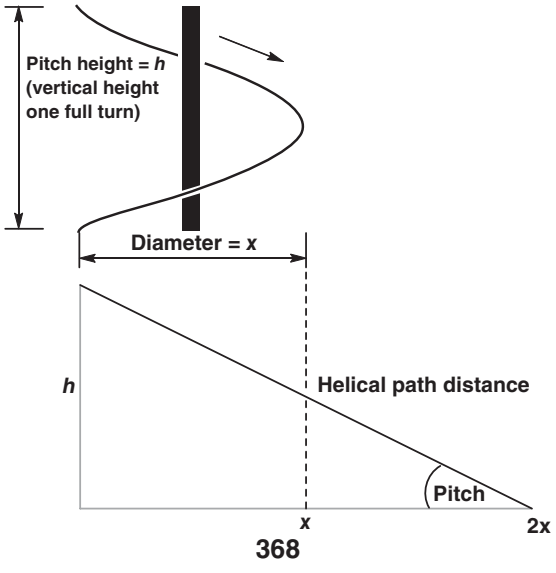

368

To construct a 3_1 screw displacement, arbitrarily start with position No. 1 in drawing **369**. A consecutive series of clockwise 120° rotations and translations equal to one-third of a full turn on the helix axis will bring us to position No. 2 (in front of the drawing plane), then on to position No. 3 (in back of the drawing plane), until we arrive at a new position No. 1 in the drawing plane. The order in which the two operations are performed is not important. The new position No. 1 has been translated along the helix axis by pitch height distance-*x* (i.e., one complete turn of the helix). It is relatively easy to see that continued application of the 3_1-screw operation will build up an ordered array of infinite repeat units in which no point remains invariant in space. This is the reason why all transformations based on *pure translation, rotation plus translation* (screw-rotation), or *reflection plus translation* (glide reflection) are to be found only in space groups. One vertical *x*-axis (helical axis) repeat unit designates a *unit cell* and encompasses half-No. 1 → No. 2 → No. 3 → half-No. 1 points from top to bottom. Periodic drawing **369** portrays three stacked adjacent unit cells within an infinite 3_1-helix.

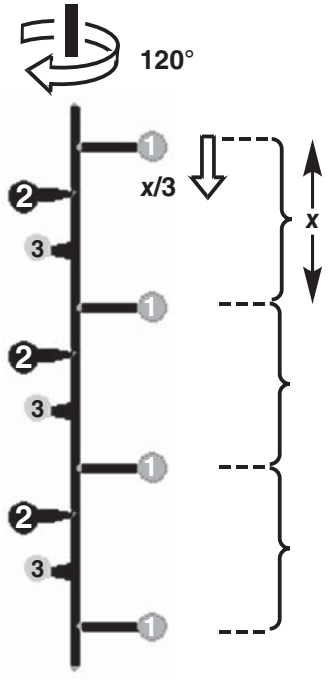

369

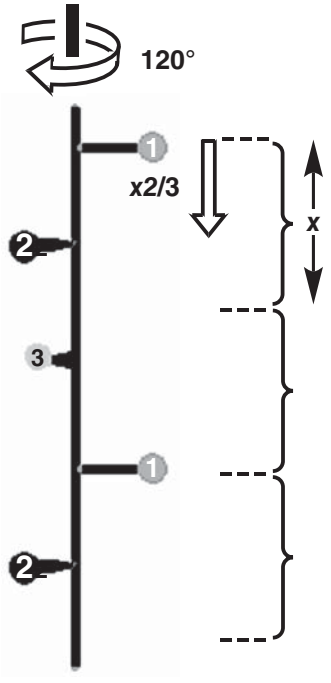

370

Enantiomorphous left-handed helices (*anticlockwise*-rotated when viewed down the axis from close to far) are affixed with n_{n-1} descriptors (e.g., 3_2, 4_3,

5_4, etc.). They are also designated as (*M*, −)-helices. However, an *extremely important point* to note is that in *all* symmetry operations, the tropicity of rotation operations is *arbitrarily, but always consistently, in a clockwise direction.* As a result, the *initial set* of three 3_2 generated points gives the *illusion* of being an "elongated" right-handed helix whose pitch height is twice as long as that for 3_1 (see **370**). The reason for this is that the translation was equal to two-thirds of a full turn on the helix axis to bring us from the top to position No. 2 in **370** (still in front of the drawing plane), and then on to position No. 3 (in back of the drawing plane), until we arrive at a new position No. 1, which has been translated by *distance-2x* along the helix axis. Careful inspection of **370** shows that there clearly is something amiss with the *periodicity* of the new helix (position No. 3 resides in the *second* periodic unit, and translated position No. 1 is located between the *second* and *third* periodic units). Since we are dealing with a space group operation, the contents of every unit cell *must be identical* to that of every other within the extended array. But this is clearly not the case. Point No. 3 in the middle unit cell does not exist in the highest unit cell. Point No. 2 does not exist in the middle unit cell. Also, point No. 1 between the middle and lowest unit cells is not present between the highest and middle unit cells. To rectify this periodicity problem, the missing points must be *added* so that the contents of each unit cell will be invariant. In other words, points No. 3 and new No. 1 in **370** must both be *translated upwards* by distance *x* into the original (upper) unit cell by (see **371**). The original numbering of the points in drawing **370** is then renumbered as in **372.** When this is performed, (i) the contents of all three unit cells in the drawing will be identical and (ii) the actual tropicity of the 3_2 helix is now *anticlockwise* (see **372**). Bottom line: a rotation of $-120°$ (disallowed in symmetry) gives the same result as an allowed rotation of $\underline{+2} \times 120° = 240°$.

Another extremely important point must also be emphasized. The 3_1 arrangement of *point positions* in **369** and the enantiomeric 3_2 arrangement of these *point positions* in **372** have nothing to do with either connecting them together one after the other (i.e., ligation) or with their connectivity to a central support pole as if one is dealing with spiral staircases. In drawings **369**, **372**, the points just happen to be arbitrarily drawn as being attached to the vertical axis line as an illustrative heuristic device. In actuality, the axis line is *imaginary* but the point positions are *real.* What does this mean? It means that the 3_1 arrangement of points in **369** and the enantiomorphous 3_2 spatial arrangement in **372** remain even when the imaginary axis line and wedges in the drawings are erased (i.e., so that the points just *float in space*). Therefore, molecules "floating in space" at defined positions constitute a helical arrangement within a real crystal. They can be thought of as steps of a spiral staircase magically *levitating in space* without any physical connection to a central pole for support. The same exact helical symmetry arrangement will exist if the molecules are bound together as in a polymeric chain. The ligation

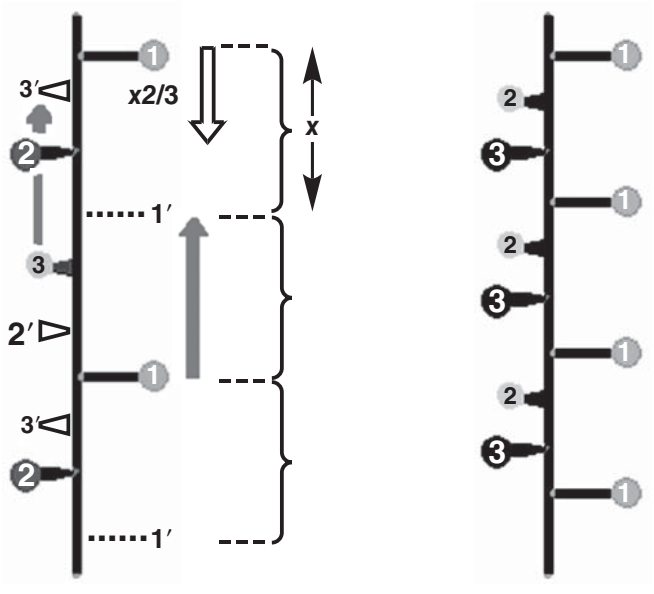

371 372

of monomer residues is only a *chemical constraint* completely unrelated to the symmetry relationship of the polymer. Similarly, the central pole in a spiral staircase is only a *mechanical constraint* unrelated to the symmetry arrangement of the steps themselves.

17.2
$2n_n$-Symmetry Achiral Helical Pathways

What about the special case of achiral helical arrangements alluded to earlier? These achiral helices exhibit $2n_n$ descriptors, that is, the standard "n_m" descriptor, where $n = 2n$ and $m = n$ (e.g., 2_1, 4_2, 6_3, etc.). With the exception of the prototypical achiral 2_1 single helix, all the other higher "homologous" examples of this family represent *multiplexes* (i.e., duplexes (double helices), triplexes, etc.). In other words, these descriptors of multiplexes are affixed to *inherently achiral pathways* of monomeric subunits within *intertwined n*-multiple screw arrangements. The operative concept is that a C_n-axis must be *coincidental* with the $2n_n$-axis. These $2n_n$ pathways only become chiral when the subunits are constrained by *chemical*

ligation to each other (e.g., (X–X–X–X), etc., polymers/oligomers) into *n*-helical strands of *parallel* strands within double-, triple-, or multiple-stranded polymers. In other words, it is only the *chemical ligation* (for molecules) or *mechanical connectivity* (for objects) that imposes chirality to a $2n_n$ arrangement. Moreover, we will see that the ligation/connectivity can be made by one of two ways to engender either two homotopic intertwined C_n-related $2n_1$ ***right-handed*** helices or two $2n_{n-1}$ ***left-handed*** helices.

Consider the four "quarter-sphere" asymmetric units of a 4_2-helix to be spatially disposed as in **373**. Do not be overly concerned that the quarters do not look asymmetrically chiral since we are using a modicum of artist's license in order to illustrate a concept. According to the 4_2 screw rotation descriptor, asymmetric unit *black*-1 quarter is rotated $360°/4 = 90°$ and then translated $2/4 = 1/2$ of the length of the helix axis so that it is transformed quarter-sphere *black*-2. The C_2-axis (coincidental with the 4_2-helical axis) further transforms black-1 into white-1 and black-2 into white-2. Next, if we desire to connect a top quarter apple with a bottom unit (via *mechanically constraining* them with cyanoacrylic "super-glue"), then notice that there are two possibilities (see **374**). Option one is to fuse black-1

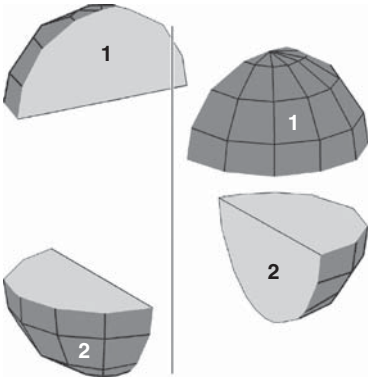

373

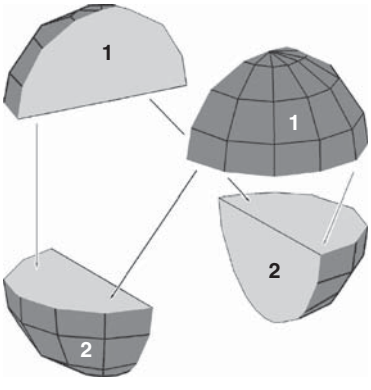

374

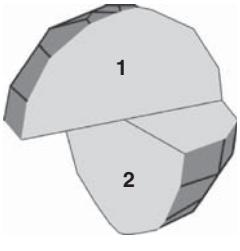

375

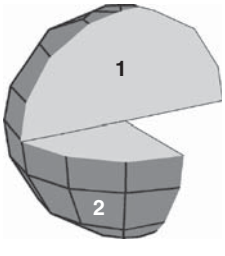

376

to black-2 via the black arrow to produce a *right-handed* helical construct **375**. But, one could have just as readily connected black-1 to white-2 via the gray arrow to form a *left-handed* helical building-block **376**.

Next, let us consider a pair of two right-handed helical building blocks (black-1 fused to black-2) and (white-1 fused to white-2) as in **377**. One may form a sphere consisting of two *homochiral* halves if the two helical constructs are *laterally intermeshed* together (see **378)**. Notice that the same sphere is formed if one pushes all of **373**'s four asymmetric units inward to the center (see 4_2 unit cell **379)**. If we disregard the superglued 1/8-th overlapped sections, then the achiral spatial arrangements of the four subunits in both spheres are *identical.* In other words, **378**'s two *mechanical constrained* chiral right-handed constructs (white-1/white-2) and (black-1/black 2) have the same identical 4_2-symmetry as **379**'s four subunits *levitating in space.* By this we mean that mechanically constraining two subunits to join is *not a symmetry operation* and, thus, has nothing to do with the subunits' 4_2-symmetry spatial relationship.

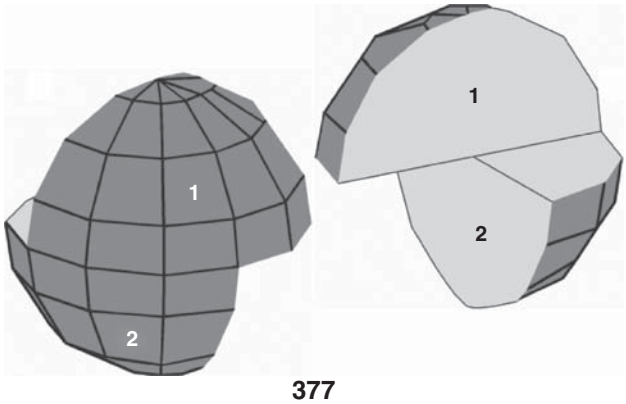

377

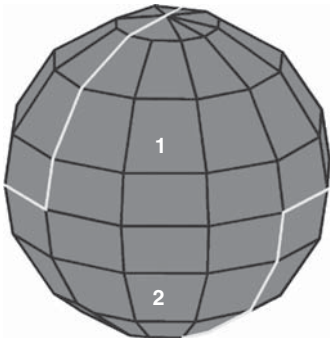

378

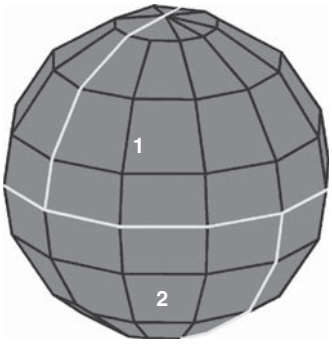

379

The next step is take the mechanical constraints into consideration and ask ourselves "if both (white-1/white-2) and (black-1/black-2) are right-handed helical building-blocks, then what is their geometrical relationship when they laterally *intermesh* to form a sphere?" The two homochiral constructs become intimately nestled around the 4_2-helical axis (and the coincidental C_2 axis) to form a 1/2-turn of a *parallel* homotopic right-handed double-helical assembly **378** unlike the *antiparallel* DNA duplex. Notice that one could have just as easily produced an enantiomorphous *parallel* left-handed double helix from (black-1/white-2) and (white-1/black-2) constructs. Finally, let us vertically stack (white-1/white-2) on top of (black-1/black-2) (see **380)**. Begin at white-1 and then diagonally transit 90° clockwise to white-2, and another 90° clockwise diagonal motion to black-1, followed by yet an additional 90° clockwise diagonal passage to black-2 to sweep out a one full-turn 4_1-helical pathway (**380**). In other words, the (white-1/white-2, **380**-*top*) 1/2-turn helical unit is the *vertical continuation* of its (black-1/black-2, **380**-*bottom*) 1/2-turn helical partner within the 4_1 stack. This is due to the coaxial C_2-axis within the four asymmetric unit's 4_2-symmetry arrangement.

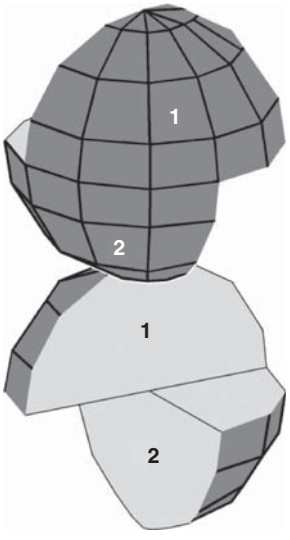

380

Are there chemical examples of $2n_n$ arrangements? The answer is indeed yes. In molecular biology, the poly(rA)-poly(rA) parallel double helix is just such a case [223]. A full turn of the biopolymer duplex consists of two 8_1-symmetry parallel strands. However, this is NOT the unit cell repeat unit. The 1/2-turn *tetranucleotide* 4_2-symmetry double helix is the polymer's *translational repeat*

unit (unit-cell, **381**), and its asymmetric unit is a *single dinucleotide* 1/4-turn segment. If the repeat unit is *excised* out of the polymer, then the *intertwined tetranucleotide* strands are said to be *nonplectonemically* coiled since the four base-pair duplex segment enables facile strand *separation without prior*

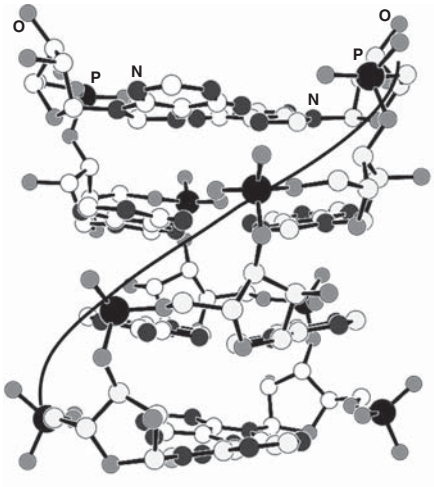

381

382

383

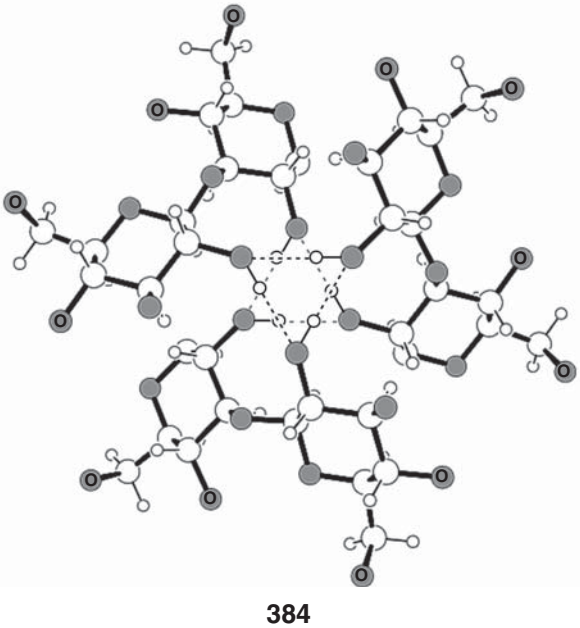

384

unwinding [224, 225]. This is not the case with DNA-like antiparallel unit cells of one full turn (although there probably is no biological significance to this observation). Another very important structural feature to stress is that **381**'s vertical C_2-axis not only results in homotopic symmetry-related poly(rA) strands, but also *equivalences the two grooves* themselves. The identical grooves and the 1/2-turn repeat unit of a *stylized* 4_2 duplex are depicted in drawings **382** and **383**, respectively. This is in marked contrast to the diastereotopic major and minor grooves of B-DNA (see **366**) and in the more stereoregular double-helical poly(dA-dT)-poly(dA-dT) [226] analogue. Similar to the mechanically constrained helical units **377**, ligation of the rA monomers is a *chemical constraint* that is also irrelevant to the 4_2-symmetry of the homopolymer duplex.

A similar example to poly(rA)-poly(rA) is the repeat unit of the polysaccharide Curdlan [227], a 6_3 triplex of intertwined parallel $(1 \rightarrow 3)$-β-D-glucan chains [224, 225]. The 1/3-turn unit cell is composed of three disaccharide units. The monosaccharide asymmetric unit undergoes a 60° rotation (360°/2*n*) followed by a translation of $n/2n = 3/6 = 1/2$ of the unit cell. The C_3-axis, coincidental with the 6_3-helix axis, then generates the two other disaccharide residues. A layer of three laterally related monosaccharides constitutes an $R_3^3(6)$ hydrogen-bonded ring graph set (see **384**). Similar to the 4_2-duplex example, stacking disaccharide units one on top of the other generates one full turn of a single 6_1- or 6_5 helix.

17.3 "*La Coupe du Roi*": Chiral Apple Halves Produced by a 4_2-Bisection

As noted by Mislow [228], the well-known French stereochemist Alain Hoareau performed a parlor trick known as *la Coupe du Roi* (the King's or Royal cut) during the first Bürgenstock Conference on Stereochemistry in May 1965. One vertical half-cut from the top to the equator (**385**) is made into an apple (idealized as sphere). The original K_h-symmetry is then lowered to C_s. A second vertical half-cut, 90° from the first slice, is then made from the bottom up to the equator. The symmetry of the double-cut apple is now D_{2d} (**386**). The final steps are two consecutive clockwise **387** (or two anticlockwise **388**) *nonadjacent* equatorial quarter-cuts that produce two 90° arcs. The chiral sense of the pair of C_2-symmetry apple halves is determined by the tropicity of these two lateral quarter-cuts. The net result of the Coupe du Roi bisected assembly **378** is that all symmetry transformations inverting the handedness of the two half-subunits (i.e., those of the Second Kind) have been effectively removed from the original sphere. The C_2-axis between the pair of chiral apple halves obligates them to be *homochiral* (see the **377** pair).

385

386

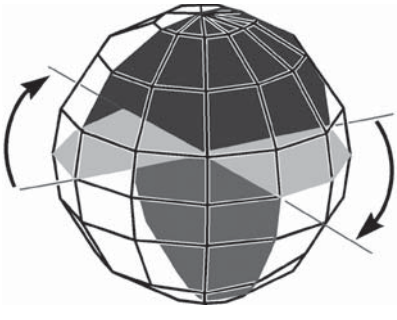

387

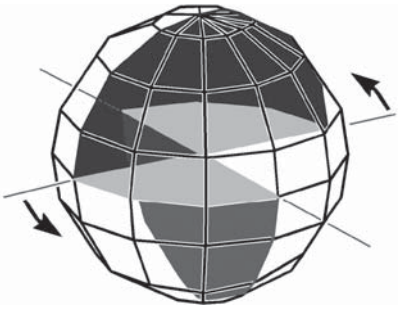

388

Kurt Mislow (after a trip to Paris to see Hoareau) challenged his group to find some chemical relevance to La Coupe du Roi during one of the weekly meetings in Princeton in 1978. The result was three very different approaches to this subject. Franco Cozzi returned to Italy and published, along with Cinquini *et al.* [229], an elegant chemical analogue of a Coupe du Roi bisection. Achiral *cis*-3,7-dimethyl-1,5-cyclooctanedione (C_{2v}-symmetry, **389**) was transformed via a double Baeyer–Villiger oxidation into a diastereomeric mixture of chiral (±)-*cis*-4,9-dimethyl-1,6-dioxacyclodecane-2,7-dione (C_2-symmetry, **390**) and an achiral C_s-symmetry constitutional isomer **391**. The two products were readily separated by column chromatography, and then the racemic ring-enlarged diester **390** underwent subsequent $LiAlH_4$ reduction to yield two *identical* molecules of asymmetric (2-methyl-1,4-butanediol, **392**). One should not be concerned that diol **392** is racemic since each (+)-or (−)-diester only affords homochiral diols. Had the Italian chemists so desired, they could have reduced the separated **391** and obtained a 2-methyl-1,3-propanediol and 3-methyl-1,5-pentanediol product mixture.

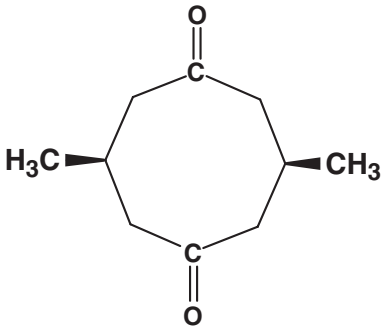

389

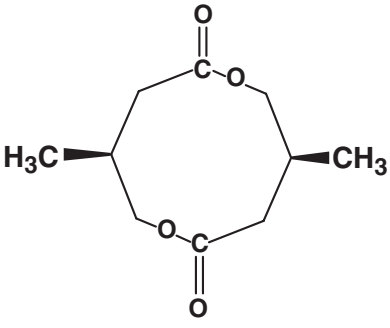

390

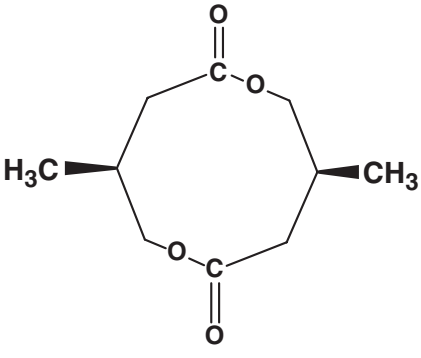

391

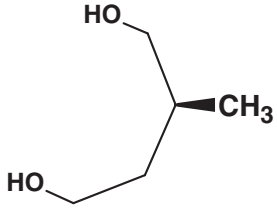

392

Five years earlier, Anet, Mislow, and coworkers [230] published a *retro* Coupe du Roi example inspired by the observation of *chiral discrimination* in ensembles composed of either a pair of C_2-symmetry *homochiral apple halves* or a pair of C_i-symmetry *heterochiral* enantiomorphs. In the Mislow–Anet work, an achiral C_{2v}-symmetry *cis*-dimer was produced in a stereospecific manner by self-coupling of (+)-4-(bromomethyl)-6-(mercaptomethyl)[2.2]metacyclophane [230]. On the other hand, self-coupling between a pair of enantiomers in a racemic mixture produced the diastereomeric C_{2h}-symmetry *trans*-dimer [230]. This same chiral discrimination has been seen already when the homochiral pair (**377**) reforms the original D_2-symmetry bisected apple, but the highest symmetry that the heterochiral pair (**375**, **376**) can exhibit is a C_i-symmetry assembly.

Another intriguing aspect of La Coupe du Roi is the symmetry basis for the homochirality of the halves produced by the apple's chiral bisection of an achiral object. Plexiglas (Perspex) Coupe du Roi cubes were constructed to eliminate undesirable rapid air-oxidation of cut apples (R. Glaser, unpublished results). One

evening, a chiral right-handed half-cube was translated upward and its bottom vertically stacked upon its partner's head to afford a very amazing (and *totally unexpected*) right-handed 4_1-summetry full-turn helical segment **380** [224, 225]. With this knowledge in hand, a literature search for 4_2-symmetry duplexes and 6_3-symmetry triplexes uncovered the two chemical examples discussed earlier (**385** and **388**). During a later scientific visit to Cordoba, Argentina (2007), the lapidary artisan Sr Miguel Castillo was requested to produce a set of very esthetically pleasing lapis lazuli blue-color Coupe du Roi oppositely cut cubes (see 4_2-symmetry **393**) that readily separated into homochiral halves (**394**) and then could be stacked (**395**).

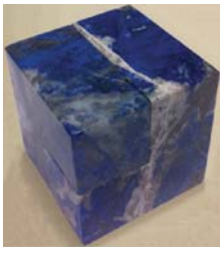

393

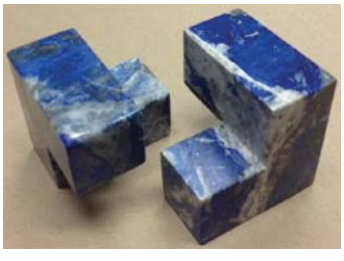

394

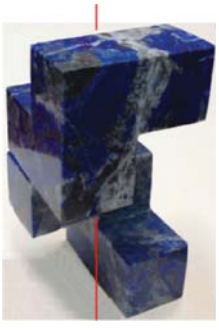

395

The chemical relevance of the Coupe du Roi apples is that they represent a readily obtainable model for $P2n_n$ space group unit cells of parallel $2n_n$-multiplexes. With dexterity (and a modicum of practice), an apple can be trisected to afford a 6_3-triplex assembly of homochiral apple thirds. On a very practical level, most of the time our daily laboratory successes cannot be readily communicated to the important (nonchemist) people sharing our daily lives. A common bond with our audience can be created by an impressive after-dinner demonstration of chiral apple cutting and a brief explanation of its chemical and symmetry significance. Try it out.

17.4 Intermeshing Molecular Threefold Helices: Symmetry, Chemical, and Phase Considerations

We have discussed the handedness of intertwining multiplexes in the previous chapter, but what about a *braid*? It is something we all know, but can one describe its handedness? Photograph **396** is a 10-wick Havdalah candle composed of five braided twinned-candle strands lighted by Hebrews on Saturday night to signify the separation of the Sabbath from the beginning of the secular week. A careful

inspection shows that the braiding process *reverses the handedness* of each strand.

Both heterochiral and homochiral screws can *intermesh* in the macro world. This intermeshing is the well-known "tongue-in-groove" phenomenon of stationary objects and gears. Like the nestling of ensembles of homochiral apple halves noted earlier, it also represents another classic example of *chiral recognition* (otherwise referred to as *chiral discrimination*). Heterochiral single helices (*M*- on the left and *P*- on the right in **397**) readily *intermesh over their entire length* to form a construct with parallel axes. Homochiral single helices undergo only *local intermeshing* in which the axes are skewed (**398**). Plastic models show that a mirror-image heterochiral pair arrangement must have the *phase* of one of its partners changed by 120° to enable lateral intermeshing.

396

397

398

Similarly, C_3-symmetry gear wheels also show chiral discrimination in which a heterochiral pair intermeshes over its entire length (**399**) and exhibits parallel axes, while the tongue-in-groove interaction is *localized* in the homochiral analogue **400**. Drawing **401** depicts a heterochiral C_{2h}-symmetry mirror-image arrangement of laterally abutting triple-helices that has been desymmetrized to *i*-symmetry by coloring the three strands (or tongues) of one end of each triple-helix black. The two enantiomorphous nonpalindromic helices are *out of phase* and, thus, clearly cannot undergo intermeshing. Comparison of **399** and **401** will show that the *M*-triple helix on the left in **401** has to be rotated by 60° to enable the intermeshing depicted in **399**. Note also that a phase change is a *mechanical constraint* and *not a symmetry operation.* Successful lateral intermeshing in

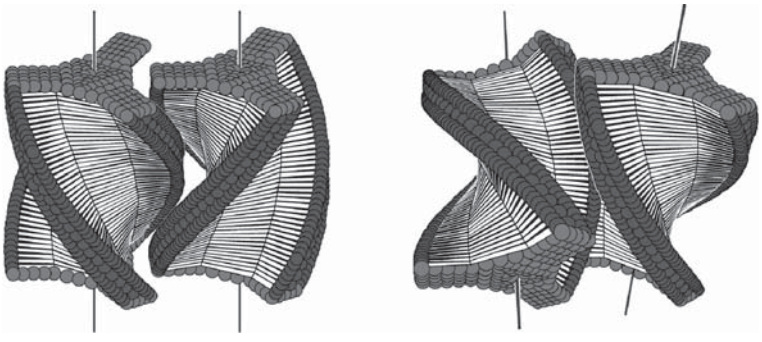

399 **400**

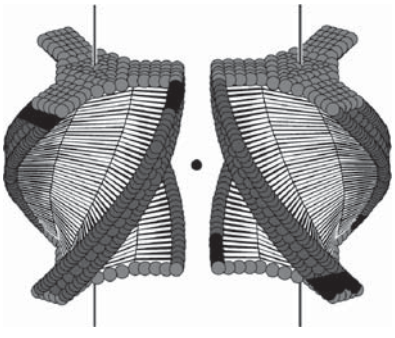

401

399 results in the loss of the inversion relationship in **401** and has removed all symmetry equivalence between the two triple helices, thereby making them *diasteromorphous* when intermeshed.

The remainder of this section discusses an elegant chemical example of intermeshing triple helices. It is based upon the preparation, by David Perkins and Leonard Lindoy (University of Sydney), of a cage compound with a tripod-type cap at each end (**402**). The relatively flexible free ligand was achiral as shown by two methylene-proton *time-averaged singlet* resonances at either 298 or 318 K: δ 2.80 (C$\underline{\boldsymbol{H}}_2$N–) and δ 5.02 (C$\underline{\boldsymbol{H}}_2$O–) [231, 232]. The *dynamic enantiotopic* relationships result in isochronicity for each set of methylene protons as a result of rapid conformational interconversion affording time-averaged D_{3h} symmetry. The ligand then becomes rigid as a result of divalent metal (Ni^{II}, Cu^{II}, Fe^{II}, and Mn^{II}) binding to the three *o,o′*-bipyridinyl units to produce a tris-chelate three-bladed propeller with chiral (Δ,Λ)-geometry. The chiral propeller's (Δ,Λ)-helicity then induces the appropriate twist sense into each of the salicyl terminal units on either side whereby enabling the entire molecule to concertedly coil into a short triple-helical rigid unit (**403**, **404**).

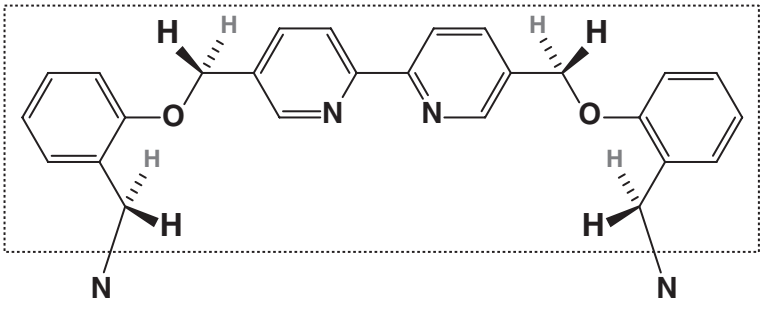

402

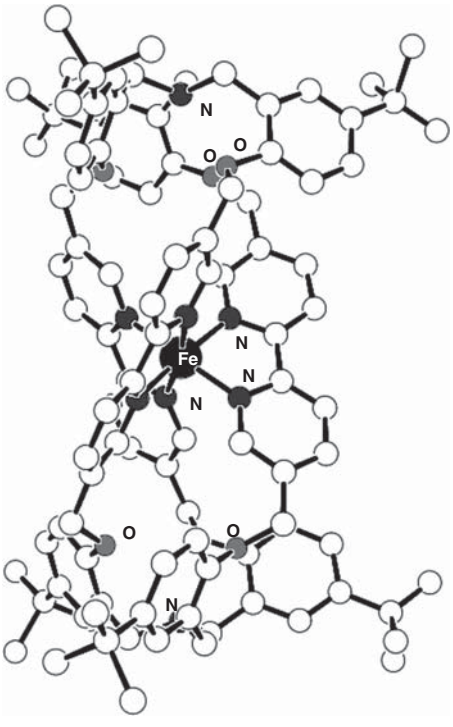

403

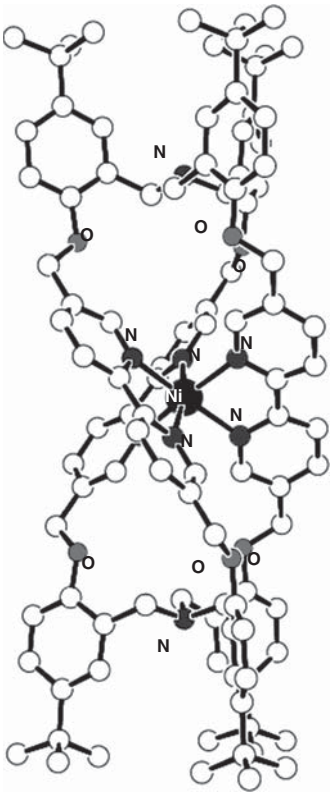

404

Ligation of Fe^{II} to the cage ligand (or to its open-end noncapped dialdehyde precursor) generated a chiral complex whose ^1H NMR shows AB-quartets that now testify to the presence of chemical shift nonequivalent methylene protons, that is, a chiral molecule. The methylene-proton's anisochronicity was attributed by the Australian group to a *fixed conformation* in the case of the cage-complex and to *restricted rotation* about the Ar–C$\underline{H_2}$–O bonds in the open-end dialdehyde (nontripod capped) precursor [231, 232]. However, there is absolutely no need to propose a "restricted rotation" argument since the chiral propeller rigid geometry of the dialdehyde metal-complex generates diastereotopic AB-methylene protons even under conditions of complete rotational freedom about the unconstrained aforementioned bonds.

Structures **403** and **404** (Refcodes ECAKAV [232] and IRACIN [231]) depict the respective Fe^{II} and Ni^{II} complexes as determined by *X-ray* crystallography. The Mn^{II} and Cu^{II} complexes are isostructural with their respective **403** and **404** analogues. Inspection of the structure's termini shows two structural types differing in the *syn-/anti*-tropicity of the tripod's lone pair toward the metal and concomitant *tert*-butyl *exo-/endo*-orientation (see **405** and **406**). One can imagine a downward force on the *anti-to-metal* tripod nitrogen lone-pair resulting in the parallel-to-axis *endo*-oriented *tert*-butyls (Ir^{II}/Cu^{II}, **406**) springing outward to more sterically demanding lateral *exo*-dispositions in the *syn-to-metal* tripod nitrogen lone-pair Fe^{II}/Mn^{II} complexes **405**. This explanation appears to be consistent with the finding that **407**'s asymmetric unit contains a dimer of two heterochiral helical intermeshed units, whereas the steric barrier of the *laterally exo*-oriented *tert*-butyls in the **405** complex most likely prevents intermeshing.

Inspection of the beautiful Ir^{II} (IRACIN, **407**) intermeshed crystal structure provided the impetus for a detailed stereochemical study of the crystal structure [233], since this was lacking in the literature. Analysis of the structure showed that eleven 5.6(7) Å $centroid_{helix\text{-}A}\cdots centroid_{helix\text{-}B}$ mean distance *edge-to-face* aromatic–aromatic electrostatic interactions were responsible for the intermesh phenomenon in **408**. These omnipresent interactions in protein structures have been extensively commented upon by Burley and Petsko [136].

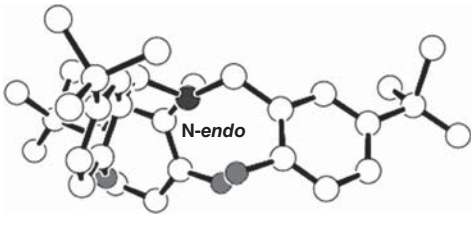

405

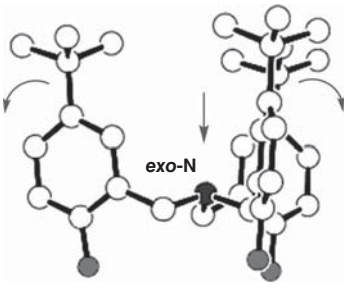

406

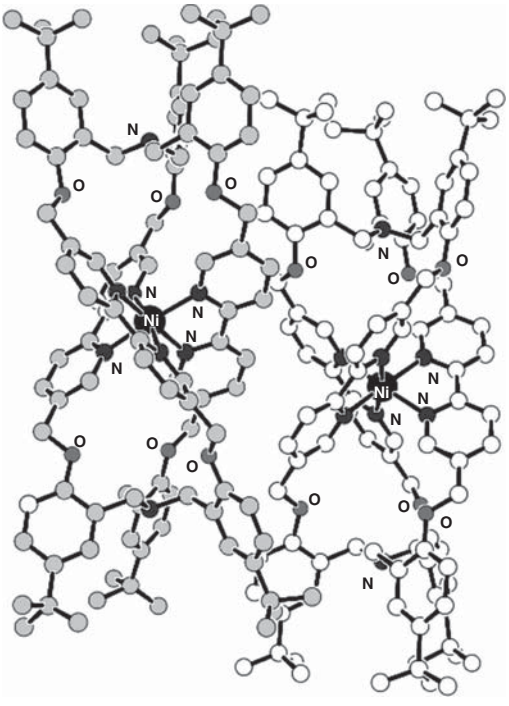

407

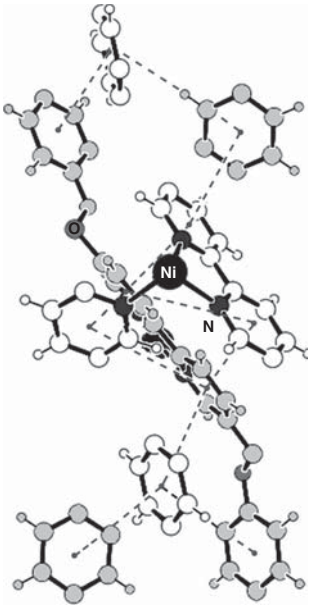

408

The first point that had to be addressed was "were the intermeshing helices **407** related as enantiomers" as claimed by the Lindoy group in their first article of 2004 where it was stated "*one enantiomer slots into the groove of the complementary enantiomer*" [231]. In the second article, it was written "*two crystallographically independent complexes, each located on a threefold axis and having opposing helical twists … define a dimeric unit*" [232]. However, from this present text, it is very clear that symmetry relationships may *not* exist between multiple molecules within an asymmetric unit by definition, no matter if it resides within a kryptoracemate chiral crystal or in **407**'s trigonal $P\bar{3}$ space group achiral crystal. Therefore, logically, the dimer is simply composed of two oppositely handed similar structure diastereomers.

Let us take a close look at IRACIN's 60° *acute* angle rhomboid-base prism unit cell, ($Z = 4$, $Z' = 0.67$, and $Z/Z' = 6$) (see **409**). Sides $a = b$, and the unique unit-cell length c is perpendicular to the rhombic base. The 120° *obtuse angle* of the rhomboid base may be mentally bisected so that the unit cell now contains two parallel adjacent equilateral triangular subprisms sharing a common face containing the short diagonal. The *center axis* of each prism (parallel to side c) is a threefold rotation axis (see **409**). Each intermeshed triple-gear molecule occupies a *different* special position of threefold rotational symmetry (hence $Z' = 0.67$), i.e.

each occupies a different laterally adjacent C_3-axis. *Centers of inversion* coincide with the midpoints at each of the five rectangular sides, and obligate the gear-like molecules to be heterochiral. The cell's four *c* sides are also threefold rotation-axes and inversion centers are located at their midpoints. In other words, the *c*-sides are *inversion* triads (*rotoinversion* axes, that is, the coincidence of an inversion center on a C_3-axis). The coincidence of a three-fold rotation and the inversion center is depicted by a special symbol consisting of a white equilateral triangle with a dot at its center. Noncoordinating $[PF_6]^{-1}$ anions occupy special positions of rotoinversion symmetry on these axes, plus one general position.

If only one triplex occupied a different special position of threefold rotational symmetry and they were related by the inversion center on the common diagonal face between them, then the volume of the unit cell would comprise one *d,l*-pair, that is, two specially positioned triple-helices, and the asymmetric unit would be only one-third of a single molecule: $Z = 2$, $Z' = 0.33$, $Z/Z' = 6$. But, how would these enantiomers intermesh? They could not be laterally adjacent to each other since there would be a *phase mismatch* as in **401**. One of them would have to move one-quarter of the *c*-distance *upward* on the equilateral subprism's central C_3-axis while the enantiomer moves one-quarter of the distance *downward* (see **410**) in the subprism's lateral neighbor. In this manner, the inversion center on the midpoint of the common face between the two subprisms would indeed relate the molecules as *bone-fide* enantiomers that could intermesh. However, the electrostatic interaction nature of the *interhelical glue* has already been discussed. So, how reasonable is it for a *d,l*-complex to share only a common one-half molecule-length intermeshing region? Answer: not very reasonable at all! Obviously, the greater the overlapping intermeshing region, the larger the number of possible edge-to-face interactions. In addition, unacceptable void regions would be created within the crystal.

Moreover, the crystallographer notes that actual unit-cell volume holds *four* specially positioned C_3-symmetry molecules, so $Z = 4$, $Z' = 0.67$, $Z/Z' = 6$. We already know that the asymmetric unit comprises two diastereomeric one-third molecules since this is what is observed. There is a distinct advantage that homochiral helices be vertically stacked upon a single triangular sub-prism's central C_3-axis. Why? If there is a ~60° phase difference *mechanical constraint* between the two differently colored stacked homochiral triplexes as in **411**, then the inversion center on the rectangular face common to the two triangular subprisms will now generate the enantiomeric stacked pair on the C_3-axis of the second subprism. Is this good? It is not only good, but wonderful! Why? If the interaxial distance is appropriate (and it is due to the many electrostatic edge-to-face interactions, that is, a *chemical constraint*), then two *laterally adjacent* one-third (*P*)-A and (*P*)-B units will have the auspicious 60° phase difference required to intermesh over almost all their entire lengths (actually ~90% of their length since there is no symmetry requirement that it be 100%). In this manner, we now understand why the unit cell contains $Z = 4$ complexes [(*P*)-A, (*P*)-B, (*M*)-A, (*M*)-B], the asymmetric unit $Z' = 0.67$ (e.g.,

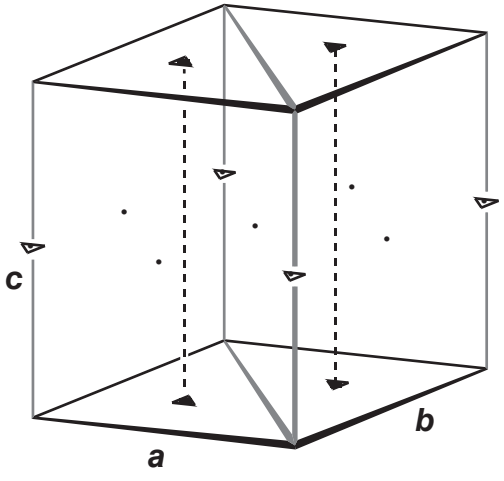

409

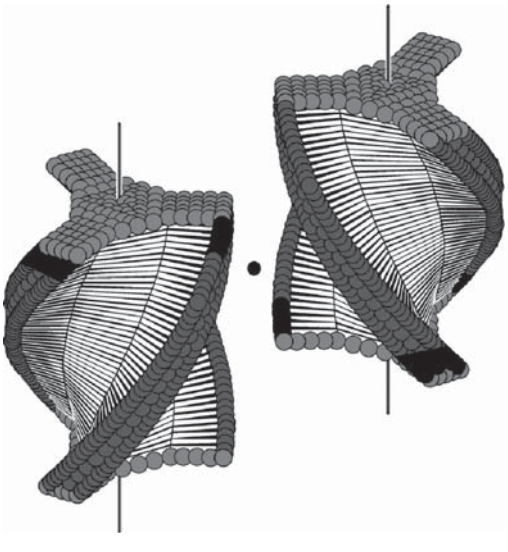

410

0.33 (*P*)-A plus 0.33 (*P*)-B), and $Z/Z' = 6$ required by the $P\bar{3}$ space group symmetry.

The story gets even better. The Australian group's description of the complexes as a *dimer* is really a gross underestimation. Why? Answer: the C_3-axis makes the three strands ("tongues") and three grooves of each molecule symmetry equivalent. Figure it out. In other words, each (*P*)-A complex has three intermeshed (*M*)-B neighbors, and in turn, each (*M*)-B neighbor has

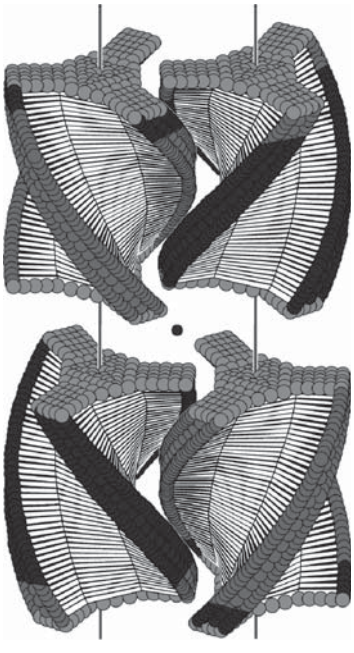

411

three intermeshed (*P*)-A complexes. Therefore, the crystal is a *supramolecular* self-assembly of intermeshed (*P*)-A:(*M*)-B complexes sandwiched between *inversion-symmetry* related layers of enantiomeric (*M*)-A:(*P*)-B moieties and vice versa. Nature indeed has an elegant esthetic sense of crystal engineering, and what a pity not to tell the story.

Finally, what are the odds of finding a crystal exhibiting homochiral intermeshing? After all, the crystallization solution was a racemic mixture of triple-helix chiral complexes. Answer: not very high since the crystallization process is under thermodynamic control. We know that parallel axes of two heterochiral crystalline complexes enable intermeshing along most of the helices' length. But, on the other hand, homochiral helices are expected to be less stable since their edge-to-face intermeshing can only occur within a limited local region. This is another elegant example of chiral discrimination.

17.5
X-Ray Fiber versus Single-Crystal Diffraction Models

In 2013, an atomic-resolution single-crystal structure of an oligo(rA)-oligo(rA) 11-mer was published by Safaee, Wilds, Sheldrick, Gehring, and coworkers [234]

(Protein Data Bank entry 4JRD), and the homotopic grooves predicted 50 years earlier by fiber diffraction [223] of poly(rA)-poly(rA) were indeed observed. The molecule crystallized in the $P4_12_12$ tetragonal chiral space group and occupied a general position of symmetry. The asymmetric unit contained one complete double helix of parallel 11-mer strands and exhibited segments of 4_2 *pseudo*symmetry tetranucleotide duplexes. An important probe of 4_2-symmetry is the fidelity of the C_2-*pseudo*symmetry axis that is coincidental to the 4_2-*pseudo*symmetry axis. The most regular tetramer was excised out of the 4JRD oligomeric duplex in order to remove the single crystal structure's end base pairs, which are slightly distorted and hence less representative of an extended polymer segment. Centroids of corresponding atoms from 131 pairs were calculated. The mean distance of the 131 centroid points from the C_2-*pseudo*symmetry axis statistical "best line" (see **412**) was only 0.49(26) Å, which is fully consistent with the 4_2-*pseudo*symmetry. Superimposition of the asymmetric poly(rA)-poly(rA) tetranucleotide segment crystal structure upon the corresponding 4_2-symmetry diffraction space-averaged model (**381**) gave an RMS difference of 0.427 Å, which is quite reasonable considering that different experimental conditions that were utilized.

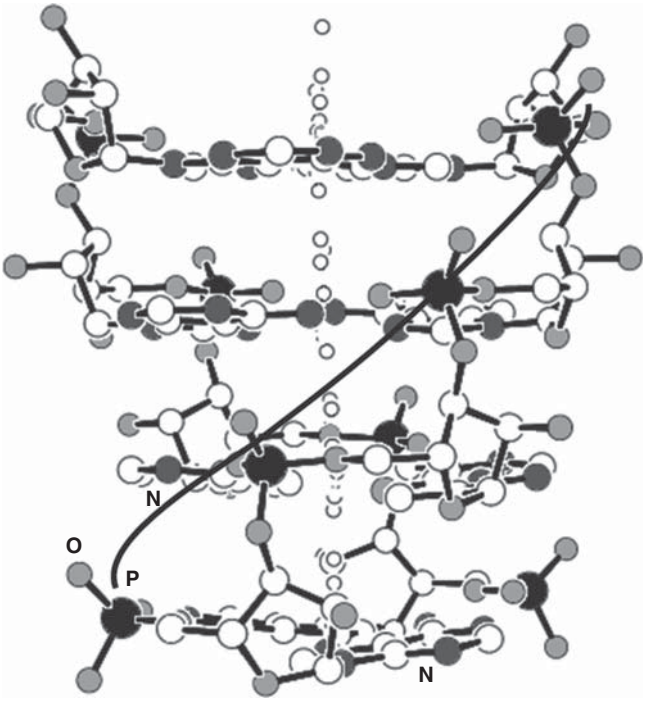

412

The atomic resolution of molecular structural models of oligonucleotide duplexes based upon single-crystal X-ray crystallography is not the only structural parameter that differs from the space-averaged models of a corresponding oriented long fibrous polymer. The end segment possesses a structural freedom that clearly is lacking in the polymer segment under bombardment by X-rays. When considering the Watson–Crick double helix model, there was a space average of the different lateral diameters of the dA:dT and dC:dG base pairs, and each base pair was artificially constrained to be ideally coplanar. In addition, the less regular ends of the fiber were never irradiated, so end geometries exhibiting increased structural freedom did not influence the model building efforts. The single-crystal oligonucleotide duplexes in the Protein Data Base provide a wealth of structural information lacking in the fiber diffraction space-averaged models. Nevertheless, in their time, these models enabled molecular biology to progress beyond the imagination of the model builders. Why? Their basic dimensions and structural hypotheses were correct (even if they were a bit "fuzzy," and perhaps "myopic," so that atomic resolution was lacking). It is awe-inspiring that with metal models that reached from floor-to-chest height in the Langridge laboratory, fiber diffraction crystallographers were able to determine the *space-averaged* structure of numerous polynucleotide duplexes that have withstood the test of time vis-à-vis today's atomic resolution oligomeric structures. As an anecdote of those times, when the "powers that be" refused Langridge's request for more model building space, ingenuity stepped in, and the novel idea was born that "*perhaps we can build a DNA model in a computer*." Using a US Navy line-drawing console and a PDP-8 Computer filling up most of the adjoining room, the author had the pleasure to be present in 1971 when Arthur Lesk put the first DNA structure on the black-and-white screen, and we all proceeded to look from the ends (and from the sides) at this veritable marvel of technology (R. Glaser, unpublished results). Now, we do it on our own desktop computers whenever we desire. Then, there were no molecular graphics programs. We have indeed come a long way.

References

1. Sargusti, I., Sharon, I., Katzenelson, O., and Avnir, D. (1998) *J. Archeolog. Sci.*, **25**, 817–825.
2. Eaton, P. and Cole, T. (1964) *J. Am. Chem. Soc.*, **86**, 3157–3158.
3. Paquette, L., Ternansky, R.J., Balogh, D.W., and Kentgen, G. (1983) *J. Am. Chem. Soc.*, **105**, 5446–5450.
4. Stewart, P.L., Fuller, S.D., and Burnett, R.M. (1993) *EMBO J.*, **12**, 2589–2599.
5. Glaser, R. (1997) *Enantiomer*, **2**, 479–483.
6. Goodsell, D. (2010) Adenovirus Capsid: Molecule of the Month, *Protein Data Bank Internet Site.* December 2010. doi: 10.2210/rcsb_2010_12
7. Liu, H., Jin, L., Koh, S.B., Atanasov, I., Schein, S., Wu, L., and Zhou, Z.H. (2010) *Science*, **329**, 1038–1043.
8. Reddy, V.S., Nachiar, S.K., Stewart, P.L., and Nemerow, G.R. (2010) *Science*, **329**, 1071–1075.
9. Djerassi, C., Records, R., Bunnenberg, E., Mislow, K., and Moscowitz, A. (1962) *J. Am. Chem. Soc.*, **84**, 870–872.
10. Gal, J. (2011) *Chirality*, **23**, 1–16.
11. Zabrodsky, H., Peleg, S., and Avnir, D. (1992) *J. Am. Chem. Soc.*, **114**, 7843–7851.
12. Zabrodsky, H., Peleg, S., and Avnir, D. (1993) *J. Am. Chem. Soc.*, **115**, 8278–8289.
13. Avnir, D., Katzenelson, O., Keinan, S., Pinsky, M., Salomon, Y., and Zabrodsky, H. (1997) in *The Measurement of Symmetry and Chirality: Conceptual Aspects* (ed. D.H. Rouray), Research Studies Press, Taunton, MA, p. 283.
14. Pinsky, M. and Avnir, D. (1998) *Inorg. Chem.*, **37**, 5575–5582.
15. Pinsky, M., Yogev-Einot, D., and Avnir, D. (2003) *J. Comput. Chem.*, **24**, 786–796.
16. Pinsky, M., Casanova, D., Alemany, P., Alvarez, S., Avnir, D., Dryzun, C., Kizner, Z., and Sterkin, A. (2008) *J. Comput. Chem.*, **29**, 190–197.
17. Pinsky, M., Dryzun, C., Casanova, D., Alemany, P., and Avnir, D. (2008) *J. Comput. Chem.*, **29**, 2712–2721.
18. Yogev-Einot, D. and Avnir, D. (2003) *Chem. Mater.*, **15**, 464–472.
19. Alvarez, S., Alemany, P., and Avnir, D. (2005) *Chem. Soc. Rev.*, **34**, 313–326.
20. Yogev-Einot, D. and Avnir, D. (2006) *Tetrahedron: Asymmetry*, **17**, 2723–2725.
21. Steinberg, A., Karni, M., and Avnir, D. (2006) *Chem.–Eur. J.*, **12**, 8534–8538.
22. Dryzun, C., Mastai, Y., Shvalb, A., and Avnir, D. (2009) *J. Mater. Chem.*, **19**, 2062–2069.
23. Dryzun, C. and Avnir, D. (2009) *Phys. Chem. Chem. Phys.*, **11**, 9653–9666.
24. Zabrodsky, H. and Avnir, D. (1995) *J. Am. Chem. Soc.*, **117**, 464–472.
25. Cirera, J., Alemany, P., and Alvarez, S. (2004) *Chem.–Eur. J.*, **10**, 190–207.
26. Alvarez, S., Avnir, D., Llunell, M., and Pinsky, M. (2002) *New J. Chem.*, **26**, 996–1009.

Symmetry, Spectroscopy, and Crystallography: The Structural Nexus, First Edition. Robert Glaser.

Companion Website: www.wiley.com/go/Glaser/Symmetry

27. Echeverria, J. and Alvarez, S. (2008) *Inorg. Chem.*, **47**, 10965–10970.
28. Cirera, J., Ruiz, E., and Alvarez, S. (2005) *Organometallics*, **24**, 1556–1562.
29. Alvarez, S. (2005) *Dalton Trans.*, 2209–2233.
30. Echeverria, J., Casanova, D., Llunell, M., Alemany, P., and Alvarez, S. (2008) *Chem. Commun.*, 2717–2725.
31. Alvarez, S., Alemany, P., Casanova, D., Cirera, J., Llunell, M., and Avnir, D. (2005) *Coord. Chem. Rev.*, **249**, 1693–1708.
32. Avnir, D. and Huylebrouck, D. (2013) *Nexus Netw. J.*, **15**, 171–182.
33. Gil-Av, E., Feibush, B., and Charles-Sigler, R. (1966) *Tetrahedron Lett.*, **7**, 1009–1015.
34. Oró, J., Updegrove, W.S., Gibert, J., McReynolds, J., Gil-Av, E., Ibanes, J., Zlatkis, A., Flory, D.A., Levy, R.L., and Clarence, J. (1970) *Science*, **167**, 765–767.
35. Feibush, B. (1971) *Chem. Commun.*, 544–545.
36. Charles, R., Beitler, U., Feibush, B., and Gil-Av, E. (1975) *J. Chromatogr.*, **112**, 121–133.
37. Byers, J.A. (2004) *J. Neurosci. Methods*, **135**, 89–93.
38. Gorbitz, C.H. (1987) *Acta Chem. Scand.*, **B41**, 87–92.
39. Yao, J.W., Cole, J.C., Pidcock, E., Allen, F.H., Howard, J.A.K., and Motherwell, W.D.S. (2002) *Acta Crystallogr.*, **B58**, 640–646.
40. Rao, S.N., Parthasarathy, R., and Cole, F.E. (1973) *Acta Crystallogr.*, **B29**, 2373–2378.
41. Caira, M.R., Botha, S.A., and Flanagan, D.R. (1974) *J. Chem. Crystallogr.*, **24**, 95–99.
42. (a) Gabbay, E.J. (1966) *Biochemistry*, **5**, 3036–3043; (b) Gabbay, E.J. (1967) *Biopolymers*, **5**, 727–727; (c) Gabbay, E.J. and Glaser, R. (1968) *Biopolymers*, **6**, 243–254; (d) Glaser, R. and Gabbay, E.J. (1970) *Biochim. Biophys. Acta*, **224**, 272–275.
43. Mondragon, A. and Harrison, S.G. (1991) *J. Mol. Biol.*, **219**, 321–334.
44. Glaser, R., Frenking, G., Loew, G.H., Donnell, D., Cohen, S., and Agranat, I. (1989) *J. Chem. Soc., Perkin Trans. 2*, 113–122.
45. Glaser, R., Cohen, S., Donnell, D., and Agranat, I. (1986) *J. Pharm. Sci.*, **75**, 772–774.
46. Shi, L., Dong, G., Duan, L., Qiu, Y., Jia, J., Guo, W., Zhao, D., Cui, D., and Tao, X. (2012) *Chem. Eur. J.*, **18**, 8092–8099.
47. Mislow, K. (1966) *Introduction to Stereochemistry*, New York, Benjamin, pp. 13–23.
48. Boese, R., Blaeser, D., and Wiess, H.–.C. (1999) *Angew. Chem. Int. Ed.*, **38**, 988–992.
49. Gong, D., Wang, B., Cai, H., Zhang, X., and Jiang, L. (2011) *J. Organomet. Chem.*, **696**, 1584–1590.
50. Gal, J. (2007) *Chirality*, **19**, 89–98.
51. Flack, H.D. (2009) *Acta Crystallogr.*, **A65**, 371–389.
52. Hope, H. and de la Camp, U. (1972) *Acta Crystallogr.*, **28**, 201–207.
53. Luner, P.E., Patel, A.D., and Swenson, D.C. (2002) *Acta Crystallogr.*, **C58**, o333–o335.
54. Brozek, Z. and Stadnicka, K. (1994) *Acta Crystallogr.*, **B50**, 59–68.
55. Mauskopf, S.H. (1976) *Trans. Am. Philos. Soc.*, **66**, 5–82.
56. McCrone, W.C. (1965) in *Physics and Chemistry of the Solid-State*, vol. 2 (eds D. Fox, M.M. Labes, and A. Weisberger), Interscience Publishers, London, pp. 725–767.
57. Kuroda, R. and Mason, S.F. (1981) *J. Chem. Soc., Dalton Trans.*, 1268–1273.
58. (a) Gal, J. (2008) *Chirality*, **20**, 1072–1084; (b) Gal, J. (2011) *Chirality*, **23**, 1–16; (c) Gal, J. (2013) *Helv. Chim. Acta*, **96**, 1617–1657; (d) Gal, J. (2013) *Top. Curr. Chem.*, **340**, 1–20.
59. Kekulé, A. (1865) *Bull. Soc. Chim. Fr.*, **3**, 98.
60. Paterno, E. (1869) *G. Sci. Nat.Econ. Palermo*, **5**, 177–122.
61. Bootsma, G.A. and Schoone, J.C. (1967) *Acta Crystallogr.*, **22**, 522–532.

62. Geresh, S., Dubinsky, O., Arad-Malis, S., and Christiaen, D. (1990) *Carbohydr. Res.*, **208**, 301–305.
63. Mislow, K. (1977) *Bull. Soc. Chim. Belg.*, **86**, 595–601.
64. Drude, P. (1900) *Lehrbuch der Optik*, 1st edn, Hirzel, Leipzig.
65. Schöck, M., Otero, R., Stojkovic, S., Hümmelink, F., Gourdon, A., Lægsgaard, E., Stensgaard, I., Joachim, C., and Besenbacher, F. (2006) *J. Phys. Chem. Lett. B*, **110**, 12835–12838.
66. Woolf, A., Chaplin, A.B., McGrady, J.E., Alibadi, M.A.M., Draper, S., Murphy, F., and Weller, A.S. (2011) *Eur. J. Inorg. Chem.*, **2011**, 1614–1625.
67. Eralp, T., Shavorskiy, A., Zheleva, Z.V., Held, G., Kalashnyk, N., Ning, Y., and Linderoth, T.R. (2010) *Langmuir*, **26**, 18841–18851.
68. Fischer, E. (1894) *Ber. Dtsch. Chem. Ges.*, **27**, 2985–2993.
69. Bijvoet, J.M., Peerdeman, A.F., and van Bommel, A.J. (1951) *Nature*, **168**, 271–272.
70. Stephens, P.J. (1985) *J. Phys. Chem.*, **89**, 748–752.
71. Polavarapu, P.L. (1990) *J. Phys. Chem.*, **94**, 8106–8112.
72. Herwig, P., Zawatzky, K., Grieser, M., Heber, O., Jordon-Thaden, B., Krantz, C., Novotný, O., Repnow, R., Schurig, V., Schwalm, D., Vager, Z., Wolf, A., Trapp, O., and Kreckel, H. (2013) *Science*, **342**, 1084–1086.
73. Karplus, M. (1963) *J. Am. Chem. Soc.*, **85**, 2870–2871.
74. Chalmers, B.A., Chen, A.P.-J., and Savage, G.P. (2011) *Aust. J. Chem.*, **63**, 1108–1110.
75. Curie, P. (1894) *J. Phys.*, **3**, 393.
76. Mislow, K. (1977) *Stereochemistry Study Guide*, Princeton University, Princeton, NJ.
77. Mislow, K. and Raban, M. (1967) Stereoisomeric relationships of groups in molecules. *Top. Stereochem.*, **1**, 1–38.
78. Giusesppetti, G., Mazzi, F., Tadini, C., Gallazi, A., Vanoni, P.C., and Gaetani, M. (1980) *Farmaco. Ed. Sci.*, **35**, 231–239.
79. Hirano, S., Toyota, S., Kato, M., and Toda, F. (2005) *Chem. Commun.*, 3646–3648.
80. Kojic-Prodic, B., Ruzic-Toros, Z., Sunjic, V., Decorte, E., and Moimas, F. (1989) *Helv. Chim. Acta*, **67**, 916–926.
81. Glaser, R. and Sklarz, B. (1989) *J. Chem. Soc., Perkin Trans. 2*, 1031–1036.
82. Reisse, J., Ottinger, R., Bickhart, P., and Mislow, K. (1978) *J. Am. Chem. Soc.*, **100**, 911–915.
83. Yufit, D.S. and Howard, J.A.K. (2012) *Cryst. Eng. Commun.*, **14**, 2003–2008.
84. Ajo, D., Casarin, M., Granozzi, G., and Busetti, V. (1981) *Tetrahedron*, **37**, 3507–3512.
85. Brunelli, M., Fitch, A.N., and Mora, A.J. (2002) *J. Solid State Chem.*, **163**, 253–258.
86. Glaser, R., Geresh, S., Blumenfeld, J., Vainas, B., and Twaik, M. (1976/1977) *Isr. J. Chem.*, **15**, 17–21.
87. Dang, T.P. and Kagan, H.B. (1971) *Chem. Commun.*, 481.
88. Kagan, H. and Dang, T.P. (1972) *J. Am. Chem. Soc.*, **94**, 6429–6433.
89. Dang, T.P., Poulin, J.-C., and Kagan, H.B. (1975) *J. Organomet. Chem.*, **91**, 105–115.
90. Ball, R.G., James, B.R., Majahan, D., and Trotter, J. (1981) *Inorg. Chem.*, **20**, 254–261.
91. Knowles, W.M., Sabacky, M.J., Vineyard, B.D., and Weinkauff, D.J. (1975) *J. Am. Chem. Soc.*, **97**, 2567–2568.
92. Drexler, H.–J., Zhang, S., Sun, A., Spannenberg, A., Arrieta, A., Preetz, A., and Heller, D. (2004) *Tetrahedron: Asymmetry*, **15**, 2139–2150.
93. Glaser, R., Geresh, S., Blumenfeld, J., and Twaik, M. (1978) *Tetrahedron*, **34**, 2405–2408.
94. Glaser, R., Geresh, S., Twaik, M., and Benoiton, N.L. (1978) *Tetrahedron*, **34**, 3617–3621.
95. Townsend, J.M. and Blount, J.F. (1981) *Inorg. Chem.*, **20**, 269–271.

96. Doherty, S., Knight, J. G., Bell, A. L., Harrington, R. W., and Clegg, W. (2007) *Organometallics*, **26**, 2465–2468.
97. Molander, G.A., Burke, J.P., and Carroll, P.J. (2004) *J. Org. Chem.*, **69**, 8062–8069.
98. Glaser, R., Twaik, M., Geresh, S., and Blumenfeld, J. (1977) *Tetrahedron Lett.*, **18**, 4635–4638.
99. Brown, J.M. and Chaloner, P.A. (1978) *Tetrahedron Lett.*, **19**, 1877–1880.
100. Glaser, R. and Vainas, B. (1976) *J. Organomet. Chem.*, **112**, 249–260.
101. Glaser, R. and Geresh, S. (1977) *Tetrahedron Lett.*, **18**, 2527–2530.
102. Glaser, R., Geresh, S., Schöllkopf, U., and Meyer, R. (1979) *J. Chem. Soc., Perkin Trans. 1*, 1746–1750.
103. Glaser, R. and Geresh, S. (1979) *Tetrahedron*, **35**, 2381–2387.
104. Brown, J.M., Chaloner, P.A., Glaser, R., and Geresh, S. (1980) *Tetrahedron*, **36**, 815–825.
105. Chan, A.S.C., Pluth, J.J., and Halpern, J. (1980) *J. Am. Chem. Soc.*, **102**, 5952–5954.
106. Drexler, H.-J., Zhang, S., Sun, A., Spannenberg, A., Arrieta, A., and Peretz, A. (2004) *Tetrahedron: Asymmetry*, **15**, 2139–2150.
107. Chan, A.S.C., Pluth, J.J., and Halpern, J. (1979) *Inorg. Chim. Acta*, **37**, L477–L479.
108. Curtin, D.Y. (1954) *Rec. Chem. Prog.*, **15**, 111–128.
109. Seeman, J.I. (1983) *Chem. Rev.*, **83**, 83–134.
110. McGinnety, J.A., Payne, N.C., and Ibers, J.A. (1969) *J. Am. Chem. Soc.*, **91**, 6301–6310.
111. Hall, M.C., Kilbourne, B.T., and Taylor, K.A. (1970) *J. Chem. Soc. A*, 2539–2544.
112. Ball, R.G. and Payne, N.C. (1977) *Inorg. Chem.*, **16**, 1187–1191.
113. Fryzuk, M.D. and Bosnich, B. (1977) *J. Am. Chem. Soc.*, **99**, 6262–6267.
114. Mislow, K. and Siegel, J. (1984) *J. Am. Chem. Soc.*, **106**, 3319–3328.
115. Sobolev, A.N., Belsky, V.K., Romm, I.P., Chernikova, N.Y., and Guryanova, E.N. (1985) *Acta Crystallogr.*, **C41**, 967–971.
116. Glaser, R., Blount, J.F., and Mislow, K. (1980) *J. Am. Chem. Soc.*, **102**, 2777–2786.
117. Glaser, R. (1992) in *Acyclic Organonitrogen Stereodynamics* (eds J.B. Lambert and Y. Takeuchi), VCH Publishers, New York, pp. 123–148.
118. Eliel, E.L. (1977) *Isr. J. Chem.*, **15**, 7–11.
119. Mislow, K. (1976) *Acc. Chem. Res.*, **9**, 26–33.
120. Kurland, R.J., Schuster, I.I., and Colter, A.K. (1965) *J. Am. Chem. Soc.*, **87**, 2279–2281.
121. Chorev, M. (2005) *Biopolymers*, **80**, 67–84.
122. Glaser, R. and Shiftan, D. (1999) in *Advances in Molecular Structure Research*, vol. 5 (eds M. Hargittai and I. Hargittai), JAI Press, Stamford, CT, pp. 89–151.
123. Glaser, R., Ergaz, I., Levi-Ruso, G., Shiftan, D., Novoselsky, A., and Geresh, S. (2005) *Ann. Rep. NMR Spec.*, **56**, 143–214.
124. Ergaz, I. (2005) Ph.D. Dissertation. Ben-Gurion University of the Negev, Beer-Sheva, August 2005.
125. Glaser, R. (1996) *Enantiomer*, **1**, 233–247.
126. Bellon, P.L., Benedicenti, C., Caglio, G., and Manassero, M. (1973) *Chem. Commun.*, 946–947.
127. Glaser, R., Kountz, D.J., Waid, R.D., Gallucci, J., and Meek, D. (1984) *J. Am. Chem. Soc.*, **106**, 6324–6333.
128. Pidcock, E., Motherwell, W.D.S., and Cole, J.C. (2003) *Acta Crystallogr.*, **B59**, 634–640.
129. Brock, C.P. and Dunitz, J.D. (1994) *Chem. Mater.*, **6**, 1118–1127.
130. Robertson, D.W., Jones, N.D., Swartzendruber, J.K., Yang, K.S., and Wong, D.T. (1988) *J. Med. Chem.*, **31**, 185–189.
131. Gardner, M. (1979) *The Ambidextrous Universe: Left, Right, and the Fall of Parity*, 2nd edn, Penguin Books, London, p. 90.
132. AMES Laboratory. US Department of Energy-Public domain, *http://cmp.ameslab.gov/personnel/*

canfield/photos.html# (accessed 17 February 2015).
133. Desiraju, G.R. (2007) *Cryst. Eng. Commun.*, **9**, 91–92.
134. Steed, J.W. (2003) *Cryst. Eng. Commun.*, **5**, 91–92 and 169–179.
135. Gavezzotti, A. (2008) *Cryst. Eng. Commun.*, **10**, 389–398.
136. Burley, S.K. and Petsko, G. (1985) *Science*, **229**, 23–28.
137. Steinberg, A., Ergaz, I., Toscano, R.A., and Glaser, R. (2011) *Cryst. Growth Des.*, **11**, 1262–1270.
138. Fábián, L. and Brock, C.P. (2010) *Acta Crystallogr.*, **B66**, 94–103.
139. Bishop, R. and Scudder, M.L. (2009) *Cryst. Growth Des.*, **9**, 2890–2894.
140. Bernstein, J., Davis, R.E., Shimoni, L., and Chang, N.-L. (1995) *Angew. Chem. Int. Ed. Engl.*, **34**, 1555–1573.
141. Avnir, D. (2006) c2.exe, inv.exe, and mirror.exe programs, Department of Chemistry, Hebrew University of Jerusalem.
142. Erhardt, S., MacGregor, S.A., McCullough, K.J., Savill, K., and Taylor, B.J. (2007) *Org. Lett.*, **9**, 5569–5572.
143. Steinberg, A. (2010) PhD Dissertation, Ben-Gurion University of the Negev, Beer-Sheva.
144. Sunatsuki, Y., Fujita, K., Maruyama, H., Suzuki, T., Ishida, H., Kojima, M., and Glaser, R. (2014) *Cryst. Growth Des.*, **14**, 3692–3695.
145. Glaser, R. and Maartmann-Moe, K. (1992) *J. Pharm. Sci.*, **81**, 858–862.
146. Glaser, R. and Maartmann-Moe, K. (1990) *J. Chem. Soc., Perkin Trans. 2*, 1205–1210.
147. Brown, J.N., Bible, R.H. Jr., Finnegan, P.M., and Erickson, R.A. (1977) *Cryst. Struct. Commun.*, **6**, 343–346.
148. Wiedenfeld, H. and Knoch, F. (1987) *Acta Crystallogr.*, **C43**, 1359–1362.
149. Fleischer, E.B. (1964) *J. Am. Chem. Soc.*, **86**, 3889–3890.
150. Bertau, M., Wahl, F., Weiler, A., Scheumann, K., Wörth, J., Keller, M., and Prinzbach, H. (1997) *Tetrahedron*, **53**, 10029–10040.
151. Gallucci, J.C., Doecke, C.W., and Paquette, L.A. (1986) *J. Am. Chem. Soc.*, **108**, 1343–1344.
152. Tiritiris, I. and Schleid, T. (2003) *Z. Anorg. Allg. Chem.*, **629**, 1390–1402.
153. Glaser, R., Schoefberger, W., Beckmann, M., and Mueller, N. (2014) Central European NMR Meeting, Valtice, Czech Republic, April 27–30, 2014.
154. Kuznetsov, I.Y., Vinitskii, D.M., Solntsev, K.A., Kuznetsov, N.T., and Butman, L.A. (1987) *Zh. Neorg. Khim.*, **32**, 3112.
155. Nakazaki, M. and Naemura, K.I. (1980) *J. Chem. Soc., Chem. Commun.*, 911–912.
156. Nakazaki, M. and Naemura, K.I. (1981) *J. Org. Chem.*, **46**, 106–111.
157. Mislow, K. (1981) *J. Chem. Soc., Chem. Commun.*, 234.
158. Nakazaki, M., Naemura, K., and Hokura, Y. (1982) *J. Chem. Soc., Chem. Commun.*, 1245–1246.
159. Vögtle, F., Gross, J., Seel, C., and Nieger, M. (1992) *Angew. Chem. Int. Ed. Engl.*, **31**, 1069–1071.
160. Saalfrank, R.W., Stark, A., Peters, K., and von Schnering, H.G. (1988) *Angew. Chem. Int. Ed. Engl.*, **27**, 851–853.
161. Saalfranck, R.W., Stark, A., Bremer, M., and Hummel, H.-U. (1990) *Angew. Chem. Int. Ed. Engl.*, **29**, 311–314.
162. Saalfrank, R.W., Burak, R., Breit, A., Stalke, D., Herbst-Irmer, R., Daub, J., Porsch, M., Bill, E., Müller, M., and Trautwein, A.X. (1994) *Angew. Chem. Int. Ed. Engl.*, **33**, 1621–1623.
163. Saalfrank, R.W., Demleitner, B., Glaser, H., Maid, H., Bathelt, D., Hampel, F., Bauer, W., and Teichert, M. (2002) *Chem. Eur. J.*, **8**, 2679–2683.
164. Saalfrank, R.W., Demleitner, B., Glaser, H., Maid, H., Bauer, W., Maluenga, M., Hampel, F., Teichert, M., and Krauschield, H. (2003) *Eur. J. Inorg. Chem.*, 2003, 822–829.
165. Saalfrank, R.W., Glaser, H., Demleitner, B., Hampel, F., Chowdhry, M.M., Shünemann, V., Trautwein, A.X., Vaughan, G.B.M., Yeh, R., Davis, A.V.,

and Raymond, K.N. (2002) *Chem. Eur. J.*, **8**, 493–497.
166. Saalfrank, R.W., Hörner, B., Stalke, D., and Salbeck, J. (1993) *Angew. Chem. Int. Ed. Engl.*, **32**, 1179–1182.
167. Gütz, C., Hovorka, R., Klein, C., Jiang, Q.-Q., Bannwarth, C., Engeser, M., Schmuck, C., Assenmacher, W., Mader, W., Topić, F., Rissanen, K., Grimme, S., and Lützen, A. (2014) *Angew. Chem. Int. Ed.*, **53**, 1693–1698.
168. Granier, T., Langlois D'Estaintot, B., Chevalier, J.–.M., Precigoux, G., and Arosio, P. (2003) *J. Biol. Chem.*, **8**, 105–111.
169. Furukawa, K., Fujino, M., and Matsumoto, N. (1996) *J. Organomet. Chem.*, **515**, 37–41.
170. Wiberg, N., Finger, C.M.M., and Polborn, K. (1993) *Angew. Chem. Int. Ed. Engl.*, **32**, 1054–1056.
171. Glaser, R., Hug, P., Drouin, M., and Michel, A. (1992) *J. Chem. Soc., Perkin Trans. 2*, 1071–1079.
172. Barlow, R.B. and Johnson, O. (1989) *Br. J. Pharmacol.*, **98**, 799–808.
173. Michel, A., Drouin, M., and Glaser, R. (1994) *J. Pharm. Sci.*, **83**, 508–513.
174. Glaser, R., Charland, J.-P., and Michel, A. (1989) *J. Chem. Soc., Perkin Trans. 2*, 1875–1880.
175. Glaser, R., Shiftan, D., and Drouin, M. (1999) *J. Org. Chem.*, **64**, 9217–9224.
176. Wu, X., Burns, S.T., and Zilm, K.W. (1994) *J. Magn. Reson.*, **A111**, 29–36.
177. Glaser, R., Peng, Q.-J., and Perlin, A.S. (1988) *J. Org. Chem.*, **53**, 2172–2180.
178. Leger, J.M., Gadret, M., and Carpy, A. (1978) *Acta Crystallogr.*, **B34**, 3705–3709.
179. Riddel, F.G. and Rogerson, M.J. (1997) *J. Chem. Soc., Perkin Trans. 2*, 249–255.
180. (1989) The United States Pharmacopeia XXII, The National Formulary XVII, The United States Pharmacopeial Convention, Rockville, MD, pp. 1238–1240.
181. *www.pharmacopeia.cn/v29240/usp29nf24s0_m74520.html.*
182. Pauling, P. and Petcher, T.J. (1969) *J. Chem. Soc., Chem. Commun.*, 1001–1002.
183. Prins, L.J., Jolliffe, K.A., Hulst, R., Timmerman, P., and Reinhoudt, D.N. (2000) *J. Am. Chem. Soc.*, **122**, 3617–3627.
184. Glaser, R., Shiftan, D., Levi-Ruso, G., Ergaz, I., and Geresh, S. (2002) *J. Org. Chem.*, **67**, 5486–5496.
185. Anet, F.A.L. (1990) *Tetrahedron Lett.*, **31**, 2125–2126.
186. (a) Lambert, J.B. (1967) *J. Am. Chem. Soc.*, **89**, 1836–1840; (b) Lambert, J.B. (1971) *Acc. Chem. Res.*, **4**, 87–94.
187. Glaser, R., Shiftan, D., and Drouin, M. (1995) *Struct. Chem.*, **6**, 25–35.
188. Zhu, N., Liang, L., Trudel, M.L., and Klein-Stevens, C.L. (2004) *Struct. Chem.*, **15**, 553–565.
189. Pakhomova, S., Ondracek, J., Husak, M., Kratochvil, B., Jegorov, A., and Stuchlik, J. (1995) *Acta Crystallogr.*, **C51**, 308–311.
190. Amit, A., Mester, L., Klewe, B., and Furberg, S. (1978) *Acta Chem. Scand.*, **A32**, 267–270.
191. Caruso, F., Besmer, A., and Rossi, M. (1999) *Acta Crystallogr.*, **C55**, 1712–1714.
192. Remenar, J.F., MacPhee, M.M., Larson, B.K., Ho, J.H., McIlroy, D.A., Hickey, M.B., Shaw, B.P., and Almarson, O. (2003) *Org. Process Res. Dev.*, **7**, 990–996.
193. Novoselsky, A. and Glaser, R. (2002) *Magn. Reson. Chem.*, **40**, 723–728.
194. Harrison, W.T.A., Yathirajan, H.S., Bindya, S., Anikumar, H.G., and Devaraju (2007) *Acta Crystallogr.*, **C63**, o129–o131.
195. Froimowitz, M., Wu, K.-M., George, C., VanDerveer, D., Shi, Q., and Deutsch, H.M. (1998) *Struct. Chem.*, **9**, 295–303.
196. Giesecke, J. (1980) *Acta Crystallogr.*, **B36**, 267–270.
197. Carlstrom, D. and Bergin, R. (1967) *Acta Crystallogr.*, **23**, 313–319.
198. Froimowitz, M., Patrick, K.S., and Cody, V. (1995) *Pharm. Res.*, **10**, 1430–1434.
199. Zhu, N., Harrison, A., Trudel, M.L., and Klein-Stevens, C.L. (1999) *Struct. Chem.*, **10**, 91–103.

200. Froimowitz, M., Gu, Y., Dakin, L.A., Nagafuji, P.M., Kelley, C.J., Parrish, D., Deschamps, J.R., and Janowsky, A. (2007) *J. Med. Chem.*, **50**, 219–232.
201. Smith, M.P., Johnson, K.M., Zhang, M., Flippen-Anderson, J.L., and Kozikowski, A.P. (1998) *J. Am. Chem. Soc.*, **120**, 9072–9073.
202. Smith, M.P., George, C., and Kozikowski, A.P. (1998) *Tetrahedron Lett.*, **39**, 197–200.
203. Glaser, R., Adin, I., Shiftan, D., Shi, Q., Deutsch, H.M., George, C., Wu, K.-M., and Froimowitz, M. (1998) *J. Org. Chem.*, **63**, 1785–1794.
204. Hoffmann, R.W. (1992) *Angew. Chem. Int. Ed. Engl.*, **31**, 1124–1134.
205. Froimowitz, M., Deutsch, H.M., Shi, Q., Wu, K.-M., Glaser, R., Adin, I., George, C., and Schweri, M.M. (1997) *Bioorg. Med. Chem. Lett.*, **7**, 1213–1218.
206. Wolraich, M.L. and Doffing, M.A. (2004) *CNS Drugs*, **18**, 243–250.
207. Steinberg, A., Froimowitz, M., Parrish, D.A., Deschamps, J.R., and Glaser, R. (2011) *J. Org. Chem.*, **76**, 9239–9245.
208. Cao, L., Šekutor, M., Zavalij, P.Y., Mlinarić-Majerski, K., Glaser, R., and Isaacs, L. (2014) *Angew. Chem. Int. Ed.*, **53**, 988–993.
209. Mock, W.L. and Shih, N.Y. (1986) *J. Org. Chem.*, **51**, 4440–4446.
210. Kim, Y., Kim, H., Ho Ko, Y., Selvapalam, N., Rekarsky, M.V., Inoue, Y., and Kim, K. (2009) *Chem. Eur. J.*, **15**, 6145–6151.
211. Liu, S., Ruspic, C., Mukhopadhyay, P., Chakrabarti, S., Zavalij, P.Y., and Isaacs, L. (2005) *J. Chem. Soc.*, **127**, 15959–15967.
212. Rekharsky, M.V., Mori, T., Yang, C., Ko, Y.H., Salvapalam, N., Kim, H., Sobransingh, D., Kaifer, A.E., Liu, S., Isaacs, L., Chen, W., Moghaddam, S., Gilson, M.K., Kim, K., and Inoue, Y. (2007) *Proc. Natl. Acad. Sci. U. S. A.*, **104**, 20737–20742.
213. Marquez, C., Hudgins, R., and Nau, W.M. (2004) *J. Chem. Soc.*, **126**, 5808–5816.
214. Ong, W. and Kaifer, A.E. (2004) *J. Org. Chem.*, **69**, 1383–1385.
215. Glaser, R., Steinberg, A., Šekutor, M., Rominger, R., Trapp, O., and Mlinarić-Majerski, K. (2011) *Eur. J. Org. Chem.*, **19**, 3500–3506.
216. McInnes, F.J., Anthony, N.G., Kennedy, A.R., and Wheate, N.J. (2010) *Org. Biomol. Chem.*, **8**, 765–773.
217. Dvir, H., Jiang, H.L., Wong, D.M., Harel, M., Chetrit, M., He, X.C., Jin, G.Y., Yu, G.L., Tang, X.C., Silman, I., Bai, D.L., and Sussman, J.L. (2002) *Biochemistry*, **41**, 10810–10818.
218. Xu, Y., Colletier, J.-P., Welk, I., Jiang, H., Moult, J., Silman, I., and Sussman, J.L. (2008) *Biophys. J.*, **95**, 2500–2511.
219. Šekutor, M., Molčanov, K., Cao, L., Isaacs, L., Glaser, R., and Mlinarić-Majerski, K. (2014) *Eur. J. Org. Chem.*, **2014**, 2533–2542.
220. Zhang, J., Ren, H., and Liu, L. (2010) *Chem. Lett.*, **39**, 1016–1017.
221. Langridge, R., Wilson, H.R., Hooper, C.W., Wilkins, M.H.F., and Hamilton, L.D. (1960) *J. Mol. Biol.*, **2**, 19–37.
222. Gessner, R.V., Frederick, C.A., Quigley, G.J., Rich, A., and Wang, A.H.J. (1989) *J. Biol. Chem.*, **264**, 7921–7935.
223. Rich, A., Davies, D.R., Crick, F.H.C., and Watson, J.D. (1961) *J. Mol. Biol.*, **3**, 71–86.
224. Glaser, R. (1990) *Struct. Chem.*, **2**, 479–493.
225. Glaser, R. (1993) *Chirality*, **5**, 272–276.
226. Arnott, S., Chandrasekaran, R., Hukins, D.W.L., Smith, P.J.C., and Watts, L. (1974) *J. Mol. Biol.*, **88**, 523–533.
227. Deslandes, Y., Marchessault, R.H., and Sarko, A. (1980) *Macromolecules*, **13**, 1466–1471.
228. Mislow, K. (1994) *Bull. Soc. Chim. Fr.*, **131**, 534–538.
229. Cinquini, M., Cozzi, R., Sannicolo, F., and Sironi, A. (1988) *J. Am. Chem. Soc.*, **110**, 4363–4364.
230. Anet, F.A.L., Miura, S.S., Siegel, J., and Mislow, K. (1983) *J. Am. Chem. Soc.*, **105**, 1419–1426.
231. Perkins, D.F., Lindoy, L.F., Meehan, G.V., and Turner, P. (2004) *Chem. Commun.*, 152–153.

232. Perkins, D.F., Lindoy, L.F., McAuley, A., Meehan, G.V., and Turner, P. (2006) *Proc. Natl. Acad. Sci. U. S. A.*, **103**, 532–537.
233. Glaser, R. (2008) *Chirality*, **20**, 910–918.
234. Safaee, N., Noronha, A.M., Rodionov, D., Kozlov, G., Wilds, C.J., Sheldrick, G.M., and Gehring, K. (2013) *Angew. Chem. Int. Ed.*, **52**, 10370–10373.

Index

a

achiral helical arrangements
– asymmetric units 274
– mechanical constraints 276
– $2n_n$ descriptors 273
– poly(rA)-poly(rA) parallel double-helix 276
achirotopic stereogenic carbon 114
'acide racémique' 47
active pharmaceutical ingredients (API) 35, 200, 229
adamantane-1-NMe3 264, 265
AFMX four-spin system 210
amorphous 'frozen-liquid' 53
angiogenesis 28
α- or β-anomeric configuration
– furanose-ring anomeric hydroxyl group 64
– L-galactopyranose 64
antagonists 230
Anti-Octant Rule 10
antiperiplanar-type torsion angle 38
API *see* active pharmaceutical ingredients (API)
asymmetric carbon atom 113
asymmetric unit
– C_3-pseudosymmetric triangular array 150
– crystallographic pseudosymmetry 149
– diastereomers 151
– dynamic disorder in crystals 222
– multiple molecules 149
– RMS superimposition values 151
– (R)-symmetry cations 150
atom flipping 222
attention deficit disorder (ADD) 237
attention deficit hyperactivity disorder (ADHD) 237
Avnir CSM distortion indices 188

b

Baeyer-Villiger oxidation 279
Beer-Lambert law 70
bioactive conformation 231, 232
Biot's law 45
Bragg law 139
Brazilian twin 55
Brownian motion 165, 193
Buscopan® 196
^{13}C CP/MAS (cross polarization/magic angle spinning) pulse sequences 164

c

charge coupled device (CCD) detectors 142
chemical shift anisotropy (CSA) line-broadening 193
chiral axis 113
chiral local site-symmetry 115
chiral or asymmetric center 113
chiral periodic arrays, *see also* periodic arrays
– and chiral crystal array 134
– *chiral space groups* 133
– general position of symmetry 135
– *high fidelity pseudo*symmetry 135
– molecular structure 134
– Pasteur's crystallization 132
– Sohncke space groups 133
chiral plane 113
chiral propellers 176
chiral zero 33

Symmetry, Spectroscopy, and Crystallography: The Structural Nexus, First Edition. Robert Glaser.

Companion Website: www.wiley.com/go/Glaser/Symmetry

chirality, *see also* symmetry/psuedosymmetry
– achiral geometries 15
– amino acid chirality 23
– Cotton Effect's sign 10
– drug therapy *see* drug therapy, chirality
– extraterrestrial macro-scale chirality
– – Jovian Great Red Spot 21, 22
– – Martian dust devils 20
– – *spiral galaxies* 20
– – Venusian South Polar Giant Vortex 23
– – gastropods 18
– gustatory (taste buds) 26
– olfactory receptors 26
– pheromones 25
– progestin norethindrone, first oral contraceptive drug 10
– stereochemistry 10
– structural property 9
– symmetry *vs*. broken symmetry
– – Gakuen Spiral Towers building 16
– – Mercedes House 17
– – golden ratio 16
– tropical storms' tropicity 18
chiroptical properties
– circular birefringence 68
– circular dichroism (CD) 74
– crystallography 74
– enantiomer's configuration, gas phase 82
– isomerism 67
– Optical Rotatory Dispersion (ORD) 71
Chloride · Dihydrate quaternary ammonium salts 221
circular birefringence 45
– *index of refraction*, concept 70
– *in-phase* helical pathways 68, 69
– monochromatic light source 69
– *non-phase restricted* parallel helices 69
– photon locations 69
– quantum-mechanical phenomenon 68, 69
– *symmetry mismatch* 70
circular dichroism (CD)
– chiral medium 73
– elliptical polarized light 73
– molecular ellipticity 74
– photon locations 72
cis-geminal coupling 107
complex multiplet 207
computer assisted drug design *see* x-ray crystallography
computer assisted molecular modeling (CAMM) *see* pharmacophore method, drug design
conformational searches 234
conformationally polymorphic crystals 232
constitutional isomers 67
contact time period 166
Continuous Shape Measures (CShM) 13
'Continuous Symmetry Measures' (CSM) 13
Cotton Effect 71
Cotton Effect's sign 10
Coulomb explosion imaging (CEI) 82
cross polarization (CP) process 167
cross polarization/polarization inversion (CPPI) 194
cross-polarization (CP) 193
Crystal Structure Based Rational Design method 263
crystal, definition 148
crystallography
– fractional coordinates 74, 75
– hexagonal symmetry 77, 78
– Miller indexes 75
– rotational symmetry 76
– Scanning Tunneling Microscope (STM) 74
cubane
– adamantine, T_{CH} value 167
– *Boltzmann distribution* of nuclei 165
– cross polarization (CP) process 167
– phase coherence 166
– 'plastic crystals' 166
– *radio frequency* (RF) 165
– *relaxation mechanisms* 165
– solid-state NMR spectroscopy 164
Curtin-Hammett principle
– Z-α-benzamidocinnamic acid 106
– CH_3 OC(=O)– methoxy carbon 108
– chiral diphosphines 109
– cis-geminal coupling 107
– cis-hydrogenation, kinetically controlled 108
– cyclopropyl analogue 105
– diastereomeric transition-states 109
– -menthyl/(–)-bornyl chiral ester substrates 104
– methyl α-acetamidocinnamate, *re-si* prochiral face 106, 107
– N-acetyl-(R)-phenylalanine ethyl ester product 110
– $^{31}P^{1}H$ NMR spectroscopy 106

– $[Rh^{I}/(DIPHOS)]^{+}$. BF_4^- π-complex bounding 110
– (*R,R*)-trans-1,2-cycloalkyl analogues 105
– slow magnetic site-exchange line-broadening 106
– (*S,S*)-DIPAMP catalyst 109
– stereogenic carbons 104
– stereogenic phosphorus atoms 104
cyclononenes 214
cyclooctenes, olefinic stereochemistry 214

d
Density Functional Theory (DFT) 79, 215
desymmetrization
– Avnir CSM distortion indices 188
– chemically significant divergences 188
– chiral space group lattice 186
– diffraction pattern 163
– dirubidium closo-dodecaborate 163
– distortion, Avnir CSM programs 161
– dodecahedrane 162
– *high symmetry* point groups 161
– partial desymmetrization 163
– platonic-solid geometry compounds 187
– substituted Platonic-solid geometry molecules 188
– symmetry equivalent methyl groups 186
– *symmetry point group's order* 161
diamantane-4,9-di(NMe_3) 265
diastereomers 67, 115
dihedral angles
– NMR data 34
– torsion angles 35
3,5-dimethyladamantane-1-NH_3 Cl 258
dipolar line-broadening 193
divalent anions
– lobeline 189, 190
– *hydrogen-bonding template* 191
– monoammonium conformations 191
– muscarine 189
– nicotine 189
– ring hydrogen-bonding pattern 190
dodecahedrane 145
– desymmetrization 162
– mobility 166
– solids-NMR technique 164
dodecahedrane *see also* cubane
dopamine (DA) reuptake
– cocaine
– – ammonium NH proton 242
– – aromatic ring centroid 241
– – axial NH back-bridged analogue 243, 244
– – equatorial NH 'front-bridged' 242
– α-iso-pentyl methylphenidate-surrogate incorporation 252
– non-N-methylated compound 252
– ritalin's concentration 241
– site pharmacophore 233
drug therapy, chirality
– angiogenesis 28
– clinical trials 30
– electrostatic interactions 28
– embryopathy 27
– enantiomeric purity 27
– ethical drugs 30
– peniciliamine 27
– phocomelia 30
– placebo effect 31
– thalidomide 27, 29, 30
– transcription 28
– transcription factor 28
dynamic disorder in crystals
– asymmetric unit 222
– atom flipping 222
– atom-flip BB/TCC dynamic conformational interconversion 228
– lattice expansion 222
– local magnetic fields 228
– *gem-N,N*-dimethyl quaternary ammonium salts 222
– medium rings, conformational interconversion mechanism 222
– methohalide isostructural crystals 226
– nefopam methohalide quaternary ammonium ions 223
– non-quaternary and non-methyl suppression (NQS) partial spectrum 226
– space filling 222
– spin-lattice relaxation time constant 227
– synclinal torsion angles 222
dynamic light scattering (DLS) 184
dynamic NMR (DNMR)
– cyclohexane ring-inversion 94
– diastereomeric C_2-symmetrical trans-1,2-dicholorocyclohexane invertomers 94
– diastereomerization 95
– diastereotopic anisochronous signals 90

dynamic NMR (DNMR) (*contd*.)
– diltiazem · HCl, dissolution 97
– enantiomeric cis-1,2-dichlorocyclohexane invertomers 94
– ethyl-group diastereotopic methylene-protons 97
– interaction distance 90
– intrinsic diastereotopism 98
– magnetic site exchange permutations 93
– peak's line-width 90
– rotamers 92
– Slow Exchange Limit (SEL) 90
– sterically-hindered bond-rotation 96
– temperatures exchange rates 92
– time scale 90
– topomerization 93
– variable-temperature 90, 91

e
ebola virus 9
ECD *see* electronic circular dichroism (ECD)
electronic circular dichroism (ECD) 185
embryopathy 27
enantiomerization 94
enantiomers 42
enantiomorphous 50
enantiotopic subunits, prochirality *see* prochirality
end group modified retro-inverso (EGMRI) transformations 123
endocyclic dihedral angles 219
endocytosis 9
β-endorphins 123
ethano-bridge enantiomerization *see* T-symmetry chiral organic molecule
ethical drugs 30
exohedral guests 178

f
fast magnetic site exchange broadening temperature conditions 181
ferritin 185
fragrances 26

g
gas-liquid chromatography chiral columns 23
golden ratio 1, 3, 16, 146, 147
Group Theory 4
^{1}H CRAMPS (combined rotation and multiple pulse sequence 164

h
helical stereochemistry
– B-DNA[231] 269
– 3_1 screw displacement 271, 272
– 3_2 spatial arrangement 272
– translation and *rotation,* components 269
– Z-DNA 269
hemihedralism, crystalline tartaric acid salts
– 'acide racémique' 47
– amorphous 'frozen-liquid' 53
– chiral crystals, conglomerate 51
– isomerism 47
– molecular chirality 51
– as mordant 46
– optical activity 48
– optical rotation and crystal properties 48
– paratartaric acid 47
– phenomenon of dissymmetry 53
– polymorphism 49
– sodium ammonium paratartrate 49
"Herkimer diamonds" 42
high-fidelity pseudosymmetry 135
– concept of chirality 15
– Continuous Chirality 13
– Continuous Shape Measures (CShM) 13
– 'Continuous Symmetry Measures' (CSM) 13
– *genuine symmetry, distortions* 13
– pseudosymmetry fidelity 11
– reflection symmetry 11
– 'Vitruvian Man' 11
– X-symmetry 13, 14
homomers 67
homotopic symmetry equivalent protons 215
hybridization index 39
hybridization of atomic orbitals 39

i
integrins 8
interferogram phenomenon
– *charge coupled device* (CCD) detectors 142
– data measurements 141
– diffraction pattern 140
– *direct methods* 142
– *final residual discrepancy index* or R-factor 143
– Fourier transformation 140, 141
– isotropic or anisotropic parameters 142

– iterative calculation process (*refinement)* 142, 143
– Karle-Hauptman *tangent formula* 142
– *phase problem,* X-ray crystallography 142
– *riding method* 143
– *sphere of reflection* 140
intermeshing molecular helices
– chemical constraint 287
– dimer, complexes 288
– electrostatic interaction 287
– enantiomers' 286
– Fe^{II} and Ni^{II} complexes 285
– heterochiral and homochiral screws 282
– homochiral intermeshing 289
– inversion symmetry 287
– Ir^{II} crystal structure 285
– mechanical constraint 282, 287
– Mn^{II} and Cu^{II} complexes 285
– three-fold rotational symmetry 287
– triple helices 283
International Union of Crystallography 148
isomerism
– anisometric isomers 67
– bonding parameters 68
– diastereo-isomerism 68
– *isometric isomers* 67
isosteric replacements 251
I-symmetry of viral capsids
– asymmetric and chiral 7
– capsid's structure 7
– dissymmetric 9
– ebola 9
– function 8
– *I-pseudo* symmetry 8
– rod units 8

j

J_{AX} and $J_{AX'}$ coupling constants 208
J-coupling 207

k

Karle-Hauptman *tangent formula* 142
K_i concentration 239
kryptoracemate chiral crystals
– advantages of pseudosymmetry 154
– higher order achiral crystals 153
– *n-glide reflection pseudo* symmetry 156
– $P2_1$ monoclinic chiral space group 153, 154, 159
– pseudo-X diastereomers 152
– ring hydrogen-bonding pattern 154
– rmS(*inversion dislocation*) 156
– symmetry elements 156

l

la Coupe du Roi
– achiral cis-3,7-dimethyl-1,5-cyclooctanedione (C_{2v}-symmetry) 279
– Bürgenstock Conference on Stereochemistry 278
– chemical relevance 281
– chiral discrimination, observation 280
– Plexiglas(Perspex) coupe du roi cubes 280
Larmor frequencies 165
'lead nitrate thermometer' 200
L-galactopyranose 64
ligand exchange 113
local environment effect, molecular structure
– bioactive conformation 35
– bonding parameters 34
– computational models 35
– crystal form, packing arrangement 35
– dihedral angles 34
– NMR data 34
– time-averaged structures 34
– X-ray crystallography 34
local site-symmetry 114
lysergic acid diethylamide (LSD) 233

m

medium ring stereochemistry
– 2,6-benzoxazonine compound, crystalline-state 218
– butano-bridged epimeric cyclononene derivatives 213
– cyclooctenes, olefinic stereochemistry 214
– NMR structure determination
– – antiperiplanar and synclinal vicinal protons 218
– – antiperiplanar relationships 218
– – broad-band proton decoupled 217
– – crystalline N-desmethyl-2,6-benzoxazonine · HCl 217
– – dihedral angles 220
– – homonefopam analog 219
– – N-desmethyl 2,6-benzoxazonine, twist-chair-boat(type III) conformation 220

medium ring stereochemistry (*contd.*)
– – nefopam · HCl 217
– – solvated molecules 221
– – vibrational frequency calculation 219
– – *X-ray* crystallography 220
– saturated 214
– synperiplanar torsion angle constraint 214
– transannular interactions 214
meso-cyclopropanes 114
methylphenidate
– attention deficit disorder (ADD) 237, 241
– attention deficit hyperactivity disorder (ADHD) 237, 241
– axial N-methyl epimeric partner 244
– binding affinity 240
– cocaine 239, 240
– equatorial N-methyl species 244
– half maximal inhibitory concentration (IC_{50}) 239
– hydrogen-bonding acceptor site 244
– hydrophobic collapse phenomenon 246
– K_i concentration 239
– mirror symmetry 245
– norepinephrine (NE) 237, 239, 250
– ritalin 237, 239, 240
– serotonin reuptake inhibitor (SSRI) drug 236
– stress 236
Miller index 74
molar ellipticity coefficient 74
'molecularly active' materials 44
molecular subunits, symmetry comparison
– coded methane H-atoms 88
– diastereotopic molecule 88
– diastereotopism 89
– isochronicity 87
– racemic solvent 88
– solvated dodecahedrane 87
– solvent shell calculations 88
molecular symmetry
– NMR anisochronism
– – anisochronous signals 206
– – D_3-symmetry chiral diastereomer 205
– – hydrogen-bonded barbiturates/cyanurates 205
– – hydrogen-bonding arrays 206
– – rosettes 205
– pattern recognition
– – AFMX four-spin system 210
– – digital resolution problem 207
– – estimated standard deviation 207
– – first order multiplet patterns 209
– – homonuclear decoupling (HD) experiments 208
– – inversion in transition order 211
– – J_{AX} and $J_{AX'}$ coupling constants 208
– – J-coupling 207
– – multiple-intensity peaks 207
– – non-symmetry equivalent coupling constants 209
– – nuclear Overhauser effect (NOE) experiments 208
– – number of transitions 208
– – proton-proton vicinal coupling constants 207
'molécules intégrantes' 44

n

nefopam methohalide quaternary ammonium ions 223
nicotine 189
N-methylritalin crystals
– compact epimeric diastereomer 247
– dopamine reuptake inhibitor pharmacophore 248
– nefopam methohalides 248
– prototropic shift/nitrogen inversion 248, 249
– static disorders in 246
non-symmetry equivalent coupling constants 209
Nuclear Magnetic Resonance (NMR) spectroscopy
– coplanar arrangement 85
– cubane 86
– geminal and vicinal coupling 85
– Karplus relationship 85
– non-equivalent proton nuclei 85
Nuclear Overhauser Effect (NOE) intensity enhancements 37

o

Octant Rule 10
octa-t-butyl-octasila-cubane 186
olefins, homogeneous hydrogenation
– achiral gas chromatography 103
– (RS,RS)-alkane racemic mixture product 102
– Curtin-Hammett principle 104
– dideutero-alkane, reductive elimination 102

– dihydrogen activation 103
– (*re-re*)-enantiotopic face 102
– trans-dideutero-olefin 101
Optical Rotatory Dispersion (ORD)
– achiral chromophore 72, 73
– Beer-Lambert law 70
– chiroptical data 71
– circularly polarized photons 72
– Cotton Effect 71
– photon locations 71
ORD *see* Optical Rotatory Dispersion (ORD)
organic substances, structural representation
– bonding geometries 57
– cis-1,2-dimethyloxirane 63
– configuration 59
– dibromoethane 57
– double-bond compounds 58
– Dutch liquid 57
– enantiomorphous orientation 63
– ethanol 56
– meso-tartaric acid 60
– sodium ammonium paratartrate 55
– staggered conformers 62
– stereochemistry 59
– sugars 60
– tartaric acids 56
– *X-ray crystallography* 59
O-symmetry chiral molecules
– atropoisomeric edge-linkers 185
– atropoisomeric ligands 184
– ferritin 185
– X-ray structure determination 184

p

partially modified retro-inverso (PMRI) 123
$P2_1/c$, nature's favorite space group 153
peniciliamine 27
Penrose tiling matching rules 145
periodic arrays
– extended arrays/molecular crystals
– – achiral space groups 127
– – chiral and asymmetric units 129
– – chiral space groups 127
– – quazicrystals 127
– – symmetry, general and special positions 130
– – 'trivial' operations 129
– – unit cell 127
– general positions
– – *cis/trans* core geometries 138
– – molecular occupancy 136
– – second order spin system 132
– *special positions*
– – first order splitting 131
– – inversion symmetry 138
– – molecular occupancy 137
periodic lattice 44
permutational isomers
– aryl C(ipso) carbons 117
– chemical shifts 122
– exo/endo rotamers 117
– graph theory 121
– helicity 118
– helicity interconversion 119
– interconversion 122
– one-ring flip diastereomerization mechanism 120
– ortho edge-label exchange 119
– orthogonal-ring hub transition state 119
– polymorphous triarylamine crystals 117
– residual diastereomers 122
– 'standard dextro reference orientation' 119
– standard orientation labeled 116
– trialkylamines, pyramid geometry 117
– triarylamine helicity interconversion 119
– triarylamine propeller 121
– triarylamines maximally stereochemically labeled 116
pharmacophore method, drug design
– active pharmaceutical ingredient (API) 229
– artificial intelligence superimposition techniques 232
– binding affinities 231
– bioactive conformation 232
– chemical groups, 3D arrangement 229
– conformational searches 234
– dopamine (DA) 233
– drugs peripheral functionalities 229
– energy conformer 231
– nanomolar concentration therapeutic activities 231
– neurotransmitters binding 229
– pharmacophoric bioactive arrangement 232
– pharmacotherapeutic agents 231
– selective reuptake inhibitor (SRI) 230
– steady-state neurotransmitter equilibrium concentration 230

pharmacotherapeutic agents 231
phase coherence 166
pheromones 25
phocomelia 30
placebo effect 31
'plastic crystals' 166
platonic-solid geometries *see* platonic-solid geometry hydrocarbons
prochirality
– double-bond faces 100
– enantiotopic faces 100
– prochiral descriptors 100
– prochiral protons 99
– *Re,si* descriptors 100
progestin norethindrone, first oral contraceptive drug 10
Protein Data Base 291
proton-proton vicinal coupling constants 207
pseudoasymmetric carbon atoms 114
pseudoscalar phenomenon 33
pseudosymmetry *see* symmetry/psuedosymmetry
pseudosymmetry emulation
– Avnir *inv.exe* program 155
– chiral crystal lattice 152
– diphenhydramine derivatives 159, 160
– *intermolecular pseudosymmetry* fidelity 151, 155
– iron(II) complex 159
– kryptoracemates 152
– N-desmethylnefopam.HCl kryptoracemate molecules 156
– *n-glide reflection pseudo*symmetry 156
– $P2_1/c$, nature's favorite space group 153
– pseudoglide or pseudoscrew-rotation 157
– pseudoinversion symmetry 153
– ring hydrogen-bonding pattern 154
– rmS(inversion dislocation) 156
– Second Kind, operations 152
– *X-pseudo*symmetry, *rmS(X)* calculations 159

q

quartz crystals hemihedralism
– circular birefringence 45
– D_3 chiral pseudosymmetry 43
– D_{3d} and D_{6h} achiral symmetry 42
– double-headed 42
– 'enantiomorphism in quartz' 43
– enantiomorphous 42
– hemihedral faces 43
– holohedral faces 42
– optical rotation 45
– subgroups 44
quartz crystals, *u', x'*-hemihedral faced right- and left-handed 54
quazicrystal packing 146

r

racemic compound crystal lattices 132
refinement 142, 143
retro-inverso (RI) isomers
– *boat-boat* chiral conformation 124
– end group modified retro-inverso (EGMRI) transformations 123
– partially modified retro-inverso (PMRI) 123
– peptide transformations 122, 123
– pharmacokinetics 122
– ring-chirality 124
– stereogenic element 124
rigid conformational analogue 232
ritalin 237, 239, 240

s

saturated medium rings 214
sausage formulae, benzene six carbon atom 56
Scanning Tunneling Microscope (STM)
– Cu-surface electrode 81
– Density Functional Theory (DFT) 79
– desymmetrization 81
– homochiral dimers 82
– mechanical cleavage or electrochemical etching 78
– molecular chirality 81
– *organizational chirality* 79
– pseudosymmetry 81
– quantum mechanical phenomena 78
– *quantum tunneling* 78, 79
– symmetry relationship 74
Scopolamine Hydrobromide
– anhydrate and hydrated forms 201
– API (active pharmaceutical ingredient) 200
– Atropos Belladonna 191
– Boehringer-Ingelheim and Phytex samples 199
– bromide vs. chloride anions 202
– Brownian motion 193

– conformational structure 194
– CPPI (cross polarization/polarization inversion) 194
– desolvated crystals 203
– π-flip kinetic phenomenon 196, 197
– and HCl salts 195
– hydrogen-bond donors 203
– *hydrophobic collapse* 195
– magic angle spinning (MAS) 193
– SELTICS pulse-program 198
– single crystal *X-ray* diffraction 192
– solid-state CP/MAS ^{13}C NMR spectroscopy 197
– solid-state NMR spectroscopy 193
– 'trihydrate' form 197, 200
– variable amplitude cross polarization (VACP) pulse-program 198
SDRI *see* specific dopamine reuptake inhibitors (SDRI)
selectivereuptakeinhibitor(SRI) 230
SELTICS pulse-program *(side band elimination by temporary interruption of the chemical shift*) 198
single crystal X-ray crystallography *see* interferogram phenomenon
slow magnetic site exchange broadening temperature conditions 181
sodium ammonium paratartrate
– double salt 51
– hemihedral facets 49
sodium-D line 44
solid-state NMR spectroscopy
– *chemical shift anisotropy (CSA) line-broadening* 193
– *dipolar line-broadening* 193
solid-state *racemic compound* 132
specific dopamine reuptake inhibitors (SDRI) 244
– back-bridged tropane derivative 250
– C_α-alkyl *'methylphenidate-like'* surrogates 250
– DA/NE relative binding affinity 250
– i-Pnt test compound 251
– isosteric replacements 251
– methyl branched-chain analogues 251
– methyphenidate, branched-chain α-alkyl analogues 251
– p-Cl aromatic ring substitution 250
spherical $(CH)_n$ crystalline molecules *see* cubane
spherical $(CH)_n$ crystalline molecules *see* dodecahedrane
spin-lattice time constant *see* time constant number one (T1)
spin-spin time constant *see* time constant number two (T2)
SRI *see* selective re up take inhibitor(SRI)
stereogenic elements 113
STM *see* Scanning Tunneling Microscope (STM)
Structure-Based Molecular Design technique 258
sweeteners 26
symmetry
– dynamic stereochemistry 90
– molecular subunits *see* molecular subunits, symmetry comparison
– in NMR spectroscopy *see* Nuclear Magnetic Resonance (NMR) spectroscopy
symmetry arguments 33
symmetry molecules
– chiral/achiral symmetry 171
– crystal lattice 169
– crystallization 169
– duals in solid-geometry 170
– O_h-symmetry, cube 171
symmetry/psuedosymmetry
– apparent symmetry *see* high-fidelity pseudosymmetry
– asymmetric vs. chiral *see* I-symmetry of viral capsids
– chirality 9
– 'golden-ratio' 1, 3
– *Group Theory* 4
– handedness or chirality 5
– – chiral point groups 6
– – First Kind 5
– – Second Kind 5
– *'high symmetry'* 3
– isometry 4
– *point groups* 4
– stone axe-heads, study 2
– *symmetry operation* 5, 6
– *symmetry transform* 6
– *unit cell* 6
– 'Vitruvian Man' drawing 1
synclinal torsion angles 222

t

tartaric acid
– isolation 45
– molecular chirality *see* hemihedralism, crystalline tartaric acid salts

tetradentate edge-linker units 183
thalidomide
– adverse effects 30
– advertisements 29
– chirality, role 27
– *over-the-counter remedy* 29
– safety and effectiveness 30
time constant number one (T_1) 166
time constant number two (T_2) 166
topomerization 93
torsion angles and molecular conformation
– anhydrate and monohydrate crystal structures 36
– *boat-boat* conformation 37
– bond angles 35
– bond lengths 35
– dihedral angles 36
– molecule's environment 36
– non-symmetry equivalent molecules 37
– Nuclear Overhauser Effect (NOE) intensity enhancements 37
– semi-quantitative descriptors 38
– spatial arrangements 35
– stereochemical terms 39
– symmetry dependent 38
transcription factor 28
transmission electron microscopy (TEM) 184
triarylamine propellers 115
T-symmetry chiral organic molecule
– ammonium ions 178
– asymmetric unit building-block unit 176
– chiral propellers 176
– crystallographic T-point group symmetry 178
– C_3-symmetry 1,3,5-trisubstituted phenyl hexadentate ligands 180
– D_2 symmetry 172
– enantiomers 174
– ethano-bridge protons 175
– magnesium^{II}ions 176
– molecular chirality 174
– pseudosymmetry mimics 174
– rhombohedral R3 chiral space group 173
– spheriphane 175
– synthesis 171
– X-ray crystallography 174
T-symmetry clusters, enantiomerization
– Bailar Twist 180
– coplanar transition-state 181
– diastereotopic methylene protons 181
– energy of activation 182
twist-boat-chair (TBC) conformation 220, 221
– cyclononane 214, 215
twist-chair-chair (TCC) conformation
– atom flip 228
– atom-flip dynamic interconversion 222
– halide anion's van der Waal radii 222
– temperature measurement 228

v

Valence Shell Electron Pair Repulsion (VSEPR) paradigm 39
variable amplitude cross polarization (VACP) pulse-program 198
vibrational circular dichroism 82
vibrational Raman optical activity 82
'Vitruvian Man' drawing 1, 11

w

Watson and Crick's DNA model 144
Watson-Crick double helix 291

x

x-ray crystallography 161
– computer assisted drug design
– – adamantane-1,3-di(NMe_3 I) 262
– – asymmetric units 260
– – avidin biotin complex 256, 257
– – Avnir S(C7) parameter 260
– – bonding and non-bonding interactions 263
– – CB host 266
– – C_7 pseudosymmetry 267
– – *Crystal Structure Based Rational Design* method 263
– – cucurbit[n]urils 257
– – 3,5-diMe-Ada-1-NH_3 Cl composite 264
– – electrostatic interactions 265
– – ^{1}H NMR competition experiments 257
– – memantine 259
– – quaternary-NMe_3 salt 263
– – sodium acetate-*d3* buffer 258
– – *Structure-Based Molecular Design* technique 258
– – unused potential binding sites 255
X-ray diffraction
– *Bragg condition* 140
– by crystals
– – aperiodic (quazicrystals) 139
– – periodic (crystal lattice) 139

– – *'single crystals'* 139, *see also* interferogram phenomenon
– fiber diffraction
– – B-DNA 143
– – helical diffraction patterns 144
– – *Patterson Function* 144
– – Watson and Crick's DNA model 144
x-ray fiber vs. single crystal diffraction models
– DNA, dimensions and structural hypotheses 291
– Protein Data Base 291
– 4_2 pseudo symmetry tetranucleotide duplexes 290
– Watson-Crick double helix 291
X-symmetry
– distance geometry algorithm 14
– pseudo- and genuine symmetry 15
– 'S(X)' CSM numerical index 13
– – high-fidelity pseudo symmetry 15
– – *integer number zero* 14, 15
– – low-fidelity pseudo symmetry 15
– – moderate-fidelity pseudo symmetry 15
zero-point energy 40